

Investigation of the Ultrasonic Based Hydrogen Production Process: *Sonohydrogen*

by

Sherif Samir Ahmed Rashwan Seifeldin

A thesis submitted to the
School of Graduate and Postdoctoral Studies in partial
fulfillment of the requirements for the degree of

Doctor of Philosophy in Mechanical Engineering

Mechanical and Manufacturing Engineering Department/Faculty of Engineering
and Applied Science

University of Ontario Institute of Technology (Ontario Tech University)

Oshawa, Ontario, Canada

April 2021

THESIS EXAMINATION INFORMATION

Submitted by: **Sherif Seifeldin**

Doctor of Philosophy in Mechanical Engineering

Thesis title: Investigation of the Ultrasonic Hydrogen Production Process: Sonohydrogen

An oral defense of this thesis took place on April 9th, 2021, in front of the following examining committee:

Examining Committee:

Chair of Examining Committee	NAME
Research Supervisor	IBRAHIM DINCER
Research Co-supervisor	ATEF MOHANY
Examining Committee Member	MARTIN AGELIN-CHAAB
Examining Committee Member	AMIRKIANOOSH KIANI
University Examiner	RACHID MACHRAFI
External Examiner	YUN HANG HU, Michigan Tech

The above committee determined that the thesis is acceptable in form and content and that a satisfactory knowledge of the field covered by the thesis was demonstrated by the candidate during an oral examination. A signed copy of the Certificate of Approval is available from the School of Graduate and Postdoctoral Studies.

ABSTRACT

The present work carries out various sets of numerical investigations to link the primary effect of the acoustic parameters with the secondary effect of developing a chemical reaction mechanism for water vapor dissociation into hydrogen and radicals. The first set of numerical modeling predicts the acoustic pressure distribution inside a typical geometry cylindrical sonoreactor. The study validates the acoustic pressure according to different geometrical and acoustical parameters. Secondly, the analysis and assessments give access to the sonication process's acoustic streaming. The second set validates the acoustic streaming result according to the velocity profile and streamlines, which gives an excellent agreement with the literature's experimental data. Analysis of variance ANOVA investigates the performance of 27 different configurations for the sake of optimization and determines the most influential factors for the design of a sonoreactor. Nevertheless, the chemical reaction module develops a chemical kinetics model and simulates the sonohydrogen process. The reaction kinetics mechanism consists of 19 reversible reactions and investigates the effect of the acoustic bubble temperature and the dissolved gases on the hydrogen production rate. The study quantifies the amount of hydrogen produced from the sonohydrogen process successfully and reveals the energy consumption to produce one μmol of hydrogen per kWh.

The chemical kinetics results reveal that the higher the bubble temperature, the higher the chemical reaction rate. In the case of the $\text{H}_2\text{O}/\text{O}_2$ bubble, the energy consumption ranges between 1.05-1.63 $\mu\text{mol}/\text{kWh}$, with a maximum hydrogen yield of 4% and a maximum energy efficiency of 2% depending on the bubble's temperature. However, in the $\text{H}_2\text{O}/\text{Ar}$ bubble, the hydrogen production shows an outstanding improvement with energy efficiency in the range 20-30 $\mu\text{mol}/\text{kWh}$ with a maximum hydrogen yield of 35% and a maximum overall efficiency of 15%. The theory beyond this finding lies in the lower thermal conductivity, higher heat capacity, and lower thermal diffusivity of water vapor and carbon dioxide composition. We find this study is promising as a start for a new technique for hydrogen production.

Keywords: sonochemistry, sonohydrogen; sonoreactor performance; sonohydrogen efficiency; ultrasonic hydrogen production.

AUTHOR'S DECLARATION

I hereby declare that this thesis consists of original work of which I have authored. This is a true copy of the thesis, including any required final revisions, as accepted by my examiners.

I authorize the University of Ontario Institute of Technology to lend this thesis to other institutions or individuals for the purpose of scholarly research. I further authorize the University of Ontario Institute of Technology to reproduce this thesis by photocopying or by other means, in total or in part, at the request of other institutions or individuals for the purpose of scholarly research. I understand that my thesis will be made electronically available to the public.

Sherif Samir Ahmed Rashwan
Seifeldin

STATEMENT OF CONTRIBUTIONS

Part of the work described in Chapter 1 considering the development of the ultrasonic hydrogen production concept has been published as:

- [1] Rashwan SS, Dincer I, Mohany A. Sonication to hydrogenization: Sono-hydro-gen. *International Journal of Energy Research*. 2019 10;43, (3):1045-8. doi.org/10.1002/er.4339

Part of the work described in Chapter 2, considering the introduction and comprehensive literature review, are performed and published:

- [2] Rashwan SS, Dincer I, Mohany A, Pollet BG. The Sono-hydrogen process (Ultrasound induced hydrogen production): Challenges and opportunities. *International Journal of Hydrogen Energy*. 2019, 7;44, (29):14500-26. doi.org/10.1016/j.ijhydene.2020.05.022

Part of the work is described in Chapter 3, and Chapter 4, considering the sonoreactor acoustics modeling, analyzing, and simulating the acoustics field characteristics of the sonoreactor, is performed numerically using COMSOL and published as follows:

- [3] Rashwan SS, Dincer I, Mohany A. Investigation of acoustic and geometric effects on the sonoreactor performance. *Ultrasonics Sonochemistry*. 2020 May 16:105174. doi.org/10.1016/j.ultsonch.2020.105174
- [4] Rashwan SS, Dincer I, Mohany A. Effect of Ultrasonic Frequency on Sonic Hydrogen Production. 4th International Hydrogen Technologies Congress (IHTEC-2019).
- [5] Rashwan, S. S., Dincer, I. & Mohany. Investigation of Efficient Sonoreactor Geometries for Hydrogen Production. *International Journal of Hydrogen Energy*. Under Review. 2021

The work described in Chapter 4 considering the chemical kinetics modeling considering parametric studies for the chemical kinetics, and quantifying the hydrogen production based on the acoustic bubble temperature and different dissolved gases.

- [6] Rashwan SS, Dincer I, Mohany A. An investigation of ultrasonic based hydrogen production. *Energy*. 2020 Jun 10:118006. doi.org/10.1016/j.energy.2020.118006
- [7] Rashwan SS, Dincer I, Mohany A. A unique study on the effect of dissolved gases and bubble temperatures on the ultrasonic hydrogen (sono-hydrogen) production. doi.org/10.1016/j.ijhydene.2020.05.022
- [8] Rashwan, S. S., Dincer, I. & Mohany, A. The role of CO₂ in improving sonic hydrogen production. *International Journal of Energy Research* (2020). <https://doi.org/10.1002/er.5827>
- [9] Rashwan, S. S., Dincer, I. & Mohany, A. Journey of Wastewater to Clean Hydrogen: A Perspective. *International Journal of Energy Research* (2021). <https://doi.org/10.1002/er.6279>

For all the journal articles mentioned above, I have been responsible for the majority of the modeling, simulation of the proposed systems, reviewing and writing the manuscripts.

DEDICATION

I would like to dedicate this Ph.D. Thesis and the Doctorate Degree from Ontario Tech University to my passed away, Father, Samir Rashwan, may his soul rest in heaven.

ACKNOWLEDGEMENTS

First and foremost, I'm eternally grateful and would like to express my sincerest thanks to my mentors and supervisors, Prof. Dr. Ibrahim Dincer and Prof. Dr. Atef Mohany, for their support at the beginning of my Ph.D. Journey at Ontario Tech University. I will treasure their support for the rest of my life. I am in debt gratitude to them for all the guidance, patience, and encouragement throughout this research work and during the past three years. Their trust and high expectations pushed me to finish this thesis and develop a new hydrogen production field and gain a new level of experience. I shall also state my most profound appreciation and admiration for their exceptional enthusiasm and interest in my work. Our fruitful discussions on the subject made enormous contributions to this thesis. I also would like to express gratitude to the Government of Ontario, Canada, for providing the Ontario Trillium Scholarship (OTS) in each year of full-time study at Ontario Tech University.

My wholehearted gratitude is to my family for their invaluable patience, trust, and encouragement during this Ph.D. Journey. Words cannot express how grateful I am to my mother and father for all of the sacrifices they have made on my behalf. They never stop believing in me, even the times, I have lost my confidence and hope. I would certainly not be where I stand today without their unconditional love. Your prayers are what sustained me thus far in many injustice situations. Your continuous encouragement gave me the strength to reach my goal and carry on with my own plan throughout the years. I could not stand here today and make this Ph.D. Thesis without acknowledging the heartfelt support my family has given me. Your kindness and affection have carried me through some of the most difficult periods. Moreover, always your love and care have eased that journey, and for that, I thank you from the bottom of my heart.

TABLE OF CONTENTS

ABSTRACT	ii
AUTHOR’S DECLARATION	iii
STATEMENT OF CONTRIBUTIONS	iv
DEDICATION	v
ACKNOWLEDGEMENTS	vi
TABLE OF CONTENTS	vii
LIST OF TABLES	xii
LIST OF FIGURES	xiii
NOMENCLATURE	xviii
Chapter 1. Introduction	1
1.1 Hydrogen as a potential fuel	1
1.2 Potential ultrasound applications	3
1.3 Research gaps and motivations	4
1.4 Novelty statement	5
1.5 Thesis objectives.....	5
1.6 Contributions.....	6
1.6.1 Acoustic pressure model of sonoreactor	6
1.6.2 Acoustic streaming model of sonoreactor.....	6
1.6.3 Chemical kinetics mechanism model.....	7
1.6.4 Hydrogen yields	7
1.7 Thesis outline	7

Chapter 2. Literature Review	9
2.1 Hydrogen Production Processes	10
2.1.1 Thermochemical Process	10
2.1.2 Electrochemical Process	10
2.1.3 Photobiological Process	11
2.1.4 Photoelectrochemical Process.....	11
2.1.5 Sonochemical Process.....	12
2.2 Sonochemistry Technology	13
2.2.1 Sonoelectrochemistry.....	13
2.2.2 Benefits from sonochemistry	14
2.2.3 Sonohydrogen system Illustration.....	15
2.3 Factors affecting the sonohydrogen process.....	19
2.3.1 Ultrasonic Frequency	19
2.3.2 Dissolved gas	20
2.3.3 Acoustic power	21
2.3.4 Bulk liquid temperature	22
2.3.5 Bubble temperature.....	22
2.4 Previous numerical and experimental studies.....	25
2.4.1 Numerical modeling studies	26
2.4.2 Recent experimental studies	30
2.5 Challenges for Sonohydrogen reactor design.....	35
Chapter 3. System Development and Modeling	38
3.1 Sonoreactor Acoustic Modeling.....	38
3.1.1 Computational domain.....	38
3.1.2 Governing equations	41
3.1.3 Physical models	43
3.1.4 Boundary conditions	44
3.1.5 Modeling of acoustic streaming.....	45
3.1.6 Thermodynamics analysis and efficiency.....	47

3.1.7	Sonoreactor parameters and simulation plan	49
3.2	Bubble Dynamics Modeling	50
3.2.1	Background	50
3.2.2	The bubble dynamics model	52
3.3	Chemical Kinetics Modeling	55
3.4	Modeling Procedure	59
Chapter 4.	Results and Discussion	61
4.1	Acoustic Modeling Results	61
4.1.1	Mesh independency study	61
4.1.2	Acoustic model validation	62
4.2	Effect of Acoustical/Operational Parameters	65
4.2.1	Effect of ultrasonic frequency.....	65
4.2.2	Effect of acoustic power	67
4.3	Effect of Geometrical Parameters	69
4.3.1	Effect of immersion depth	69
4.3.2	Effect of scaling-up the sonoreactors.....	70
4.3.3	Effect of probe diameter	72
4.3.4	Effect of the boundary conditions.....	73
4.4	Analysis of variance and optimization	78
4.5	Acoustic Streaming	84
4.4.1	Acoustic streaming validation.....	84
4.4.2	Acoustic streaming analysis.....	86
4.4.3	Density effects on acoustic streaming.....	88
(a)	Constant density.....	88
(b)	Linear density result.....	89
(c)	Non-linear density result.....	90
4.4.4	Acoustic streaming for different geometries.....	91
(a)	Geo.1 – Cylindrical sonoreactor with 1 ultrasonic transducer.....	93

(b)	Geo.2 – Cylindrical sonoreactor with 3 ultrasonic transducers	93
(c)	Geo.3 – Cylindrical sonoreactor with 5 ultrasonic transducers	94
(d)	Geo.4 – Hexagonal sonoreactor with 5 ultrasonic transducers.....	95
(e)	Geo.5 – Square sonoreactor with 5 ultrasonic transducers	96
4.6	Geometric parametric study and Optimization	97
4.5.1	Effect of the number of sonotrodes.....	98
4.5.2	Effect of the outer sonoreactor geometry.....	102
4.5.3	Characterization of the cavitation zone.....	107
4.7	Chemical Kinetics Modeling Results.....	109
4.6.1	Bubble Dynamics Results	109
4.6.2	Chemical kinetics validation.....	111
4.6.3	Effect of Bubble Temperature	113
(a)	H ₂ O/O ₂ bubble case	113
(b)	H ₂ O/CO ₂ bubble case.....	116
(c)	H ₂ O/Ar bubble case	121
(d)	H ₂ O/Air bubble case	122
(e)	Hydrogen production & quantification.....	124
(f)	Energy consumption	126
4.6.4	Effect of dissolved gases.....	128
(a)	Quantification of hydrogen production.....	129
(b)	Comparison between H ₂ O/CO ₂ and H ₂ O/O ₂ bubbles.....	132
(c)	Energy consumption analysis	134
(d)	Effect of bubble composition.....	139
(e)	Energy Performance Analysis	142
4.7.1	Hydrogen yield.....	142
4.7.2	Sonohydrogen energy efficiency	143
4.7.3	Comparison of energy efficiency.....	147
4.7.4	Cavitation and sonohydrogen efficiency	149
Chapter 5.	Conclusions and Recommendations.....	154

5.1	Conclusions.....	154
5.2	Recommendations.....	155
	REFERENCES.....	158
	APPENDICES.....	171
Appendix A.	Copy righted articles.....	173
A1.	Copy rights permission by ELSEVIER of published articles.....	173

LIST OF TABLES

Table 2.1: A comparison between different hydrogen production technologies	12
Table 2.2: A summary of the experimental studies on H ₂ O ₂ production using the ultrasound	19
Table 2.3: A summary of the numerical studies on H ₂ -production using the ultrasound waves..	20
Table 2.4: H ₂ -production (Mole) at different acoustic power amplitude and frequencies. Data extracted from Kerboua and Hamdaoui [63]	21
Table 2.5: Summary table of the bubble temperature and pressure ranges as reported in the literature with corresponding references.....	24
Table 2.6: H ₂ -production at bubble temperature [K] by Merouani et al. [57]	25
Table 2.7: Sonochemical reaction steps by Cotana et al. [92]	34
Table 3.1: Acoustic investigation plan and parametric study	50
Table 3.2: Ultrasonic H ₂ -production chemical kinetic model inside an O ₂ cavitation bubble. M is the third body species. Subscript (f) denotes the forward and (r) denotes the reverse reactions.	57
Table 3.3: NASA polynomial coefficients for the species thermodynamic expressions to be used in the expressions of specific heat at constant pressure, enthalpy, and entropy.	58
Table 3.4: The physical, acoustical, thermodynamic input parameters	60
Table 4.1: The experimental parameters used by Gogate et al. [49]	63
Table 4.2: The acoustic parameters corresponding to different ultrasound probe diameters	73
Table 4.3: Input factors and 3 levels selected for ANOVA (3X3)	79
Table 4.4: Geometries' dimension used in ANOVA for the 27 runs. Note that (sonoreactor diameter D = 135 mm and length L = 170 mm)	81
Table 4.5: ANOVA Data Points for the 27 runs	82
Table 4.6: Minitab output: Analysis of variance (Two-Way ANOVA)	83
Table 4.7: Optimization and comparison of the effect of the number of sonotrodes	102
Table 4.8: Optimization and comparison on the effect of different geometries for the 5 sonotrodes analysis	105
Table 4.9: The initial concentration of the mixture species present study.....	111
Table 4.10: Energy consumption comparison between the most common H ₂ -production technologies	128
Table 4.11: Tabulated properties of H ₂ O/Air and H ₂ O/Ar mixture [154]. The negative sign refers to a decrease in the tabulated properties	129
Table 4.12: Tabulated properties of H ₂ O and different bubble mixtures at 298 K [154]. All at the same WVF of 0.39	131
Table 4.13: Tabulated properties of H ₂ O and different bubble mixtures at 8000 K [154]. All at the same WVF of 0.39	131
Table 4.14: Tabulated properties of H ₂ O and H ₂ O/CO ₂ mixture at 298 K [154]. The negative sign refers to a decrease in the tabulated properties	131
Table 4.15: Tabulated properties of H ₂ O and H ₂ O/CO ₂ mixture at 8000 K [154]. The negative sign refers to a decrease in the tabulated properties	132
Table 4.16: Select properties of H ₂ O/O ₂ and different H ₂ O/CO ₂ mixtures at 298 K [154]. WVF is the water vapor fraction. The negative sign refers to a decrease in the tabulated properties.	133

LIST OF FIGURES

Figure 1.1: Energy demand over the years up to 2040 in Petajoule [PJ]. Note that PJ equal to $1.0E+15$ Joules [1]	2
Figure 1.2: A summary of ultrasound applications at different ultrasonic frequencies	3
Figure 2.1: Different processes and technologies for hydrogen production	9
Figure 2.2: Design configurations of a sonoreactor	15
Figure 2.3: Schematic of the ultrasound generator probe showing H_2O/CO_2 bubbles and the dissociation mechanism	16
Figure 2.4: The sequence of acoustic cavitation bubble collapse	17
Figure 2.5: Factors governing the hydrogen production of sonohydrogen process	18
Figure 2.6: Space-time evolution of temperature during the collapse at an equilibrium radius of $R_0 = 4.5 \mu m$ driven at 26.5 kHz and 1.3 bar. Adapted from Schanz et al. [77]	23
Figure 2.7: (a) Oscillating pressure field in the domain; (b) the pressure fluctuation at the center of the bottom (blue) and the bottom displacement (pink) by Osterman et al. [80]	26
Figure 2.8: Active cavitation zones simulated by CFD technique for the reactor filled with saturated crude oil at a temperature of 25 °C by Niazi et al. [83]	27
Figure 2.9: Pressure profile (a), pressure contour (b), and temperature contour (c) with ultrasonic power of 300 W, the liquid medium is water by Kim et al. [78]	28
Figure 2.10: Pressure field distributions inside the sonoreactor; (a) pressure contours of the vertical transducer, (b) Axial pressure amplitude distribution, (c) pressure field of longitudinal transducer (d) radial pressure amplitude and the direction of the transducer at $z=0.095$ from the bottom by Sutkar et al. [84]	29
Figure 2.11: Different experimental configuration of sonoreactors in three different laboratories (a) AIST 96k, (b) Nagoya 130k and (c) Shiga 200k by Koda [89]	31
Figure 2.12: (a) Detail normalized ultrasonic intensity distribution at the ultrasonic horn tip, (b) comparison between the experimental sonoreactor (water, 20 kHz, ultrasonic power = 10 W) and the predicted intensity distribution for the same geometry by Klima et al. [47]	32
Figure 2.13: The Sono-chemiluminescence images under different input power for 30, 60, and 90 W by Son et al. [91]	33
Figure 2.14: Hydrogen production versus time for different pressure conditions reprinted from [92]	35
Figure 2.15: Challenges associated with sonoreactors	37
Figure 3.1: (a) The developed sonoreactor model with an aspect ratio, $H/D = 1.26$, (b) boundary conditions of the sonoreactor, (c) Computational quarter domain in 3D, same boundary conditions as the 2-D domain showing the meshing	39
Figure 3.2: Computational domains of unique sonoreactor geometries with a sonotrode introduced from the top side	41
Figure 3.3: Thermodynamics basic concept of the sonohydrogen process	48
Figure 3.4: Classification of sonoreactor parameters	49
Figure 3.5: Bubble radius expansion with an initial diameter of 1.5 μm and wave frequency of 20 kHz [106]	52

Figure 3.6: The regions for each category of bubbles in terms of the ambient radius R_0 and acoustic amplitude PA when exposed to ultrasonic frequency of 20 kHz [50]	55
Figure 4.1: Grid independency study at different number of elements, where $f = 20$ kHz	62
Figure 4.2: Validation of the numerical model with experimental results by Gogate et al. [49] .	64
Figure 4.3: The effect of ultrasonic frequencies on the acoustic pressure distribution, the average pressure P_{avg} is taken over the volume	66
Figure 4.4: Acoustic pressure operating range at various ultrasonic frequencies for sonoreactor	67
Figure 4.5: Axial acoustic pressure distribution at different frequencies	68
Figure 4.6: Minimum pressure at various acoustic power for sonoreactor.....	68
Figure 4.7: Effect of transducer immersion depth on the maximum/minimum acoustic pressure	69
Figure 4.8: Effect of transducer immersion depth on the axial acoustic pressure distribution.....	70
Figure 4.9: Pressure distribution in the mid-plane of the small-scaled GEO.1 (left) and 10-times scaled-up sonoreactor GEO.1 (right) at an ultrasonic frequency of (a) 20 kHz and (b) 30 kHz ..	71
Figure 4.10: The transducer probe diameter on (a) the pressure map, max and mini acoustic pressure (b) on the axial pressure distribution	74
Figure 4.11: Effect of absorbing boundary conditions on wave propagation for an ultrasonic frequency of 20 kHz.....	75
Figure 4.12: Axial acoustic pressure for 4 different geometries with absorbing boundaries	76
Figure 4.13: Effect of absorbing boundary conditions on wave propagation for an ultrasonic frequency of 20 kHz.....	77
Figure 4.14: Axial acoustic pressure distribution at different geometries with reflecting boundaries	78
Figure 4.15: Pareto chart of the standardized effects.....	83
Figure 4.16: Velocity streamlines due to acoustic streaming (left), Axis-symmetrical velocity distribution predicted (right) compared to the experimental results of laboratory horn at 300 W (left) by Dahlem et al. [139]	84
Figure 4.17: The predicted axial velocity distribution at different distances from the transducer tip $Z = 10, 50, \text{ and } 65$ mm.....	85
Figure 4.18: Acoustic streaming induced flow at different time scales.....	86
Figure 4.19: Streamlines induced by acoustic streaming at different time scales	87
Figure 4.20: Time evolution of the velocity magnitude contours and velocity streamlines while using constant density relation in the flow module	89
Figure 4.21: Time evolution of the velocity magnitude contours and velocity streamlines while using linear density relation in the flow module.....	90
Figure 4.22: Time evolution of the velocity magnitude contours and velocity streamlines while using linear density relation in the flow module.....	91
Figure 4.23: Time evolution of the velocity magnitude contours overlaying velocity streamlines with nonlinear density module for Geo. 1 – Cylindrical sonoreactor with 1 ultrasonic transducer	92
Figure 4.24: Time evolution of the velocity magnitude contours overlaying velocity streamlines with nonlinear density module for Geo. 2 – Cylindrical sonoreactor with 3 ultrasonic transducers	93
Figure 4.25: Jet-like flow simulation for CLY-3P.....	94

Figure 4.26: Time evolution of the velocity magnitude contours overlaying velocity streamlines with nonlinear density module for Geo. 3 – Cylindrical sonoreactor with 5 ultrasonic transducers	95
Figure 4.27: Time evolution of the velocity magnitude contours overlaying velocity streamlines with nonlinear density module for Geo. 4 – Hexagonal sonoreactor with 5 ultrasonic transducers	96
Figure 4.28: Time evolution of the velocity magnitude contours overlaying velocity streamlines with nonlinear density module for Geo. 5 – Cylindrical sonoreactor with 5 ultrasonic transducers	97
Figure 4.29: Acoustic shapes and modes for sonoreactors at 20 kHz (left) and corresponding Eigen frequencies (right) with different ultrasonic probes; the average pressure is taken over the volume from the COMSOL Acoustic Module Solution. Note that the vapor pressure for cavitation is 3171.47 Pa at 25.0 °C.....	100
Figure 4.30: Maximum and minimum acoustic pressure for all geometries at (a) 20kHz and (b) Eigen frequencies.....	101
Figure 4.31: Acoustic shapes and modes for sonoreactors at 20 kHz (left) and corresponding Eigen frequencies (right) with different ultrasonic probes; the average pressure is taken over the volume from the COMSOL Acoustic Module Solution. Note that the vapor pressure for cavitation is 3171.47 Pa at 25.0 °C.....	103
Figure 4.32: Acoustic shapes and modes for sonoreactors at 20 kHz (left) and corresponding eigenfrequency (right) with 5 transducers each; the average pressure is taken over the volume from the COMSOL Acoustic Module Solution. Note that the vapor pressure for cavitation is 3171.47 Pa at 25.0 °C.	104
Figure 4.33: Maximum and minimum acoustic pressure for all geometries at (a) 20kHz and (b) Eigen frequencies for geometries featured with 5 probes.....	106
Figure 4.34: Blake Cavitation Threshold concerning the nuclei radius,.....	107
Figure 4.35: Cavitation percentage over the sonoreactor volume	108
Figure 4.36: The simulated bubble dynamics results at 20 kHz for a bubble radius of 1.5 μm and acoustic amplitude of 0.1 MPa (a) the pulse pressure introduced to the bubble, (b) bubble radius expansion at the aforementioned conditions.....	110
Figure 4.37: Validation of the chemical kinetics mechanism used in this study with the work done by Merouani et al. [57].....	112
Figure 4.38: Evolution of the kinetic mechanism involving hydrogen with time at different bubble temperatures for a single bubble initially composed of H ₂ O/ O ₂	114
Figure 4.39: Evolution of the mole number of H ₂ concerning the time at different bubble temperatures	115
Figure 4.40: Evolution of the mole number of *H concerning the time at different bubble temperatures	115
Figure 4.41: The hydrogen and hydrogen radical produced in moles	116
Figure 4.42: Predicted species production vs. time at different bubble temperatures for H ₂ O/CO ₂	117
Figure 4.43: Predicted H ₂ production vs. time of reaction at different temperatures for the H ₂ O/O ₂ bubble	118

Figure 4.44: Predicted H ₂ production vs. time of reaction at different temperatures for the H ₂ O/CO ₂ bubble.....	118
Figure 4.45: Predicted H ₂ production vs. time of reaction at different temperatures for the H ₂ O/Ar bubble	119
Figure 4.46: Predicted H ₂ production vs. time at different bubble temperatures for the H ₂ O/Air bubble.....	119
Figure 4.47: Predicted species production vs. time at different bubble temperatures for H ₂ O/Ar	121
Figure 4.48: Predicted species production vs. time at different bubble temperatures for H ₂ O/Air	123
Figure 4.49: Predicted H ₂ output rate in μmol/hr at f = 20 kHz and 30 kW using different experimental models	125
Figure 4.50: Predicted H ₂ energy consumption in μmol/kWh at f = 20 kHz and 30 kW using different experimental models	127
Figure 4.51: The predicted output of H ₂ from a single bubble vs. the reaction time for various dissolved gases.....	130
Figure 4.52: Predicted species production of the O ₂ /H ₂ O bubble concerning the time.....	132
Figure 4.53: Predicted species production from the H ₂ O/CO ₂ bubble concerning the time.....	133
Figure 4.54: Predicted number of moles of H ₂ and *H vs. at different bubble temperatures for CO ₂ /H ₂ O (left Y-axis) and O ₂ /H ₂ O (right Y-axis).....	135
Figure 4.55: Predicted H ₂ production in μmol/kWh for CO ₂ /H ₂ O (left y-axis) and O ₂ /H ₂ O (right y-axis)	135
Figure 4.56: Predicted number of moles of H ₂ and H vs. at different bubble temperatures for Air/H ₂ O (left Y-axis) and O ₂ /H ₂ O (right Y-axis)	137
Figure 4.57: Predicted H ₂ production in μmol/kWh for Air/H ₂ O (left y-axis) and O ₂ /H ₂ O (right y-axis)	137
Figure 4.58: Predicted number of moles of H ₂ and H vs. at different bubble temperatures for Ar/H ₂ O (left Y-axis) and O ₂ /H ₂ O (right Y-axis)	138
Figure 4.59: Predicted H ₂ production in μmol/kWh for Ar/H ₂ O (left y-axis) and O ₂ /H ₂ O (right y-axis)	138
Figure 4.60: The predicted output of H ₂ from a single bubble vs. the reaction time for various dissolved gases at a water volume fraction WVF =39%	140
Figure 4.61: The predicted output of H ₂ from a single bubble vs. the reaction time for various dissolved gases at a water volume fraction WVF =50%	140
Figure 4.62: The effect of the initial bubble concentration on H ₂ production of an H ₂ O/CO ₂ bubbles	141
Figure 4.63: The effect of the initial bubble concentration on H ₂ O ₂ production of an H ₂ O/CO ₂ bubbles	141
Figure 4.64: Hydrogen yield and energy efficiency vs. acoustic bubble temperature of H ₂ O/CO ₂ bubble.....	145
Figure 4.65: Hydrogen yield and energy efficiency vs. acoustic bubble temperature of H ₂ O/O ₂ bubble.....	146

Figure 4.66: Hydrogen yield and energy efficiency vs. acoustic bubble temperature of H ₂ O/Air bubble.....	146
Figure 4.67: Hydrogen yield and energy efficiency vs. acoustic bubble temperature of H ₂ O/Ar bubble, argon bubble.....	147
Figure 4.68: Hydrogen yield Comparison for different bubble temperatures and different dissolved gases.....	148
Figure 4.69: Energy Efficiency Comparison for different bubble temperatures and different dissolved gases.....	149
Figure 4.70: Average sonoreactor temperature with sonication time.....	150
Figure 4.71: Input power vs. Cavitation Energy (y-axis-left) and Energy Conversion Efficiency (y-axis-right).....	151
Figure 4.72: Input power vs. Cavitation Energy y-axis-left and Sonoxygen Efficiency y-axis-right.....	152
Figure 4.73: Input power vs. Cavitation Energy (y-axis-left) and Energy Conversion Efficiency (y-axis-right).....	153
Figure 4.74: Input power vs. Cavitation Energy (y-axis) left and Sonoxygen Efficiency (y-axis) right.....	153

NOMENCLATURE

a	NASA polynomial coefficient
A	Transducer probe surface area [m^2]
B/A	Nonlinear parameter
c	Speed of sound [m/s]
C_j	Molar concentration of the specie j [Mole]
C_p	Specific heat at constant pressure [$kJ/kg \cdot K$]
CLY-1P	Cylindrical sonoreactor with 1 Probe
CLY-2P	Cylindrical sonoreactor with 2 Probes
CLY-3P	Cylindrical sonoreactor with 3 Probes
CLY-4P	Cylindrical sonoreactor with 4 Probes
CLY-5P	Cylindrical sonoreactor with 5 Probes
D_p	Probe diameter [m]
E	Energy density [kW]
f	Ultrasound frequency [kHz]
HEX-3P	Hexagonal sonoreactor with 3 Probes
HEX-5P	Hexagonal sonoreactor with 5 Probes
h_j	Specific enthalpy of specie j [kJ/kg]
H_j	Enthalpy of specie j [kJ]
I	Intensity [W/m^2]
I_A	Acoustic intensity [W/m^2]
k_0	Liquid rate constant
K_{fi}	Forward equilibrium constant
K_{ri}	Reverse equilibrium constant
m	Mass of water [kg]
n	Number of moles
N	Number of bubbles
P	Acoustic power [W]
p	Acoustic pressure [kPa]
p_0	Acoustic amplitude [kPa]
p_v	Vapor pressure [kPa]
p_{go}	Gas pressure in the bubble at ambient conditions [kPa]
p_{max}	Maximum bubble pressure [kPa]
p_t	Total pressure [kPa]
PZT	Piezoelectric transducer
Q_j	Heat of reaction of specie j [kJ/kg]
Q_m	Monopole domain source
Q_d	Dipole domain source
r	Rate of reaction of any specie [Mole/s]
R	Rate of reaction with respect to time [Mole/s]
R_0	Ambient bubble radius [μm]
R	Bubble radius [μm]
R_{max}	Maximum radius of the bubble [μm]
R_{min}	Minimum radius of the bubble [μm]

R'	First derivative of the radius
R''	Second derivative of radius
s_j	Specific entropy of specie j [kJ/kg .K]
S_j	Entropy of specie j [kJ/ K]
SQR-3P	Square sonoreactor with 3 Probes
SQR-5P	Square sonoreactor with 5 Probes
t	Time [s]
T	Temperature [K]
T_∞	Bulk liquid temperature [K]
T_{max}	Maximum bubble temperature [K]
u	Velocity [m/s]
ν_j	The stoichiometric coefficient of specie j
W	Watt
WVF	Water vapor fraction
x	Position in x-direction [m]
∇	Partial derivative

Greek symbols

β	Nonlinear coefficient
γ	Specific heat ratio
η	Efficiency
λ	Wavelength [m]
μ	Dynamic viscosity [kg/m s]
ρ	Density [kg/m ³]
ν	Stoichiometric coefficient of any specie j
σ	Surface tension [N/m]
ω	Angular frequency [rad/s]

Subscripts

∞	Ambient state
A	Acoustic amplitude
g	gas
v	vapor
j	species
prod	Products
react	Reactants
US	Ultrasonic

Species

CO	Carbon monoxide
CO ₂	Carbon dioxide
H	Hydrogen radical
He	Helium
H ₂	Hydrogen

H_2O	Water
H_2O_2	Hydrogen peroxide
HO_2	Hydroperoxyl
O	Oxygen
OH	Hydroxyl radical

Chapter 1. Introduction

How will the world solve the problem of reducing our carbon emissions? The solution would be to replace coal, oil, and gas in the long-term with primary energy from solar-generated electricity and wind-generated electricity. However, wind and solar electricity do not form a complete picture of our clean energy solution. Within the mix, we will need a more high-density transportable fuel. Imagine that a supertanker will pick up a hundred thousand tonnes of iron from the port of Vancouver in western Canada and take it to the eastern part of Toronto. Now, we realize that it uses bunker fuel; we immediately think it is terrible. Would it be great if we could replace that with batteries? The answer is no because it is not realistic. It is hard to see the batteries achieve the energy density that would allow us to power the ship or a plane. However, it is doable with hydrogen because hydrogen has a much higher energy density than batteries. Hydrogen is a clean fuel that does not produce any carbon emissions because carbon and its derivatives (C, CO₂, CO) are eliminated from the combustion process; instead, it produces water as a combustion product. The question is, where do we get the hydrogen? Hydrogen is a secondary energy source, which means it needs to be produced from other substances; we can generate it from water using renewable energy, which releases no carbon emissions. We can also produce hydrogen from natural gas, coal, and biomass using heat to drive chemical reactions with water. This method does release carbon emissions that need to be captured and stored safely. In this Ph.D. thesis, hydrogen is produced by an ultrasound source. This method is clean, has no carbon emissions. Once we made it, it is convenient to use hydrogen as an alternative to oil for transport and natural gas for heating. Hydrogen is an effective way to store and transport energy. With an abundance of natural resources, Canada can make clean hydrogen, ensuring it becomes a key part of our energy solution.

1.1 Hydrogen as a potential fuel

The total energy demand mainly consists of residential, commercial, and industrial demands. Due to the industrial energy demand growth, researchers have been probing different opportunities to secure an alternative fuel to switch to clean and sustainable fuel. Figure 1.1 shows that the energy demand grows steadily in the early part of the projection, driven mainly by an increase in industrial-scale production of goods, manufacturing, forestry, fisheries, agriculture, construction, mining, and oil and natural gas extraction. The industrial section is taken a huge part of the total energy demand.

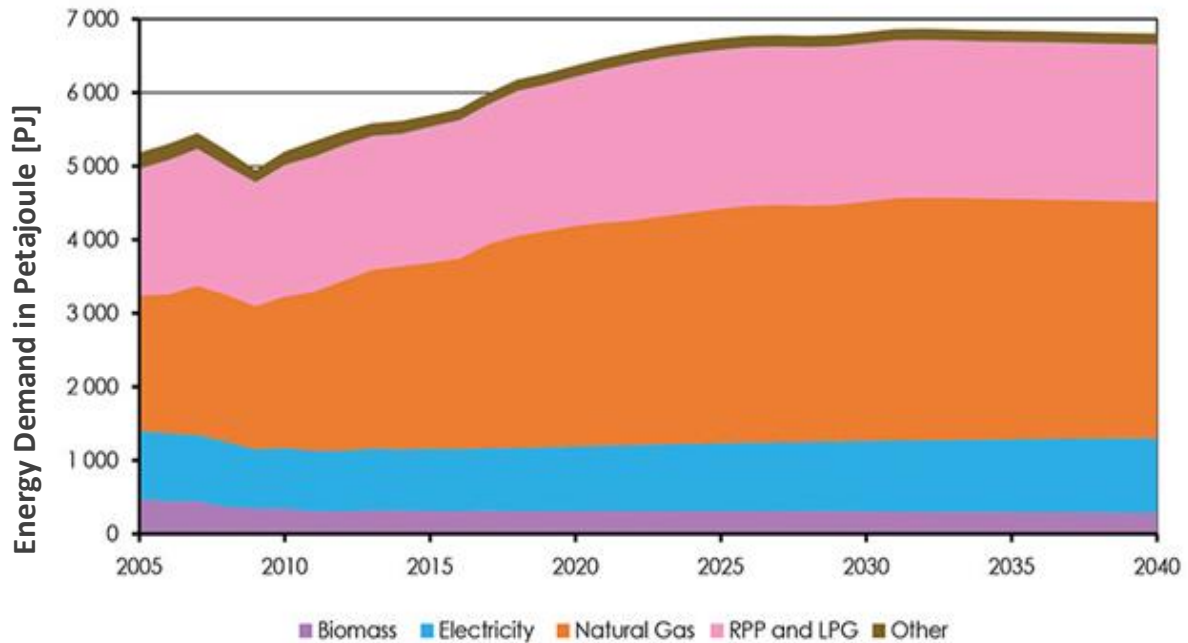


Figure 1.1: Energy demand over the years up to 2040 in Petajoule [PJ]. Note that PJ equal to $1.0E+15$ Joules [1]

The aim of the research studies in the incoming decades will focus on fuel substituting to reduce greenhouse gas emissions from gas turbine applications, such as flight transportation and other industrial applications. The challenge is to research developing the advanced and innovative sonohydrogen system as a clean energy source. The thesis contributes to evaluate the feasibility of producing hydrogen and identifying the fundamentals of the sonochemical process. There are five reasons why hydrogen is the future fuel and a secure, clean, and affordable alternative to fissile fuels. Here are five reasons why hydrogen has been touted as an energy source of the future and is the key to the future of renewables:

1. Zero emissions on roads, hydrogen-powered vehicles emit only heat and water as by-products.
2. More extended driving range, hydrogen-powered vehicles can travel for longer on less energy.
3. Decarbonizing industrial sectors, hydrogen could be a substitute energy source for manufacturing and emissions-heavy industries.
4. Secure storage and usage, hydrogen can be easily stored, shipped, and used by businesses.
5. Proven use case in space travel, hydrogen has been successfully used as a rocket propellant in aerospace ships and would undoubtedly play a more significant role in powering the future.

1.2 Potential ultrasound applications

Ultrasound of high frequency can travel long distances, even through obstacles. Power ultrasound is used in many medical and engineering applications. One of the medical applications is that ultrasound is used in scanning body parts of a human being, for example, echocardiography and imaging of organs. Electrocardiography is the non-invasive recording used to detect heart conditions; the record is called an electrocardiogram. A stress electrocardiogram is the record of heart response to the stress of physical exercise. The instrument records the changes in the electrocardiograph. The electrocardiogram's baseline voltage is the isoelectric line, which measures electric potentials using a biomedical amplifier. Ultrasound also has surgical uses; it cures medical conditions like cataracts, stones in the kidneys. The ultrasonic waves' ability to cause particles of a substance to vibrate rapidly and break into small pieces is used in ultrasound surgery cataract is removed by using this technique. Ultrasound is also used in breaking the small stones in the kidney into fine particles, and these fine particles are flushed out along with urine. Arafa and Mohany reviewed the recent patents associated with ultrasonic applications [2].

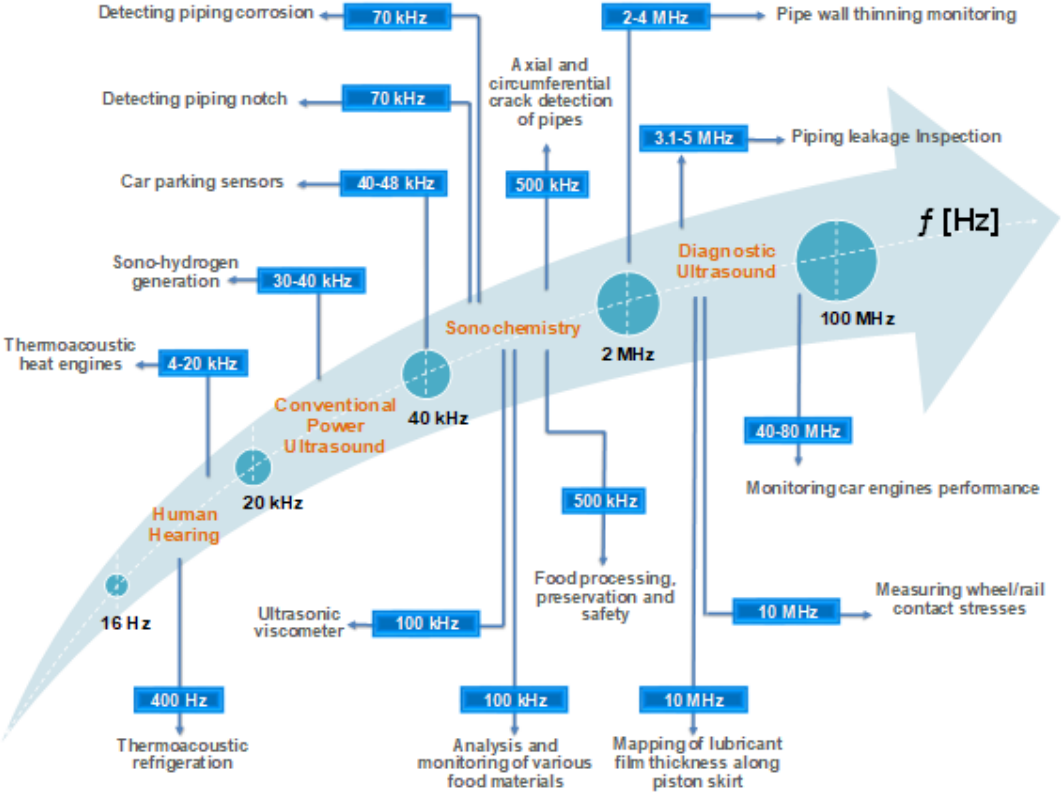


Figure 1.2: A summary of ultrasound applications at different ultrasonic frequencies

Moreover, power ultrasound has many uses in engineering. Ultrasound has a massive history of use in many engineering devices for diagnostics processes [3]. Ultrasound is used to clean parts of smaller diameter, for example, a spiral pipe. Ultrasounds are used to detect cracks in metal blocks after ultrasonic waves are allowed to pass through the metal block, and detectors are used to detect the flaws because ultrasound is reflected from the flaws portion. Nevertheless, the expansion of sonar is sound navigation and ranging. It is a device used to measure the distance, direction, and speed of underwater objects using ultrasonic waves. In order to detect the existence of submarines in the seas, inaudible ultrasonic sound signals are sent; the reflected sound waves are received again and give access to all measurements. In Figure 1.2, several applications are presented at a particular ultrasound frequency range as per previous research reports. This thesis is concerned with using ultrasound in hydrogen production [4]. Until recently, researchers haven't discovered that ultrasound can be used for producing useful gases such as hydrogen.

1.3 Research gaps and motivations

Producing hydrogen via sound waves offers a tremendous opportunity. Introducing high-frequency sound waves to liquid water provides an environmentally friendly way to produce hydrogen. This innovative approach is named: Sonohydrogen. Research gaps and motivations are as follows:

- Sonoreactors are still designed and optimized for conventional/large-scale operations.
- Previous efforts do not solve the design challenges associated with a full domain of sonoreactor.
- There is a need for a drastic cut in carbon emissions; thus, hydrogen is one of the most powerful fuels and highly suitable for clean energy production.
- Probing the opportunities and challenges of hydrogen-for-future-energy by producing it sustainably enough and clean to meet a low-carbon economy's needs.
- There is a need to enhance our fundamental understanding of the unexplored ultrasonic hydrogen production approach.
- There is a need to enhance our knowledge about the factors affecting the hydrogen production rate from the sonohydrogen process.

1.4 Novelty statement

The challenge is to research developing the undiscovered, advanced, and innovative sonohydrogen system as a clean energy source. The novelty of this Ph.D. work is that it contributes to evaluating the feasibility of producing hydrogen and identifying the sonochemical process's fundamentals. This Ph.D. work's novelty is to extend the up-to-date contributions made in this field, which is still limited to many factors that govern the sonohydrogen process for hydrogen production. This Ph.D. thesis aims to overcome the lack of data on the operation of the sonoreactor under different physical and geometrical conditions. It also proposes a novel energy-efficiency sonoreactor system for sustainable and eco-friendly hydrogen production.

1.5 Thesis objectives

This work aims to develop a novel ultrasonic hydrogen production process named the Sonohydrogen process. The concept is based on when ultrasound waves are introduced to liquid; they result in generating acoustic cavitation bubbles; when these bubbles collapse, a tremendous amount of energy is produced in the microscale, which is enough to dissociate the water molecules through a series of chemical kinetics reactions into hydrogen, and other radicals. The present Ph.D. thesis provides researchers with an in-depth knowledge of the novel H₂ production method using the power of ultrasound. The thesis objectives are as follows:

- To model, analyze, and simulate the acoustic and flow field characteristics of sonoreactors:

This objective is aimed at drawing the CFD domains of the sonoreactors, perform grid orientation and grid independence studies for each studied domain, and implement model validation studies using experimental data. It will also conduct parametric studies to investigate numerous geometries, configurations under different operating conditions.

- To perform various parametric studies considering the acoustic streaming

The acoustic streaming study aimed to investigate the effects of varying geometrical and operational parameters on the sonoreactor performance, compare and contrast the nonlinear density with linear and constant densities. Perform a parametric study on the effect of sonotrode number on acoustic streaming, and estimate the velocity profile and the formation of the vortices in order to assure a good premixing between the liquid levels.

- To develop the chemical kinetics mechanism for the sonohydrogen process:

The chemical kinetics mechanism consisted of 19 chemical reactions is developed based on previous combustion studies and is solved using the chemical engineering model. Validation of the chemical kinetics model is carried out with data available in the literature. A parametric study on the effect of the acoustic bubble temperature and on the effect of dissolved gases is performed, writing a perspective on the role of CO₂ in enhancing the hydrogen production from the sonohydrogen process.

- To perform energy efficiency analysis and geometric-parametric study:

To probe the best geometry in terms of pressure distribution, acoustic streaming, and velocity streamlines. An energy analysis study is conducted on the cavitation energy, cavitation yield, and the corresponding energy consumption. The study also examines the acoustical parameters and factors that govern the sonohydrogen process, including ultrasound frequencies and acoustic power. Evaluate the performances of the reactors under various efficiency criteria and parameters.

- To optimize the design of an ultrasonic sonoreactor for hydrogen production:

The first objectives will consider designing various configurations of “sonohydrogen” reactors for ultrasonic hydrogen production. Perform analysis of variance ANOVA in order to optimize the geometrical and acoustical effects and determine a designing point for a single probe sonoreactor geometry.

1.6 Contributions

1.6.1 Acoustic pressure model of sonoreactor

Novel sonoreactor geometries are proposed and validated to estimate the performance that explicitly incorporates the ultrasonic waves' influence on the pressure distribution inside the sonoreactors. The results revealed that sonoreactor performance is linked to the geometry and operation parameters that trigger the sound waves' constructive interference.

1.6.2 Acoustic streaming model of sonoreactor

The unsteady acoustic module is used along with CFD to simulate the acoustic streaming model is of importance to assure premixing of liquid levels. The analysis showed that the acoustic

streaming induced by the ultrasonic transducer is a jet-like flow inside the sonoreactor to assure mixing between the liquid levels.

1.6.3 Chemical kinetics mechanism model

To completely dissociate a 1 mole of water vapor requires around 15000 K; the reaction mechanism consisted of 19 reversible chemical reactions is simulated, validated, and extended to include the effect of the bubble temperature and different dissolved gases. The calculations provided a Guideline for quantifying the H₂ production from the sonohydrogen process using the developed chemical kinetics mechanism.

1.6.4 Hydrogen yields

Design a sonoreactor that provides the maximum cavitation energy, cavitation yield, and energy efficiency. Increasing the input power is not always in favor of hydrogen production or energy consumption.

1.7 Thesis outline

Chapter 2 presents a comprehensive literature review according to different hydrogen production methods while comparing their environmental and economic perspectives. It sheds light on the innovative hydrogen production technique given the name: “Sonohydrogen”. It compares the five main categories before illustrating the physics related to the sonohydrogen process and the factors that govern the hydrogen production rate of the sonohydrogen process. All factors are illustrated in-depth, explaining the physics beyond increasing or decreasing the hydrogen production rate. Chapter 3 presents the development and modeling of the sonohydrogen process using three consecutive models, including the acoustics model, bubble dynamics model, and the chemical kinetics model. This Ph. D. thesis's main objective of this Ph.D. thesis is to link all models together and establish a relation between the acoustic model associated with the sonoreactor and the chemical kinetics model associated with the water dissociation reactions for hydrogen production. In chapter 4, the results related to each model are presented in the following order: (1) acoustic model results of the sonoreactor that give insight into the acoustic pressure distribution of the sonoreactor, including validation study and a parametric study investigating different acoustical and geometrical parameters. (2) An acoustic streaming study is conducted at which different geometries are examined, and results are presented in terms of velocity profiles and streamlines.

(3) Geometric optimization is taking place to select the best geometry that provides a high possibility of generating acoustic cavitation bubbles and thus more hydrogen production. (4) The chemical kinetics modeling study at which hydrogen quantification is reported based on different operational parameters and different acoustic cavitation bubble conditions. (5) Performance parameters such as the cavitation energy, hydrogen yield, and the energy consumption associated with the sonochemical process are presented and illustrated. Finally, the work summary and some unknown aspects, which are left to subsequent studies, are mentioned in chapter 5.

Chapter 2. Literature Review

Energy is all around us; even so, it is often not in the right place or the exact time we need it. However, what if we combine new ways of looking at it with creative ways of converting and storing it. We can then transform electrons into hydrogen using a novel sonochemical system or electrolyzer systems. We can use high-performance reactors to make synthetic fuels and sustainable chemicals. Now we can burn metal powder to fuel our industry, and we can warm out cities with heat from thermochemical batteries. Nowadays, a smart energy grid can transform, store, and trade energy carriers between all our devices every second across the globe. It is believed that this future is now working and collaborates on creating systems for sustainable energy production, conversion, and storage. We can provide essential knowledge, high-tech engineering, and excellent research. We can drive the energy revolution, but we need to know what previous research fellows have done so far. This is the aim of the literature review chapter.

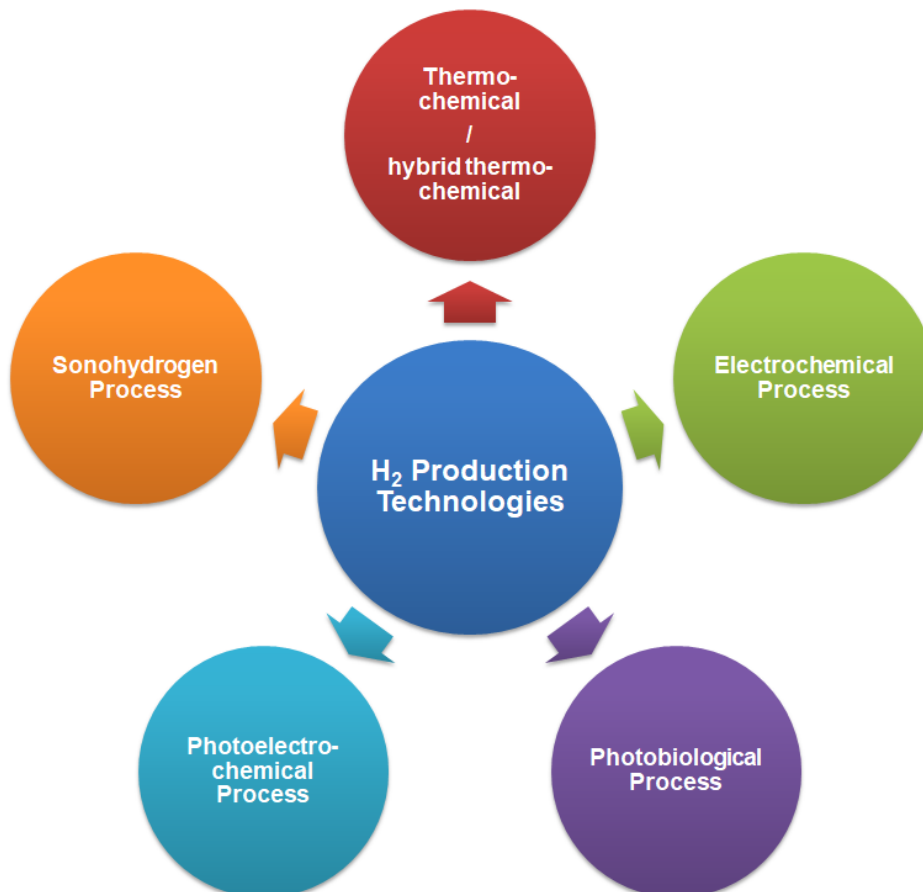


Figure 2.1: Different processes and technologies for hydrogen production

2.1 Hydrogen Production Processes

In this section, different hydrogen production methods are reviewed, and they are compared according to environmental and economic perspectives. Hydrogen is not only very powerful and efficient, but also it is a renewable source of energy, as it can be produced via five main categories of technology, namely, thermochemical [5], (ii) electrochemical [6], (iii) photobiological [7], (iv) photoelectrochemical [8], and (v) *Sonohydrogen* [3], which are all summarized in Figure 2.1.

2.1.1 Thermochemical Process

The thermochemical process means that the hydrogen production involving the steam gas reforming (SMR) of natural gas or liquefied petroleum gas (LPG) [9], which is considered one of the widely used means of hydrogen production from a gas material such as methane, ethanol, and methanol. In the steam reforming process, natural gas is used as feedstock for hydrogen generation and fuel for the reformer furnace's burners. Then steam is generated in the waste heat recovery unit by cooling the hot flue gases and process gas. The reaction requires heat, which is generated by the combustion of tail gas and natural gas. Natural gas and steam mainly react to produce hydrogen and carbon dioxide, and a catalyst activates the reaction. The effect of the adsorptive separation produces hydrogen, and the product purity can be as high as 99.999 Vol.%. The tail gas contains combustible gases and is used as fuel for the burners. The steam reforming plants are required in many applications such as the metallurgical applications, chemical industry, food & beverages, glass industry, petrochemical & refinery, and hydrogen peroxide production. However, the gasification processes are used when the raw material is solid such as coal or biomass [10–12]. This technique has broad sustainability problems. Therefore, Dincer and Acar [13] reviewed and evaluated different hydrogen production methods for enhancing the sustainability of such an approach. Steam gas reforming is not an environmentally friendly way for hydrogen production, as Haryanto et al. [14] reported because of the massive amount of carbon dioxide produced from the reforming process.

2.1.2 Electrochemical Process

This technique is considering hydrogen electrolysis in charge of water electrolysis (WE) to produce hydrogen [14]. This method using a low voltage (9 Volts DC power) to create reactions in various solutions; this is the electrolytic process and can be used to split water into hydrogen

and oxygen; the machine that does this is a hydrogen electrolyzer. The hydrogen electrolysis is used to convert electrical energy and store it into tanks in hydrogen, transformed later and back into electricity. Hydrogen Electrolysis from water is usually undertaken with liquid alkaline or polymer electrolyte membrane electrolyzers. There are different electrolyzers; the alkaline electrolyzer works by immersing two electrodes in a liquid electrolyte. When a voltage is applied, the released product gases are oxygen and hydrogen. However, it poses some problems; it cannot efficiently use intermittent power supplies, meaning it is incompatible with renewables. It also compromises efficiency during storage. To store enough hydrogen for regular use, we would need either a giant tank or an additional compressor. Simultaneously, the polymer electrolyte membrane (PEM) electrolyzer overcomes some of these issues by using a solid polymer electrolyte, the membrane responsible for the conduction of protons, the separation of hydrogen oxygen, and the electrical insulation of the electrodes. It can use the fluctuating power supply from renewables and results in pure hydrogen due to the electrolyte's solid structure. It is easy and more efficient. However, it has a prohibitively high cost due to its required use of gold, iridium, and platinum. This technique is high-energy demanding with an overall efficiency of 60%. It can be very efficient if the electricity cost is below 2 cents/kWh.

2.1.3 Photobiological Process

The photobiological technology uses the natural photosynthesis activity of bacteria and green algae to produce hydrogen [15]. Algae produce hydrogen at certain conditions, and it is an entirely renewable source that is made from sunlight and carbon dioxide, and water, and it is a sustainable renewable fuel. Concerning photobiological production, some algae and bacteria produce hydrogen, using sunlight as their energy source to decompose water into hydrogen and oxygen in a series of complex chemical reactions. One main problem is that the production rate is prolonged. Detailed reviews associated with this technique can be found in [16,17].

2.1.4 Photoelectrochemical Process

The photoelectrochemical technology is producing hydrogen in only one-step using the water-splitting phenomenon via illuminating a water-immersed semiconductor with sunlight [18]. The photoelectrochemical production or photoelectrolysis uses sunlight to split water into hydrogen and oxygen. A semiconductor absorbs solar energy and acts as an electrode to separate the water

molecules. The research will make this process more efficient and prevent semiconductors from eroding too quickly to have a useful surface life. A better technique to produce cleaner hydrogen is the so-called “Photocatalytic water splitting,” which can decompose oxygen and hydrogen by utilizing sunlight with photocatalyst aid [19–22]. One obstacle to this method is that the instability of the semiconductor materials in the aqueous phase. Other disadvantages are provided by Haryanto et al. [23].

2.1.5 Sonochemical Process

Sonochemistry is defined as how the power of ultrasound can be utilized in chemistry. It has been recognized that hydrogen can be produced by introducing ultrasound waves to liquid water. As compared to the other non-renewable energy sources, hydrogen can be produced infinitely by simple means of separation from water molecules. The Sonohydrogen approach can provide this and can produce hydrogen peroxide for medical and industrial use. This technique is not fully discovered to the best of our knowledge, and more research studies have to be conducted on it.

Table 2.1 draws a comparison between the different hydrogen production techniques, including differences in the theory and the hydrogen production rate.

Table 2.1: A comparison between different hydrogen production technologies

H ₂ -production methods	Theory beyond each method	H ₂ -Production rate and cost
Thermochemical (steam reforming)	$CH_4 + 2 H_2O + h_{thermal} \rightarrow 4 H_2 + CO_2$	9-12 tons of CO ₂ / 1 ton H ₂ [24].
Electrochemical (water electrolysis)	$H_2O + h_{electrical} \rightarrow H_2 + \frac{1}{2} O_2$	53.4-70.1 kWh/ 1 kg of hydrogen [25].
Photobiological	$2 H_2O + CO_2 + Algae/Cyanobacteria + h_{solar} \rightarrow O_2 + 4 e^- + 4 H^+ \rightarrow 2 H_2$	0.07-96 mmol H ₂ L ⁻¹ h ⁻¹ [26]
Photoelectrochemical	$H_2O + h_{solar} \rightarrow H_2 + \frac{1}{2} O_2$	39 kWh/ kg [27] or 17.3 \$/kg of H ₂ [28].
Sonochemical	$H_2O + h_{sound} \rightarrow OH + H$ $OH + H \rightarrow H_2 + O$ [29]	0.8 μM min ⁻¹ at acoustic intensity of 0.6 W cm ⁻² [30].

From the above discussion, we conclude that further investigation shall be conducted in the sonochemical process and incoming is a detailed illustration of the sonochemical technology, benefits of sonochemistry, Sonohydrogen theory, and the system design are considered the focus of this Ph.D. work. It will give a snapshot of the *Sonohydrogen* theory.

2.2 Sonochemistry Technology

In this section, the review associated with the sonochemistry approach is presented, and then an insight review of the *Sonohydrogen* process will be illustrated. In chemistry, the study of sonochemistry is concerned with understanding the effect of ultrasound in forming acoustic cavitation in liquids resulting in the initiation or enhancement of chemical activity in the solution. Therefore, the chemical effects of ultrasound do not originate from the ultrasonic wave's direct interaction with the solution's molecules. The simplest explanation for this is that sound waves propagate through a liquid at ultrasonic frequencies with a significantly longer wavelength than the bond length between atoms in the molecules. Therefore, the sound wave cannot affect the bond's depression energy and, consequently, directly increase a molecule's internal energy. Instead, sonochemistry arises from acoustic cavitation. The formation, growth, and implosive collapse of bubbles in a liquid, the collapse of these bubbles is an almost adiabatic process. It is thereby resulting in the massive buildup of energy inside the bubble, resulting in extremely high temperatures and pressures in the sonicated liquid's microscopic region. The high temperatures and pressures result in chemical excitation of any matter inside or in the bubbles' immediate surroundings as it rapidly imploded. A wide variety of outcomes can result from acoustic cavitation, including sonoluminescence, increased chemical activity in the solution due to the formation of primary and secondary radical reactions, and increase chemical activity through the creation of new, relatively stable chemical species that can diffuse further into the solution to create the chemical effect. Penconi et al. [31] reported the hydrogen production rate using different liquid mediums. In the case of using water as a liquid medium, the hydrogen production rate is around 80 $\mu\text{moles/h}$, while in the case of ethanol, the hydrogen production rate is 5.5 $\mu\text{moles/h}$. A critical experimental comparison is made to investigate the effect of the liquid medium on the hydrogen production rate while using a sample of 300 mL of water and ethanol separately at 38 kHz. It is found that while using water as the liquid medium, the hydrogen production rate is 15 times higher as compared to ethanol.

2.2.1 Sonoelectrochemistry

Sonoelectrochemistry is defined as a combination of three fields, including electrolysis, ultrasound, and electrochemistry, which is initially reported by Morigushi [32] in 1934. In the electrolysis process, hydrogen is produced at the decomposition potential in the molecular form,

taking place on the electrodes' surface via an electrochemical reaction. The molecular hydrogen gas nucleate at the electrode surface's cavity to hydrogen gas bubbles at the cathode active sites. The hydrogen gas bubbles start to enlarge at the surface of the electrode. Early in the 1990s, Sheng-De Li et al. [33] and Richard et al. [34] reported that introducing ultrasonic waves to an electrolysis process would considerably increase energy efficiency. In the next sub-sections, we gave a snapshot of the fundamental aspects, benefits, approach, acoustic cavitation bubble, and factors affecting the hydrogen production rate.

2.2.2 Benefits from sonochemistry

The ultrasound is widely used for several applications in different fields, including acoustic cavitation bubble [35], hardening by immersed metals [36], several medical and clinical applications, for example, drug delivery and other therapeutic applications [37], enhanced electrospinning [38], enhanced bladder cancer therapy [39] and accelerating chemical reactions and processes. The ultrasonic waves and irradiation are associated with potent chemical and physical effects for driving, enhancing the chemical reactions and yields. The idea beyond using ultrasound is to use less hazardous chemicals and solvents and to reduce energy consumption. There are several benefits beyond the sonochemistry approach, such as it can enhance the electrochemical diffusion processes. Ultrasound waves are used to enhance the chemical reactions and to provide a unique chemical environment. For example, organic syntheses can be significantly improved by the use of ultrasound. A comprehensive review is performed on the ultrasound in synthetic organic chemistry concentrated on the applications in organic synthesis by Mason [40]. Many other researchers, e.g., Cravotto and Cintas [41] and Bang and Suslick [42] have successfully performed synthetic organic reactions using ultrasound. Production of nanomaterials, environmental treatment, purifying water, corrosion of metals, cleaning polymeric membranes, food processing, cavitation bubble dynamics, and hydrogen production. Chen [43] performed a comprehensive review in their handbook published in 2011 on ultrasound applications in water and wastewater treatment. Many other researchers are performed in synthetic organic chemistry using ultrasound, and it is found by Tao and Sun [44], Jayani et al. [45], and Ashokkumar [46].

2.2.3 Sonohydrogen system Illustration

When the sound waves with high frequency are passing through a liquid such as water, it will lead to the vibration of liquid water mechanically; it is so-called “Water Sonolysis” or “Water Sonication.” There are three main configurations used to introduce ultrasound waves into sonoreactors, as shown in Figure 2.2.

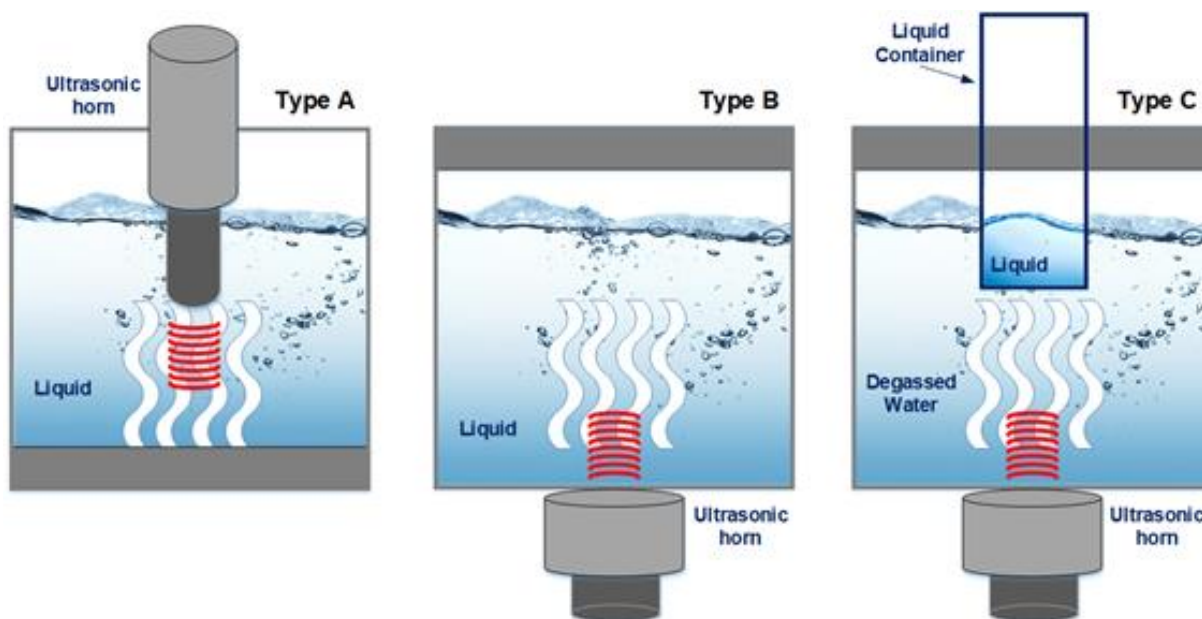


Figure 2.2: Design configurations of a sonoreactor

These configurations are the ultrasonic transducer horn or probe (type-A), the ultrasonic transducer bath (type-B), and the indirect irradiation ultrasonic bath (type-C). In the case of the ultrasonic horn-type A, the transducer is immersed inside the liquid container, and the ultrasound waves are introduced from the horn tip with a diameter smaller than the acoustic wavelength $\lambda = c/f \leq 3.0 \text{ cm}$ [47]; consequently, the acoustic cavitation bubbles are generated. While in the case of the ultrasonic bath type-B, where it is mainly used for cleaning purposes, the ultrasonic waves are introduced at the bottom of the liquid container. Indirect propagation of ultrasound waves is also possible, as shown in type-C. This configuration consists of an ultrasonic bath within which a small water container exists. The ultrasonic bath is filled with degassed water, so bubbles cannot be formed [48]. However, more considerable concentrated energy will be available in type-A (immersed ultrasonic probe reactor), and almost 15% lower power dissipation is found in the case of type-B (ultrasonic bath reactor) [49]. Therefore, type-A has been selected in this investigation,

as it will contribute to the generation of more acoustic cavitation bubbles. Thus, more hydrogen will be generated because of the higher energy dissipation associated with this sonoreactor type [50]. Figure 2.3 shows and illustrates the schematic of the sonoreactor model. The ultrasound probe immersed in a water container emits sound waves through the water by a frequency range between 20-40 kHz. Ultrasound also generates acoustic cavitation bubbles within the liquid at the tip of the ultrasound probe. The typical ultrasound wave has compression and rarefactions acoustic pressure that will accumulate energy inside the acoustic cavitation bubble. This energy is in the form of several thousand temperatures in kelvin and several hundreds of pressures in atmospheres, which is enough to dissociate the water vapor trapped inside the bubble, the so-called sonolysis process [51]. The acoustic cavitation bubbles take place when ultrasound is introduced to liquid water.

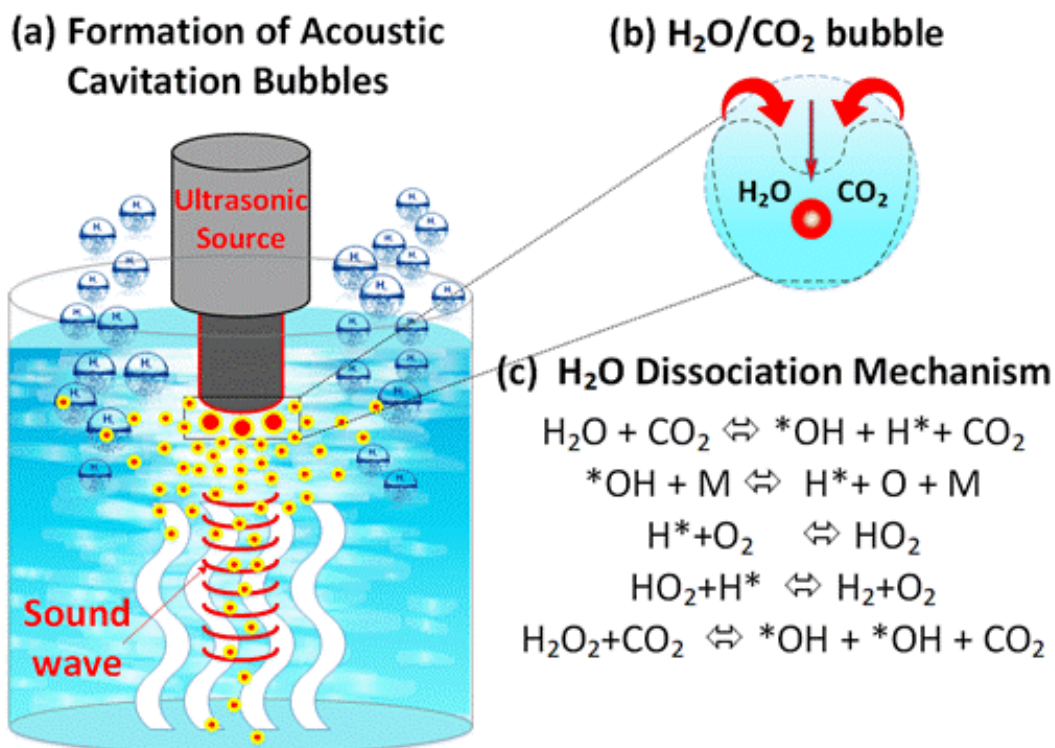


Figure 2.3: Schematic of the ultrasound generator probe showing H₂O/CO₂ bubbles and the dissociation mechanism

The medium goes through a series of compression and rarefaction cycles. As rarefaction and compression high-frequency sound waves travel through water, the expansion will push or stretch the molecules apart and give the intense negative pressure to overcome the intermolecular forces. In contrast, the compressions push the molecules together through intense positive pressure. If the

sound waves strong enough and in succeeding cycles, this will lead to a sudden pressure drop at which the cavitation phenomenon occurs, and the creation of gaseous bubbles in liquid takes place. These bubbles grow, oscillate, and collapse violently; this phenomenon is called the acoustic cavitation bubble.

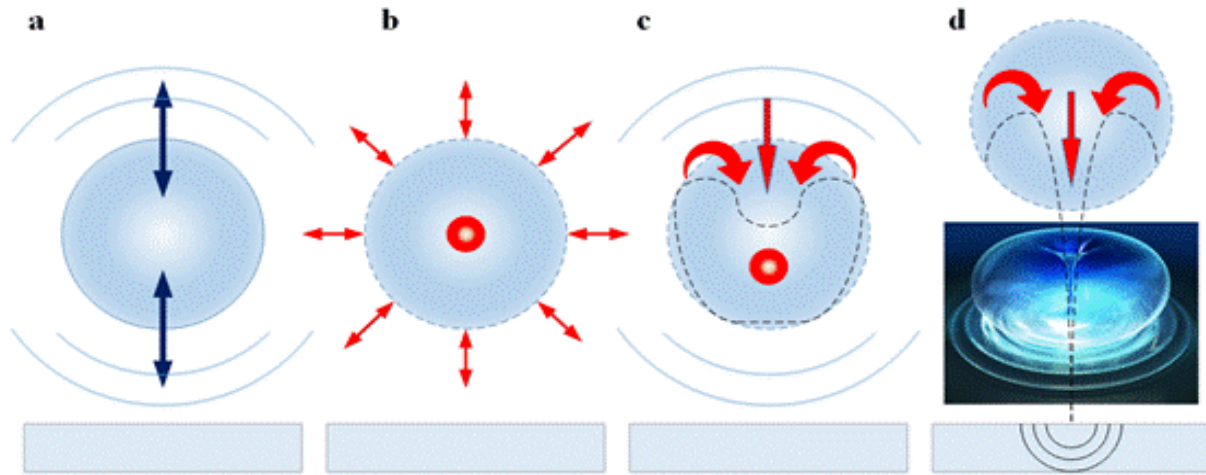


Figure 2.4: The sequence of acoustic cavitation bubble collapse

The mechanism has four consecutive and instantaneous stages, as seen in Figure 2.4; (a) bubble formation, (b) continuous growth, (c) collapse, (d) micro-jets [37], and as reported by Lee et al. [52,53]. The first stage is the acoustic cavitation bubble formation due to introduce the ultrasound waves to the liquid water. The second stage is the bubble enlarges and grows in successive cycles, after which the bubble reaches the unstable mode at which it is about to collapse. The third stage is the acoustic cavity implosion, at which a violent bubble collapses, leading to the release of high energy. The sonication of liquid water depends on the physical effects of quick heating and rapid cooling resulting from the acoustic cavity bubble's implosion. However, a detailed system description can be found in the recent perspective article by Rashwan et al. [54].

The reaction mechanism inside a single-bubble saturated with water vapor during a water sonolysis experiment has great interest. The rapid heating phase is described as heat generated from the cavity implosion is enough to dissociate the water molecule (H_2O) into highly reactive hydrogen radicals H and hydroxyl radicals OH . While the quick cooling process is responsible for recombining the highly reactive radicals H and OH to form hydrogen H_2 . Merouani et al. [55] reported the most two essential reactions that 99.9% of the hydrogen is produced from the gas phase recombination reaction; the reaction can be given as follows:



However, another recombination reaction takes place at the surface of the bubble shell with a minor impact in H₂-production can be given as follows [56]:



Merouani et al. [57] performed a water sonolysis (water dissociation to OH+H). They reported that water's sonolysis process via low ultrasound frequencies results in thermal dissociation of water into hydrogen radicals H and hydrogen oxide radical OH. This process is driven by a tremendous amount of heat accumulated inside the bubbles due to a very high temperature, and high pressure resulted from cavitation bubbles collapse. Ultrasonic cavitation of water has a subsequent collapse of microbubbles. This is considered a unique phenomenon that leads to hydrogen production during the water sonolysis process. Water sonolysis is a promising and clean technique to produce hydrogen, mainly if the water is used as the hydrogen source. The effect of the Sonohydrogen parameters is not clarified yet. This will be the aim of the next section and the corresponding subsections. In the next section, several factors governing the H₂-production rate during the sonohydrogen process will be reviewed.

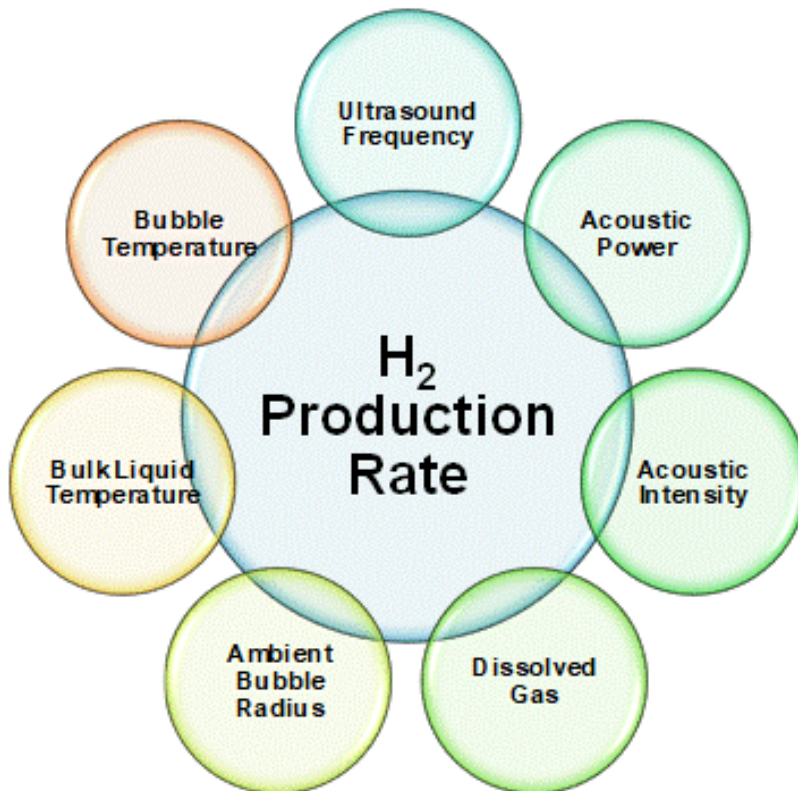


Figure 2.5: Factors governing the hydrogen production of sonohydrogen process

2.3 Factors affecting the sonohydrogen process

Several essential parameters govern the rate of hydrogen production, as shown in Figure 2.5, foremost the acoustic frequency, acoustic power, acoustic intensity, dissolved gas, ambient bubble radius, the water bulk temperature, and the gas bubble temperature [55]. However, quantifying the hydrogen production rate has not yet been fully developed and still needs many numerical and experimental investigations.

2.3.1 Ultrasonic Frequency

It is noticed that the amount of hydrogen produced from such a process is considered highly frequency-dependent as it is the most crucial parameter in sonohydrogen generation—the hydrogen production rate increases with the increase of applied frequency [58]. Several dynamic factors govern the hydrogen production rate with frequency, such as the maximum bubble core temperature and pressure, the amount of water vapor trapped, and the collapse time. At low frequencies, the bubble will have more time to expand and enlarge. This would allow more water vapor to be trapped inside the bubble core. As a result, the bubble collapse will be extreme and will generate a higher pressure and temperature, which will promote the chemical reaction producing more radicals. The collapse time will be short at higher frequencies, and the bubbles will not have enough time to generate a radical as the bubbles' reaction will be very fast. Combining all these factors, we figure out why the applied ultrasound frequency has a significant impact on the hydrogen production rate.

Table 2.2: A summary of the experimental studies on H₂O₂ production using the ultrasound

	The production rate of H ₂ O ₂ (μmol/min)		
Frequency [kHz]	Petrier & Francony [59]	Jian et al. [60]	Merouani et al. [61]
20	0.7	1.1	-
200	5	5.2	-
300	-	-	2.5
500	2.1	3	-
585	-	-	4.2
800	1.4	2	-
860	-	-	3.4
1140	-	-	2.1

In Table 2.2, a summary of the conducted studies on H₂O₂ production using the ultrasound waves is presented while comparing different studies at different ultrasonic frequencies. Petrier & Francony [59] and Jian et al. [60] conducted experiments where ultrasonic waves at 20 kHz emitted from a titanium horn (diameter 3.5 cm) connected to a commercial supply “Branson Sonifier 450”. While the high frequencies transducers operated at a piezoelectric disc (diameter 4cm) supplies (200, 500, and 800 kHz) and it is connected to a high-frequency power supply from “Electronic Service”. Whereas, Merouani et al. [61] conducted their experiments using a 300 kHz piezoelectric disc at which ultrasonic waves are emitted from the bottom. Additionally, they performed another experiment at higher frequencies 585, 860, and 1140 kHz using a Meinhardt multi-frequency transducer (model E/805/T/M) with a diameter of 5.3 cm. It can be seen that the H₂O₂ production rate is increasing while increasing the frequency until it reaches an optimum point, then the rate goes down back. This can be attributed to the formation of bubble clouds that attenuate the acoustic intensity, which will reduce the production rate of H₂O₂.

2.3.2 Dissolved gas

The effect of dissolved gas on the hydrogen production performance lies between two significant physical properties; (1) specific heat capacity ratio ($\gamma = C_p/C_v$) and (2) thermal conductivity (k). The dissolved gas that has higher heat capacity could accumulate at higher temperatures. Simultaneously, dissolved gases with low thermal conductivity will have low heat dissipation, which will allow more temperature to be trapped inside the bubble. Consequently, selecting a dissolved gas with high heat capacity and low thermal conductivity will be the optimum selection for enhancing water vapor's dissociation process, hence, more hydrogen generation in return.

Table 2.3: A summary of the numerical studies on H₂-production using the ultrasound waves

Input Frequency	Dissolved Gas	H ₂ -output rate	References	Analysis
20 kHz	Argon	0.8 to 5 μMol/min	Venault [30]	Numerical
1000 kHz	Argon	13.6 μMol/min	Margulis and Didenko [62]	Numerical
1000 kHz	Air	0.22 μMol/min	Margulis and Didenko [62]	Numerical
1100 kHz	Argon	10 ⁻¹⁷ Mol/s	Merouani [57]	Numerical
1100 kHz	Argon	10 ⁻¹³ Mol/s	Merouani [55]	Numerical

A summary of the numerical work carried out on the hydrogen production using ultrasound is presented compared to the hydrogen production rate at different frequencies and different dissolved gases from the available literature review and shown in Table 2.3.

2.3.3 Acoustic power

The hydrogen production rate is highly dependent upon the acoustic intensity. This is attributed to the fact that during the collapse, the acoustic bubble is acting as a micro-combustor in which a high-temperature chemical reaction occurs. Highly reactive radicals are the product of such a chemical reaction. The chemical reaction is governed by three factors: bubble temperature, collapse time, and bubble size, which correspond to the amount of water vapor trapped in the bubble. With the increase of the acoustic intensity, the bubbles' expansion ratio will increase, allowing more water vapor to be trapped in every single bubble—similarly, the compression ratio increases, leading to a higher bubble temperature. As a result, the increase in the bubbles' expansion and compression ratios will promote an unusual chemical reaction leading to produce more free radicals from the dissociation of the water molecules inside the bubbles. In addition, increasing the acoustic intensity will increase the collapse time, so the chemical reaction will have more time to produce more reactive-radicals. When we combine all of these factors, including bubble expansion, promoting chemical reactions, and collapse time, this will lead to higher H₂ generation. Kerboua and Hamdaoui [63] performed a numerical estimation of hydrogen production at different operating conditions of acoustic power and frequencies. They confirmed that the theory of increasing acoustic intensity leads to an increase in the hydrogen production rate. Their results are reported in Table 2.4.

Table 2.4: H₂-production (Mole) at different acoustic power amplitude and frequencies. Data extracted from Kerboua and Hamdaoui [63]

	Acoustic Pressure Amplitude			
Acoustic frequency	1.5 [atm]	2.0 [atm.]	2.5 [atm.]	3.0 [atm.]
200 [kHz]	1.33×10^{-19}	2.53×10^{-17}	7.35×10^{-17}	1.30×10^{-16}

2.3.4 Bulk liquid temperature

The cavitation is considered a dynamic phenomenon, strongly affected by the operating parameters such as bulk liquid temperature, static pressure, and geometry of the sonoreactor. The sonochemical process's reaction mechanism is influenced by the bulk temperature, as pointed out by Sutkar and Gogate [64]. Any tiny changes in the temperature will alter the liquid medium's pressure and acoustic intensity, yielding a dramatically different cavitation effect [65]. Few studies have considered the quantitative determination of the parameters such as temperature and pressure field over an entire range of operation as a function of different operating parameters by Marangopoulos et al. [66] and Zeqiri et al. [67,68]. Kim et al. [69] studied the effect of ultrasound irradiation on the temperature and pressure distribution inside the sonoreactor. In all liquid media, the temperature increases with time. However, the differences in all liquid media's physical and thermodynamic properties are why the variation of the temperature trends concerning time. The effect of the liquid bulk temperature is scarce in the literature, and the precise mechanism of this effect remains unclear. The liquid bulk temperature has a significant impact on bubble temperature and the hydrogen production rate in return. The liquid bulk temperature is critical as it is considered the surrounding medium of the acoustic cavitation bubbles. When bulk fluid temperature increases, the bubble temperature increases leading to liquid-vapor pressure increases and more vapor is trapped inside the bubble. However, increasing the bulk temperature will make the bubbles collapse less violent, affecting the decomposition process of water molecules causing fewer active radicals. Combining these two essential factors should lead to an optimum liquid bulk temperature at which the maximum hydrogen production rate is achieved.

2.3.5 Bubble temperature

It is all about how much energy is required to take hydrogen H_2 out of a single water molecule H_2O . Firstly, in order to dissociate a water molecule H_2O into hydroxyl radical OH and hydrogen radical H , this would require the energy of approximately 497.1 kJ/mol. Secondly, to dissociate the hydroxyl radical OH into hydrogen radical H and oxygen radical O , this would need an energy of approximately 425.9 kJ/mol. Thus, collectively, the total amount of energy required to dissociate a single water molecule entirely is 920 kJ/mol, equivalent to 51 MJ/kg. Based on a simple energy balance equation and 1st law of thermodynamics: $Q = m c_p \Delta T$, by substituting the value of the heat per unit mass and the specific heat of constant pressure of water vapor, at an

average temperature of 6000 K, $c_p = 3.350$ kJ/kg. K. We will find out that the bubble temperature required to dissociate a single water molecule completely is around 15000 Kelvin. Gallego et al. [70] reported single bubble sonoluminescence to reach temperatures up to 20,000 K as measured from light-emission spectra. Therefore, the quest for ever-higher temperatures began soon after discovering single-bubble sonoluminescence by Gaitan and Crum [71] and still undergoing. **While measurements from the light spectrum peak around 20,000 K for water.** This shows that the acoustic cavitation bubble's body allows a dense plasma or micro-combustion at higher temperatures [72–74]. However, in water, water vapor's dissociation in the bubble upon its collapse quenches the high temperatures as per Toegel et al. [75]. This, indeed, is suggested by experiments performed at 30.4 kHz (with the addition of the second harmonic) in sulfuric acid as reported by Rossello et al. [76] though not by measuring the light-emission spectrum. Instead, the maximum temperatures in the bubbles have been estimated by fitting the measured radius time curves to a bubble model. A temperature of 76,000 K is predicted from bubble oscillation curves obtained at 1.8 bar driving pressure. Another example, Schanz et al. [77] a single bubble with an equilibrium radius $R_0 = 4.5$ μm saturated with water vapor and argon at 1.3 bar in a sound field of 26.5 kHz. The maximum temperature reached in this case is 16,450 K as determined from the kinetic energy of the molecules. This compares well with the spectroscopic measurements of single bubble sonoluminescence.

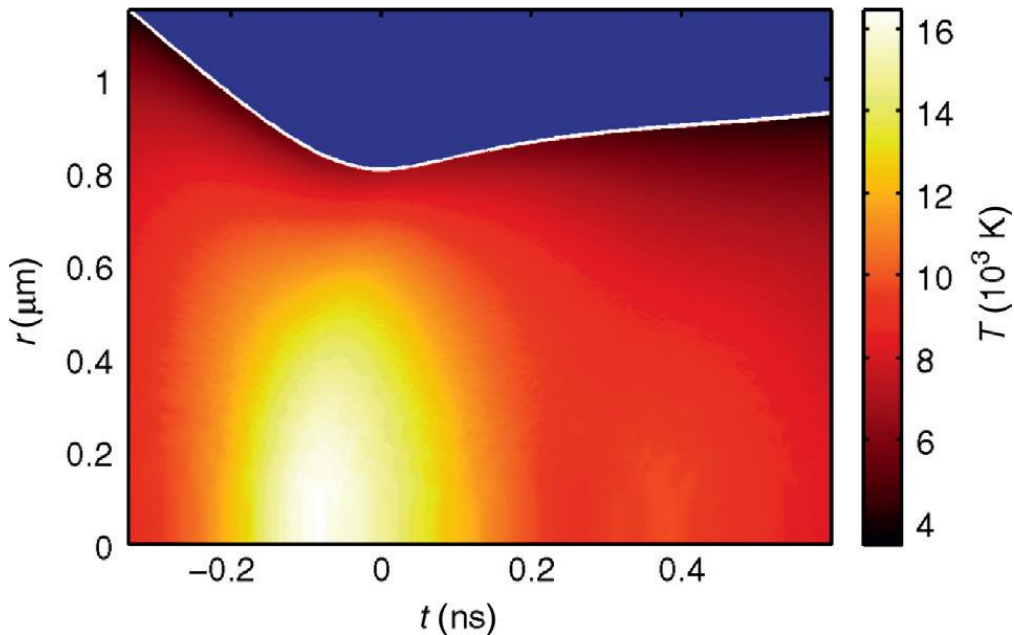


Figure 2.6: Space-time evolution of temperature during the collapse at an equilibrium radius of $R_0 = 4.5$ μm driven at 26.5 kHz and 1.3 bar. Adapted from Schanz et al. [77]

On the other hand, some researchers reported severe and extreme temperatures in the literature. For instance, in 2007, Kim et al. [78] performed numerical simulation analysis on the temperature and pressure fields due to a collapsing bubble under ultrasound. They reported the estimated bubble temperatures up to 150,000 Kelvin and bubble pressure up to 10,000 atm from their numerical simulation at different boundary conditions with $R_0 = 15.0 \mu m$, $P_A = 1.5 \text{ atm}$, and $f_d=37.8 \text{ kHz}$, the bubble center temperature goes up to 10,000 K. At another condition, $R_0 = 5.0 \mu m$, $P_A = 1.33 \text{ atm}$, and $f_d=12.93 \text{ kHz}$, the bubble center temperature goes up to 60,000 K. Surprisingly, at $R_0 = 4.5 \mu m$, $P_A = 1.3 \text{ atm}$, and $f_d=32.8 \text{ kHz}$. The bubble center temperature goes to 150,000 Kelvin. Recently, other researchers reported also different bubble temperatures, pressures at wide range of boundary conditions. For instance, Kerboua et al. [63] performed the numerical estimation of the ultrasonic production of hydrogen. They reported bubble temperature goes up to 15000 K. Here is a summary table for the ranges of the temperature and pressure at the collapse of an acoustic cavitation bubble exposed to an ultrasonic frequency field at different boundary conditions.

Table 2.5: Summary table of the bubble temperature and pressure ranges as reported in the literature with corresponding references

Reference	Bubble Temperature Range	Bubble Pressure Range
Colussi et al. [79], 1998	2000 - 8000 K, $R_0 = 2 \mu m$, 20 kHz, $P_A = 2 \text{ atm}$.	-
Gogate et al. [49]	1000 - 5000 K	100-50,000 bar
Kerboua and Hamdaoui [63]	1000 – 15000 K	-
Merouani [57]	1000 - 7500 K	10 MPa – 900 MPa
Merouani et al. [29]	6000 K at 20 kHz, $R_0 = 7.5 \mu m$ 5500K at 355 kHz, $R_0 = 3.2 \mu m$	10000 atm at 20 kHz, $R_0 = 7.5 \mu m$ 200 atm at 355 kHz, $R_0 = 3.2 \mu m$
Merouani et al. [61]	4000K at 21.4 kHz, $R_0 = 8 \mu m$	-
Kim et al. [78]	$R_0 = 15.0 \mu m$, $P_A = 1.5 \text{ atm}$, and $f_d=37.8 \text{ kHz}$, Bubble center temperature goes up to 10,000 K	10000 atm, $R_0 = 13.0 \mu m$, $P_A = 1.4 \text{ atm}$, and $f_d=28.5 \text{ kHz}$
Kim et al. [78]	$R_0 = 5.0 \mu m$, $P_A = 1.33 \text{ atm}$, and $f_d=12.93 \text{ kHz}$, Bubble center temperature goes up to 60,000 K	-
Kim et al. [78]	$R_0 = 4.5 \mu m$, $P_A = 1.3 \text{ atm}$, and $f_d=32.8 \text{ kHz}$, Bubble center temperature goes up to 150,000 K	-

The bubble temperature is one of the critical parameters that affect the mole fraction of the produced hydrogen. The maximum bubble temperature is associated with two operational conditions, such as the frequency and the acoustic amplitude. Merouani et al. [57] reported the amount of H₂ production for different bubble temperatures. The analysis is conducted on a single acoustic cavitation bubble. It can be seen that there is an optimum hydrogen rate recorded in the range between 5000-7000 K. The higher the bubble temperature, the higher the amount of hydrogen production as per Table 2.6. The results revealed that the amount of hydrogen production is higher at a low acoustic amplitude and high frequency. In contrast, hydrogen production is lower at a high acoustic amplitude and low frequency. On the other hand, to attain the maximum bubble temperature at the end of the bubble collapse, higher acoustic amplitude and low frequency should be applied [57].

Table 2.6: H₂-production at bubble temperature [K] by Merouani et al. [57]

Bubble Temperature [K]	1500	2000	2500	3000	3500	4000	4500	5000
H ₂ Production [mol]	2 E-33	1 E-25	2.1 E-24	3.5 E-21	0.5 E-19	7 E-18	6.3 E-18	5.1 E-15

In conclusion, many factors are governing the hydrogen generation from the sonohydrogen process. This study is obligated to quantify the amount of hydrogen produced from the sonohydrogen technology by performing numerical investigations. An acoustic model and chemical kinetics models have been developed, validated, and investigated. In the next chapter, the developed acoustic model is illustrated in detail.

2.4 Previous numerical and experimental studies

In this section, recent numerical modeling and solution for the *Sonohydrogen* approach are presented starting from the hydrodynamic modeling for the gas inside the bubble in liquid medium considering simulation about bubble behavior at different ultrasonic frequencies. Then we will be turning to some numerical simulation of the sonoreactor for characterizing the flow and the acoustic fields within the sonoreactor.

2.4.1 Numerical modeling studies

Hydrodynamic modeling and solution for the gas inside a bubble in a liquid medium is subjected to ultrasound waves triggers solving the *Navier-Stokes* equations for the gas inside the bubble. The gas conservation inside the bubble assumes that the bubble has a symmetrical and spherical shape. The governing equations associated with the gas trapped inside a bubble subjected to ultrasound waves are introduced, including mass, momentum, and energy are given by Kim et al. [78]. Numerical simulation of a near-wall bubble collapse is performed by Osterman et al. [80] in an ultrasonic pressure field. This numerical simulation has considered a 2-D and axisymmetric model. A pressure field is generated with the bottom of a container oscillating at 33 kHz. In this study, a validation of the model is successfully achieved by comparing a bubble collapsing near the oscillating wall as compared to the experimental work done by Philipp and Lauterborn [81]. Results considering the pressure contour oscillation and the pressure fluctuation are reported in Figure 2.7 (a) and (b), respectively.

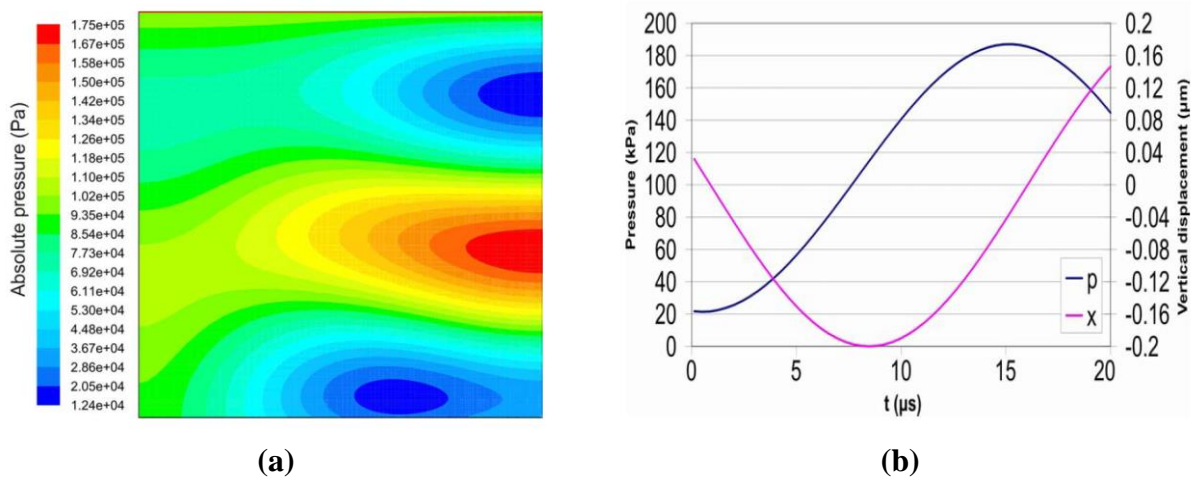


Figure 2.7: (a) Oscillating pressure field in the domain; (b) the pressure fluctuation at the center of the bottom (blue) and the bottom displacement (pink) by Osterman et al. [80]

The comparison is made in terms of the dynamics sequence of the cavitation bubble collapse concerning time. A sequence of the acoustic cavitation bubble is captured using an experiment conducted by Philipp and Lauterborn [81] and a numerical work done by Osterman et al. [80]. The difference between the experimental and numerical simulation is that the differences lie in the bubble shapes and the bubble position at the end of the collapse. This can be attributed to the numerical simulation did not consider the phase changes, and the experimental work has some uncertainties due to the gravitational effects. Another difference that can be found between both

experimental and numerical work is that the counter-jet resulted from the bubble collapse is not captured by the numerical simulation. This is also attributed to the fact that the phase change has not been considered in the numerical simulations. Many research studies are conducted to investigate the acoustic cavitation bubbles. The cavitation bubbles can be characterized by oscillations' dynamics and maximum pressure and temperature inside the bubbles before the collapse. Rooze et al. characterized [82] acoustic cavitation bubbles reporting some recent experimental reports to characterize the bubbles. In the textbook by Yasui [50], a comprehensive illustration is included for helping readers to understand the phenomenon of acoustic cavitation and bubble dynamics.

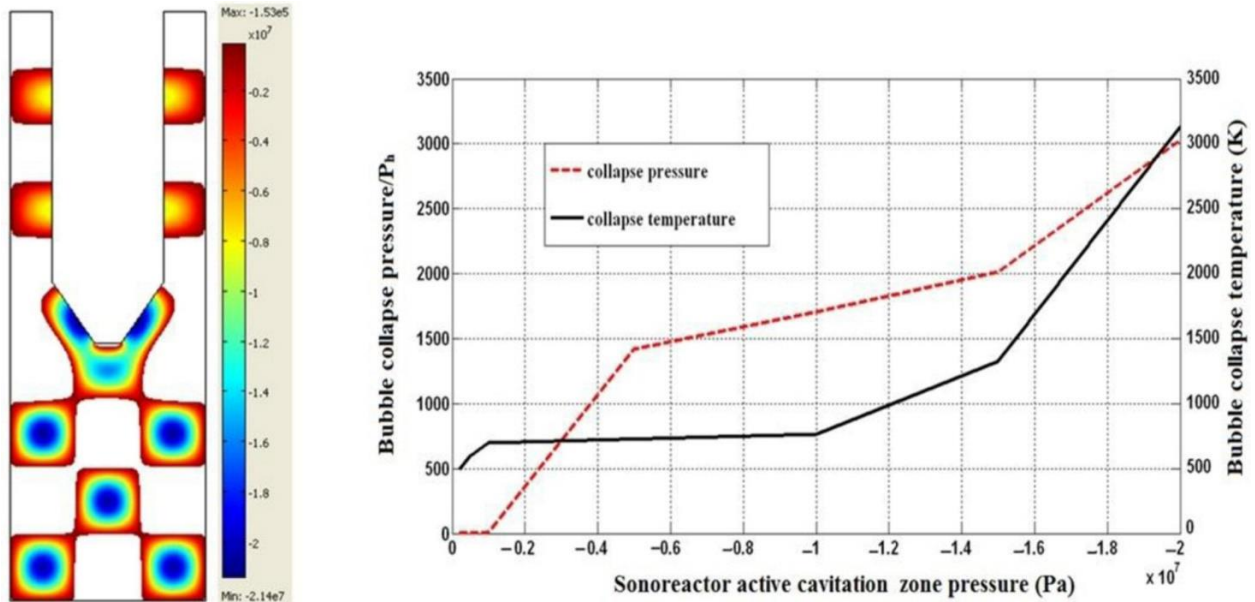


Figure 2.8: Active cavitation zones simulated by CFD technique for the reactor filled with saturated crude oil at a temperature of 25 °C by Niazi et al. [83]

CFD simulation is performed on the acoustic cavitation in a crude oil upgrading sono-reactor and prediction of collapse temperature and pressure of a cavitation bubble by Niazi et al. [83]. In this study, ultrasonic waves are introduced to liquid water contained in a sonoreactor via an ultrasound probe to investigate the pressure distribution. The experimental data is utilized from the Hielscher Ultrasound Technology website for a sono-reactor filled with water at 20 kHz and 2 kW. In the same study, CFD analysis of acoustic cavitation in a crude oil sono-reactor and prediction of collapse temperature and pressure of the cavitation bubble is conducted as well. Figure 2.8 presents the numerical results simulated to show the active cavitation bubbles zones in the sono-

reactor filled with saturated oil at a bulk temperature of 25°C. The acoustic pressure threshold for acoustic bubbles is estimated to be 0.153 MPa with an initial oil bubble size of 10 μm. On the other hand, the figure is also showing the collapse pressure and temperature of the generated acoustic cavitation bubbles while crude oil is the working medium. The collapse pressure and temperature may go up to several thousands of Pa and Kelvins, respectively.

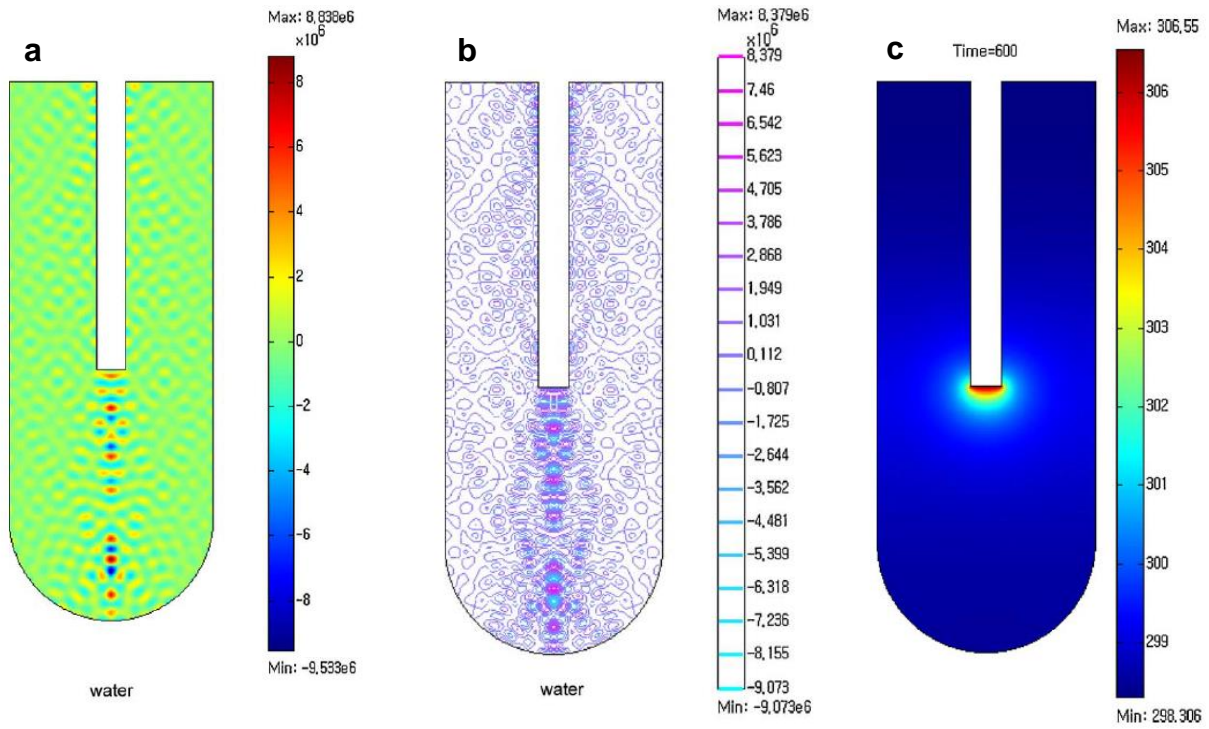


Figure 2.9: Pressure profile (a), pressure contour (b), and temperature contour (c) with ultrasonic power of 300 W, the liquid medium is water by Kim et al. [78]

The temperature and pressure fields due to the collapsing of bubbles under ultrasound conditions are predicted by Kim et al. [78] via the solution of *Navier Stokes equations* for the gas trapped inside a bubble. They compared the pressure profile of four different liquid mediums. The pressure profiles are different from each other; this can be attributed to the difference in the sound velocity and each medium's density. They reported the pressure profile and temperature contours of water, as seen in Figure 2.9. Generally, the hot spot zone usually takes place near the tip of the ultrasound probe. From the pressure profile results, it can be concluded that the pressure profile oscillates starting from the probe tip to the way down to the bottom of the container.

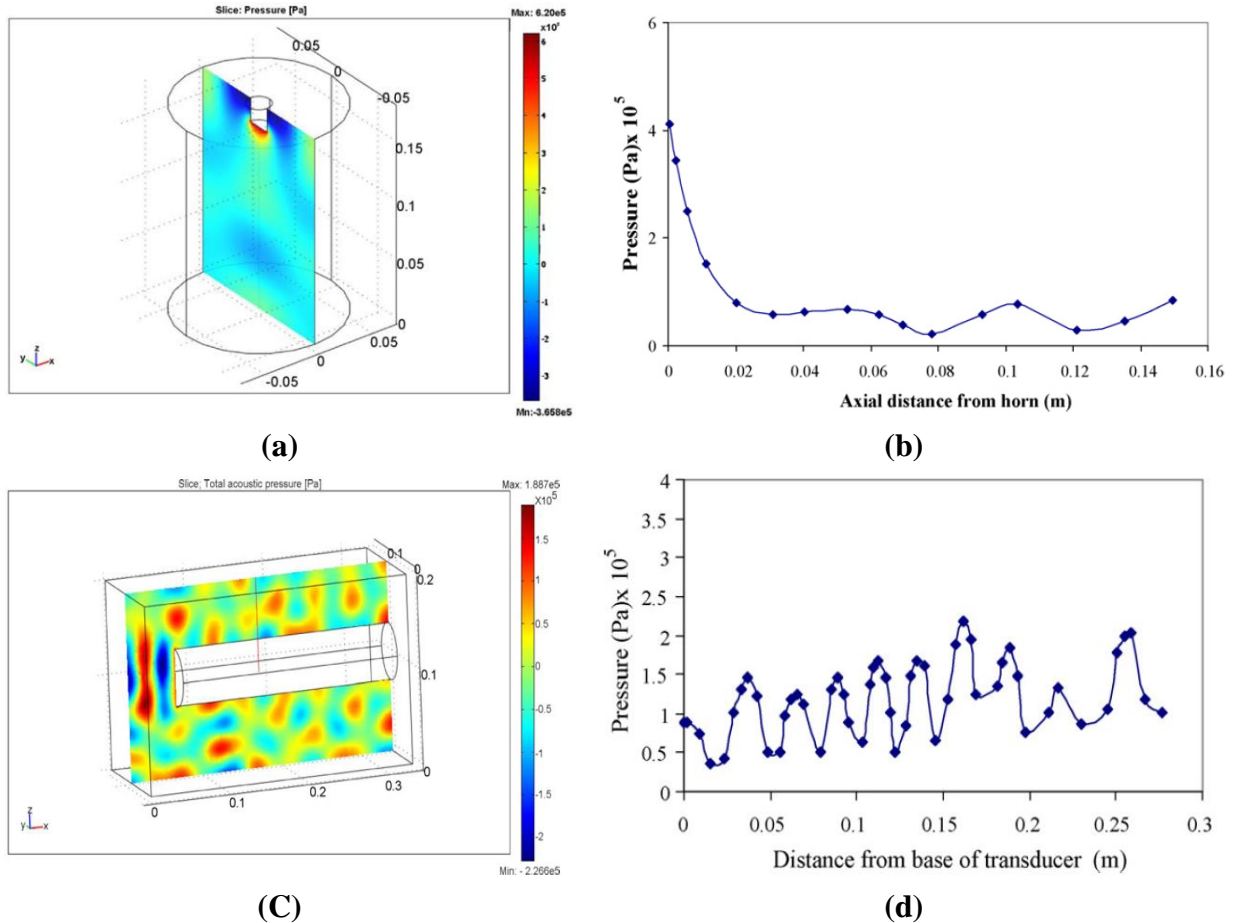


Figure 2.10: Pressure field distributions inside the sonoreactor; (a) pressure contours of the vertical transducer, (b) Axial pressure amplitude distribution, (c) pressure field of longitudinal transducer (d) radial pressure amplitude and the direction of the transducer at $z=0.095$ from the bottom by Sutkar et al. [84]

At an acoustic power of 300 W, the maximum and minimum pressure are recorded at 8.838 and -9.533 Pa, respectively. The temperature increased while increasing the acoustic power or the irradiation time. Sutkar et al. [84] performed a numerical analysis of the theoretical prediction of cavitation activity distribution in a sono-reactor. Numerical simulation is carried out and compared with experimental investigations. A 2 cm diameter ultrasonic probe with a maximum power of 240 W and a frequency of 20 kHz is being immersed in a cylindrical water bath ($D= 13.5 \text{ cm} \times H= 17.5 \text{ cm}$). The results presented the variation of the pressure distribution inside the sonoreactor, as seen in Figure 2.10. The pressure contours of the vertical transducer and its corresponding pressure amplitude in the ultrasound probe's axial direction are shown in Figure 2.10(a) and (b), respectively. It is well recognized that the maximum pressure amplitude is close to the tip of the

transducer probe and the pressure tremendously decreases on the way to the bottom of the reactor. The pressure contours of the longitudinal transducer and the corresponding pressure amplitude in the axial direction of the ultrasound probe are shown in Figure 2.10(c). Pressure fluctuation is observed along the length of the probe in the x-direction at $z = 0.095$ m, as presented in Figure 2.10(d). Many research studies considered the improvement of the acoustic and flow fields of the sono-reactor. Wei [85] performed a numerical simulation to design and characterize an ultrasonic transducer to overcome traditional transducers' disadvantages. Wang et al. [86] and Memoli et al. [87] performed characterization studies and improved a cylindrical-type sono-reactor. In the next section, different experimental configurations have been summarized and reported. Analysis of the most important findings is quantified coherently.

2.4.2 Recent experimental studies

Ultrasound-induced cavitation bubbles can be a source of acoustic waves due to bubble oscillation. The production of these sound pressure waves can be attributed to two reasons; the first reason is that these pressure waves is a result of the bubbles collapse, whereas the second reason is that these pressure waves are produced from the interaction between the bubbles, the wall and the reflected ultrasound waves from the walls. It is not yet clear that the production of these sound pressure waves is due to which of these reasons. Therefore, further experimental investigations should be carried out. An overview of different experimental configurations and recent experimental work procedure and their significance in understanding the sonohydrogen production approach will be presented. Recently, Yasui et al. [50] recommended that the liquid surface inside the small water container be aligned with the same level of the degassed water in the liquid bath to obtain the same irradiation condition. Traveling and standing waves governing equations associated with the ultrasonic transducer immersed in the sono-reactor are summarized and well-illustrated by Kinsler et al. [88]. They provided an intensive illustration of different wave shapes, such as a plane sound wave traveling through a liquid medium. Furthermore, a spherical wave can be formed if the acoustic wave source is a point source that emits an acoustic wave into a liquid medium. The authors also considered a circular plane disc emits an acoustic wave into a liquid medium. In fact, the circular disc is acting similarly to the tip of the ultrasonic probe that emits ultrasound waves to the liquid medium inside the sono-reactor.

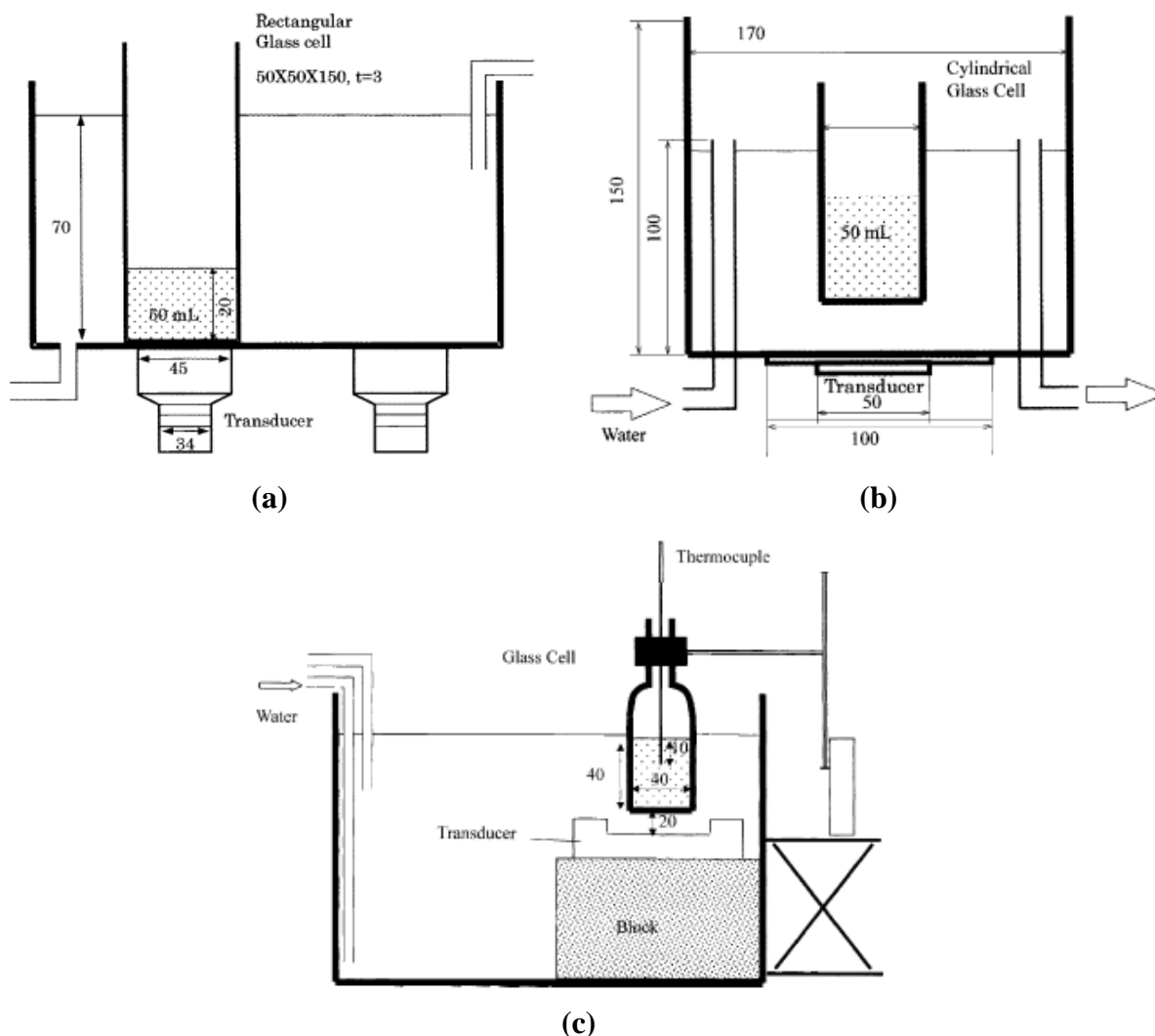


Figure 2.11: Different experimental configuration of sono-reactors in three different laboratories (a) AIST 96k, (b) Nagoya 130k and (c) Shiga 200k by Koda [89]

The generated acoustic cavitation bubbles by ultrasound are significantly affecting the density and sound velocity in the medium. In general, the density, sound velocity, and acoustic pressure amplitude decrease because of the generation and presence of bubbles under an ultrasound probe. The decrease in acoustic pressure amplitude has been studied and can be found in [90]. Koda et al. [89] compared 3 (three) different experimental setups for the sake of calibrating the sonochemical efficiency of different sono-reactor. The experimental setup (a) is built, operated, and tested in the National Institute of Advanced Industrial Science and Technology (AIST). An ultrasound transducer of 45 mm is mounted at the bottom of a water bath to sonicate a sample of a volume of 50 cm³, as seen in Figure 2.11(a). Simultaneously, Nagoya University and Shiga University of

Medical Science experiments are presented in Figure 2.11 (b) and (c). All experiments are used to create a standard method to calibrate the efficiency of the sono-reactor and sonication efficiency, and the results of this comparison study are presented in the next section. Optimization of a sono-reactor (Type-A) subjected to a frequency of 20 kHz is investigated numerically by Klima et al. [47] and compared with experimental results. The second significant important parameter affecting the sono-reactor performance is the acoustic power intensity, which comes after the ultrasound frequency.

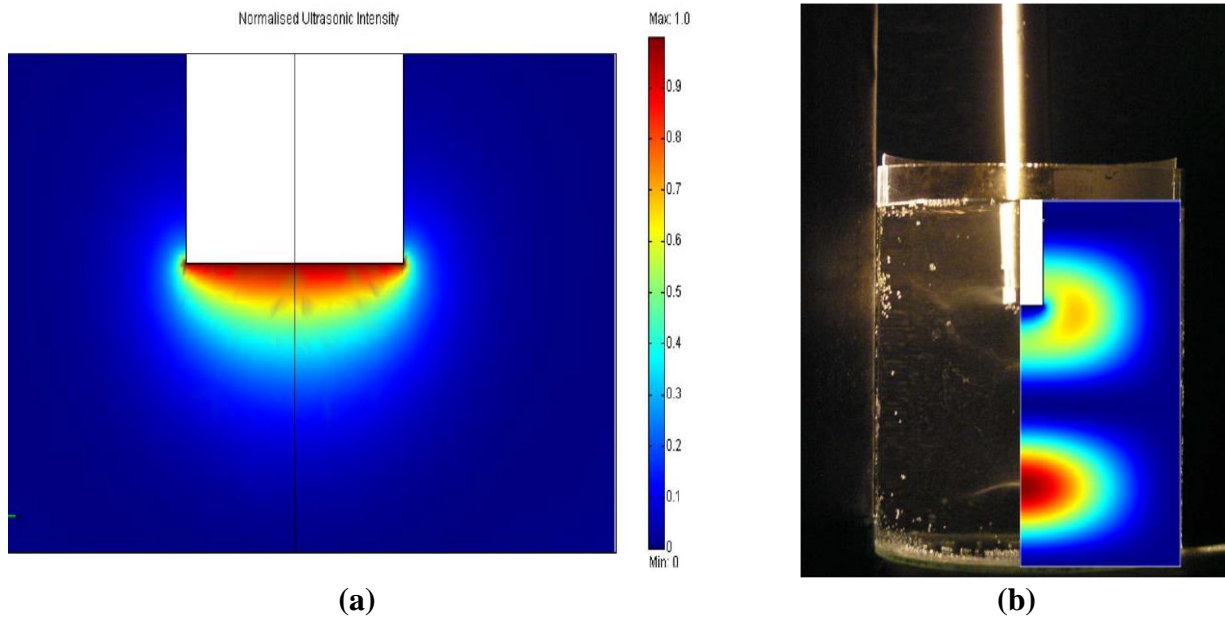


Figure 2.12: (a) Detail normalized ultrasonic intensity distribution at the ultrasonic horn tip, (b) comparison between the experimental sonoreactor (water, 20 kHz, ultrasonic power = 10 W) and the predicted intensity distribution for the same geometry by Klima et al. [47]

In this study, the effect of acoustic power intensity on the sono-reactor characteristics and the ultrasound fields are studied. In the case of low intensity, the intensity distribution's prediction is well simulated, while the opposite in the case of high intensity, the intensity distribution estimation is complex. Figure 2.12 (a) presents the intensity distribution around the tip of the ultrasound probe. It is found that the higher intensity takes place close to the probe tip. Figure 2.12 (b) presents a comparison between the experimental results and the numerical analysis, and it can be seen that both are fitted closely. Son et al. [91] performed an experimental investigation on the acoustic emissions spectral using Type-B experimental configuration. They considered different experimental parameters, including the liquid height and transducer power. The experimental setup

of the sonoreactor consists of an acrylic cylindrical sono-reactor (11 cm diameter and 110 cm height) with a transducer type piezoelectric transducer PZT. A 36 kHz frequency transducer is mounted at the bottom of the sonoreactor. The water container is filled up with water at different liquid heights, such as 100 cm. a power meter is then mounted at the exit of the ultrasonic transducer controller to control the power input. A hydrophone is used to record the acoustic emission spectra, and it is fixed at the mid-point of the sono-reactor.

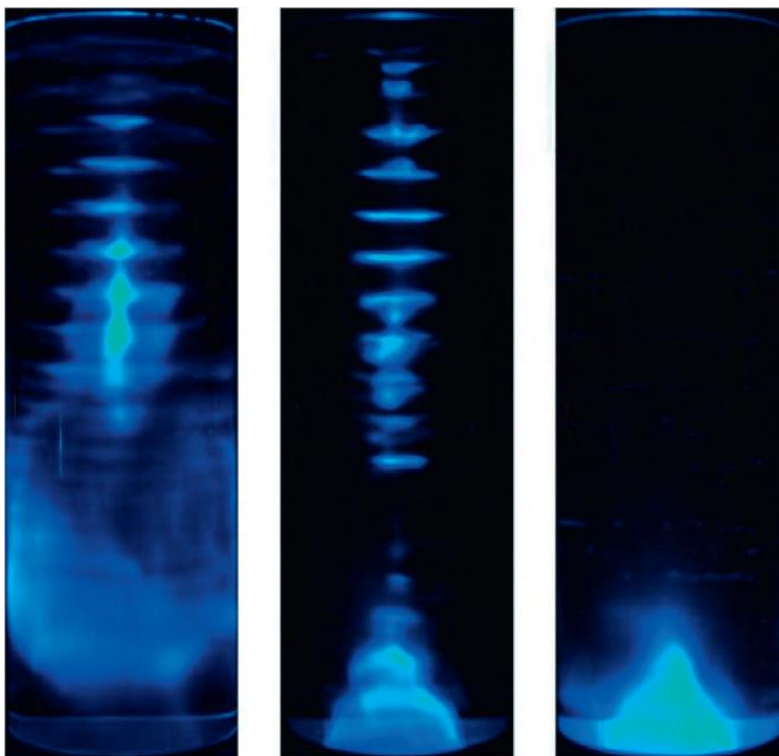


Figure 2.13: The Sono-chemiluminescence images under different input power for 30, 60, and 90 W by Son et al. [91]

They investigated 3 (three) different electrical input power, and they reported the total relative sono-chemiluminescence H_2O_2 generation and the calorimetric heat power. They reported that the H_2O_2 generation is 10.7, 30.6, and 25.6 μM at 30, 60, 90 Watts, respectively. Figure 2.13 shows the effect of increasing the transducer power on the Sono-chemiluminescence images. The water inside the sono-reactor is mechanically vibrated. The results showed that at low acoustic input power bright zone appeared as an indication for a traveling wave, and a standing wave is observed in the remaining part of the sono-reactor. At an average acoustic power, the bright conical zone is reduced, and the stripes are concentrated along the sono-reactor axis. Whereas, at high acoustic input power, the bright zone is reduced because of a cloud of bubbles formed near the transducer;

note that the transducer is mounted at the bottom of the sono-reactor. They reported a crucial observation that higher acoustic power does not significantly affect the hydrogen production yield, but it can be a reason for emitting acoustic emissions at harmonic frequencies. The more the bubbles are generated, the more the acoustic energy will be attenuated. A recent experimental work performed by Merouani et al. [61] studied different methods for estimating the active bubbles in a type-B sonoreactor. Experiments involving H_2O_2 production is carried out using an ultrasonic reactor containing 300 ml of distilled water. They conducted the experiments in cylindrical water-jacketed glass reactors. They reported some experimental procedures, including that water temperature should be kept at $25^\circ C$ by a water jacket recirculation around the cylinder. They reported that the bubble radius and H_2O_2 production rate are highly ultrasonic frequency-dependent.

A different configuration has been suggested by Cotana et al. [92] for studying water photolysis for hydrogen production. H_2O_2 and H_2 are the main products of this sonochemical reaction mechanism because of the highly reactive radicals' recombination, produced from the water molecules' dissociation at the first chemical reaction. They reported the sonochemical reaction steps in Table 2.7, corresponding to H_2 and H_2O_2 production. The experimental photolysis reactor consisted of a rectangular reactor with one glassed side to introduce photonic energy. It had 3 (three) main ducts, as highlighted in the figure, with two piezoelectric transducers mounted at the reactor's bottom. In order to generate the ultrasonic field in water, two piezoelectric transducers connected to the ultrasonic transducer controllers are attached to a power meter. The transducer generated the ultrasonic waves at a frequency of 22.5 kHz with a minimal input power of 50 W only. The experiments are carried out using the following procedure; first, the sono-reactor is filled with 0.1L of distilled water; second, the water above the water surface is injected with inert gas; thirdly, the water is subjected to the ultrasonic actions at different pressure conditions namely, 1.0, 1.5, 2.5 atm. They performed a parametric study analysis to investigate the effect of the sono-reactor pressure on the hydrogen production rate.

Table 2.7: Sonochemical reaction steps by Cotana et al. [92]

$H_2O \rightarrow H + OH$	(1)
$H+OH \rightarrow H_2 + O$	(2)
$OH+OH \rightarrow H_2O_2$	(3)
$H_2O_2 \rightarrow H_2O + \frac{1}{2} O_2$	(4)
$H+OH \rightarrow H_2O$	(5)

Figure 2.14 presents the hydrogen production in μMol concerning time (in minutes). The results show a linear relationship between the produced hydrogen and time. Furthermore, the highest production rate took place for 1.0 atm pressure condition, and the production rate of hydrogen decreased as the pressure inside the sono-reactor increased. This could be attributed to the sono-reactor is pressurized. The acoustic cavitation bubbles cannot be oscillating freely, reducing the amount of heat absorbed by the bubbles and affecting the hydrogen production rate.

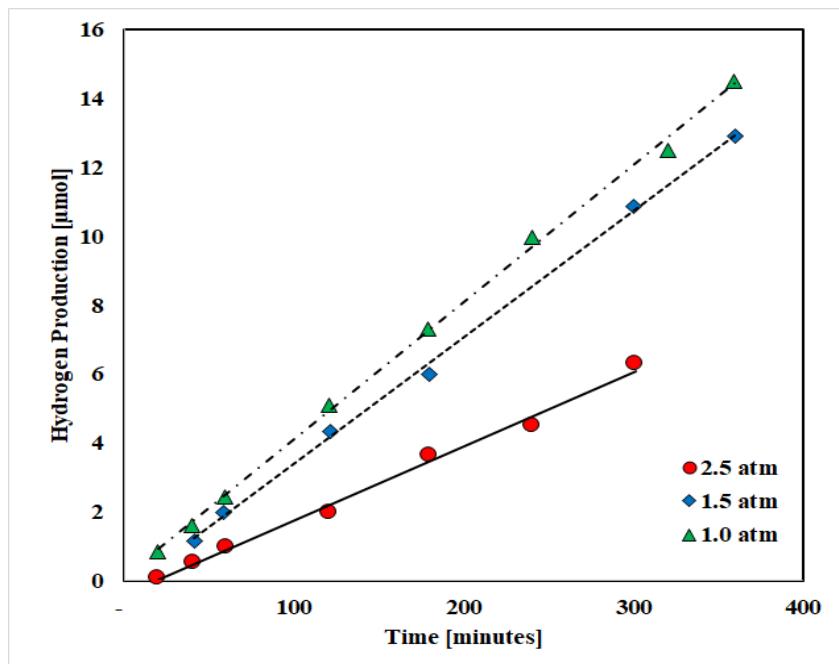


Figure 2.14: Hydrogen production versus time for different pressure conditions reprinted from [92]

The performance and efficiency assessment criteria of the sonoreactors are presented in the next section. Detailed description in the view of the sonochemical efficiency calculation procedure is presented in terms of the energy density, ultrasonic power dissipated in the liquid medium inside the sonoreactor, and cavitation energy. A comparison is made regarding the sonochemical efficiency from previous reports and studies in the literature.

2.5 Challenges for Sonohydrogen reactor design

In this section, the need for further research studies is presented. The main challenges associated with the efficient design and operation of sono-reactor are summarized in Figure 2.15. The challenges are revealed from previous and ongoing studies considering sono-reactor experiments and given in details as follows:

- 1) The acoustic field: has not been fully understood both numerically and experimentally. The acoustics field is highly complex for several reasons, such as the inhomogeneous spatial distribution of bubbles. Consequently, the speed of sound is time and position-dependent. Furthermore, the liquid container's walls are vibrating due to the pressure oscillation of the liquid medium. These vibrations emit acoustic waves back to the liquid medium, which will significantly affect the acoustic field.
- 2) Mechanism of H₂ production: this challenge lies in advancing our fundamental understanding of the mechanism of hydrogen production as the mechanism is not yet understood, and the most reported suggestions are controversial. Water-sonication experiments are still under investigation. Some research studies hypothesized that most of the H₂ production is generated inside the bubble during the gas phase. At the same time, others contradict this hypothesis by reporting that H₂ is formed on the bubble shell by the recombination of the generated radicals.
- 3) Intensity distribution: many difficulties are found in the determination of the intensity distribution inside the sono-reactor. Determination of ultrasonic intensity is well investigated in the case of low-intensity ultrasound. However, the challenge comes in when high power ultrasound is used when it exceeded the cavitation threshold. Other difficulties in the determination of ultrasonic intensity distribution lie in that ultrasound is mainly characterized by the power delivered to the system determined by calorimetry. Furthermore, the ultrasound field inside the sono-reactor is known to be a non-uniform sound field because most of the ultrasonic energy is consumed at the tip of the ultrasonic probe.
- 4) Attenuation of the sound waves in the liquid medium, as ultrasound waves are emitted and propagate through the liquid medium, the sound's acoustic intensity decreases along with the distance from the ultrasonic probe to the bottom of the liquid container. The attenuation takes place due to reflection, refraction, and absorption of the sound waves by the generated bubbles. As a result, active and passive acoustic zones will exist inside the sono-reactor. It is essential to understand the effect of these changes within the sono-reactor by probing the possibilities to reduce these attenuation effects.
- 5) Factors affecting the ultrasonic hydrogen production are the frequency of ultrasound, type of dissolved gas, acoustic power, and the bulk liquid temperature. Data concerning the effect of ultrasound frequency and the water bulk temperature are very limited and scarce in the literature and need to be furtherly investigated.

- 6) Energy conversion: one of the most important factors in developing an industrial process is the energy conversion from ultrasound waves to the required effect. The importance lies in the change of liquid properties as per the ultrasonic characteristics, which is considered very limited in the literature.
- 7) Large-scale sono-reactor: some researchers highlighted that the implementation of industrial sono-reactors had not reached full commercialization yet because most of the research studies are considered the lab-scale sonoreactors and do not provide enough information about the optimum design and optimum operating conditions of the sonoreactors. It is necessary to understand the sono-reactor characteristics, including the cavitation energy and acoustic intensity distribution.
- 8) Quantification of the produced hydrogen: few studies have considered quantification of the hydrogen production rate. Detailed quantification is essential to clearly understand the effects of different operating conditions, which is necessary to upgrade sono-reactors from the lab-scale to industrial or conventional scale.

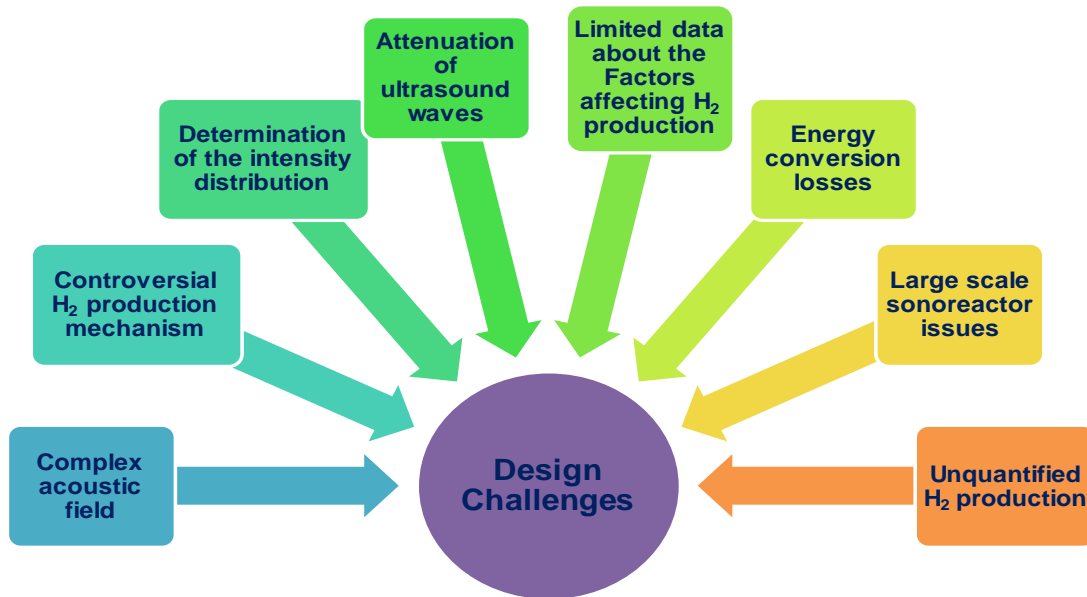


Figure 2.15: Challenges associated with sonoreactors

In order to address these challenges, an acoustic model and chemical kinetics model have been developed, validated, and investigated.

Chapter 3. System Development and Modeling

3.1 Sonoreactor Acoustic Modeling

Computational fluid dynamics (CFD) is a powerful tool used mainly to optimize and predict the characteristics of the sonoreactor model. The present numerical study aims to provide a detailed explanation and instructions to model the sonoreactor under different operating conditions. We present the computational domain, the physical models, and the boundary conditions in the following sections. Numerical models are also developed to simulate the sonication process, and they are successfully validated and compared with available data in the literature. Several numerical investigations are conducted using the finite-element method and solved by the computational acoustics module in the COMSOL Multiphysics. The acoustic and geometrical parameters' effect is considered, analyzed, and reported, including the ultrasonic frequency, acoustic intensity, and the reactor's scaling-up. The present results include a parametric study examining the change of the ultrasonic frequency, power, and other geometrical effects.

3.1.1 Computational domain

The numerical modeling is performed in 2D and 3D domains for the sonoreactor model under different operating conditions. The numerical study investigates the acoustic and flows fields' characteristics in a sonoreactor with an immersed-type transducer. An axisymmetric 2-D geometry of the sonoreactor is going to be modeled. The sonoreactor model domain and dimensions are inspired by the experimental work conducted and published by Gogate et al. [49], and it can be seen in Figure 3.1 (a). The basic sonoreactor computational domain consists of an acrylic glass cylindrical container with an internal diameter, $D = 135$ mm, and a height, $H = 170$ mm with an aspect ratio $[H/D = 1.26]$. The sonoreactor is filled with liquid water at the ambient temperature of 25 °C. The ultrasound transducer probe is immersed in water at a distance, $d = 20$ mm, from the top side of the glass cylinder with the following specifications (20 kHz, 36 W, and tip-diameter, $DP = 20$ mm). The 3D domain is built up, as shown in Figure 3.1 (c), to examine the sonoreactor under different operating conditions and consider the curvature of the wall. The sonoreactor geometry is axisymmetric; thus, a quadrant 3-D domain is built up to decrease the computational time and cost. Grid generation is carried out with a small mesh close to the ultrasonic transducer probe, which has the highest acoustic intensity.

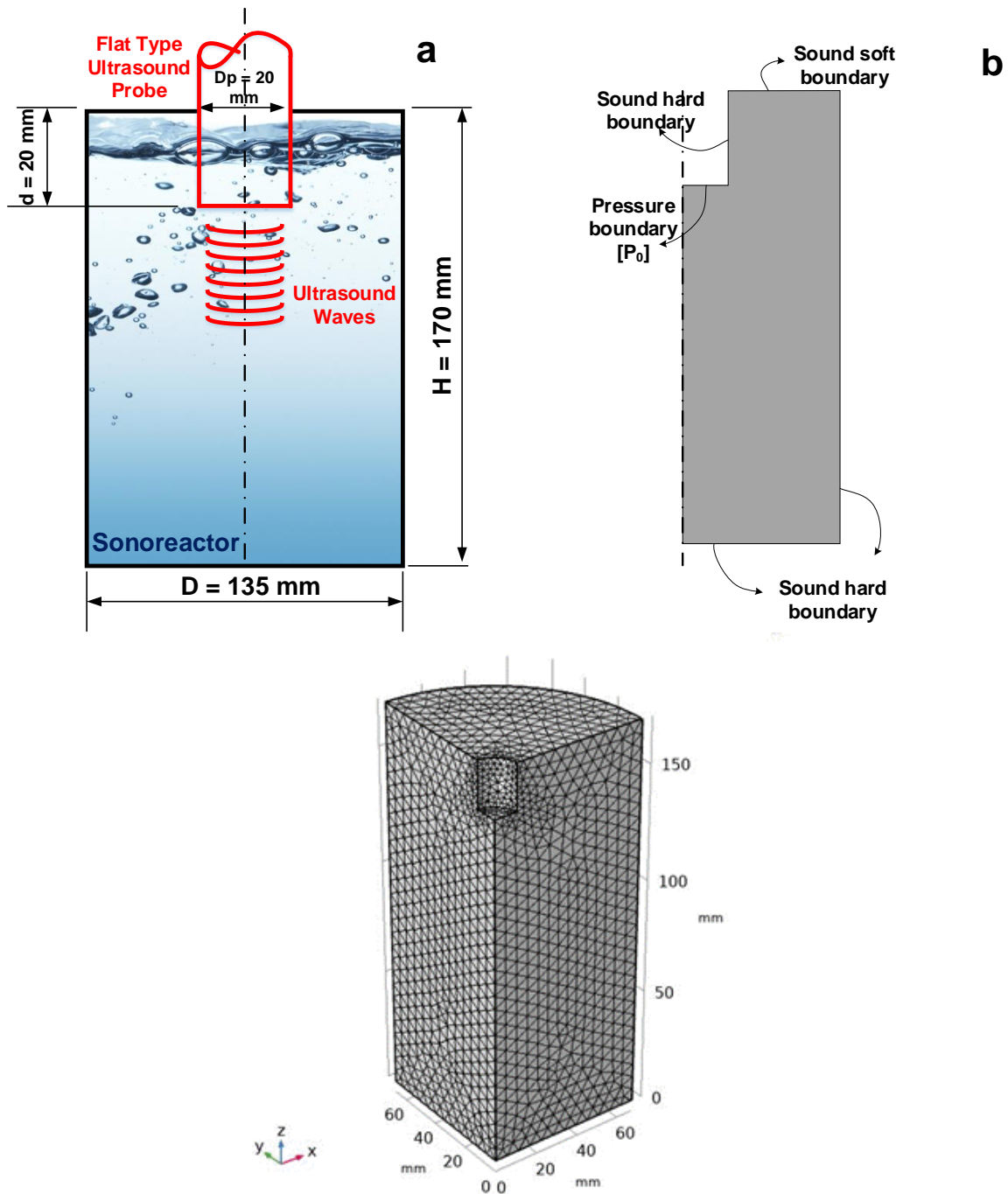
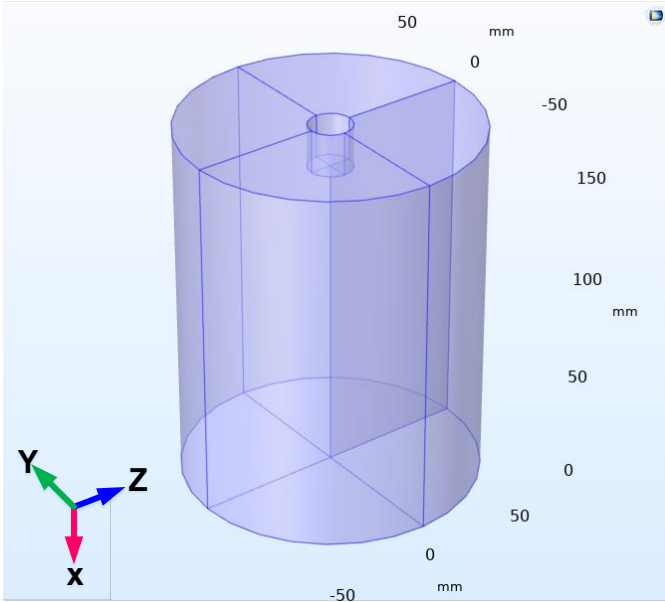


Figure 3.1: (a) The developed sonoreactor model with an aspect ratio, $H/D = 1.26$, (b) boundary conditions of the sonoreactor, (c) Computational quarter domain in 3D, same boundary conditions as the 2-D domain showing the meshing

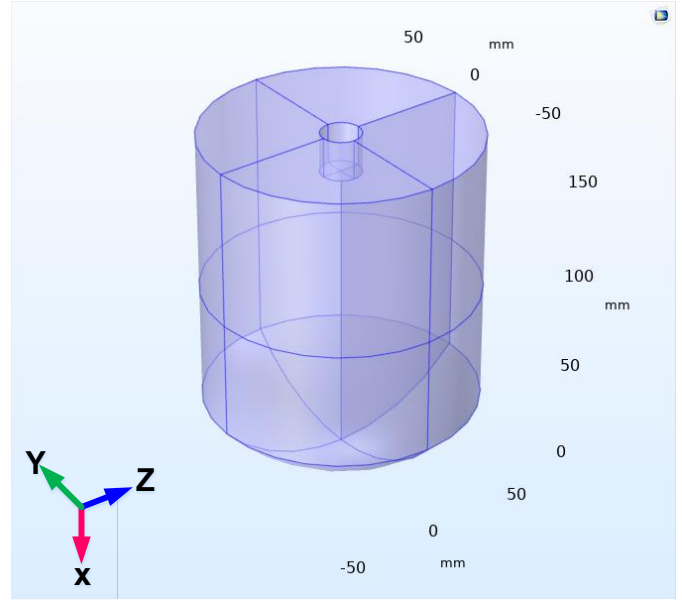
In order to check the mesh accuracy and quality, a grid independence study is carried out to eliminate the effect of the mesh size on the results. Different meshes are used with different densities, namely, finer mesh 12345 elements, extra-fine mesh 48697 elements, and the extremely

fine mesh 263273 elements. It is found that any further increase in the mesh density would not alter the results. Because of this study, the extra fine mesh is used with 48697 elements chosen to continue the simulation study. Moreover, different geometries are investigated, which is shown in Figure 3.2. COMSOL Multiphysics is used to draw all of the geometries. GEO.1 is a typical sonoreactor configuration inspired by an experimental work reported by [49] and validated for benchmarking. While GEO.2 is an inverse cone configuration, GEO.3 is a typical cylinder sonoreactor with a curved bottom wall, and GEO.4 is a regular cone shape with a broader bottom area. The geometries are built and inspired by [93], who conducted research studies on analytical applications for sonochemistry. These geometries are customary geometrical shapes of sonoreactors used in chemical industries. The geometries developed based on how the sonoreactor wall and base will influence the computational results, including a contracting wall and base (GEO.2), a concave base (GEO.3), and an expanding wall and base (GEO.4). At an ambient temperature of 25 ° C and atmospheric pressure, all sound reactors are filled with water. The ultrasound transducer is immersed in the water at a certain distance, and $d = 20$ mm (20 kHz, 36 W, and a tip-diameter, $DP = 200$ mm) from the top of the acrylic glass cylindrical cylinder. The acoustic pressure-frequency domain COMSOL module is used mainly to predict the acoustic and flow fields' characteristics of the sonoreactor models.

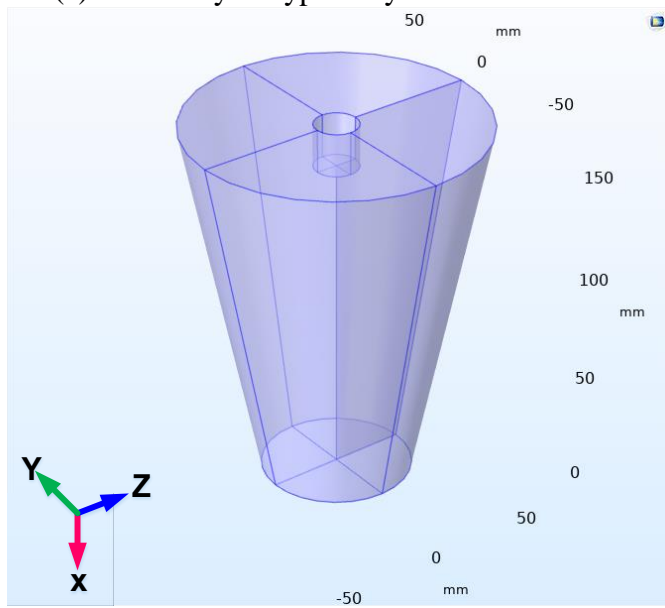
Four sonoreactor geometries will be simulated using the finite-element method and solved by the available computational fluid dynamics tool in COMSOL Multiphysics. This study's second objective is to investigate the influence of the geometrical parameters such as the sonoreactor geometry, wall boundary, and conditions on the acoustic pressure distribution inside the sonoreactor. This includes varying the outer sonoreactor geometries, namely, the typical cylindrical sonoreactor shape, the hexagonal sonoreactor, and the square sonoreactor. Additionally, the effect of adding multiple sonotrodes is also investigated, and the acoustic pressure distribution is quantified, compared, and reported. Finally, the input power effect on the cavitation energy and sonochemical hydrogen yield is investigated while varying the input power through having multiple sonotrodes.



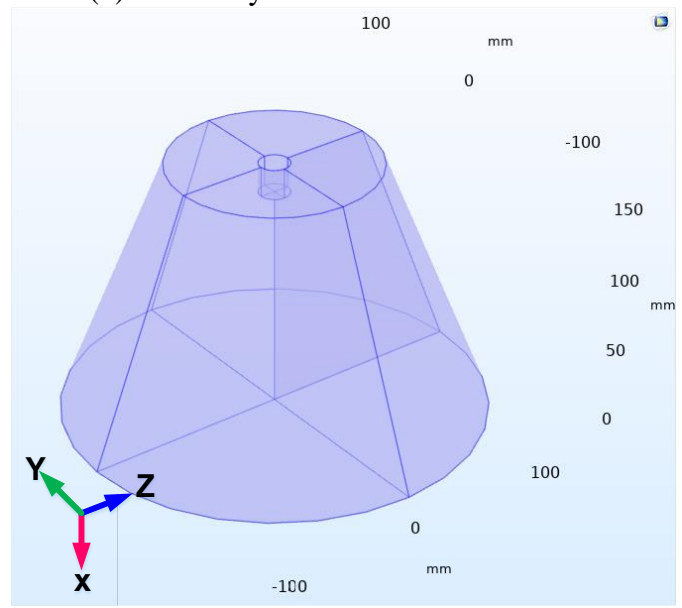
(a) Geometry 1-Typical cylindrical sonoreactor



(b) Geometry 2- Concave base sonoreactor



(c) Geometry 3 – Narrow base sonoreactor



(d) Geometry 4 – Wide base sonoreactor

Figure 3.2: Computational domains of unique sonoreactor geometries with a sonotrode introduced from the top side

3.1.2 Governing equations

The most fundamental equation in acoustic is the wave equation for the acoustic pressure through a liquid medium such as water. It describes the properties of the sound field in space and time, which can be given as follows:

$$\frac{\partial^2 P}{\partial x^2} - \frac{1}{c^2} \frac{\partial^2 P}{\partial t^2} = 0 \quad (3.1)$$

P is the acoustic pressure (N/m²), and c is the sound speed in the liquid medium (m/s). By extending equation (3.1), considering three dimensions in a homogenous liquid medium can be described as follows:

$$\nabla \left(\frac{1}{\rho} \nabla P \right) - \frac{1}{\rho c^2} \frac{\partial^2 P}{\partial t^2} = 0 \quad (3.2)$$

where ρ is the density. In order to carry out the numerical simulation to study the ultrasonic field propagations, some assumptions have to be made. For simplification and to simulate the propagation of the ultrasonic waves through the liquid medium, the linearity of the sound wave through the liquid medium is initially assumed, neglecting the shear stress, assuming incompressible liquid medium, and the time-harmonic pressure assumption, so the pressure can be given as follows:

$$P(r, t) = P(r) e^{i\omega t} \quad (3.3)$$

Based on these assumptions, we obtain the following equation, which is described as the Helmholtz equation:

$$\frac{\nabla^2 P}{\rho} - \frac{\omega^2}{\rho c^2} P = 0 \quad (3.4)$$

The equation is solved using COMSOL Multiphysics software to give access to the acoustic pressure distribution inside the sonoreactor after selecting the correct physical models and the suitable boundary conditions. Additionally, the following equations are used to calculate each of the following by order: the acoustic intensity, velocity amplitude, sonotrode displacement and acceleration [94] as follows:

$$I_{US} = \frac{P_{US}}{A_p} [W/m^2] \quad (3.5)$$

$$V_0 = \frac{P_0}{\rho_0 c_0} [m/s] \quad (3.6)$$

$$X_0 = \frac{V_0}{\omega} [\mu m] \quad (3.7)$$

$$a = 4\pi^2 f^2 x [m/s^2] \quad (3.8)$$

Lastly, the cavitation energy and cavitation yield are used to estimate the hydrogen quantity emitted by the sono-hydrogen sonoreactor. The cavitation yield is defined as the number of reaction

products per unit of irradiation time in seconds per unit of energy consumption in kWh. The cavitation energy gives an indication about the energy dissipated from the supplied input/electrical energy, and it can be described in terms of the input power as [95]:

- Cavitation energy:

$$\text{Cavitation Energy} = -0.0008 (\text{input energy})^2 + 0.4699 (\text{input energy}) \quad (3.9)$$

- Sonochemical energy consumption:

$$\text{Sonohydrogen Yield} = 0.0003 (\text{cavitation energy})^2 + 0.0140 (\text{cavitation energy}) \quad (3.10)$$

The selected physical models and boundary conditions will be illustrated in the next sections. However, in a later study concerning the acoustic streaming induced by the sonication effects, the compressibility effects have been involved in the study through a comparison study when using three different densities, namely, the constant density, linear density, and nonlinear density effects on the acoustics streaming.

3.1.3 Physical models

In order to model a continuous wave excitation and get a steady-state time-harmonic solution, the pressure acoustics, frequency domain physics with a frequency-domain study have been selected. The amplitude of the excitation at the source location should be an input parameter based on the acoustic intensity and acoustic power. Information regarding the pressure amplitude is provided in the boundary conditions section. For the acoustic module, the pressure acoustics frequency-domain has been selected. Within this model, the linear elastic fluid model has to be chosen with attenuation. The attenuation of the liquid medium is significant, which has a considerable value of the absorption coefficient (α). The attenuation losses of the acoustic pressure can be obtained from calculating the attenuation coefficient that can be given as follows:

$$\alpha = \frac{8\mu\pi^2 f^2}{3\rho c^3} \quad (3.11)$$

where f is the ultrasound frequency, ρ is the water density, and c is the sound speed. By direct substitution, the absorption coefficient of water is found to be 0.0125 m⁻¹. The computational fluid dynamics CFD tool is added to the study to simulate the acoustic velocity streaming induced by the ultrasonic transducer to relate the acoustic pressure field to the flow dynamics field. The fluid

flow module is selected with the laminar flow-interface with gravity referred to the following researchers; Gogate et al. [49]; Acoustic Module, pressure acoustics frequency-domain interface] Niazi et al. [83]; Rubinetti et al. [94]; Fluid Flow, Laminar flow-interface with gravity, Rubinetti et al. [94].

3.1.4 Boundary conditions

The computational domain with all boundary conditions required to solve the case is shown in Figure 3.1 (b). The simulations incorporate a linear model with boundary conditions summarized below while assuming infinitely rigid and perfectly reflective acoustic boundaries in all cases, except one special case with absorbing boundaries. This assumption is changed during the study about the effect of different types of boundaries. Since most ultrasonic sources emit sinusoidal waves, the pressure wave can be assumed as harmonic. The conversion factor of the ultrasonic probe is assumed to be 0.85. Lastly, during the acoustic streaming validation, it is assumed that the probe's acoustic streaming pattern is a jet inlet that is used regularly over the years [96,97]. The boundary conditions are implemented based on COMSOL 5.4 library modules [98] and previously reported studies Gogate et al. [49]; Sutkar et al. [84]; Niazi et al. [99] can be given as follows: At the transducer probe tip, the pressure boundary condition will be applied as $[P=P_0]$ based on the calculation of acoustic power and intensity. Therefore, the pressure amplitude at the probe surface can be given as follows [47,69,99]:

$$I_{US} = \frac{P_{US}}{A} = \frac{P_0^2}{2\rho_0 C_0} \quad (3.12)$$

where I_{US} is the acoustic intensity in $[W/m^2]$, the acoustic power P_{US} unit is in $[W]$, and A is the transducer probe surface area $[m^2]$. The sonoreactor side walls are set to sound-hard boundary condition as well as the sides of the ultrasound transducer probe is defined as a sound-hard boundary wall and can be given as follows:

$$\left. \frac{\partial P}{\partial x} \right|_{x=0} = 0 \quad (3.13)$$

The sonoreactor walls are set to be sound-soft boundary conditions where $(P=0)$; this corresponds to a soft obstacle to allow the pressure P_0 to vanish at this boundary. Furthermore, this is also a so-called pressure release surface, which applies to underwater noise problems.

3.1.5 Modeling of acoustic streaming

In order to include the nonlinear effects of the vortex shedding, the acoustics are modeled using the full compressible Navier-Stokes (NS) Equation in the vicinity of the sonoreactor [100]. The compressible flow is important here because, in the case of the sonoreactor, the flow velocity is large enough to introduce significant changes in the density. The changes can be neglected when the Mach number lower than 0.3. However, the coupling between the velocity and pressure fields becomes so strong that the NS and continuity equations need to be solved together. Compressible flow can be laminar or turbulent. In this case, the model combines pressure acoustics, transient module, and Laminar flow module. The vortices are resolved, so no turbulence model is used (DNS). The acoustic and flow coupling is valid as long as vorticity is small at the interface boundary. On the acoustic side, the velocity is set, and on the flow side, the pressure is set to be a transient equation. The transient pressure acoustics model equation extracted from COMSOL can be expressed as follows:

$$\frac{1}{\rho c^2} \frac{\partial^2 p_t}{\partial t^2} + \nabla \cdot \left(-\frac{1}{\rho} (\nabla p_t - q_d) \right) = Q_m \quad (3.14)$$

$$p_t = p_2 + p_b \quad (3.15)$$

Where p_t is the total pressure, ρ is the fluid density, c is the speed of sound, q_d is the dipole domain source. This term represents a volumetric domain force, and it could be used to represent a uniform constant background flow convecting the sound field, and monopole domain source Q_m that can represent a domain heat source, causing pressure variations. The background pressure field node to model a background/incident pressure wave to study the scattered pressure field p_2 , which is defined as the difference between the total acoustic pressure p_t and the background pressure field p_b . In the case of compressible and laminar flow, the term $(\nabla \cdot u)$ is not neglected because the flow is compressible and the density changes concerning time and also we can not remove the term $(\frac{2}{3}\mu(\nabla \cdot u))$ from the viscous force term in the NS equation in the case of the compressible flow. After taking into considerations all of the previous assumptions, the laminar flow equation extracted from COMSOL:

$$\rho \frac{\partial u}{\partial t} + \rho(u \cdot \nabla)u = \nabla \cdot [-pi + K] + F \quad (3.16)$$

$$\frac{\partial \rho}{\partial t} + \nabla \cdot (\rho u) = 0 \quad (3.17)$$

$$K = \mu(\nabla u + (\nabla u)^T) - \frac{2}{3}\mu(\nabla \cdot u)i \quad (3.18)$$

The sound-hard boundary (wall) adds a boundary condition for a sound-hard boundary (wall), a boundary at which the normal component of the acceleration and the velocity is zero. It can be expressed as follows:

$$-n \cdot \left(-\frac{1}{\rho}(\nabla p_t - q_d) \right) = 0 \quad (3.19)$$

For zero dipole-domain source $q_d = 0$ and a constant fluid density, this means that the normal derivative of the pressure is zero at the boundary:

$$\frac{\partial p_t}{\partial n} = 0 \quad (3.20)$$

The compressible pressure waves in the flow equations are included through the linear and non-linear density relations, we needed to use the linear, and the non-linear density relation is defined according to the following equations:

$$\rho_L = \rho_0 + \frac{p}{C^2} \quad (3.21)$$

$$\rho_{NL} = \rho_0 + \frac{p}{C^2} - \frac{1}{\rho_0 C^4}(\beta - 1)p^2 \quad (3.22)$$

Where ρ_L is the linear density distribution concerning the acoustic pressure, while ρ_{NL} is the nonlinear density distribution concerning the acoustic pressure, speed of sound, and the nonlinearity coefficient, and β is the nonlinear coefficient and expressed as:

$$\beta = 1 + \frac{B}{2A} \quad (3.23)$$

Where B/A is the nonlinear parameter that changes when the sonication medium changes, the nonlinear acoustic coefficient is of importance in our study; this is because at medium to high acoustic pressure amplitudes and sound pressure levels, the local particle velocity can be so large that the linear assumptions of acoustics break down. Typically, vortex shredding takes place in the vicinity of that region. This leads to nonlinear losses and, in audio applications, the nonlinear distortion of the sound signal. The nonlinear effects are sometimes included through semi-empirical parameters in analytical transfer impedance models. In this section, an immersed type sonoreactor contained a particular volume of liquid water medium, and the losses are modeled

directly. The model couples pressure acoustics and the laminar flow interface in a transient simulation to model the complex nonlinear losses associated with the vortex shedding. The incident acoustic field has an amplitude of 234 dB SPL corresponding to 5 bar. The amplitude is considered typical for most of the sonoreactor applications and configurations. To the best of our knowledge, and it is evident that the best agreement with the velocity measurements is observed with an acoustic pressure at the tip of the horn of about 500 kPa.

$$P_{in} = P_A \sin(\omega_0 t) \quad (3.24)$$

Where P_{in} is the incident pressure, P_A is the acoustic pressure amplitude, ω_0 is the angular frequency of the driving frequency $f_0 = 20 \text{ kHz}$. The model is simulated using different densities as per the previous set of equations. A comparison is made accordingly on constant density, Linear density, and non-linear density on the flow field inside the sonoreactor. The benefit of the streaming study is to assure a good premixing of the liquid levels, which will affect the chemical yields.

3.1.6 Thermodynamics analysis and efficiency

In order to scale-up sonochemical reactors for industrial use, one needs to investigate the efficiencies and the factors affecting the sonochemical process. The most important two parameters for developing performance and efficiency criteria are the energy density and the ultrasonic power dissipation. In fact, energy density E_{US} is related to the temperature change of the liquid medium during irradiation time t_{US} that can be measured in a flask filled with the required liquid to estimate the “real” ultrasound power. This experiment is suggested by Zarzycki et al. [101]. The energy density with the irradiation time is calculated using the following equation as follows:

$$E_{US} = P_{US} \cdot \frac{t_{US}}{V_I} \quad (3.25)$$

While the following equation can calculate the ultrasonic power dissipation into a liquid:

$$P_{US} = m_{US} C_{pUS} \frac{\Delta T}{\Delta t} \quad (3.26)$$

where m_{US} the mass of water in kg, C_{pUS} is the specific heat capacity of water at a constant pressure of 4.19 kJ/kg/K, and $(\Delta T/\Delta t)$ is the temperature rise per second. The calorimetric measurement is based on thermodynamic calculations to show how much power is transferred

from the transducer to the liquid medium. The calorimetric measurement is for the sake of investigating the energy efficiencies of the sonication process. The thermodynamics analysis is also of importance. Figure 3.3 presents a thermodynamics concept of the sonoreactor, including the distribution of all input and output energies involved in the sonohydrogen process. The thermodynamics analysis and equations, including mass balance, energy balance, and sonohydrogen efficiency, can be given as follows:

$$m_{w_i} = m_{w_f} + \sum_{i=products}^i m_i \quad (3.27)$$

$$P_{US} \times \Delta t_{US} + m_{w_i} \times h_{w_i} = m_{w_f} \times h_{w_f} + \sum_{i=products}^i m_i \times h_i \quad (3.28)$$

$$\eta_{sonohydrogen} = \left. \frac{n_{H_2}(t) * \overline{H\bar{V}}_{H_2}}{P_{US} \cdot \Delta t_{US}} \right]_{H_2O/dissolved_gas} \quad (3.29)$$

Where m_{w_i} and m_{w_f} is the initial and final water masses, m_i is the mass of the dissociation reaction products, including hydrogen, hydroxyl radicals, hydrogen peroxide, and other products.

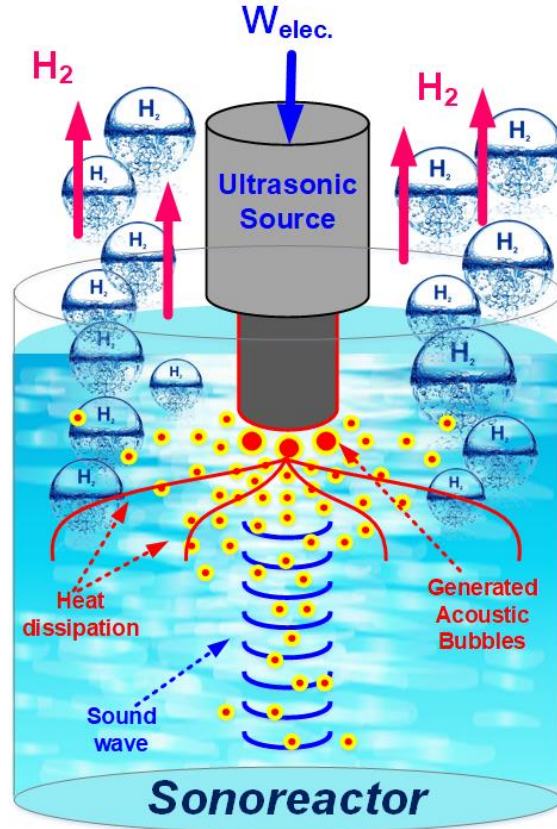


Figure 3.3: Thermodynamics basic concept of the sonohydrogen process

The energy balance equation includes the ultrasonic power input or the electrical power input multiplied by the irradiation time. The sonohydrogen efficiency is defined as the output over the input, which is equal to the energy output of hydrogen produced over the electrical power supplied to the sonoreactor.

3.1.7 Sonoreactor parameters and simulation plan

This numerical investigation will study the effect of different sonoreactor parameters. These essential parameters have been classified as physical, geometrical, and operational parameters. Several factors that affect the sonoreactor characteristics, including the acoustic and flow fields, are organized and summarized in Figure 3.4.

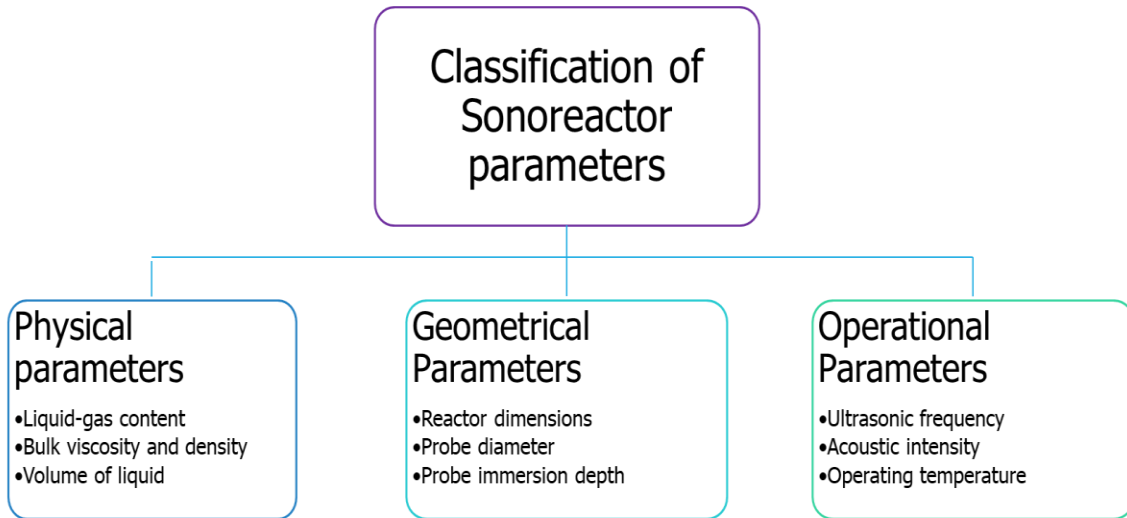


Figure 3.4: Classification of sonoreactor parameters

The numerical investigation plan is summarized in Table 3.1. Four sets of numerical investigations will be conducted, including (a) building up the computational domain based on the experimental sonoreactor model established by Gogate et al. [49], (b) model(s) validation and comparison will be made, (c) studying the effect of the geometrical parameters, (d) investigating the impact of operational parameters, and finally (e) the geometric optimization study.

Table 3.1: Acoustic investigation plan and parametric study

A	Establish the computational domain	1) The model is built and inspired by a previous experimental work	<i>Results presented in section 4.1</i>
B	Model validation	2) The model is going to be validated with previous experimental work	<i>Results presented in section 4.1</i>
C	Study the effect of geometrical parameters	3) The effect of reactor dimensions 4) The effect of the transducer probe diameter 5) The effect of immersion depth	<i>Results presented in section 4.2 and 4.3</i>
D	Study the effect of operational parameters	6) The effect of ultrasonic frequency 7) The effect of acoustic intensity	<i>Results presented in section 4.2 and 4.3</i>
E	Study the acoustic streaming induced	8) The effect of acoustic streaming 9) The effect of sonoreactor geometries on acoustic streaming	<i>Results presented in section 4.4</i>
F	Geometric parametric/optimization study	10) Effect of different outer geometries 11) Effect of the number of sonotrodes 12) Cavitation energy and conversion efficiency	<i>Results presented in section 4.5</i>

3.2 Bubble Dynamics Modeling

In order to create a relation between the primary effect of the operation of the acoustic cavitation bubble and the consequent effect of the chemical kinetics mechanism associated with the sonochemical process, a detailed numerical study is performed. We studied a potential reaction kinetics mechanism to develop sonochemical hydrogen in this work, which we called the sonohydrogen process. The reaction kinetics mechanism consists of 19 reversible reactions that take place at different conditions within the acoustic cavitation micro-bubble. The reaction kinetics simulation is validated and used to calculate the amount of hydrogen that is initially saturated with water/oxygen H_2O/O_2 emitted by a single bubble. Two related studies in the literature compare the bubble dynamics model's findings and the chemical kinetics model.

3.2.1 Background

The concept of using hydrogen from the sonochemical process depends on two consequences; the primary effect is the acoustic cavitation behavior. The chemical reaction mechanism associated with the activity of the cavitation is the secondary influence. The primary consequence is that few

attempts are made at high frequency to build large-scale sonochemical reactors to boost cavitation operation in multiple areas within the sonoreactor. For example, Asakura et al. [102] have built a broad sonochemical reactor with 12 PZT transducers operating at an ultrasonic frequency of 500 kHz and a maximum capacity of 620 kHz. While Mhetre and Gogate [103] proposed a new sonochemical reactor design with a vast capacity of 72 L using a set of 12 transducers operating at 40 kHz and a maximum rating of 2400 W. This method archives a uniform distribution of cavitation energy and can be a practical method for the industrial scale. Gleb et al.[104] studied acoustic streaming's effect on continuous sound crystallization in channels using an ultrasonic horn with a 20 kHz frequency. Gogate et al. [49] reviewed functional mapping studies of sonochemical reactors and carried out experimental verification. They suggested that extra efforts should be made to compare the pressure pulse values at different locations within the sonoreactor with the chemical effects of various chemical reactions. Besides, further work is needed to predict the number of free radicals produced by the sonochemical method. Subsequently, Sutkar and Gogate [64] presented a description of the various techniques used to explain cavitation activity distribution in the reactor. They clarified that the dependence of acoustic cavitation on the nature of sonochemical reactors and the operating parameters recommended that multi-frequency reactors be a better alternative to single-frequency reactors due to higher cavitation activity leading to higher chemical yields. However, Sutkar et al. [84] researched the distribution of cavitation energy using COMSOL Multiphysics software in the sonochemical reactor, which would impede the efficient design of large-scale sound reactors. This theoretical simulation helped them to predict cavitation behavior. However, these studies lack the secondary impact or influence of the consequence chemical reaction process that will be our study's subject.

The secondary effect is the chemical reaction mechanism associated with the primary effect of the sonohydrogen process, which is rarely introduced in the literature. A simple sounding method will produce hydrogen by immersing the ultrasonic horn in a pure water jar. The combined effects of the primary and secondary effects of the sonohydrogen process can contribute to the evolution of hydrogen, which is highly dependent on the acoustic parameters (main effect). It is ascribed to the fact that, during the collapse of a single bubble, the bubble acts as a micro-combustor with a high-temperature chemical reaction up to thousands of Kelvins, and highly reactive radicals such as OH, H, O, and HO₂ are formed. Three variables regulate the chemical reaction mechanism: (a) the temperature of the bubble, (b) the time of the collapse, and (c) the size of the bubble [4]. The effect

of the pressure outside and inside the bubble, however, is also significant. The external bubble pressure field depends on the acoustic operating parameters used, such as the acoustic strength. In this regard, the inside pressure of the bubble is influenced by how long the bubble is exposed to the bubble's outside pressure, which may amount to thousands of ATMs. Both stresses are important because they profoundly influence and regulate the collapse of the bubbles. As the bubble collapse's peak temperature is a crucial parameter for the sonochemical reactors' design, Kim et al. [78] estimated the maximum temperature and pressure due to the collapsing bubble under the acoustical impact. He proposed a specific analytical model. They say that the bubble's maximum temperature can be up to 60000 K in the ultrasonic frequency range of 10-40 kHz. The variation of the radicals generated by the bubble's temperature is examined by Yasui et al. [105].

3.2.2 The bubble dynamics model

This section discusses the numerical approaches used for solving the bubble dynamics model and the chemical kinetics mechanism model associated with the sonohydrogen process. The radial bubble dynamics model is explained by introducing the Keller & Miksis equation.

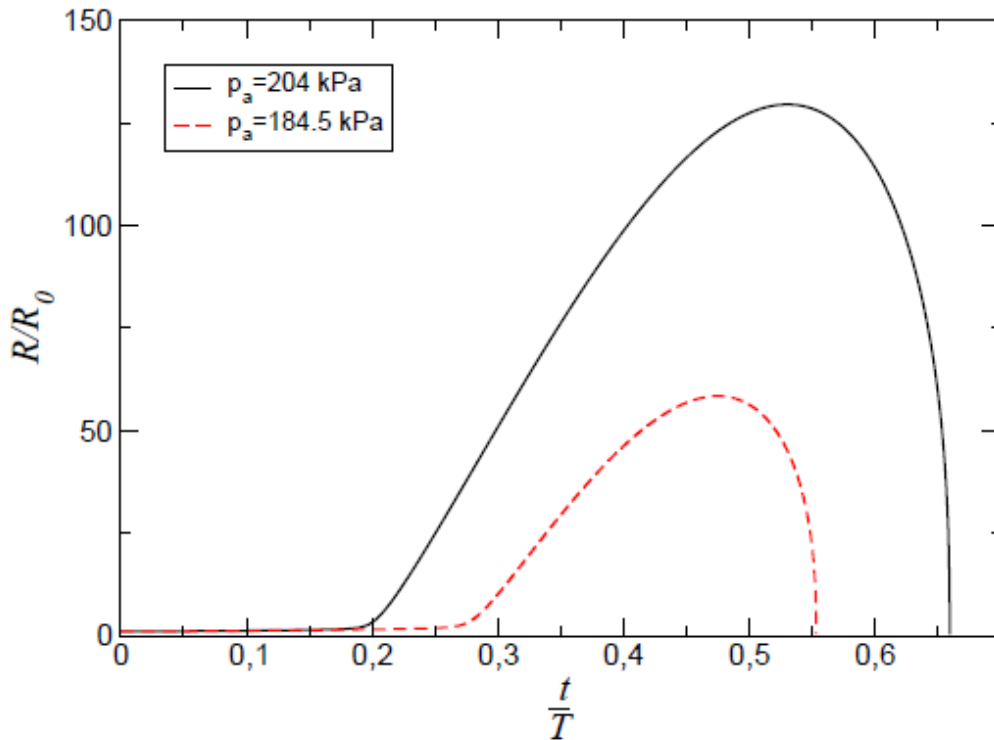


Figure 3.5: Bubble radius expansion with an initial diameter of $1.5 \mu m$ and wave frequency of 20 kHz [106]

The equation relates to the evolution of the acoustic cavitation bubble radius concerning the time when the bubble is exposed to an external ultrasound wave source. Jamshid et al. [106] have reported the collapse of a bubble with an ambient diameter of 1.5 μm for two different acoustic pressure amplitudes at an ultrasonic frequency of 20 kHz. It is supposed that after the collapse of a bubble at higher pressures, it is fragmented into smaller bubbles. The higher the value of the pressure, the higher the number of children produced by the initial nuclei. Due to the lack of sufficient knowledge about the physical background, a linear function is applied here for this proportionality, and the method of its application is described. While the chemical kinetics model is concerned with the possible dissociation reaction mechanism of the water vapor trapped inside a single bubble, both models are combined. The following is a detailed description. The radial dynamics of a spherical bubble saturated with vapor gas trapped inside and oscillating due to an outer ultrasonic wave's exposure is a non-linear ordinary differential equation. The equation described as Keller & Miksis equation [107], and is written as follows:

$$\left(1 - \frac{\dot{R}}{c}\right)\dot{R}\ddot{R} + \frac{3}{2}\left(1 - \frac{\dot{R}}{3c}\right)\dot{R}^2 = \frac{1}{\rho_L}\left(1 + \frac{\dot{R}}{c} + \frac{R}{c}\frac{d}{dt}\right)\left[p - p_\infty - \frac{2\sigma}{R} - 4\mu\frac{\dot{R}}{R} + p_A \sin(2\pi ft)\right] \quad (3.30)$$

where R is the bubble radius, \dot{R} , \ddot{R} are the first and second derivatives of the radius R concerning time. ρ_L is the density of the liquid medium, c is the speed of sound, p is pressure inside the bubble, p_∞ is the ambient static pressure of the medium surrounded the bubble, σ is the surface tension, μ is the liquid viscosity, f is the ultrasonic frequency, and p_A is the acoustic pressure amplitude obtained from the acoustic intensity I_A , and it is written as follows:

$$I_A = \frac{p_A^2}{2\rho_L c} \quad (3.31)$$

The gas model is assumed as adiabatic. The adiabatic collapse model is adopted by Rashwan et al. [108,109], and Merouani et al. [29,57] would lead to hot spot temperature. Moreover, at any instantaneous point during the adiabatic phase, the pressure inside the bubble calculated from knowing the bubble size using:

$$p = \left[p_v + p_{go} \left(\frac{R_0}{R_{max}} \right)^3 \right] \left(\frac{R_{max}}{R} \right)^{3\gamma} \quad (3.32)$$

$$T = T_\infty \left(\frac{R_{max}}{R} \right)^{3(\gamma-1)} \quad (3.33)$$

where p_v is the vapor pressure, and p_{g0} is the gas pressure in the bubble at its ambient state ($R = R_0$). R_0 is the ambient bubble radius, T_∞ is the bulk liquid temperature, R_{max} is the maximum radius of the bubble, and $\gamma = 1.4$ is the ratio of the specific heats capacities (C_p/C_v).

$$p_{g0} = p_\infty + \left(\frac{2\sigma}{R_0}\right) - p_v \quad (3.34)$$

The maximum bubble pressure P_{max} and bubble temperatures T_{max} will be reached at the collapse phase at which the chemical kinetics model starts and are written as follows:

$$p_{max} = \left[p_v + p_{g0} \left(\frac{R_0}{R_{max}}\right)^3 \right] \left(\frac{R_{max}}{R_{min}}\right)^{3\gamma} \quad (3.35)$$

$$T_{max} = T_\infty \left(\frac{R_{max}}{R_{min}}\right)^{3(\gamma-1)} \quad (3.36)$$

An empirical correlation is determined by Mason and Lorimer [110] to correlate the maximum bubble radius in terms of the frequency and the acoustic pressure amplitude as follows:

$$R_{max} = (3 \times 10^3 / f)(P_A - 1)(P_A)^{-1/2} [1 + 2(P_A - 1)/3]^{1/3} \quad (3.37)$$

where P_A is the acoustic pressure amplitude in atm, and f is the frequency in kHz. Colussi et al. [79] verified this correlation in sonochemistry's chemical bubble dynamics in 1998. Moreover, Yasui et al. [50] has classified the regions of the acoustic cavitation bubble in regard to the ultrasonic frequency, acoustic amplitude, and the ambient bubble radius (f , P_A , R_0). The figure is presented at an ultrasonic frequency of 20 kHz. Assuming a acoustic amplitude of 0.1 MPa and an ambient bubble radius of 1.5 μm , the bubble will be located in the dissolving bubbles zone. In order to move from the dissolving bubbles zone to a stable bubble zone, it can be by either increasing the acoustic amplitude, in accordance with the below diagram. In addition, by comparing the phase diagrams at different ultrasonic frequencies, namely 20 kHz and 140 kHz as seen in Figure 3.6 (a) and (b), respectively. It can be seen that the unstable bubble zone where the bubble goes under explosive conditions, is reduced, giving a smaller room for the acoustic operating conditions that leads to an explosive bubble. The degas bubbles zone has been increased while leaving the dissolving bubble region with almost no change. In conclusion, the dynamic bubble model depends on the applied acoustical parameters such as the acoustic amplitude and the ultrasonic frequency. The bubble dynamics model's output parameters, such as the bubble maximum pressure and temperature, will be used in the following chemical kinetics model. The next section will focus on the chemical kinetics model of the sonohydrogen process.

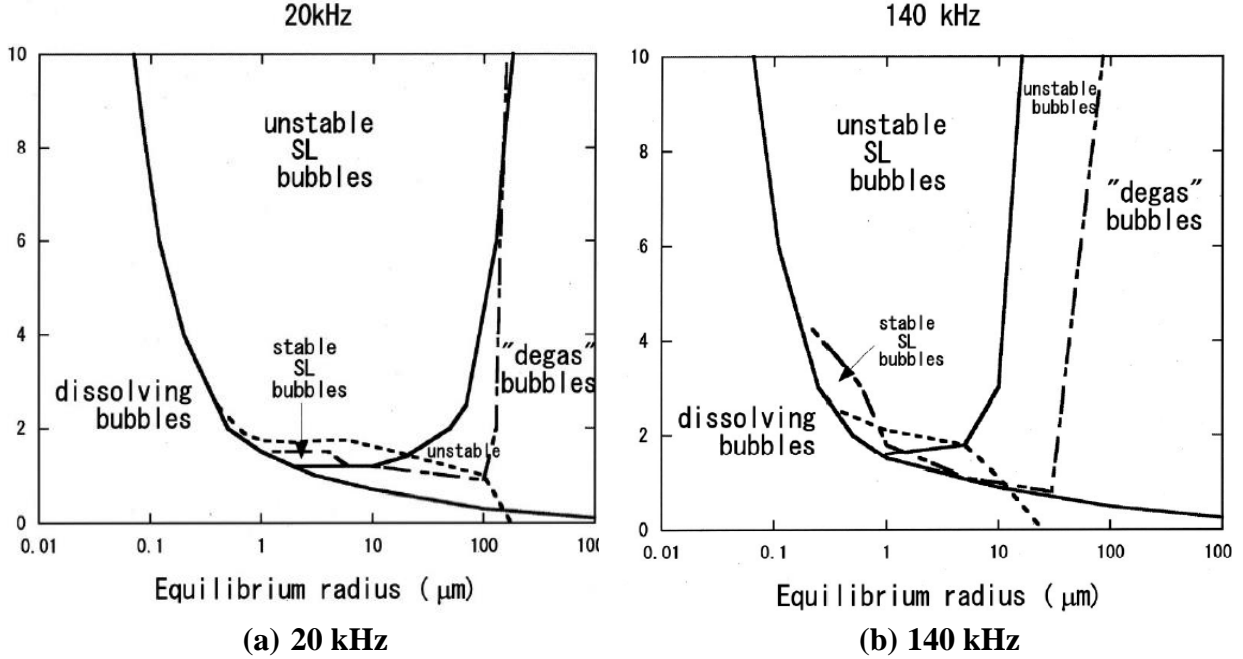


Figure 3.6: The regions for each category of bubbles in terms of the ambient radius R_0 and acoustic amplitude P_A when exposed to ultrasonic frequency of 20 kHz [50]

3.3 Chemical Kinetics Modeling

The bubble is acting as a micro combustion reactor at which a series of chemical reactions are taking place. The Chemical Species Transport module in COMSOL Multiphysics 5.4 is used with the Reaction Engineering approach submodule to investigate the chemical kinetics. For a bubble initially containing H_2O/O_2 and, a chemical kinetic mechanism consisted of 19 reversible chemical reactions where the reaction formulas described in Table 3.2. All chemical reactions are reversible, and the general equation of the reaction rate written as follows:

$$\frac{dc_j}{dt} = R_j = \nu_j r \quad (3.38)$$

where C_j is the molar concentration of the j th species, R_j is the rate of reaction of species j concerning time t , and the stoichiometric coefficient of species j is ν_j . The rate of reaction r_i of the i th reaction is given by the difference of the forward rates subscripted by (react) and the reversible rates subscripted by (prod) and can be written as follows:

$$r_i = k_i^f \prod_{j \in \text{react}} C_j^{-\nu_j} - k_i^r \prod_{j \in \text{prod}} C_j^{-\nu_j} \quad (3.39)$$

The forward and reverse rate constants used with the Arrhenius expressions written as follows:

$$K_{fi} = A_{fi} \left(\frac{T}{T_{ref}} \right)^{b_{fi}} \exp \left(-\frac{Ea_{fi}}{R_g T} \right) \quad (3.40)$$

$$K_{ri} = A_{ri} \left(\frac{T}{T_{ref}} \right)^{b_{ri}} \exp \left(-\frac{Ea_{ri}}{R_g T} \right) \quad (3.41)$$

where R_g is the universal gas constant $8.314 \text{ J}/(\text{mol}\cdot\text{K})$, A_{fi} and A_{ri} are the pre-exponential factors, b_{fi} and b_{ri} are the temperature exponent and the Ea_{fi} and Ea_{ri} are the activation energies for the forward and reversible reactions. These values are obtained from the utilization of multiple experimental data to find the Arrhenius parameters attained from the NIST Chemical Kinetics Database [111]. The ‘‘Reaction Engineering’’ module in COMSOL Multiphysics will require the ‘‘species thermodynamic expressions for each species during the setup. Therefore, each species should be identified separately by importing the thermodynamics data file previously reported by NASA [112]. The Species Thermodynamic Expressions are given as follows:

$$C_{p_j} = R_g (a_1 + a_2 T + a_3 T^2 + a_4 T^3 + a_5 T^4) \quad (3.42)$$

$$h_j = R_g \left(a_1 T + \frac{a_2}{2} T^2 + \frac{a_3}{3} T^3 + \frac{a_4}{4} T^4 + \frac{a_5}{5} T^5 + a_6 \right) \quad (3.43)$$

$$s_j = R_g \left(a_1 \ln \left(\frac{T}{T_0} \right) + a_2 T + \frac{a_3}{2} T^2 + \frac{a_4}{3} T^3 + \frac{a_5}{4} T^4 + a_7 \right) \quad (3.44)$$

where the NASA polynomial coefficients supplied in thermodynamic are a_{1-7} . The first 7 numbers starting on the second line of each species entry are the seven coefficients (a_1 through a_7 , respectively) for the high-temperature range (above 1000 K, the upper boundary specified on the first line of the species entry). The following seven numbers are the coefficients (a_1 through a_7 , respectively) for the low temperature range (below 1000 K, the lower boundary specified on the first line of the species entry). All thermodynamic constants are given in [112], which is easily imported to COMSOL in the Thermo data input under the thermodynamics properties and reported in Table 3.3. These constants are used to determine the specific heat, enthalpy, and entropy for each species (i) to obtain the thermodynamic reaction properties that are given as follows:

$$H_j = \sum_{j \in prod} (v_j j) h_j - \sum_{j \in react} (-v_j j) h_j \quad (3.45)$$

$$S_j = \sum_{j \in prod} (v_j j) s_j - \sum_{j \in react} (-v_j j) s_j \quad (3.46)$$

$$Q_j = -r_j H_j \quad (3.47)$$

The reaction kinetics mechanism is given in Table 3.2, and all chemical reaction data obtained from previous kinetic data for combustion and sonolysis. For example, Hart and Henglein [113] studied the sonochemistry approach, while the combustion of a mixture consisting of

hydrogen/oxygen is taking place in cavitation bubbles. When the reaction kinetics mechanism starts, the dissociation of H_2O takes place, and highly reactive radicals such as OH, H, O, HO_2 are formed in the bubble as well as hydrogen peroxide H_2O_2 as a by-product. Thus, the composition of the all formed species is estimated at different bubble temperatures by the reactions system's computer simulation.

Table 3.2: Ultrasonic H_2 -production chemical kinetic model inside an O_2 cavitation bubble. M is the third body species. Subscript (f) denotes the forward and (r) denotes the reverse reactions

	Reactions	A_f	b_f	E_{af}	A_r	b_r	E_{ar}	Ref.
1	$H_2O + M \leftrightarrow H^* + ^*OH + M$	1.9E23	-1.83	1.1E5	2.2E22	-2.00	0.00	Misik and Riesz [114] Hart and Henglein [115]
2	$O_2 + M \leftrightarrow O + O + M$	4.5E17	-0.64	1.2E5	6.2E15	-0.50	0.00	Kamath et al. [116]
3	$^*OH + M \leftrightarrow O + H^* + M$	9.8E17	-0.74	1.02E5	4.7E18	-1.00	0.00	Didenko and Pugach [117]
4	$H^* + O_2 \leftrightarrow O + OH$	1.9E14	0.00	1.65E4	5.5E11	0.39	-2.9E2	Ashokkumar et al. [118]
5	$H^* + O_2 + M \leftrightarrow HO_2 + M$	1.5E12	0.60	0.00	3.1E12	0.53	4.9E4	Leighton [51]
6	$O + H_2O \leftrightarrow ^*OH + ^*OH$	2.9E6	2.02	1.3E4	1.5E5	2.11	-2.9E3	Lofstedt et al. [119]
7	$HO_2 + H^* \leftrightarrow H_2 + O_2$	1.6E13	0.00	8.2E2	3.2E12	-0.35	5.5E4	Wu and Roberts [120]
8	$HO_2 + H^* \leftrightarrow ^*OH + ^*OH$	7.1E13	0.00	2.95E2	2.0E10	0.72	3.7E4	Hua and Hoffman [121]
9	$HO_2 + O \leftrightarrow ^*OH + O_2$	3.2E13	0.00	0.00	3.25E12	0.33	5.3E4	
10	$HO_2 + ^*OH \leftrightarrow H_2O + O_2$	2.9E13	0.00	-5E2	5.9E13	0.24	6.9E4	Baulch et al. [122]
11	$H_2 + M \leftrightarrow H^* + H^* + M$	4.6E19	-1.40	1.04E5	1.15E20	-1.68	8.2E2	Hart and Henglein [123]
12	$O + H_2 \leftrightarrow H^* + ^*OH$	3.8E12	0.00	8E3	2.67E4	2.65	4.9E3	Hua and Hoffman [121]
13	$^*OH + H_2 \leftrightarrow H^* + H_2O$	2.1E8	1.52	3.4E3	2.3E9	1.4	1.8E4	Lohse and Hilgenfeldt [124]
14	$H_2O_2 + O_2 \leftrightarrow HO_2 + HO_2$	4.6E16	-0.35	5.06E4	4.2E14	0.00	1.2E4	Flynn [125]
15	$H_2O_2 + M \leftrightarrow ^*OH + ^*OH + M$	2.9E14	0.00	4.8E4	1.E14	-0.37	0.00	Rayleigh [126]
16	$H_2O_2 + H^* \leftrightarrow H_2O + ^*OH$	2.4E13	0.00	3.9E4	1.3E8	1.31	7.1E4	Naidu et al. [127]
17	$H_2O_2 + H^* \leftrightarrow H_2 + HO_2$	6.0E13	0.00	7.9E3	1.0E11	0.70	2.4E4	Tsang and Hampson [128]
18	$H_2O_2 + O^* \leftrightarrow ^*OH + HO_2$	9.55E6	2.00	3.9E3	8.7E3	2.68	1.8E4	Sochard et al. [129]
19	$H_2O_2 + ^*OH \leftrightarrow H_2O + HO_2$	1.0E12	0.00	0.00	1.8E10	0.59	3E4	Colussi et al. [79]

Where A is the pre-exponential factor, B is the exponential temperature factor, activation energy E_a . For two species reaction, A is in $cm^3 mol^{-1} s^{-1}$, For three species reaction, A is in $cm^6 mol^{-2} s^{-1}$.

Table 3.3: NASA polynomial coefficients for the species thermodynamic expressions to be used in the expressions of specific heat at constant pressure, enthalpy, and entropy.

Species	H_2O	H	OH	O_2	O	HO_2	H_2	H_2O_2	AR
T_{low} [K]	200	200	200	200	200	200	200	200	300
T_{mid} [K]	1000	1000	1000	1000	1000	1000	1000	1000	1000
T_{high} [K]	3500	3500	3500	3500	3500	3500	3500	3500	5000
$a_{low,1}$ [1]	4.2	2.5	3.99	3.78	3.16	4.30	2.34	4.27	2.5
$a_{low,2}$ [1/K]	-0.002	7.05E-13	-0.0024	-0.003	-0.003	-0.004	0.008	-5.42E-4	0
$a_{low,3}$ [1/K ²]	6.52E-6	-1.99E-15	4.61E-6	9.85E-6	6.64E-9	2.11E-5	-1.95E-5	1.67E-5	0
$a_{low,4}$ [1/K ³]	-5.48E-9	2.30E-18	-3.88E-9	-9.68E-9	-6.12E-9	-2.42E-8	2.01E-8	-2.16E-8	0
$a_{low,5}$ [1/K ⁴]	1.77E-12	-9.2E-22	1.36E-12	3.24E-12	2.11E-12	9.2E-12	-7.3E-12	8.62E-12	0
$a_{low,6}$ [K]	-30293.72	25473.65	3615.08	-1063.95	29122.25	294.80	-917.93	-17702.8	-745.7
$a_{low,7}$ [1]	-0.84903	-0.44	-0.104	3.65	2.05	3.72	0.68	3.43	4.36
$a_{high,1}$ [1]	3.0339	2.5	3.09	3.28	2.56	4.02	3.33	4.165	2.5
$a_{high,2}$ [1/K]	0.002	-2.3E-11	5.48E-4	0.00148	-8.59E-5	0.002	-4.94E-5	0.005	0
$a_{high,3}$ [1/K ²]	-1.64E-7	1.61E-14	1.26E-7	-7.58E-7	4.19E-8	-6.34E-7	4.99E-7	-1.9E-6	0
$a_{high,4}$ [1/K ³]	-9.70E-11	-4.74E-18	-8.8E-11	2.09E-10	-1.0E-11	1.14E-10	-1.79E-10	3.71E-10	0
$a_{high,5}$ [1/K ⁴]	1.68E-14	4.98E-22	1.17E-14	-2.16E-14	1.22E-15	-1.1E-14	2.00E-14	-2.87E-14	0
$a_{high,6}$ [K]	-30004.29	25473.66	3858.657	-1088.46	29217.58	111.856	-950.16	-17861.8	-745.35
$a_{high,7}$ [1]	4.9667	-0.45	4.47	5.45	4.78	3.78	-3.20	2.92	4.36

3.4 Modeling Procedure

This section will present the modeling process in a straightforward step-by-step procedure, including both the bubble dynamics and the chemical kinetics models. We will begin with the assumptions made for the bubble dynamics model. It includes the following: the acoustic intensity assumed to be constant, the ambient pressure and temperature assumed to be constant, the vapor trapped inside the bubble assumed to be an ideal gas, and the gas model considered adiabatic. Additionally, since the acoustic bubble radius varies with the acoustic pressure amplitude derived from the Keller & Miksis equation, the linear function is assumed to change the bubbles' number with the pressure. The most important boundary conditions that have to be specified based on previous literature observations are the ultrasonic frequency, initial bubble radius, and acoustic pressure amplitude. All boundary conditions have been chosen based on literature reports. The ultrasonic frequency used is 20 kHz, and the acoustic amplitude is 0.1 MPa as per Burdin et al. [130] and Tsochatizidis et al. [131]. The range of the initial bubble radius reported by those authors ranges between 1-25 μm . Recent and old numerical simulations have reported boundary conditions within this range. For example, in 1998, Colussi et al. [79], $R_0 = 2 \mu m$, 20 kHz, $P_A = 2 atm$. In 2015, Merouani et al. [29] studied the acoustic bubble characteristics at 20 kHz and $R_0 = 7.5 \mu m$ and 20 kHz, $R_0 = 7.5 \mu m$. I have selected 1.5 μm in my simulation to be conservative. The modeling procedure performed as follows:

1. Solving the radial bubble dynamics by solving the non-linear second-order ordinary differential Keller & Miksis equation using the built-in Matlab Function “ode45 function”, the physical, acoustic, and thermodynamics input parameter are given in Table 3.4. Additionally, the ODE solver is the Runge-Kutta 4-5 solver, while the initial conditions: $t = 0, R(0) = R_0$ and $\dot{R}(0) = 0$.
2. Solving the variation of pressure and temperature inside the bubble by Matlab.
3. Solving for the bubble radius concerning the time by Matlab.
4. Solving the chemical kinetics model, knowing that started at the beginning of the adiabatic phase, or when the bubble radius reaches its maximum value. Therefore, the chemical kinetics mechanism is solved using the chemical Engineering module of COMSOL Multiphysics using the pressure, temperature, and maximum radius ($R = R_{max}$ obtained from the first three steps while solving the bubble dynamics model).

Table 3.4: The physical, acoustical, thermodynamic input parameters

R_0 [μm]	1.5
f [kHz]	20
p_∞ [kPa]	101.325
p_A [MPa]	0.1
p_v [kPa]	2.33
γ	1.4
μ [$\text{Pa}\cdot\text{s}$]	0.001
σ [N/m]	0.0725
ρ_L [kg/m^3]	1000
c [m/s]	1500

At these set of conditions, it leads to a specific variation of R, T, and P with respect to time. Based on the maximum bubble temperature, the chemical kinetics mechanism is solved. The value of the maximum bubble temperature is necessary to solve the chemical kinetics model, therefore, a set of temperatures are assumed and investigated, namely, 2000, 4000, 6000, 8000, and 10000 K. Based on these temperatures, the hydrogen production is estimated, and quantified. As the bubble temperature increases, all species' reaction rate increases due to the water vapor's dissociation trapped inside the bubble. Some input parameters are required to solve this chemical reaction mechanism, including the initial concentrations of water vapor/oxygen and the maximum pressure and temperature at which the bubble collapse and chemical reaction will start. These parameters are obtained by solving the Keller-Miksis equation for bubble dynamics. Hence, all species' concentration at the end of the bubble collapse is quantified at the maximum temperature. It is very challenging to conduct experimental evidence for the chemical kinetics mechanism because of two reasons. The first reason is the short reaction time that undertook in microseconds μs . Simultaneously, the second reason is that the highly reactive radicals are produced and combined quickly. However, the chemical kinetics module compared to a corresponding numerical work from the literature.

Chapter 4. Results and Discussion

In this chapter, the developed numerical tool's guideline is discussed to simulate the sonoreactor model's characteristics and the sonochemical process for hydrogen production. The following studies are considered; the grid independency study, model validation study, and parametric study considering the change of the ultrasonic frequency, probe diameter, probe immersion depth, ultrasonic intensity, acoustic streaming, and solution for the chemical kinetics mechanism.

4.1 Acoustic Modeling Results

In this work, three design configurations of a sonoreactor are considered under various operating conditions. The acoustic characteristics are investigated during water sonication while using an immersed-type ultrasonic flat transducer probe in a sonoreactor model. Numerical models are also developed to simulate the sonication process, and they are successfully validated and compared with available data in the literature. Several sets of numerical investigations are conducted using the finite-element method and solved by the computational acoustics module in the COMSOL Multiphysics. The acoustical and geometrical parameters' effect is considered, analyzed, and reported, including the ultrasonic frequency, acoustic intensity, and the reactor's scaling-up. The present results include a parametric study examining the change of the ultrasonic frequency, intensity, and probe immersion depth on the performance.

4.1.1 Mesh independency study

Mesh independency study is conducted for both the 2-D geometry and the 3-D geometry to assure that the results are independent of the mesh size. The triangular mesh is automatically generated in the 2-D model. In contrast, the tetrahedral mesh is generated in 3-D using the built-in facility of COMSOL based on the selected physics, including the pressure acoustic frequency domain interface and the laminar flow-interface with gravity. The 2-D computational domain is examined with a different number of elements based on different mesh sizes. Four different mesh sizes are generated, namely, the fine-mesh (4568 elements), finer-mesh (10168 elements), extra-fine mesh (23464 elements), and extreme-fine mesh (49488 elements). Figure 4.1 presents the grid-independency study results while comparing four different mesh elements. The results show that there are no significant differences among all mesh elements. Therefore, the intermediate mesh elements 23.5k are used in this study to save computational power and time.

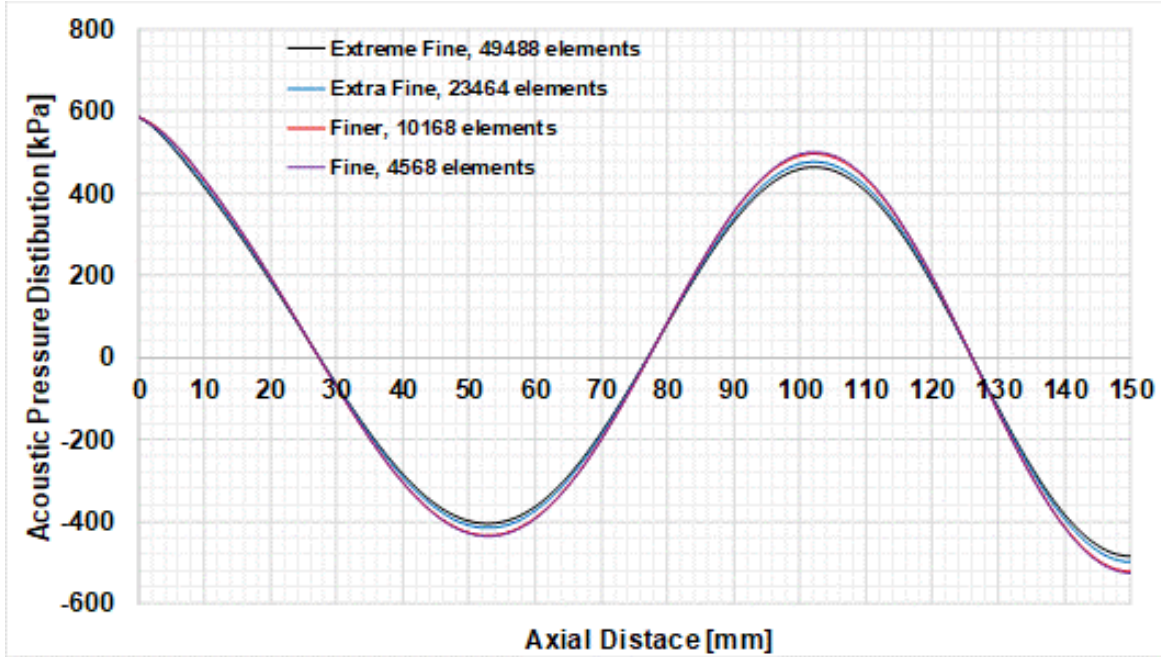


Figure 4.1: Grid independency study at different number of elements, where $f = 20 \text{ kHz}$

Accordingly, the 3-D domain is built to check mesh accuracy and quality. A grid independence study is carried out following the same procedure used with the 2-D domain to eliminate the mesh size effect on the results. Different meshes are used with different densities, namely, finer mesh 12345 elements, extra-fine mesh 48697 elements, and the extremely fine mesh 263273 elements. It is found that any further increase in the mesh density would not alter the results. As a result, the extra fine mesh is used with 48697 elements that are chosen to continue the simulation study. In general, the maximum mesh size should be less than $1/8$ of the wavelength.

4.1.2 Acoustic model validation

The validation study is carried out to ascertain the accuracy of the proposed model. A finite element model FEM is developed to give access to the acoustic pressure field distribution inside the sonoreactor. The acoustic frequency domain model is solved using COMSOL 5.4 software by a Dell workstation with 72.0 GB RAM and Xeon 2.80 GHz processor. As previously illustrated in the computational domain section, the geometrical and operational parameters have been obtained from the experimental work reported by Gogate et al. [49]. The operating parameters are summarized as follows: the ultrasound frequency of 20 kHz and acoustic power of 36 W. They have carried out measurements for the acoustic pressure amplitude using a movable hydrophone

in the axial direction from the ultrasonic transducer probe tip to the bottom of the liquid water container with an interval of 1 cm taking up to 14 different readings. Hence, the current numerical model's acoustic pressure distribution is compared with its correspondents obtained from the experimental measurements. They investigated the mapping and experimental verification of sonochemical reactors. The input parameters for the validation study are found in Table 4.1. The comparison is drawn with the previous experimental study considering the acoustic pressure distribution along the centerline of the sonoreactor, as seen in Figure 4.2. The solid-black line with red-diamond markers denotes the experimental pressure amplitude measurement by the hydrophone. In contrast, the dashed-blue line denotes the present numerical study in the 2-D domain, and the thin-orange line indicates the present research study in the 3-D domain. The comparison results show that the present 2-D and 3-D models are such a spitting image. Both of them give an excellent agreement with the experimental work regarding the acoustic pressure values and profile.

Table 4.1: The experimental parameters used by Gogate et al. [49]

Input parameter	Value
ρ_0 [kg/m ³]	998
C_0 [m/s]	1498
Frequency [kHz]	20
Ultrasound power, P_{US} [W]	36
Transducer probe diameter [mm]	20
Intensity [kW/m ²]	114.65
Pressure amplitude, P_0 [kPa]	585.49

Furthermore, an error analysis shows that the maximum error takes place at a point of 2.0 cm away from the probe and a minimum error at a point 10 cm away from the probe surface. It is noticed that the difference between the present numerical study and the experimental measurement is found because of two reasons. The primary reason is that measurement close to the transducer probe tip is challenging. When the hydrophone is inserted close to the tip, it will interfere with ultrasonic waves and liquid processing. Another reason is that the numerical study did not consider the hydrogen bubble clouds that are very concentrated near to the transducer tip, which is regarded as another sort of acoustic pressure destruction. Moreover, based on the ultrasonic frequency of 20 kHz, the calculated wavelength is $\lambda = 7$ cm, a huge error is expected in the measurements due to the interval of the measurements and the probe size.

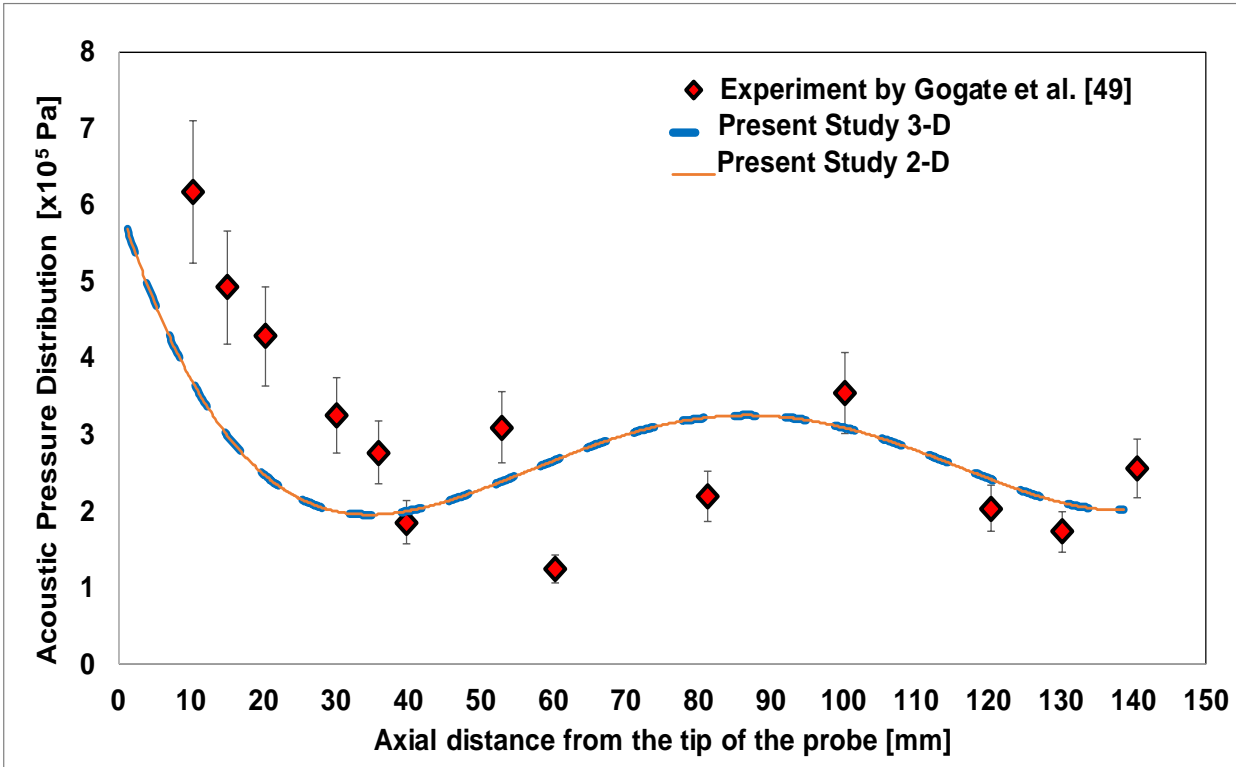


Figure 4.2: Validation of the numerical model with experimental results by Gogate et al. [49]

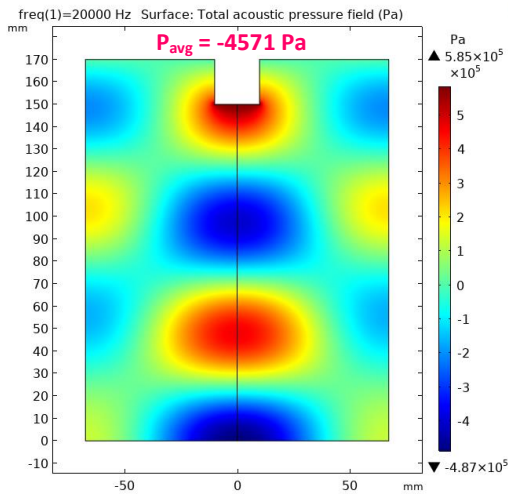
To examine the model accuracy, the 3-D model is build up and analyzed in terms of the total acoustic pressure distribution. Surprisingly, the 3-D domain results did not show any changes in the acoustic pressure values compared to the results of the 2-D domain. This is ascribed to the strong coupling between the flow and sound fields. It appears that at 20 kHz frequency coincides with the 3rd mode of an acoustic resonance frequency, and hence the flow will reorganize itself to eliminate any three-dimensional effect [132,133]. The maximum pressure field intensity is found to be 5.85×10^5 Pa that is located in the region close to the transducer tip. In contrast, the minimum pressure field intensity is found to be -4.85×10^5 Pa for both the 2-D and 3-D domains, where the speed of sound is around 1500 m/s. Note that the sound pressure will be maximum and minimum in the same location [134]. Consequently, the 2-D domain is selected to continue the study to save computational time and cost.

4.2 Effect of Acoustical/Operational Parameters

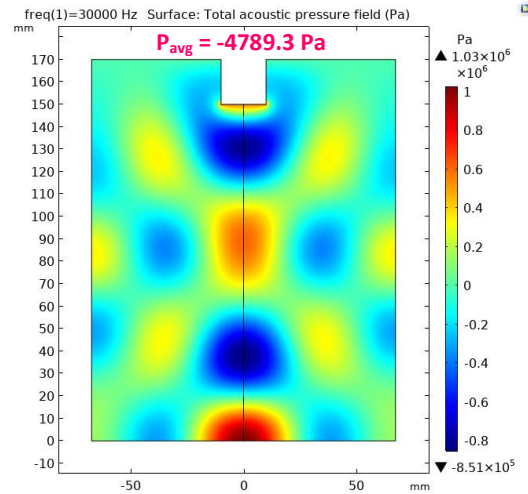
The effect of the operational and acoustical parameters such as the ultrasonic frequency, acoustic intensity, and probe immersion depth are investigated in the following sections.

4.2.1 Effect of ultrasonic frequency

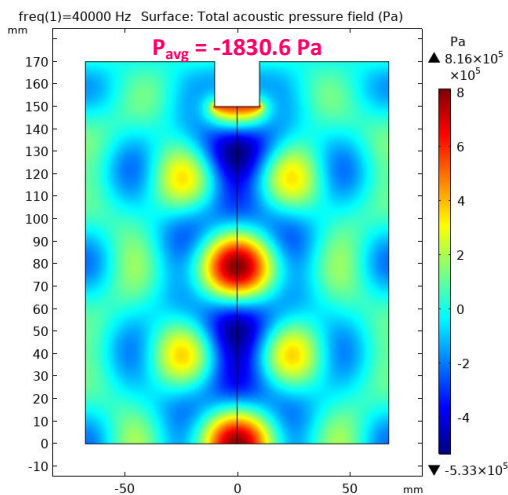
In this section, the results obtained from the numerical simulations are presented, including the acoustic pressure contours at 20 kHz frequency and ultrasonic intensity of 36 W, and the effect of ultrasonic frequency. It is noticed that the amount of hydrogen produced from such a process is considered highly frequency-dependent as it is the most critical parameter in the Sono-hydrogen process [3]. The ultrasonic frequency range to produce the acoustic cavitation bubbles is between 20-100 kHz [110,135,136]. The impact of the ultrasonic frequency on the sonoreactor performance is represented in Figure 4.3. The results reveal that increasing the ultrasound frequency alters the periodic time and the corresponding carrier signal wavelength and alters the reflected waves' phase from the hard wall boundaries. Simultaneously, at the same acoustic intensity of 36 W, the ultrasonic frequency change alters the acoustic pressure range and the wave interactions. We are concluding that modifying the ultrasonic frequency at the same acoustic intensity will significantly alter the maximum and minimum acoustic pressure inside the sonoreactor. For instance, as seen in Figure 4.3, at 20 kHz, the maximum and minimum pressures are $-4.87E5$ and $5.85E5$ Pa, respectively. At 70 kHz, the maximum and minimum pressures are $-8.41E6$ and $7.47E6$ Pa. The difference between the maximum and minimum pressures at 70 kHz is much higher than their correspondence at 20 kHz. The minimum and maximum pressure at various ultrasonic frequencies for the sonoreactor are presented in Figure 4.4. As the ultrasonic frequency increases, a higher amplitude of negative pressure will be obtained. At low ultrasonic frequency in the range of 20-50 kHz, the minimum pressure appears to alter insignificantly; however, in the range of 55-80 kHz, the minimum pressure sharply decreases, which will allow more hydrogen bubbles to be created. Thus, more hydrogen will be produced. At this range of frequency, the hydrogen bubble will have more time to expand and enlarge. This would allow more water vapor to be trapped inside the bubble core. The unstable zone can be defined as the zone at which the acoustic cavitation bubbles will not be generated at different frequencies based on the maximum and minimum pressures estimated inside the sonoreactor.



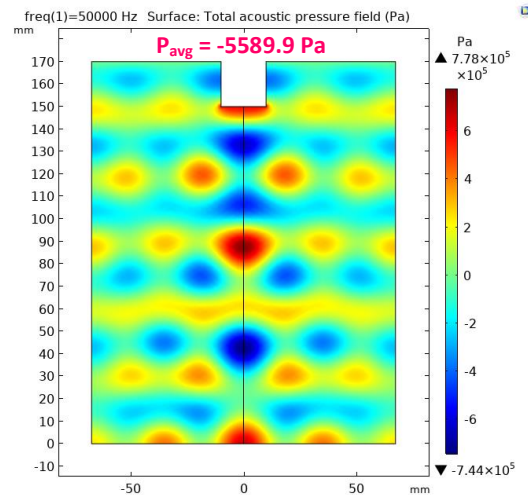
$f = 20 \text{ kHz}$, Max = $5.85 \text{ E}5$, Min = $-4.87 \text{ E}5$



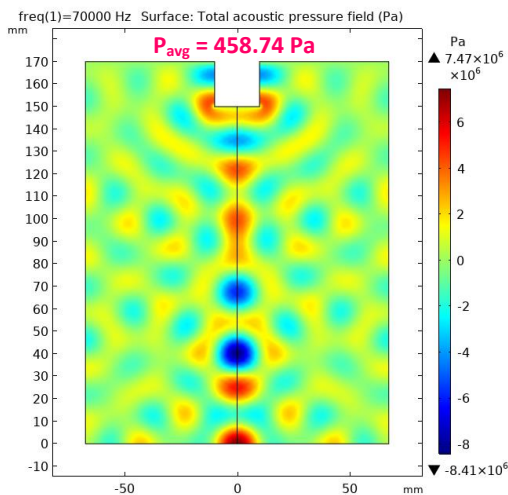
$f = 30 \text{ kHz}$, Max = $1.06 \text{ E}6$, Min = $-8.51 \text{ E}5$



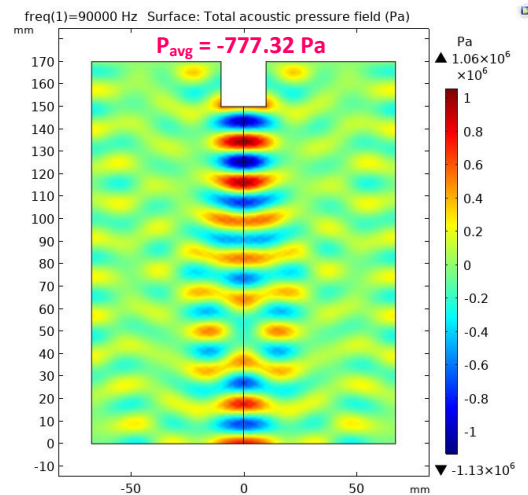
$f = 40 \text{ kHz}$, Max = $8.16 \text{ E}5$, Min = $-5.33 \text{ E}5$



$f = 50 \text{ kHz}$, Max = $7.78 \text{ E}5$, Min = $-7.44 \text{ E}5$



$f = 70 \text{ kHz}$, Max = $7.47 \text{ E}6$, Min = $-8.41 \text{ E}6$



$f = 90 \text{ kHz}$, Max = $1.06 \text{ E}6$, Min = $-1.13 \text{ E}6$

Figure 4.3: The effect of ultrasonic frequencies on the acoustic pressure distribution, the average pressure P_{avg} is taken over the volume

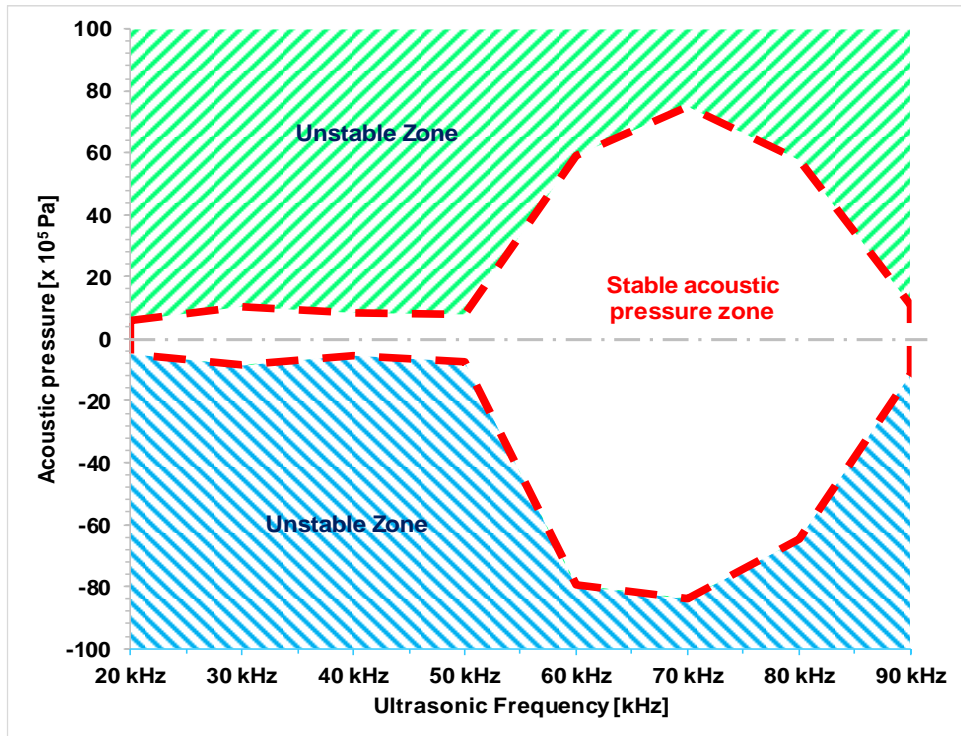


Figure 4.4: Acoustic pressure operating range at various ultrasonic frequencies for sonoreactor

As a result, the bubble collapse will be powerful and generate a higher pressure and temperature, which will promote the chemical reaction producing more radicals. Whereas, at higher frequencies than 80 kHz, the bubbles' response will be swift and fewer radicals will be generated because of the shortage of collapse time. Combining all these factors, we expect why the applied ultrasound frequency has a significant impact on the minimum pressure until it reaches an optimum point, then it goes down back. Figure 4.5 presents the acoustic pressure distribution at the centerline of the sonoreactor with various ultrasonic frequencies. It is emphasized that increasing the ultrasonic frequency will reduce the periodic time of the wave cycle. The higher the ultrasonic frequency, the lower the periodic time, and consequently, the shorter wavelength is expected. This might be taken negatively as the bubble will not have enough time to properly perform the collapsing mechanism.

4.2.2 Effect of acoustic power

The second primary important parameter is acoustic power. At the probe tip, the pressure boundary condition will be applied as pressure amplitude based on the calculation of acoustic power and intensity related by the probe area as per equation (3.6). The effect of changing the acoustic power

of the ultrasonic transducer probe is presented in Figure 4.6. As seen, the acoustic power enhancement reduces the minimum pressure, which will improve the cavitation process. Hence, more hydrogen bubbles will be generated. This is ascribed to the fact that increasing the acoustic power will increase the pressure amplitude leading to more sound pressure levels in the sonoreactor.

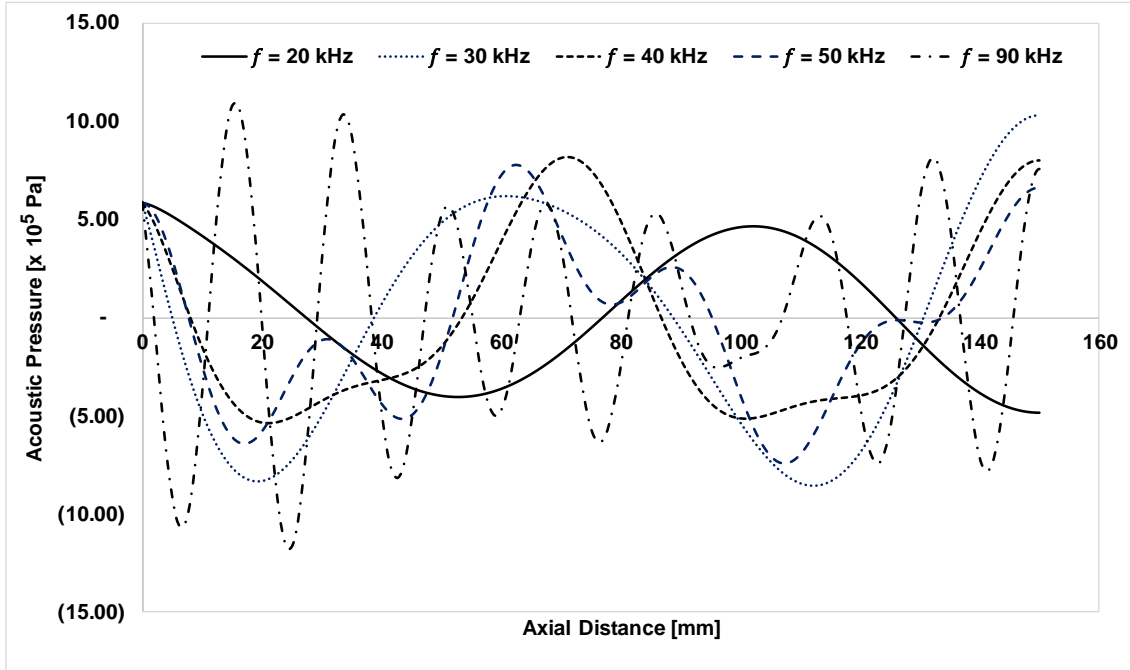


Figure 4.5: Axial acoustic pressure distribution at different frequencies

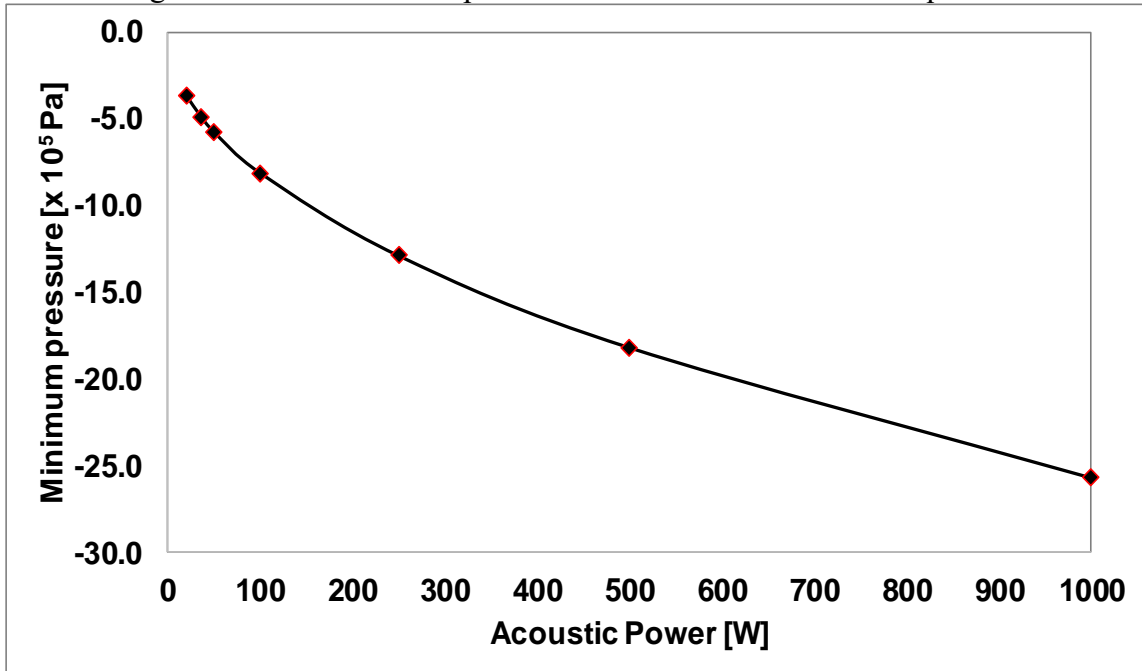


Figure 4.6: Minimum pressure at various acoustic power for sonoreactor

4.3 Effect of Geometrical Parameters

4.3.1 Effect of immersion depth

The probe immersion depth is also considered one of the essential geometrical parameters that affect sonoreactor performance significantly. The acoustic pressure of the fluid inside the sonoreactor is affected by changing the ultrasonic transducer depth. Therefore, this study investigates the effect of the transducer diameter on the sonoreactor performance. The effect of the probe immersion depth on acoustic pressure distribution in the sonoreactor is investigated, as shown in Figure 4.7. Generally, the stable acoustic pressure zone did not alter significantly by changing the transducer probe's depth. Surprisingly, the maximum pressure remains constant while the minimum pressure slightly fluctuates while increasing the immersion depth. This is because when the acoustic waves reflect off from the sonoreactor bottom walls, the reflected wave interferes with the incident wave, leading to either construction or destruction wave interference.

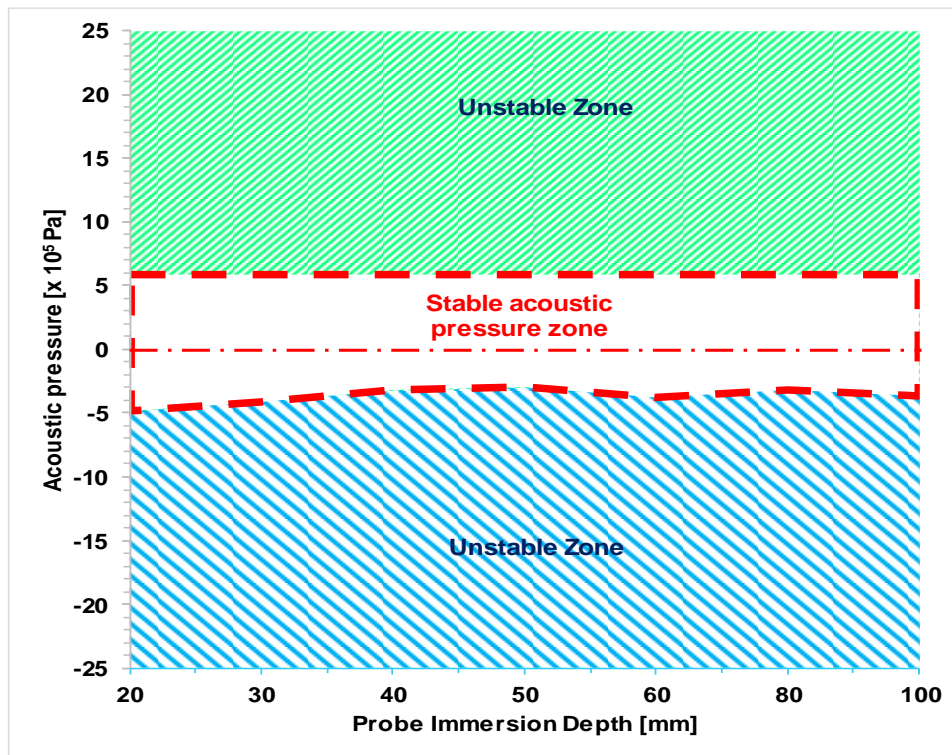


Figure 4.7: Effect of transducer immersion depth on the maximum/minimum acoustic pressure

For better illustration, Figure 4.8 presents the transducer probe immersion-depth effect on the acoustic pressure distribution. If there is a node on the sound-hard boundary, the acoustic pressure

amplitude will be enhanced because the reflected wave will add to the incident waves as seen at the end of the axial distance in the cases with an immersion depth of 50, 60, and 80 mm. On the other hand, if there is an antinode on the sound-hard boundary, the pressure antinode destroys the incident wave. It decreases the acoustic pressure as seen at the end of the axial distance in the cases that have an immersion depth of 20, 30, 40, and 100 mm, highlighting the need for complete and consecutive cycles to allow the formation of the acoustic cavitation bubbles.

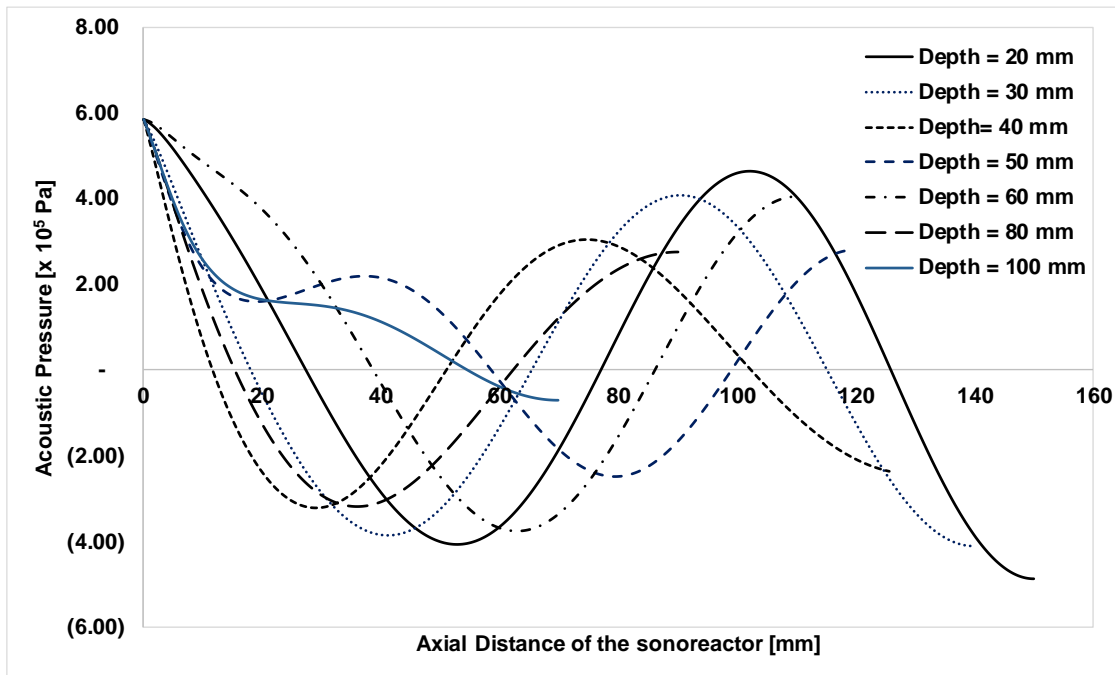


Figure 4.8: Effect of transducer immersion depth on the axial acoustic pressure distribution

4.3.2 Effect of scaling-up the sonoreactors

For commercialization, scaling-up the sonoreactor is of importance because it indicates the conventional performance and operation of the sonoreactor. Therefore, the effect of upscaling GEO.1 10 times on the acoustic pressure distribution is investigated. The sonoreactor is scaled up 10 times with the acoustic power source. Pre-calculation of the acoustic pressure amplitude should be done before upscaling the sonoreactor. It is because changing the diameter 10 times should reflect on the pressure amplitude. Both geometries are investigated at the same acoustic power of 36W. The acoustic pressure amplitude reduced from 585.49 kPa in case of a probe diameter of 20 mm to 117.1 kPa in a 100 mm diameter. The results showed that the peaks of pressure along the axis of the sonoreactor have a smaller magnitude in the case of the conventional sonoreactor as

compared to the lab-scale reactor. For example, as seen in Figure 4.9, the maximum amplitude of acoustic pressure is 5.85 E5 Pa for the lab-scale sonoreactor, while it shows 4.41 E5 Pa for the up-scaled sonoreactor, which is lower by 24.6%. Besides, the results showed a higher magnitude of the negative pressure in the case of conventional sonoreactor (sized 10 times bigger than GEO.1). However, the cavitation area is minimal that cannot sustain the bubble effectively. This finding has changed in the case of higher ultrasonic frequency.

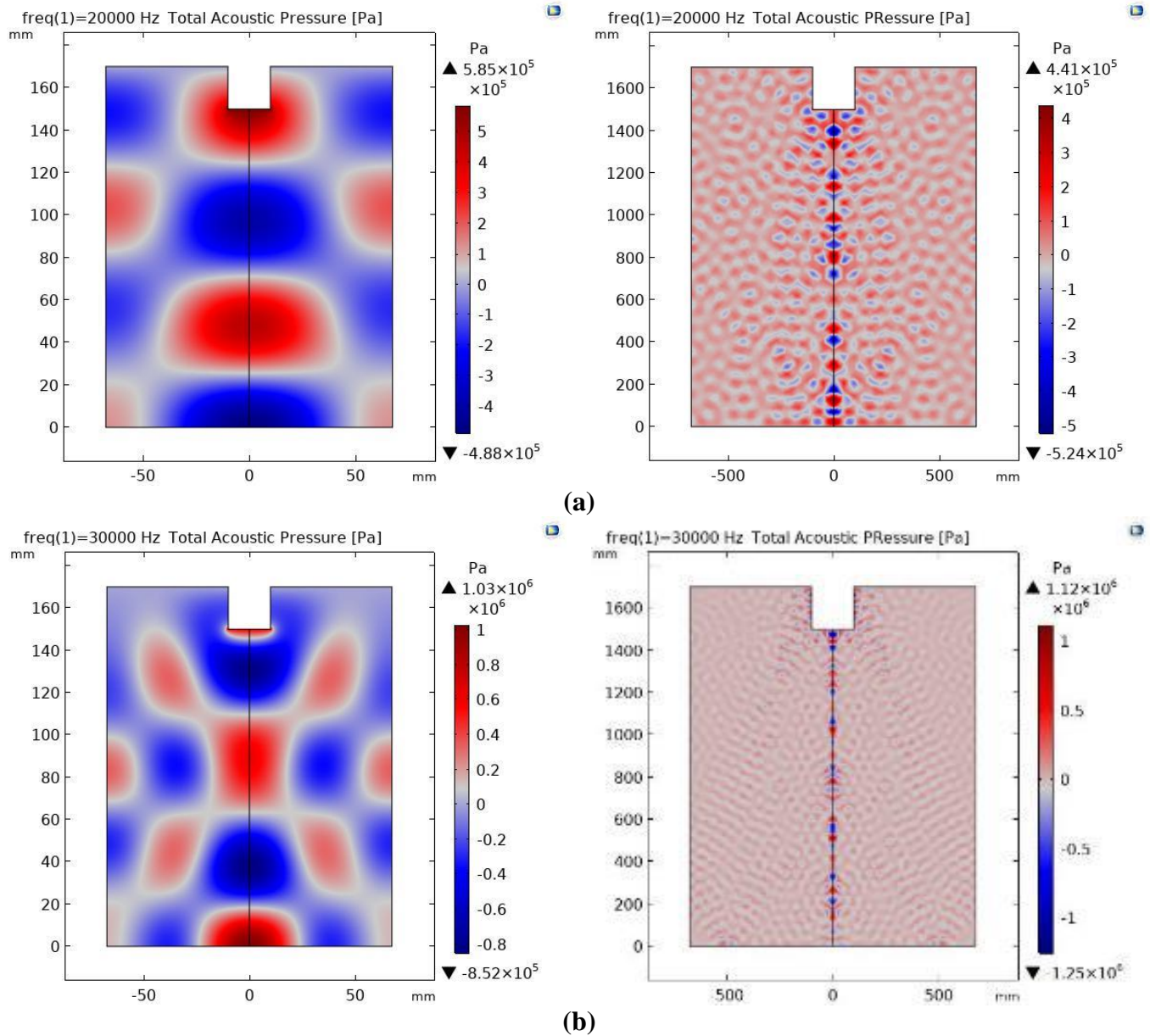


Figure 4.9: Pressure distribution in the mid-plane of the small-scaled GEO.1 (left) and 10-times scaled-up sonoreactor GEO.1 (right) at an ultrasonic frequency of (a) 20 kHz and (b) 30 kHz

The parametric study results show that the highest cavitation energy corresponds to the maximum magnitude of negative pressure that takes place in the range of 60 to 80 kHz. The cavitation energy analyses are conducted under 20 kHz of frequency and at 36 W input power. It is found that the cavitation energy of 15.87 W could produce 2.98×10^{-10} mol/J of sonochemical efficiency. Moreover, the effect of altering the transducer probe depth changes the acoustic pressure field insignificantly. A recommendation has been made to improve the sonochemical efficiency by introducing more considerable ultrasound input power while operating the sonoreactor at an ultrasonic frequency lower than 60 kHz. The results presented in this paper provide a comprehensive assessment of different sonoreactors and the feasibility of scaling-up their production rate.

4.3.3 Effect of probe diameter

In this section, the probe diameter's effect on GEO.1 is simulated, analyzed, and reported. The transducer probe diameter is also critical; thus, the study probes the diameter's influence on the sonoreactors' performance. Undoubtedly, altering the probe diameter will change the acoustic pressure amplitude. The acoustic pressure amplitude is required to set the pressure boundary condition P_0 at the probe tip concerning different probe diameters and the same acoustic intensity. The acoustical parameters at different ultrasonic transducer probe diameters are shown in Table 4.2.

The acceleration of the transducer tip in the axial direction can be given as $a_z = 4\pi^2 f^2 x$ [m/s²] which is reported by Rubinetti [94] in their recent numerical modeling study and validation concept for acoustic streaming induced by the ultrasonic transducer. This unique study sets the acoustic boundary condition for the sonotrode tip as axial acceleration. The Origin and derivation of such an equation can be found in Chapter 10, "Modeling energy in power ultrasound transducers," of the book entitled "Power Ultrasonics: Applications of High-Intensity Ultrasound" by Gallego and Graff [70]. The equation originates from the displacement equation along with the piezoelectric transducer, which is considered linear assuming Newtown's Law. The simulations reported in this book chapter give the acceleration as a function of the driving frequency under varying amplitudes levels and up to 80,000 m/s². Figure 4.10 (a) presents the max and mini acoustic-pressure variation at different probe diameters. In the stable acoustic pressure zone that there is a symmetrical behavior at the zero acoustic pressure line.

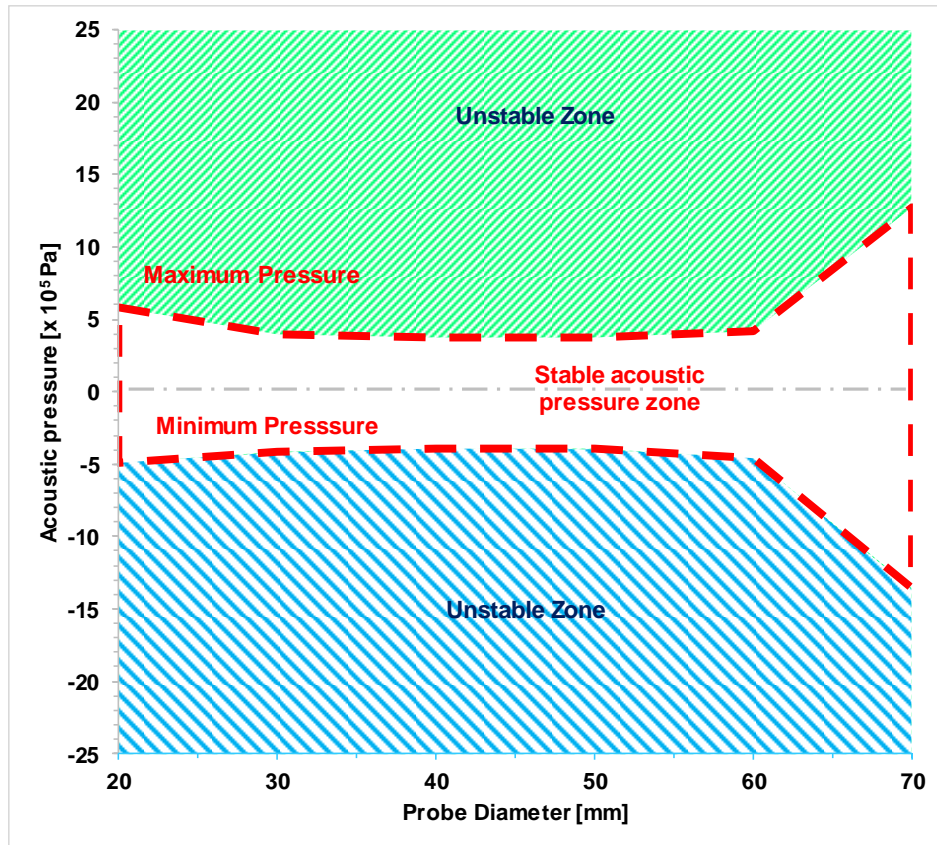
Table 4.2: The acoustic parameters corresponding to different ultrasound probe diameters

Probe diameter D_p [mm]	20	30	40	50	60	70
Probe Area A_p [m^2]	0.00031 4	0.000707	0.00125 6	0.001963	0.002826	0.003847
Ultrasound Intensity [W/m^2]	114,650	50,955	28,662	18,344	12,739	9,359
Acoustic Amplitude P_0 [kPa]	585.49	390.33	292.75	234.2	195.16	167.28
Velocity Amplitude [m/s]	0.39	0.26	0.2	0.16	0.13	0.11
Displacement [μm]	3.12	2.08	1.56	1.25	1.04	0.89
Acceleration [94] [m/s^2]	49,189.2	32,792.8	24,594.6	19,675.7	16,396.4	14,054.1

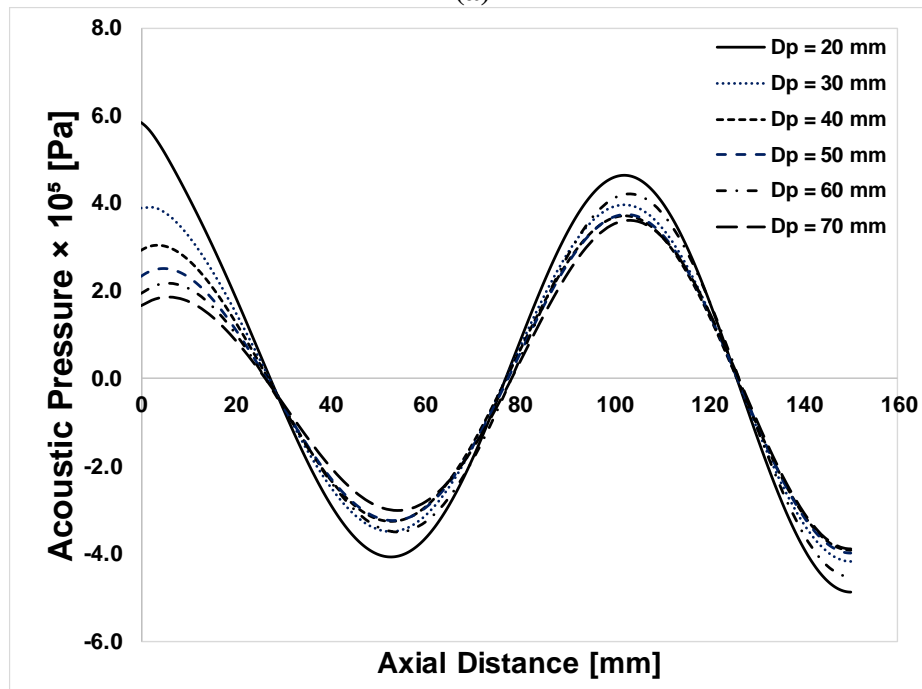
The max magnitude of the negative pressure increases while increasing the transducer diameter. It is attributed to the fact that when the transducer probe dimension alters, this will change the distance of the sound-hard boundaries and change the wave point (node or antinode) and change the phase of the reflected waves as well [99]. Figure 4.10 (b) displays the transducer probe diameter's influence on the axial acoustic pressure distribution. It is well-known that a transducer probe should introduce the ultrasound waves with a diameter smaller than the wavelength; hence the cavity bubbles could be formed. As seen, the axial location of the acoustic pressure nodes and antinodes matched at different probe diameters and did not alter; however, the acoustic pressure values did not alter considerably while increasing the probe diameter.

4.3.4 Effect of the boundary conditions

The linear wave equation has proven efficient in investigating different parameters affecting the pressure distribution inside the sonoreactor. Therefore, it is used repeatedly to examine the ultrasonic wave propagation's sensitivity to the boundary conditions for different sonoreactor geometries. Therefore, the study considered different boundary conditions for all reactors, including the effect of the absorbing and reflecting sonoreactors' walls. Klima et al. [47] performed a FEM approach to optimize a cylindrical reactor's geometry by changing the boundary conditions.



(a)



(b)

Figure 4.10: The transducer probe diameter on (a) the pressure map, max and mini acoustic pressure (b) on the axial pressure distribution

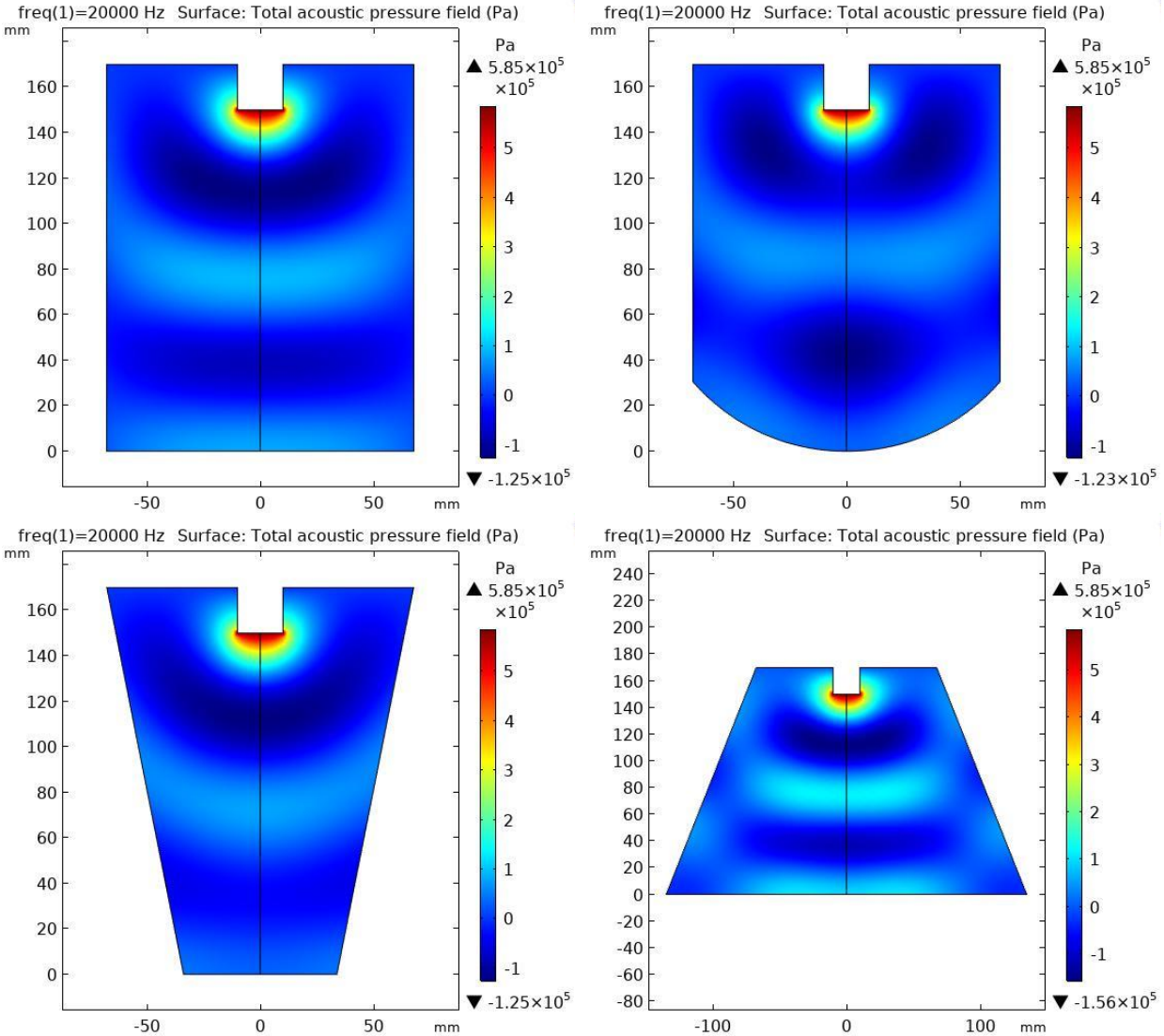


Figure 4.11: Effect of absorbing boundary conditions on wave propagation for an ultrasonic frequency of 20 kHz

The results are shown in Figure 4.11 and Figure 4.13 for the absorbing and reflecting boundaries, respectively. It can be seen in Figure 4.11 that the acoustic wave emitted from the sonotrode has created sound wave layers with the highest pressure located at the tip of the sonotrode, and the absorbing boundaries have attenuated the introduced acoustic pressure. Besides, the acoustic pressure peaks near the transducer probe tip in all geometries remained unchanged, while a slight change is noticed in the minimum pressure inside the sonoreactor. Generally, all geometries have acted the same in the case of absorbing boundaries. Furthermore, Figure 4.12 displays the pressure distribution at the transducer's axis for different geometries concerning the absorbing boundaries. Generally, the wave decays as the propagation distance increases. By comparing all geometries, it

is seen that all geometries experience almost the same pressure distribution with a slight difference in the second pressure peak location. GEO.4 has shown the maximum second peak. It is because it has the most extensive area of the bottom wall. Undoubtedly, this will directly affect cavitation possibilities. The bubbles should be introduced to many consecutive cycles to generate, enlarge, and explode to benefit from the bubble collapse's energy.

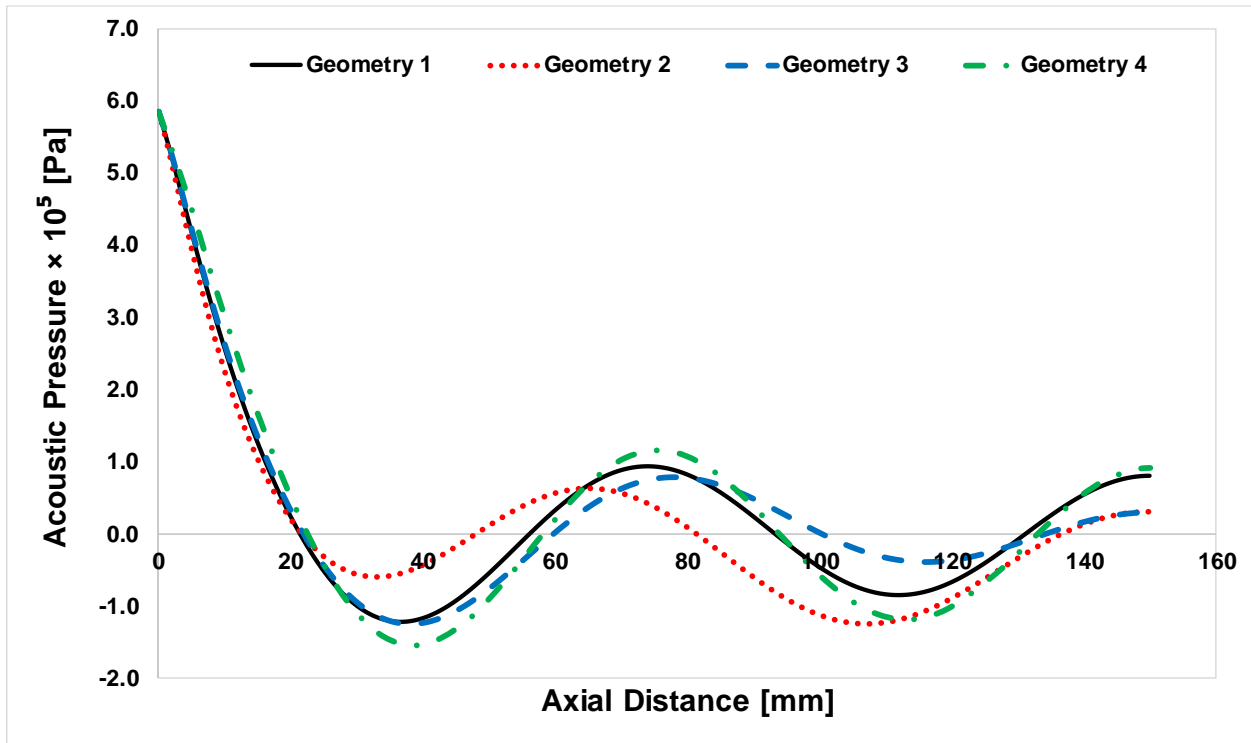


Figure 4.12: Axial acoustic pressure for 4 different geometries with absorbing boundaries

For comparison, the same simulation is performed by changing the absorbing walls to reflecting walls. The reflecting boundaries have led to a higher probability of generating acoustic cavitation bubbles and a higher number of cavitation zones. Figure 4.13 presents the effect of the sound-hard boundaries at the sonoreactor walls representing the reflected boundaries as compared to the sound-soft walls representing the absorbing boundaries. It is seen that the sound-hard boundaries help in creating high and low-pressure regions in the reactor with more significant cavitation zones. Generally, altering the wall properties, higher and lower pressure regions can be generated all over the sonoreactor.

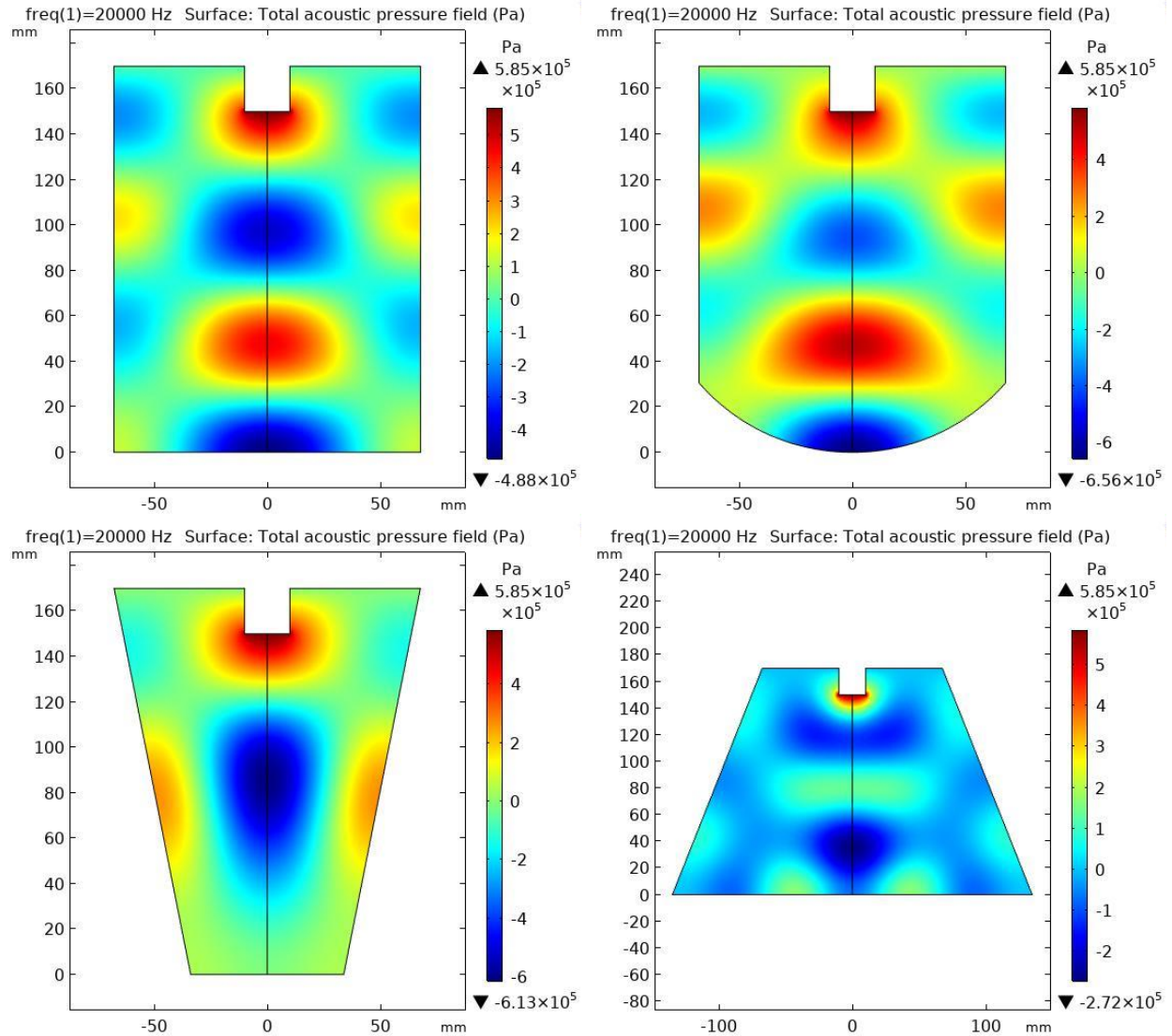


Figure 4.13: Effect of absorbing boundary conditions on wave propagation for an ultrasonic frequency of 20 kHz

Moreover, Figure 4.14 displays the acoustic pressure field at the axis of the reactor for different geometries. The first two geometries experience pressure peaks two times of the ultrasound source amplitude by comparing all geometries. It is concluded that higher and lower pressure zones can be achieved even at low frequencies by altering the wall boundary conditions. It will directly affect the cavitation possibilities as the bubbles should be introduced to many consecutive cycles to generate, enlarge, and explode to benefit from the energy produced from the bubble collapse. For this reason, GEO.3 and GEO. 4 are not preferable.

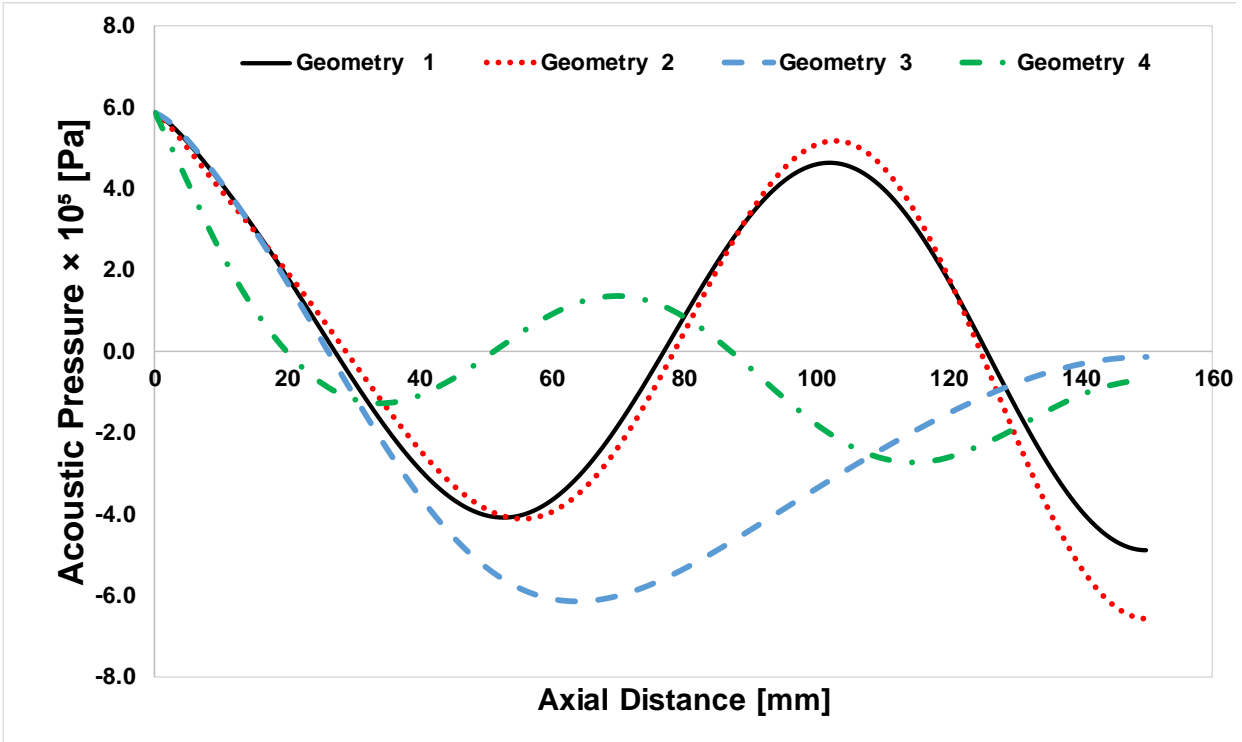


Figure 4.14: Axial acoustic pressure distribution at different geometries with reflecting boundaries

4.4 Analysis of variance and optimization

The objective of this section is to determine which variables are most influential on the response parameter. For the sake of finding the optimal geometric design for a single probe sonoreactor with a cylindrical geometry and decrease the number of the follow-up numerical simulations in the parametric studies, the analysis of variance ANOVA has been utilized. The sonoreactor geometry is presented in section 3.1.1 and figure 3.1, where all dimensions and boundary conditions are shown. The acoustical and geometrical parameters are considered the driving parameters, while the response parameter is the maximum magnitude of the negative pressure ($P_{Negative}$) for each geometric condition. This study aims to determine the acoustical and geometrical parameters that allow the largest magnitude of the negative pressure—knowing that the magnitude of the negative pressure has to be higher than the Blake cavitation threshold mentioned in the last section to have a violent cavitation collapse. The following section demonstrates the selection of the geometrical and acoustical parameters.

The diameter ratio (D/D_p) is defined as the ratio between the sonoreactor diameter and the ultrasonic probe diameter. The higher level is selected based on an ultrasonic probe diameter of 20

mm and a sonoreactor diameter of 135 mm ($D/D_p = 6.75$), which is inspired by the experimental work of Gogate et al. [49]. While the lower level is selected based on an ultrasonic probe diameter of 80 mm, and a fixed sonoreactor diameter of 135 mm, this would leave a gap of around 2.75 cm from the side of the sonoreactor diameter to the side of the ultrasonic probe diameter [137]. Based on these assumptions, the diameter ratio (D/D_p) is namely, 1.7, 3.4, and 6.75.

For the immersion depth ratio (l/D_p), is defined as the ratio between the ultrasonic probe immersion depth (l) and the ultrasonic probe diameter. Similarly, the higher level is selected based on an ultrasonic probe diameter of 20 mm, and an immersion depth of 20 mm ($l/D_p = 1.0$) [49]. While the higher level is chosen based on an immersion depth ($l = 100$ mm), and a probe diameter of 20 mm, this gives the immersion depth ratio of 5.0 [138]. This would leave a gap between the probe tip and the bottom side of the sonoreactor of around 70 mm. Based on these assumptions, the immersion depth ratio (l/D_p) is namely, 0.25, 0.5, and 1.

For the ultrasonic frequency, the lower level is selected to be 20 kHz which is the threshold of ultrasound waves. While the higher level is also found in the literature. Table 4.3 shows selected factors and levels for this study. Based on the parameters above, 27 different geometries have been built up and solved using COMSOL Multiphysics (acoustic module) for the response variable ($P_{Negative}$). Noting that, the dimension for each of the 27 geometries has been reported in Appendix A (Table A1) along with the results of each configuration summarized in Appendix A (Table A2).

A full factorial analysis of variance two-way ANOVA is performed using Minitab 19 software. The dimensions of the 27 runs are calculated and given in Table 4.4 for each probe diameter, the probe depth, and the operating frequency based on a sonoreactor diameter of 135 mm and a reactor length of 170 mm. Then 27 different geometries have been built, simulated and the results are presented in Table 4.5.

Table 4.3: Input factors and 3 levels selected for ANOVA (3X3)

Factor	Low Level	Mid-level	High level
D/D_p	1.7	3.4	6.75
l/D_p	0.25	0.5	1
f , kHz	20	50	70

The results from the two-way ANOVA reported in Appendix show that the diameter ratio (D/D_p) has the most substantial influence on the response ($P_{Negative}$). While the second major influential parameter is the ultrasonic frequency. This can be confirmed by Figure 4.4 on the effect of ultrasonic frequency. It is observed that the frequency range between 20 kHz and 50 kHz does not significantly change the maximum magnitude of the negative pressure, which matches the outcome of ANOVA as per Figure 4.4. Therefore, the ANOVA study replicated at a higher frequency of 70 kHz. Lastly, the immersion depth has no significant effect on the negative pressure. This also can be confirmed from the results presented in Figure 4.7. In conclusion, it can be observed that the diameter ratio and the ultrasonic frequency are more significant than the immersion depth ratio. As seen, in order to maximize the magnitude of the negative pressure, either geometry #1 or geometry # 14 can be selected as highlighted in red in the following tables. This indeed will enhance the cavitation activity and the corresponding cavitation volume inside the sonoreactor.

Table 4.4: Geometries' dimension used in ANOVA for the 27 runs. Note that (sonoreactor diameter $D = 135$ mm and length $L = 170$ mm)

Run#	Probe diameter (D_p), mm	Depth (l), mm	Frequency (f), kHz
1	80	20	20
2	80	40	20
3	80	80	20
4	80	20	50
5	80	40	50
6	80	80	50
7	80	20	70
8	80	40	70
9	80	80	70
10	40	10	20
11	40	20	20
12	40	40	20
13	40	10	30
14	40	20	30
15	40	40	30
16	40	10	70
17	40	20	70
18	40	40	70
19	20	5	20
20	20	10	20
21	20	20	20
22	20	5	30
23	20	10	30
24	20	20	30
25	20	5	70
26	20	10	70
27	20	20	70

Table 4.5: ANOVA Data Points for the 27 runs

	x_1	x_2	x_3	y_1
Run#	D/Dp	l/Dp	freq	P_Neg
1	1.7	0.25	20	-1.17E+07
2	1.7	0.5	20	-4.19E+06
3	1.7	1	20	-5.24E+06
4	1.7	0.25	50	-7.69E+05
5	1.7	0.5	50	-1.13E+06
6	1.7	1	50	-1.02E+06
7	1.7	0.25	70	-3.27E+06
8	1.7	0.5	70	-5.56E+06
9	1.7	1	70	-4.32E+06
10	3.4	0.25	20	-1.03E+06
11	3.4	0.5	20	-3.91E+05
12	3.4	1	20	-9.61E+05
13	3.4	0.25	50	-2.00E+06
14	3.4	0.5	50	-4.15E+05
15	3.4	1	50	-1.11E+06
16	3.4	0.25	70	-1.92E+06
17	3.4	0.5	70	-9.45E+05
18	3.4	1	70	-2.11E+06
19	6.75	0.25	20	-5.27E+05
20	6.75	0.5	20	-5.45E+05
21	6.75	1	20	-4.88E+05
22	6.75	0.25	50	-5.06E+05
23	6.75	0.5	50	-8.54E+05
24	6.75	1	50	-7.45E+05
25	6.75	0.25	70	-2.16E+06
26	6.75	0.5	70	-4.53E+06
27	6.75	1	70	-8.46E+06

Table 4.6: Minitab output: Analysis of variance (Two-Way ANOVA)

Analysis of Variance

Source	DF	Adj SS	Adj MS	F-Value	P-Value
Regression	6	1.03E+14	1.72E+13	2.37	0.068
D/Dp	1	3.55E+13	3.55E+13	4.89	0.039
l/Dp	1	2.93E+12	2.93E+12	0.4	0.471
freq	1	1.19E+13	1.19E+13	1.63	0.011
D/Dp*l/Dp	1	5.26E+12	5.26E+12	0.72	0.465
D/Dp*freq	1	2.26E+13	2.26E+13	3.11	0.025
l/Dp*freq	1	2.34E+12	2.34E+12	0.32	0.587
Error	20	1.45E+14	7.26E+12		
Total	26	2.48E+14			

Model Summary

S	R-sq	R-sq(adj)	R-sq(pred)
0.470086	92.71%	51.53%	16.03%

Regression Equation in Uncoded Units

$$P_Neg = -15395995 + 2194000 D/Dp + 6561052 l/Dp + 248245 freq - 672758 D/Dp*l/Dp - 34821 D/Dp*freq - 75640 l/Dp*freq$$

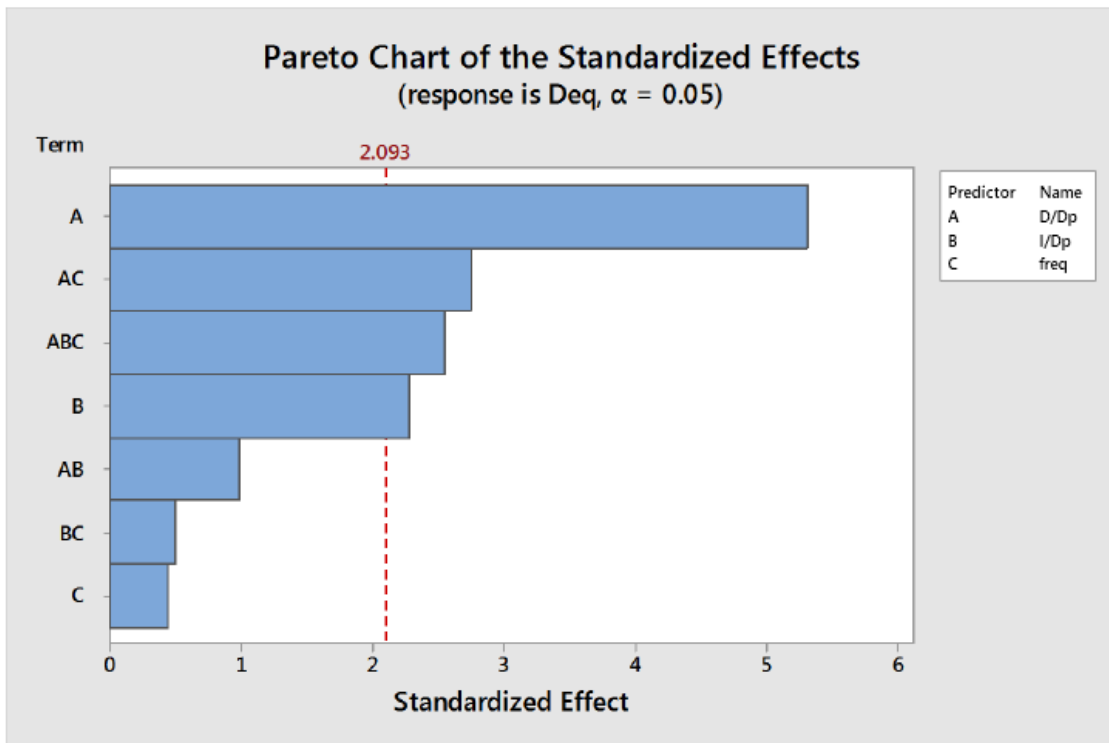


Figure 4.15: Pareto chart of the standardized effects

4.5 Acoustic Streaming

Acoustic streaming is one benefit of the non-thermal effects of ultrasound applications. Individual pulses of ultrasonic energy causing acoustical streaming, cavitation, and microstreaming. The study investigates the non-linear coupling between acoustics and CFD of sonoreactor. The coupling between the ultrasonic waves using the Helmholtz equation and the Navier-Stokes equations is complicated and rarely investigated in the literature. Therefore, this study aims to simulate the acoustic streaming inside a sonoreactor. The unsteady acoustics module and CFD are coupled to simulate the acoustic velocity streaming brought by the ultrasonic transducer to correlate the acoustic pressure field inside the sonoreactor to the flow dynamics field. The fluid flow module is selected with the laminar flow interface.

4.4.1 Acoustic streaming validation

A validated numerical model is successfully conducted with an excellent agreement with previous experimental data available in the literature to predict the behavior of the flow characteristics for parameter variations turns out to be a reasonable approach. The predicted CFD velocity profile and pattern show an excellent agreement with the experimental data available in the literature. The model successfully described hydrodynamic fields generated by high-frequency low-power ultrasound.

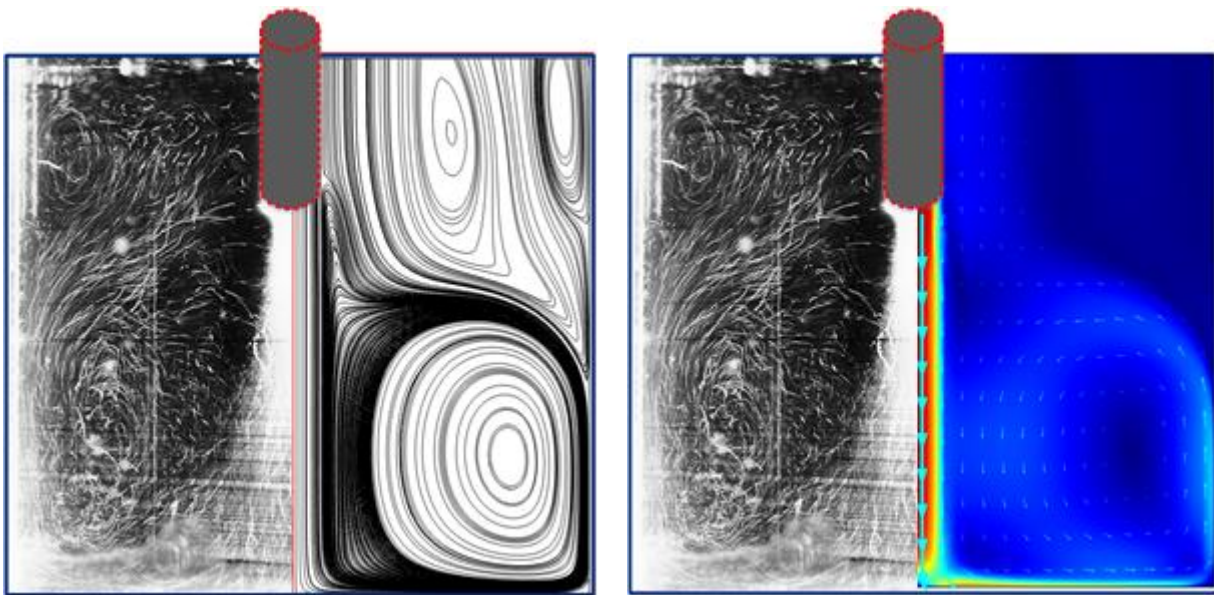


Figure 4.16: Velocity streamlines due to acoustic streaming (left), Axis-symmetrical velocity distribution predicted (right) compared to the experimental results of laboratory horn at 300 W (left) by Dahlem et al. [139]

For the sake of benchmarking, a model validation study for GEO.1 is successfully performed with respect to the pressure field at the axis of the reactor and reported by Rashwan et al. [140]. Henceforward, the acoustic streaming field of the model is successfully validated with the experimental visualization of the typical flow pattern in a half vertical plan is reported by Dahlem et al. [139] and as shown on the left side of Figure 4.16. The velocity pattern consisted of two eddies, the large eddy allocated at the bottom corner of the sonoreactor. The small vortex is shown at the top corners of the reactor. The axisymmetric model for a transducer probe is established with a no-slip boundary condition. As mentioned before, the liquid medium is initially stagnant, and the flow induced by the ultrasound effects because of the acoustics source. The comparison is made, and the model is validated by the Particle Image Velocimetry (PIV) experimental data reported by Dahlem et al. [139] considering the acoustic streaming of sonoreactor. The modeling simulations show an excellent agreement with the experiments regarding the flow pattern captured by the PIV. There are two counter-rotating eddies, as seen in the experimental results, and they are captured with the current numerical study as well, which validated the present model. These results are also following the results presented by Trujillo and Knoerzer [96], Schenker [141], and Slama [142]. They reported a similar observation of the characterization of ultrasound-induced acoustic streaming and the jet-like velocity profile.

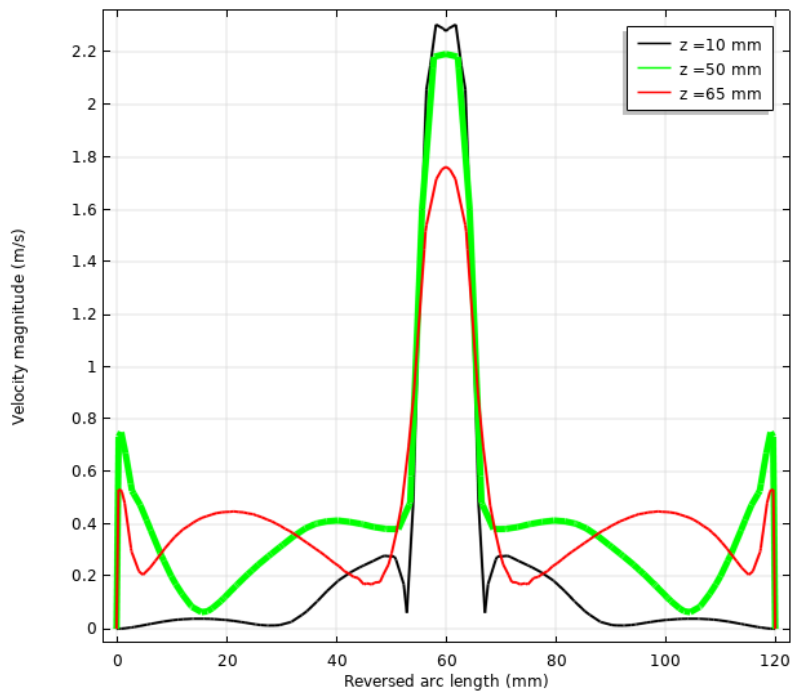


Figure 4.17: The predicted axial velocity distribution at different distances from the transducer tip $Z = 10, 50,$ and 65 mm

4.4.2 Acoustic streaming analysis

Figure 4.17 shows the axial velocity profile at different vertical positions measured from the transducer probe tip. The axial flow velocity profile matches the velocity profile reported by Schenker et al. [141]. It shows a maximum amplitude at the axis because of the location of the transducer probe. The velocity decreases, moving to the sides of the sonoreactor, where the recirculation zones take place. The developed model is simulated by the CFD module in COMSOL 5.4 using a high-performance workstation, and its specifications can be found here [140]. The simulation time is spent for one simulation to be converged for about 1 hour and 26 minutes. Figure 4.18 presents the acoustic streaming evolution pattern is shown in a sequence of images with respect to time.

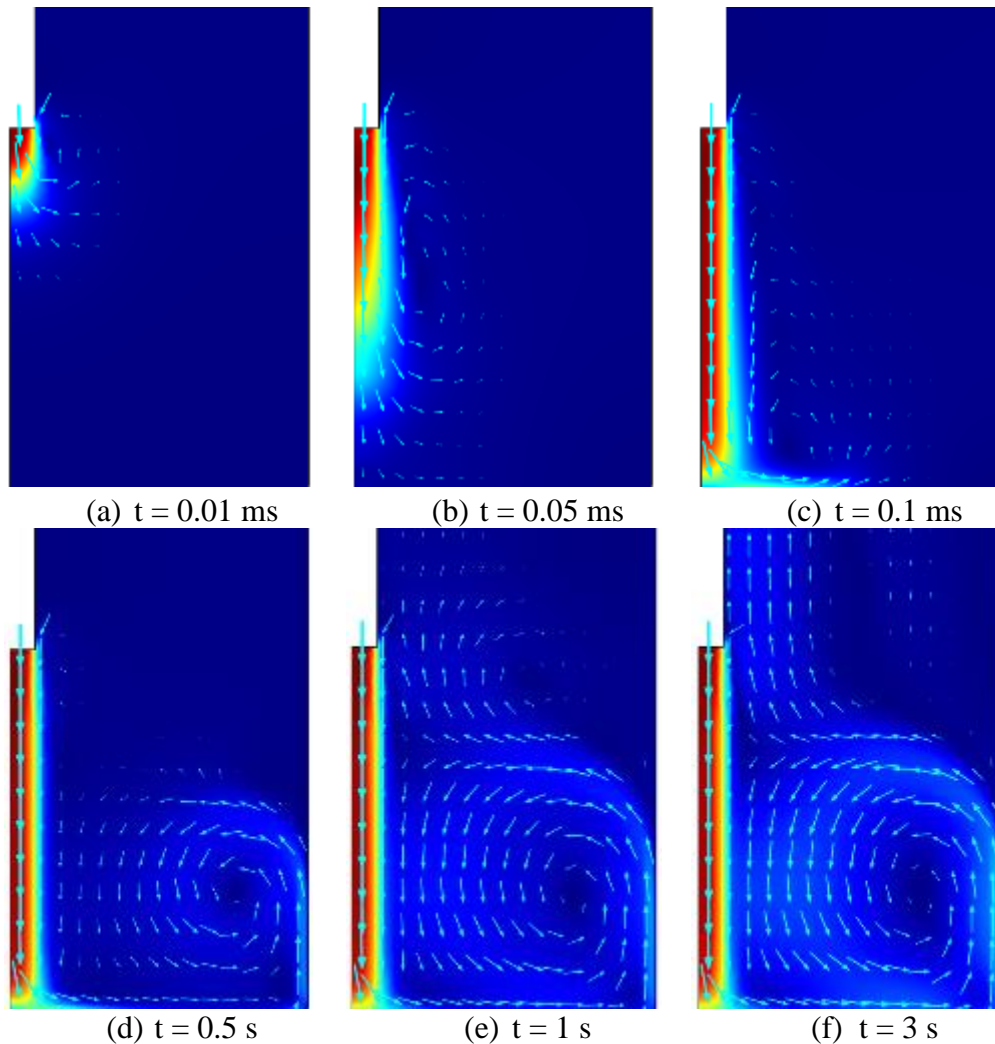


Figure 4.18: Acoustic streaming induced flow at different time scales

The flow-induced from the acoustic streaming is obtained between $t=0.05$ s and $t = 3.0$ s. The flow is initiated from the transducer's surface and travels in the direction of the bottom wall of the sonoreactor. The flow interacts with the bottom wall, and encounter recirculation zones are created; one is located at the bottom surface, and the other one moves upward along the sidewall. The velocity streamlines are also drawn and presented in Figure 4.19 for the same time intervals from $t=0.01$ ms and $t= 0.1$ ms. Generally, it is observed that acoustic streaming consists of two encounter vortices of different sizes. The most significant vortex is taking place at the bottom of the sonoreactor, while the smallest vortex is taking place close to the transducer probe tip. This formation of both vortices is due to generated boundary layers at the corner of the sonoreactor. The jet flow is moving downwards, producing more flow recirculation zones on the bottom and upper parts of the sonoreactor.

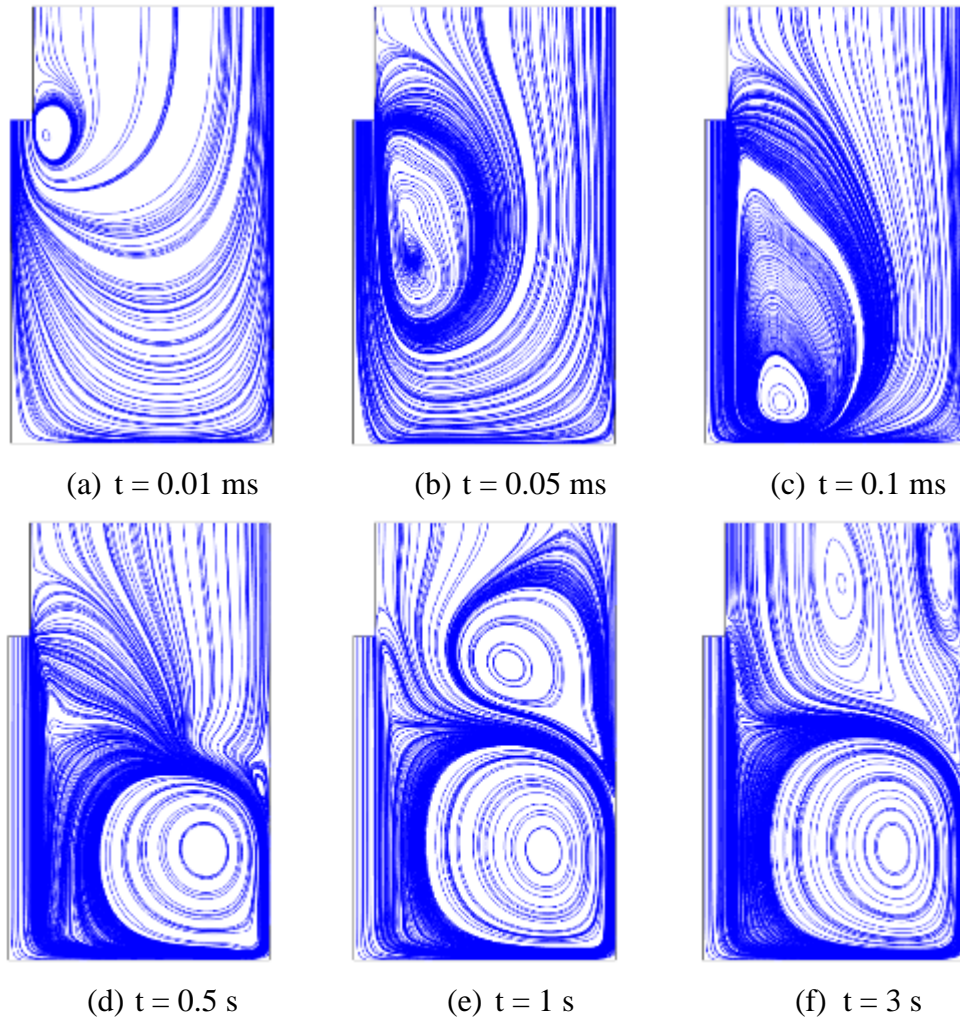


Figure 4.19: Streamlines induced by acoustic streaming at different time scales

The flow is evaluated, starting from the transducer probe where the first recirculation zone is created. After some time and when the flow becomes steady-state and consistent, three recirculation zones are created that contribute to maintaining a good premixing between the liquid levels in the sonoreactor.

4.4.3 Density effects on acoustic streaming

In this section, a comparison is drawn between the three fundamental densities, constant, linear, and non-linear density, which are illustrated in section 3.1.5.

(a) Constant density

In this section, the constant density is used in the flow field properties after setting the oscillating pressure boundary at the transducer probe tip. The main comparison is basically about how the flow pattern created and changes by the ultrasonic transducer oscillations' effect. In all cases, the flow pattern consisted of a strong downwards jet flow with a maximum velocity highlighted in red in the color label at the maps' side. Figure 4.20 presents the time evolution sequence of images of the acoustic streaming effects under a constant density. As seen, the axial downward flow jet is not visually continuous in a short time step. However, overall it will act as jet-like acoustic streaming induced by high frequency-high power horn sonoreactor. The computation of the flow field shows some recirculation zones are presented at the side of the axial jet with the corner of the sonoreactor. From the results, the jet-like acoustic streaming flow is developed within milliseconds from applying the acoustic pressure amplitude of around 5 bar corresponds to an acoustic power of 36W and an acoustic intensity of 8.5 W/cm². The results seemed to be unrealistic as the velocity magnitude goes up to 66.7 m/s as maximum velocity. This is because using the default settings for the compressible flow (density from the material) leads to the wrong (isothermal) speed of sound in the model since $\rho = \rho(p, T)$, and the temperature is kept constant. Having a velocity of 60 m/s close to the transducer probe is considered very high, and the induced jet flow continuity is not clear. A significant change in the velocity field is noticed when assuming the linear and the nonlinear density distribution, as reported in the following subsections.

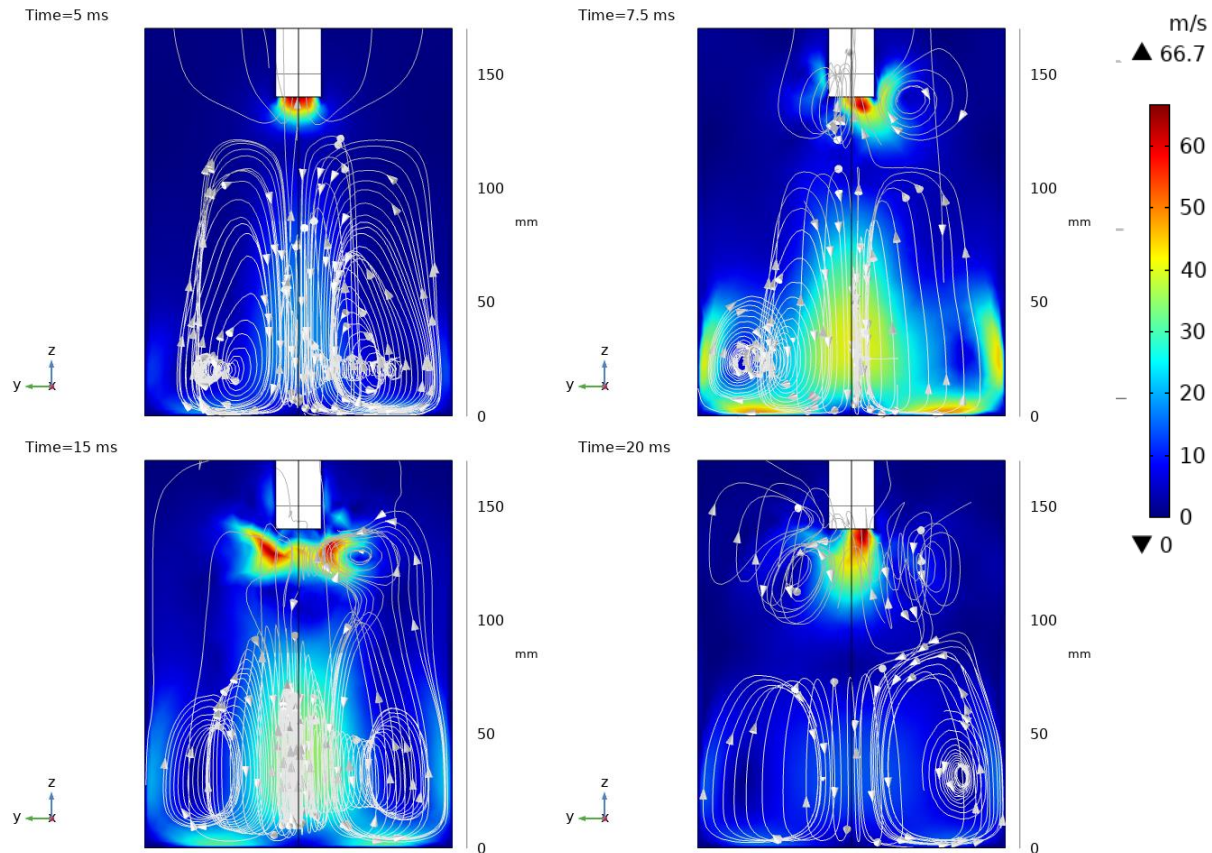


Figure 4.20: Time evolution of the velocity magnitude contours and velocity streamlines while using constant density relation in the flow module

(b) Linear density result

The linear density relation is used in the fluid module to include the effect of changing the density within the sonoreactor when the acoustic pressure varies. The linear density showed a better view than the constant density in terms of how the flow is affected by the acoustic pressure modes, namely the nodes and antinodes. Figure 4.21 shows the time evolution of the flow distribution inside the sonoreactor. The figure shows the velocity magnitude's contour overlying the velocity streamlines to show precisely the recirculation zones. As seen a significant change in the velocity after considering the effect of the fluctuating acoustic pressure into the density relation. This can be attributed to the reasonable assumption of the linear distribution of density with respect to the acoustic pressure and the speed of sound. Unlike the linear density results of the streaming jet, a full evolution of the jet has been captured, which shows that multiple recirculation zones correspond to the acoustics streaming induced by the ultrasonic transducer's effect.

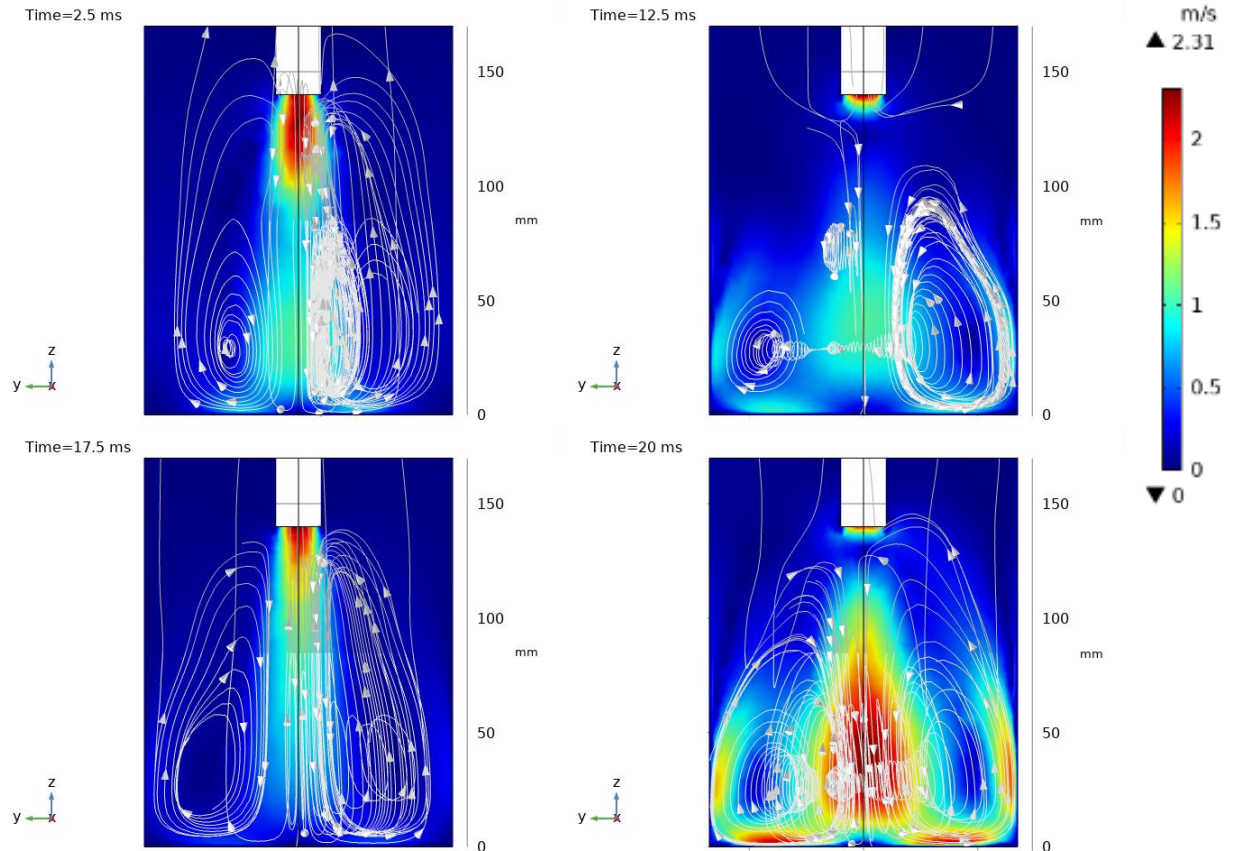


Figure 4.21: Time evolution of the velocity magnitude contours and velocity streamlines while using linear density relation in the flow module

(c) Non-linear density result

To the best of our knowledge, this work is the first one that has achieved simulation of the non-linear density contribution for acoustic streaming above the cavitation threshold. Moreover, the velocity magnitude and distribution experience indicate the degree of premixing between the liquid buckets inside the sonoreactor. In the case of liquid-liquid reactions, acoustic streaming is shown as an essential parameter for the sonochemical yield and efficiency. The nonlinear assumption is the one to believe. This can be attributed to the correct assumption of the linear distribution of density with respect to the acoustic pressure and the speed of sound. For the nonlinear density simulations shown in Figure 4.22, we can see that the flow did not evolve from the first couple of milliseconds. The time-evolution images are close to what happens to reality as the flow is not homogenous inside the sonoreactor, and the liquid levels keep mixing. One major finding is that the maximum velocities reduced in the non-linear density results as compared to the constant and the linear cases. This can be attributed to the effect of the acoustic pressure in the NL density.

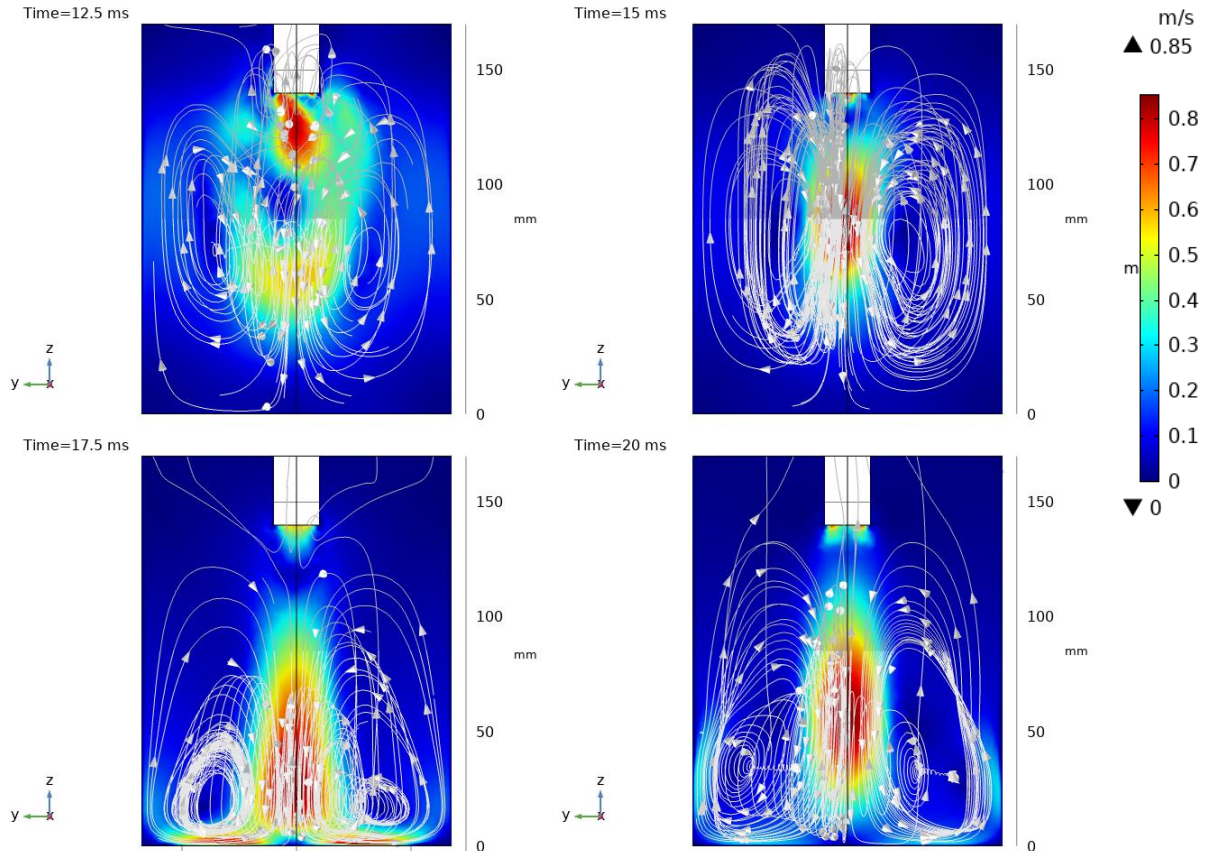


Figure 4.22: Time evolution of the velocity magnitude contours and velocity streamlines while using linear density relation in the flow module

In closing, when comparing the three cases, a significant change in the velocity values taking place inside the sonoreactor. The values went down from 60 m/s when using a constant density from the material to 0.8 m/s when using the non-linear density distribution. The nonlinear density considers the change in the acoustic pressure and includes the non-linearity efficiency and the nonlinearity parameter.

4.4.4 Acoustic streaming for different geometries

For the reason of including the nonlinearities of the vortex shedding, the acoustics are modeled using the full compressible Navier-Stokes (NS) Equation in the vicinity of the sonoreactor. The compressible flow is important here because, in the case of the sonoreactor, the flow velocity is large enough to introduce significant changes in the density. The changes can be neglected when the Mach number lower than 0.3. However, the coupling between the velocity and pressure fields becomes so strong that the NS and continuity equations need to be solved together. Compressible

flow can be laminar or turbulent. In this case, the model combines pressure acoustics, transient module, and Laminar flow module. The vortices are resolved, so no turbulence model is used (DNS). The acoustic and flow coupling is valid as long as vorticity is small at the interface boundary. Vortex shredding usually takes place in the vicinity of that area. This contributes to nonlinear losses and also the nonlinear distortion of the sound signal in audio applications. Nonlinear effects are often included in analytical transfer impedance models via semi-empirical parameters. In this section, different geometries of an immersed type sonoreactor contained a particular volume of liquid water medium are modeled. In a transient simulation, the model couples pressure acoustics and the laminar flow interface to model the dynamic nonlinear losses associated with the vortex's shedding. The acoustic field of an event has an amplitude of 234 dB SP, corresponding to 5 bars. The amplitude is considered typical for most of the sonoreactor applications and configurations. Comparisons are made based on which geometry has a better streaming distribution.

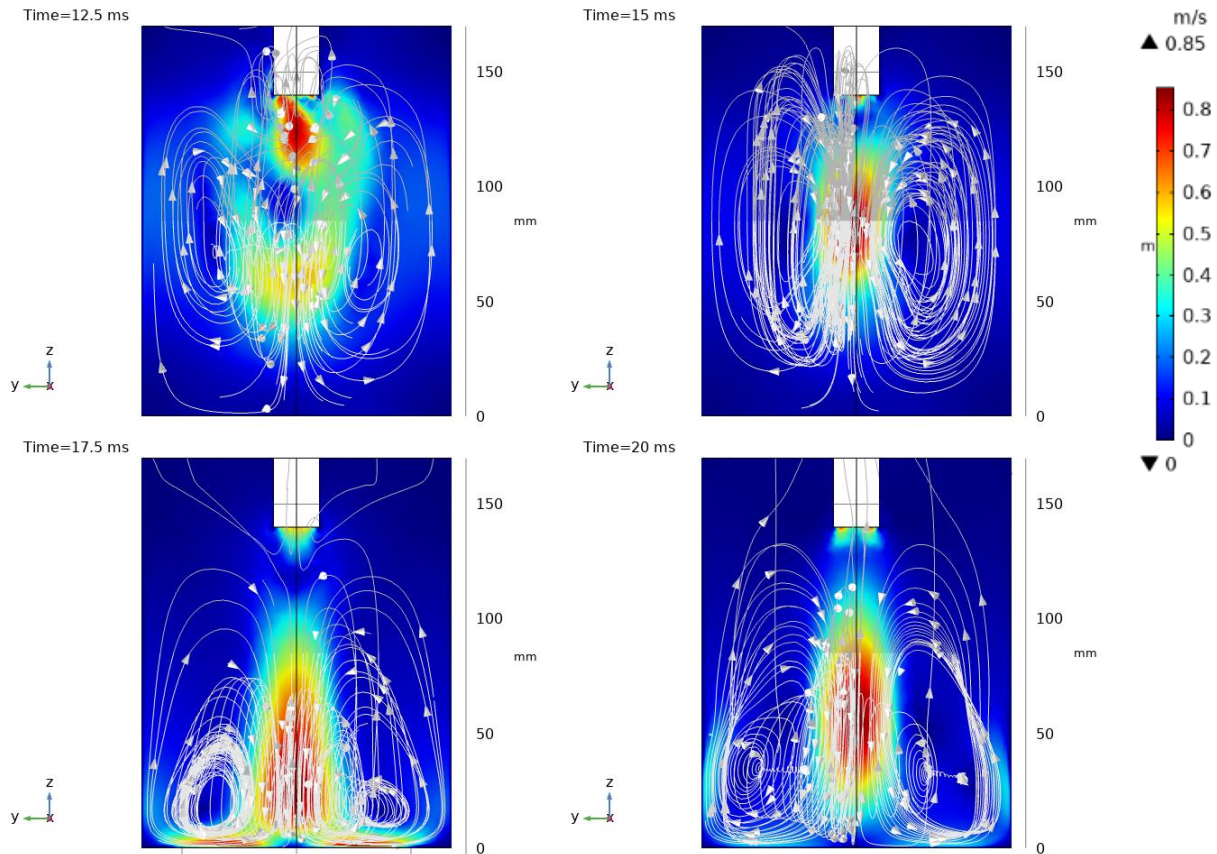


Figure 4.23: Time evolution of the velocity magnitude contours overlaying velocity streamlines with nonlinear density module for Geo. 1 – Cylindrical sonoreactor with 1 ultrasonic transducer

(a) Geo.1 – Cylindrical sonoreactor with 1 ultrasonic transducer

For the nonlinear density simulations shown in Figure 4.23, we can see that the flow did not evolve from the first couple of milliseconds. The time-evolution images are close to reality as the flow is not homogenous inside the sonoreactor, and the liquid levels keep mixing. One significant finding is that the maximum velocities reduced in the non-linear density results compared to the constant and linear cases. This can be attributed to the effect of the acoustic pressure in the non-linear density relation. The induced jet flow usually will form two large eddies or recirculation zones that help the premixing between the liquid levels inside the sonoreactor.

(b) Geo.2 – Cylindrical sonoreactor with 3 ultrasonic transducers

The cylindrical sonoreactor with 3 probes showed a better premixing as shown in Figure 4.24.

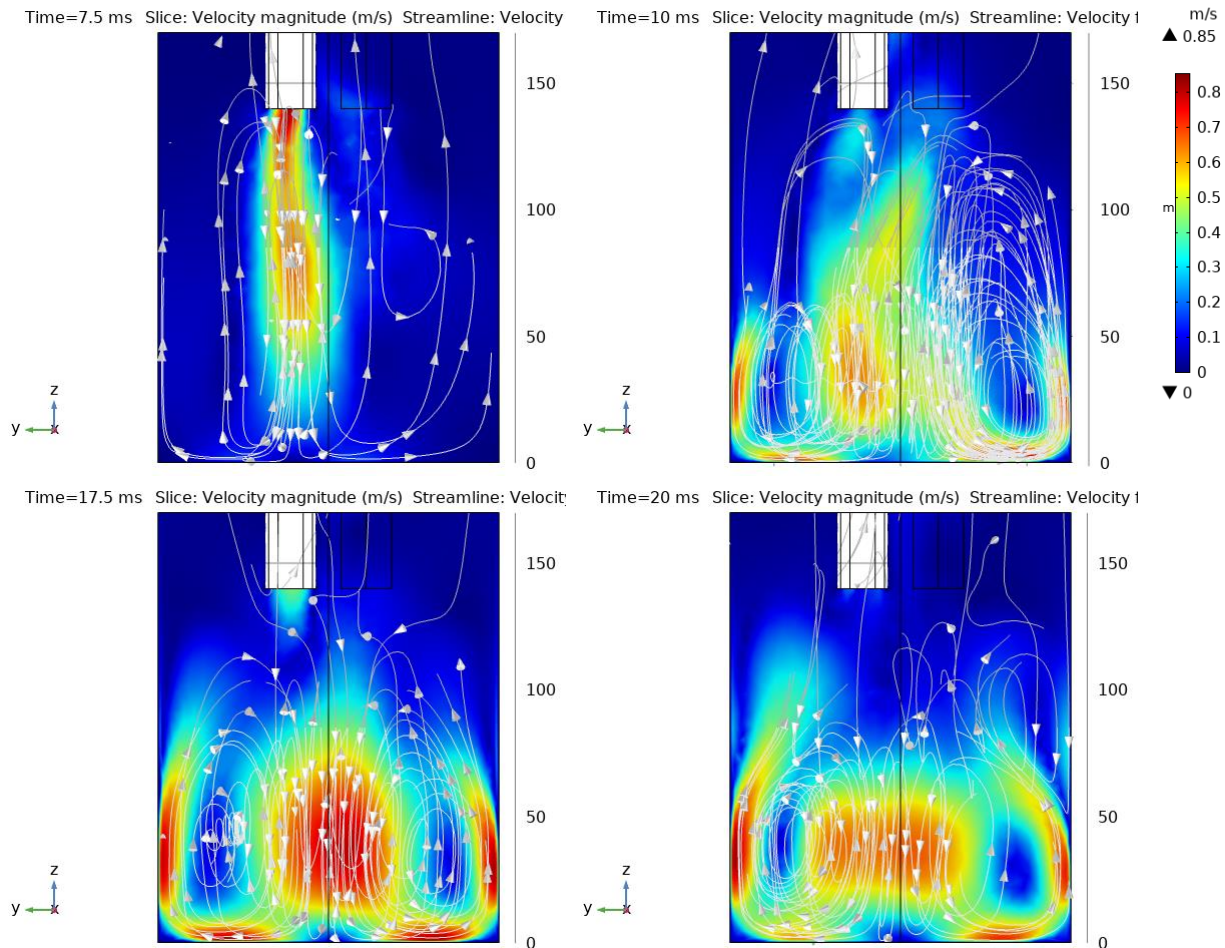


Figure 4.24: Time evolution of the velocity magnitude contours overlaying velocity streamlines with nonlinear density module for Geo. 2 – Cylindrical sonoreactor with 3 ultrasonic transducers

A sectional view at the centerline of the sonoreactor is taken shows the middle sonotrodes fires its acoustic oscillations, and the flow is triggered as captured in the sequence below. In fact, better mixing can be easily predicted from the distribution of the velocities inside the sonoreactor. The process shows proper mixing, which is why we consider geometry 2 to be one of the best to increase the sonochemical yield and sonohydrogen efficiency. The cylindrical sonoreactor with 3 probes has been selected for further numerical simulations because it has a reasonable cavitation percentage, as Figure 4.35, and perfect premixing between the liquid level. The CLY-3P geometry combines the high performance of the cavitation percentage and high-efficiency acoustic streaming. Assuming a jet-like flow, the velocity profile is re-stimulated again, and it can be presented in Figure 4.25. Comparing both profiles shows that the simulation presented in Figure 4.24 is more reasonable because it accounts for the body forces created by the combined effect of acoustic pressure nodes and antinodes created by the 3 probes.

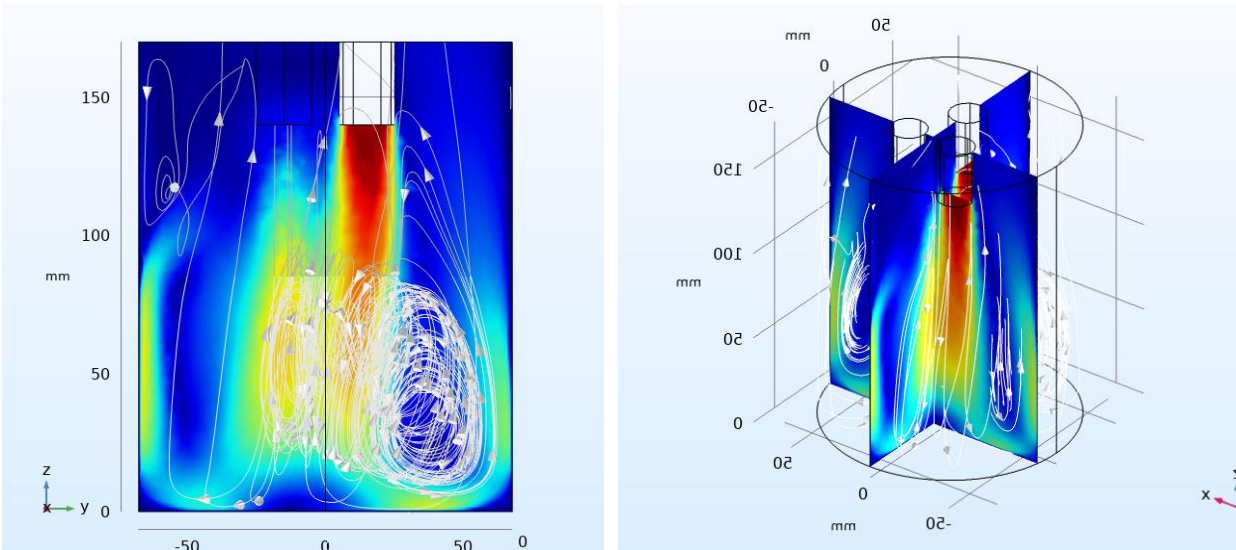


Figure 4.25: Jet-like flow simulation for CLY-3P

(c) Geo.3 – Cylindrical sonoreactor with 5 ultrasonic transducers

The cylindrical sonoreactor with 5 sonotrodes showed a reasonable premixing but not the favorable between the liquid level, as shown in Figure 4.26. A sectional view at the centerline of the sonoreactor is taken shows all the sonotrodes firing their acoustic wave and oscillations, and the flow is triggered as captured in the sequence below. In fact, this geometry does not seem to have a premixing because of the absence of the recirculation zones and the insufficient distribution of

the velocities inside the sonoreactor. The acoustic streaming process shows improper mixing, and that is why we consider geometry#3 not to help improve the sonochemical process.

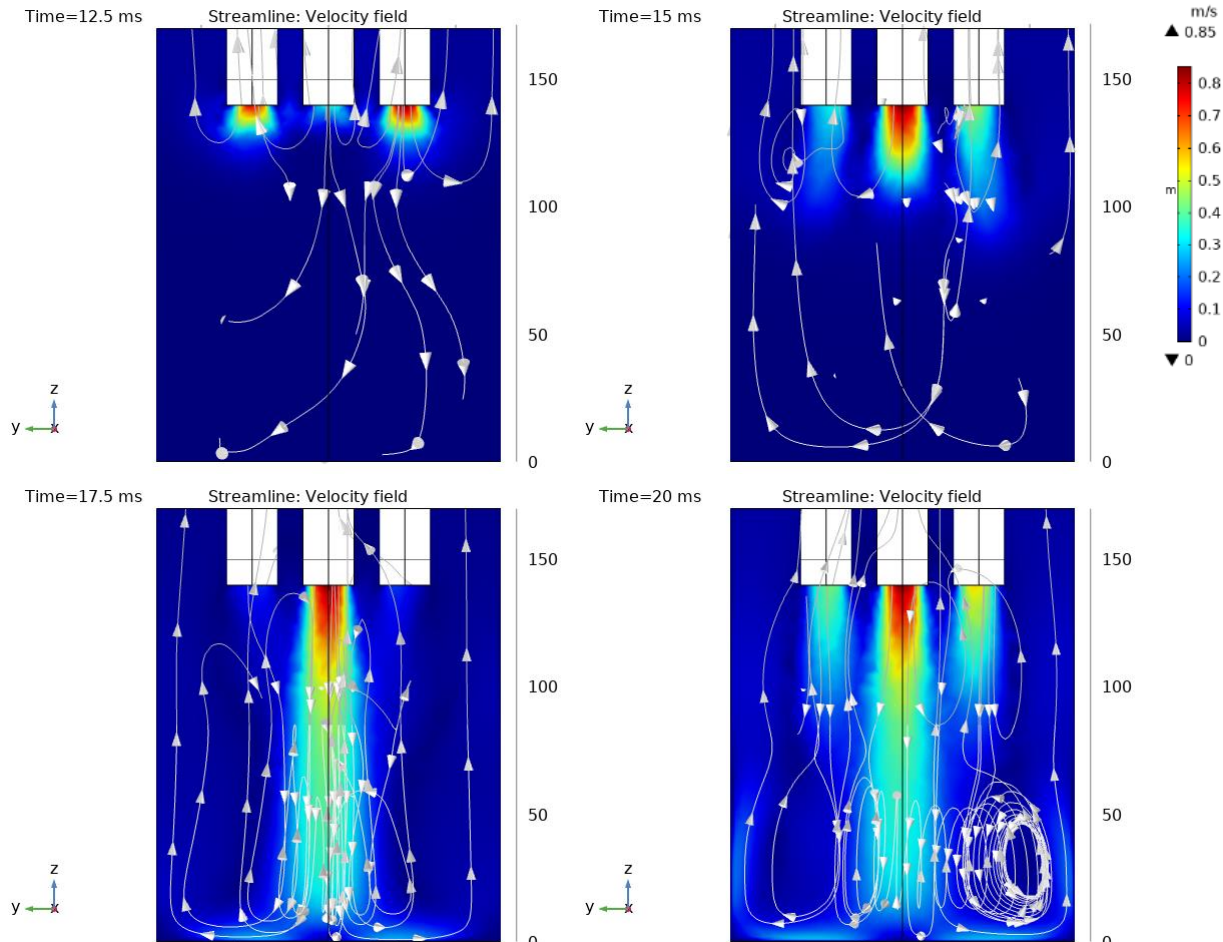


Figure 4.26: Time evolution of the velocity magnitude contours overlaying velocity streamlines with nonlinear density module for Geo. 3 – Cylindrical sonoreactor with 5 ultrasonic transducers

(d) Geo.4 – Hexagonal sonoreactor with 5 ultrasonic transducers

The hexagonal sonoreactor with 5 sonotrodes showed a better premixing between the liquid level, as shown in Figure 4.27. A sectional view at the centerline of the sonoreactor is taken shows all the sonotrodes firing their acoustic wave and acoustic oscillations, and the flow is triggered as captured in the sequence below. Actually, better mixing can be easily predicted from the distribution of the velocities inside the sonoreactor. The acoustic streaming process shows proper

mixing, and that's why we consider geometry#4 is also one of the best to increase the sonochemical yield and sonohydrogen efficiency.

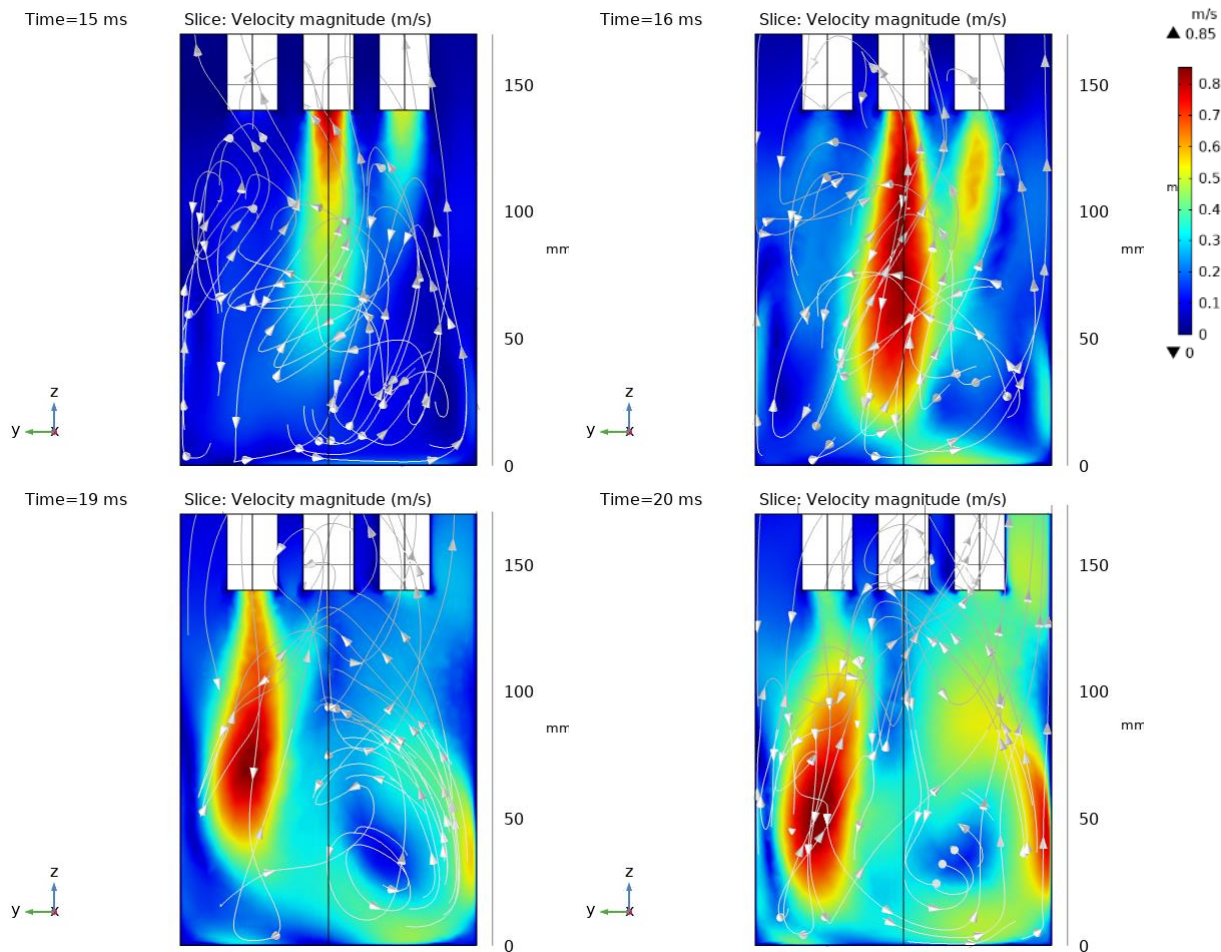


Figure 4.27: Time evolution of the velocity magnitude contours overlaying velocity streamlines with nonlinear density module for Geo. 4 – Hexagonal sonoreactor with 5 ultrasonic transducers

(e) Geo.5 – Square sonoreactor with 5 ultrasonic transducers

The square sonoreactor with 5 sonotrodes showed unfavorable premixing between the liquid levels, as shown in Figure 4.28. A sectional view at the centerline of the sonoreactor is taken shows all the sonotrodes firing their acoustic oscillations, and the flow is triggered as captured in the sequence below. This geometry does not seem to have a premixing because of the absence of the recirculation zones. In closing, for better premixing between the liquid level in the sonoreactor, we would suggest using Geotmetry#2 and Geometry#4 because both have proven a better streaming performance, which will improve the sonochemical process and the sonohydrogen yield.

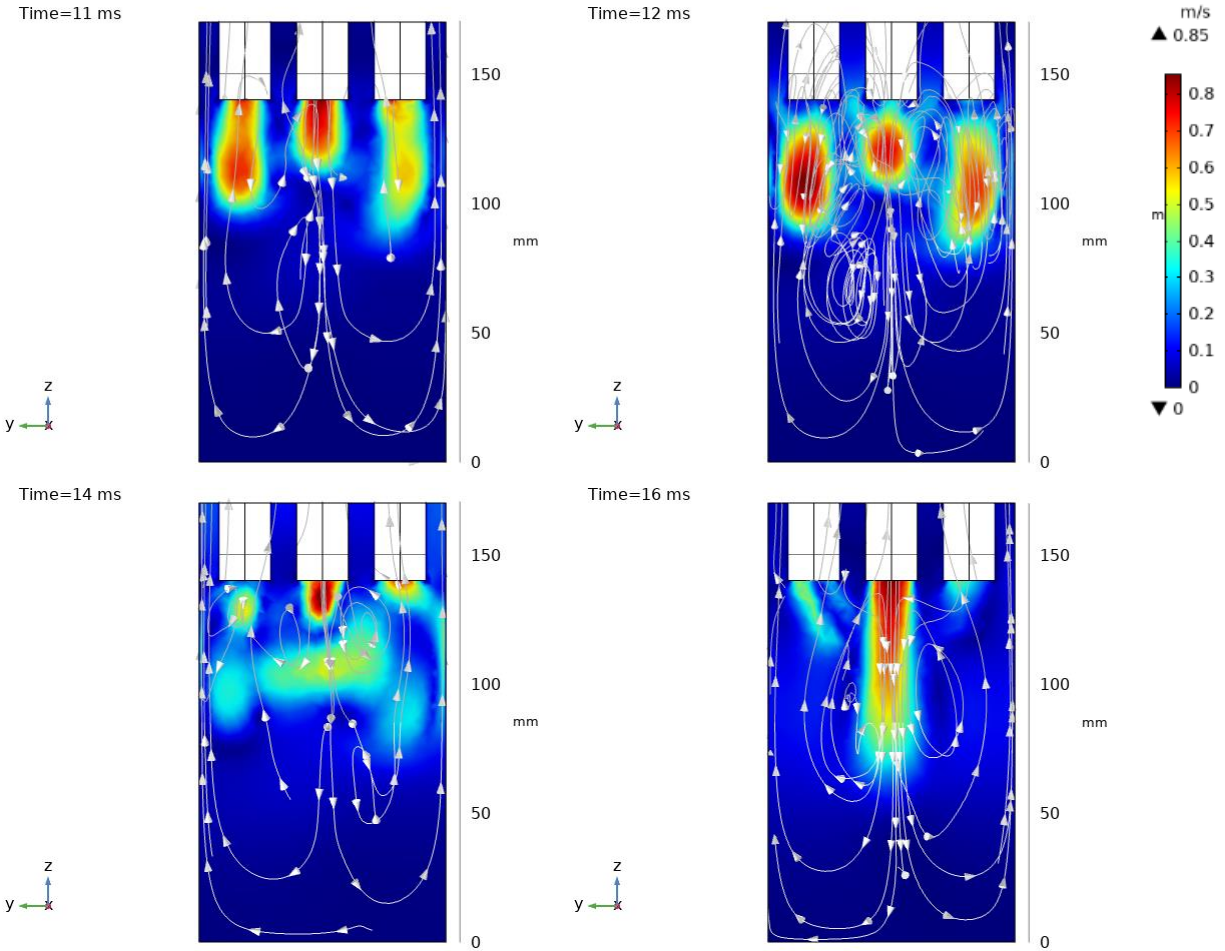


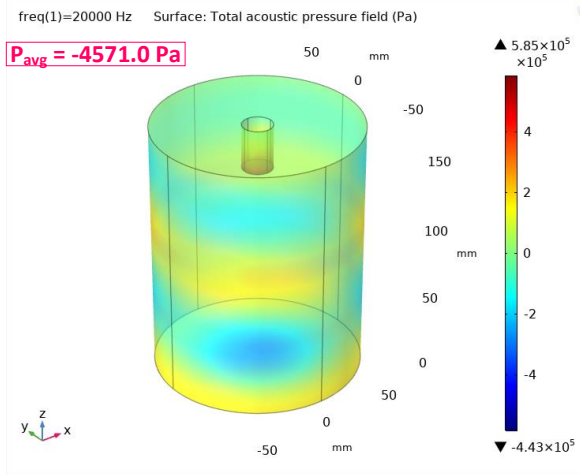
Figure 4.28: Time evolution of the velocity magnitude contours overlaying velocity streamlines with nonlinear density module for Geo. 5 – Cylindrical sonoreactor with 5 ultrasonic transducers

4.6 Geometric parametric study and Optimization

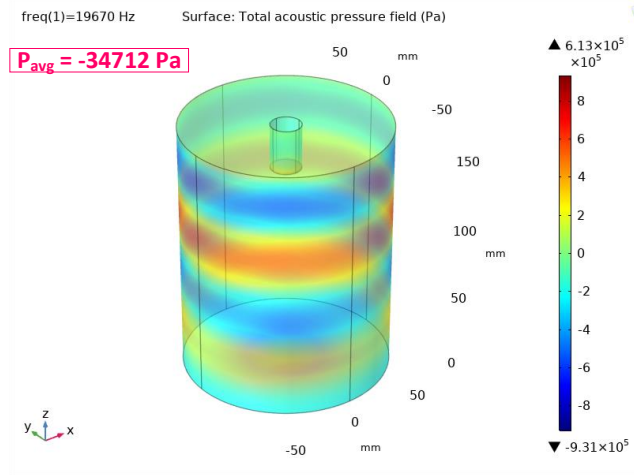
In this chapter, a geometric optimization study is performed to investigate the optimum geometry that best benefits the sono-hydrogen process. The study is considered in three phases; the first phase is conducting acoustic simulation on different arrays and geometries considering Eigen frequencies and the most typical ultrasonic frequency, 20 kHz. The second phase is to simulate the acoustic streaming in regard to the flow field distribution. The third and final phase is the hydrogen production calculation from such geometries. This is what we are going to see herein.

4.5.1 Effect of the number of sonotrodes

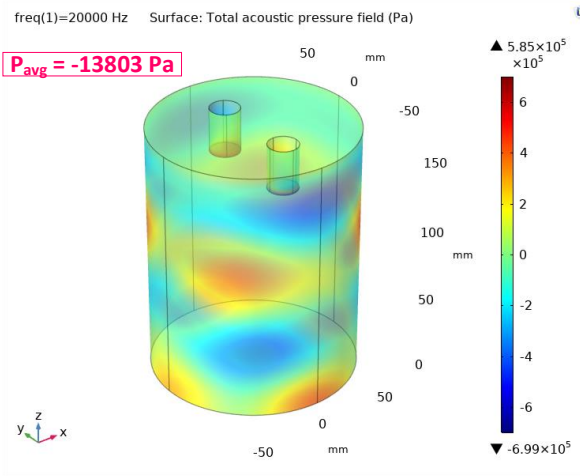
A novel simulation analysis is conducted because of the effect of having multiple probes in on sonoreactor. First of all, having studied the type-A sonoreactor contributes to the field as few studies have reported simulations about this type of sonoreactor—most of the studies available in the literature considered type-b and type-c sonoreactors. Son et al. [95,143] performed a geometric-optimization experimentally of sonoreactors to enhance the cavitation activity using a type-b bath sonoreactor. The probe is fixed at the lowest side of the sonoreactor. They considered changing the aspect ratio of the sonoreactor by varying the liquid height above the ultrasonic transducer. They concluded that as the liquid height increases, the cavitation yield increases substantially under the same input power. In this parametric study, we have considered varying the number of sonotrodes to see how this would affect the negative pressure's maximum magnitude. For this reason, 5 three-dimensional geometries are built with a different number of ultrasonic probes immersed from the top side, starting from 1 to 5. All geometries have the same dimensions and boundary conditions while changing the number of probes. We run initial acoustic simulations for all five geometries using COMSOL to determine the Eigen frequencies or what is so-called the natural frequencies and the corresponding mode shapes for all the suggested geometries. The acoustic simulations took minutes to solve the Helmholtz equation. Once the acoustic simulations are done, the excitable modes and frequencies are checked. Then, the ultrasonic probe is introduced to work at the same frequency to trigger a resonance condition. This resonance condition will enhance the sonochemical process and make it more efficient. Figure 4.29 considers the differences in the acoustic shapes and modes for different sonoreactors at 20 kHz, as shown in the figure's left column. The right column shows the pressure distribution for the same sonoreactor operating at its corresponding Eigen frequencies with different ultrasonic probes. In the case of a cylindrical sonoreactor with 3 sonotrodes, the geometry is tested regarding different Eigen frequencies. We found that, at an Eigen frequency of 20076 Hz, the sonoreactor would not hold the pressure generated and accumulated inside the sonoreactor. It may lead to damage to the sonoreactor. Therefore, another Eigen frequency is selected from the solution 19990 Hz that gives more reasonable pressure values. The cylindrical sonoreactor with 3 sonotrodes shows a higher magnitude of negative pressure, which will promote the acoustic cavitation generation process.



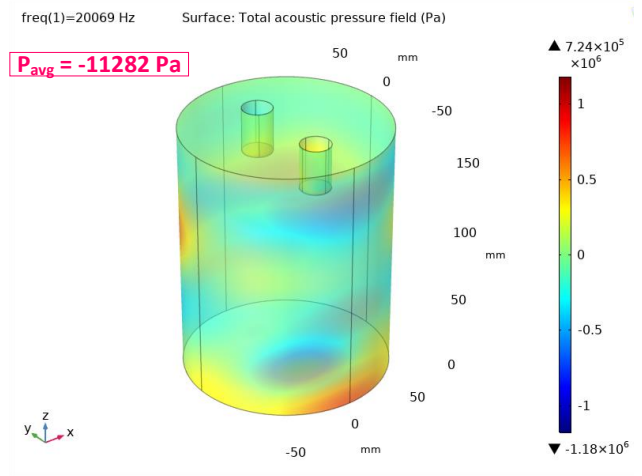
CLY-1P



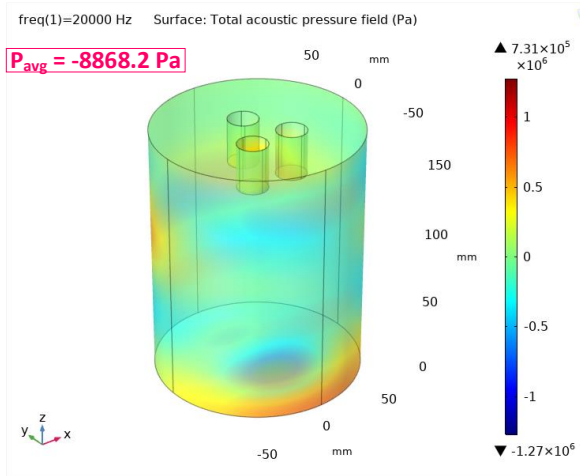
CLY-1P



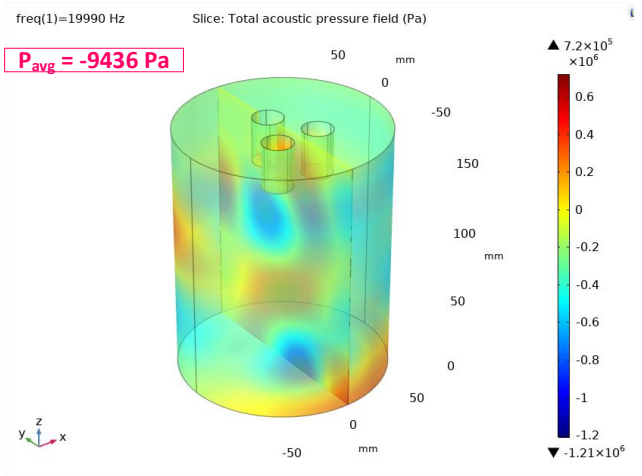
CLY-2P



CLY-2P



CLY-3P



CLY-3P

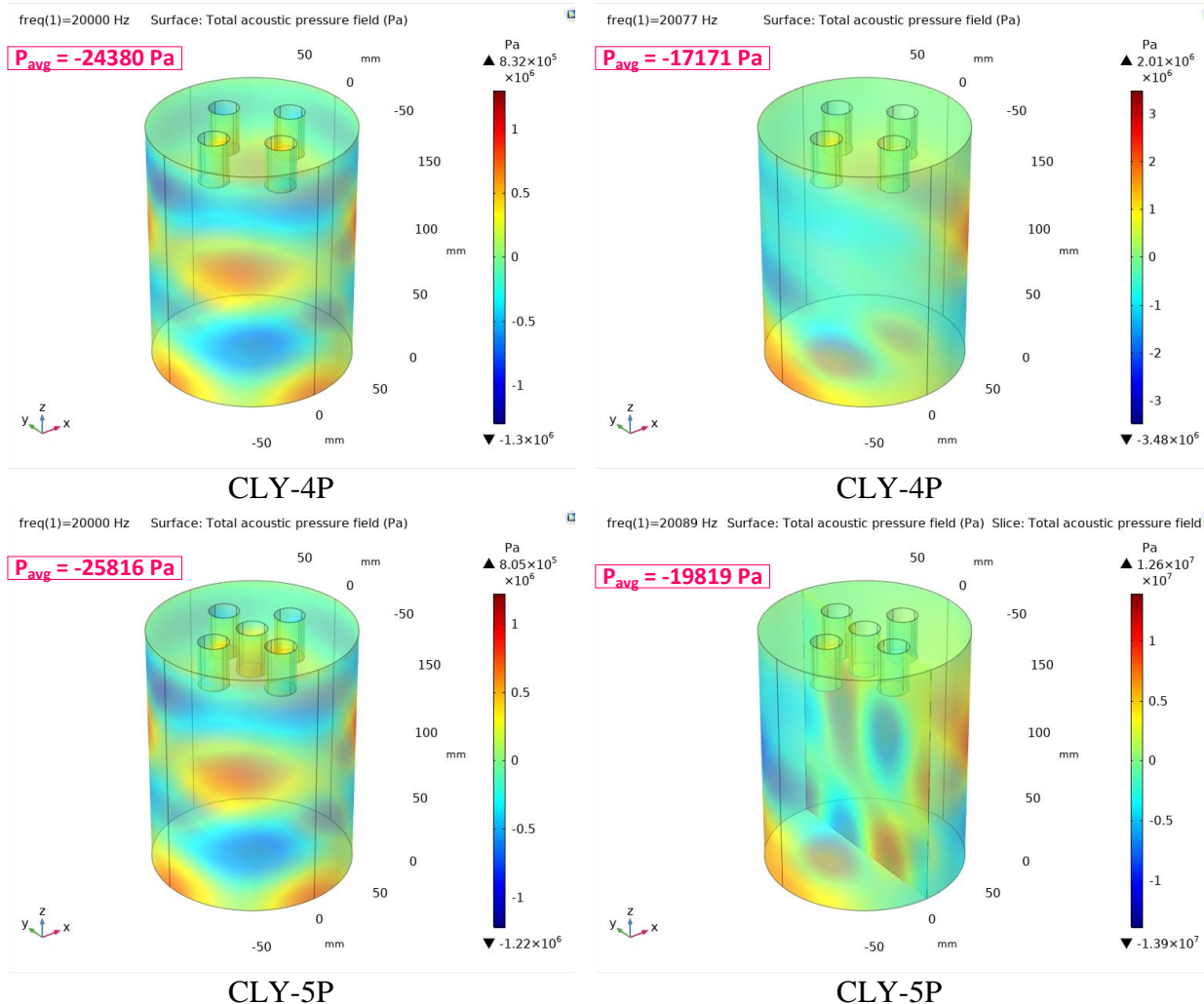
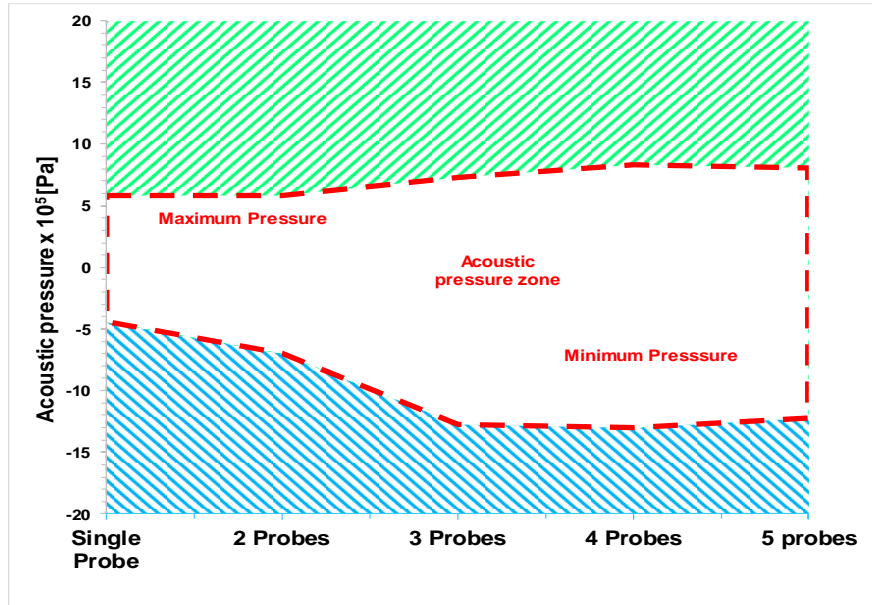
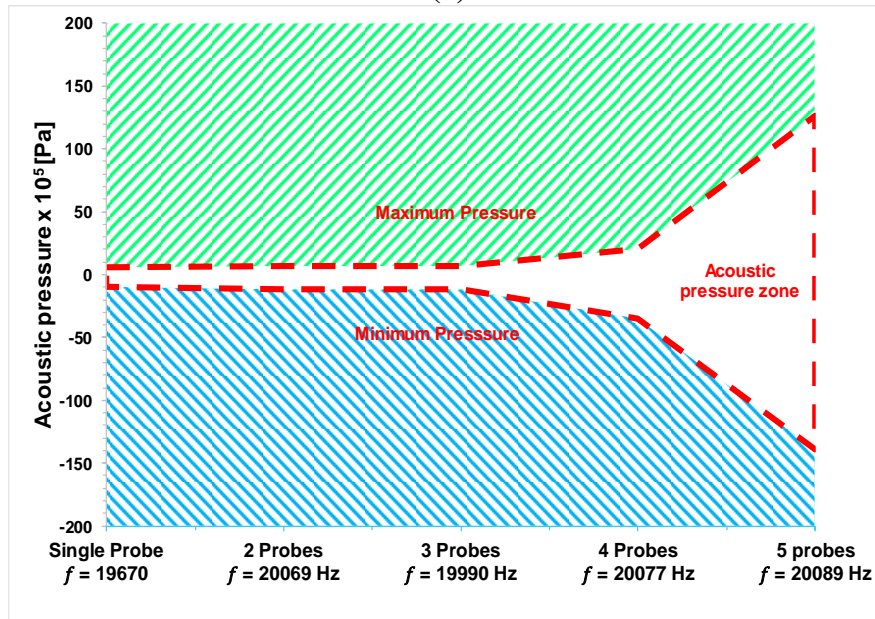


Figure 4.29: Acoustic shapes and modes for sonoreactors at 20 kHz (left) and corresponding Eigen frequencies (right) with different ultrasonic probes; the average pressure is taken over the volume from the COMSOL Acoustic Module Solution. Note that the vapor pressure for cavitation is 3171.47 Pa at 25.0 °C.

For the sake of clarification, a comparison is made to differentiate between all geometries. The comparison is drawn on the maximum and minimum acoustic pressures and reported in Figure 4.30 (a) at 20 kHz & (b) at the Eigen frequencies corresponds to each geometry. Where (a) represents the changes in the acoustic pressure at 20 kHz while changing the number of sonotrodes. There is no significant change in the maximum/minimum pressures when using one or two sonotrodes. While a major deflection is observed at 3 sonotrodes from which 4 or 5 sonotrodes would not alter the acoustic pressures. Therefore, at 20 kHz, we would recommend using a single or 3 sonotrodes because adding more sonotrodes would not be beneficial.



(a)



(b)

Figure 4.30: Maximum and minimum acoustic pressure for all geometries at (a) 20kHz and (b) Eigen frequencies

The highest sound pressure is usually related to the acoustic power supplied through the transducer probe, which has not changed significantly. In contrast, a significant change is noticed in the maximum magnitude of the negative pressure, which corresponds to the formation of acoustic cavitation bubbles. This is because the higher the magnitude of the negative pressure, the bigger the minimum pressure and the water vapor pressure. The optimum performance is recorded when the 3-sonotrodes geometry is used as the pressure drops down to down to -1.21×10^6 , enhancing

the sonochemical activity and possibly generating more bubbles. A similar observation has been found by Niazi et al. [83,99]. Table 4.7 shows the summary description of the optimization study and a comparison of the effect of the number of sonotrodes.

Table 4.7: Optimization and comparison of the effect of the number of sonotrodes

#N of Sonotrodes	1	2	3	4	5
Frequency [Hz]	$f=20000$				
Minimum pressure [Pa]	-4.43×10^5	-6.99×10^5	-1.27×10^6	-1.30×10^6	-1.22×10^6
Eigen Frequency [Hz]	19670	20069	19990	20077	20089
Minimum pressure [Pa]	-9.31×10^5	-1.18×10^6	-1.21×10^6	-3.48×10^6	-1.39×10^7

4.5.2 Effect of the outer sonoreactor geometry

In this section, a novel study is conducted considering the effect of having different outer sonoreactor geometries built in three dimensions, namely, the typical cylindrical sonoreactor, Hexagon reactor, and square sonoreactor. This study is made in two phases; the first phase is building those unique three-dimensional geometries with 3 ultrasonic transducer probes. While the second phase, all unique geometries are featured with 5 ultrasonic transducer probes. In this parametric study, we have considered varying outer geometry to see how this would affect the negative pressure's maximum magnitude. For this reason, 3 three-dimensional geometries are built. All geometries have the same diameter length and boundary conditions. The hexagon and the square are drawn inside the circular cylinder diameter given earlier. The same simulation procedure used in the previous section is used herein. An initial acoustic simulation is run for all three geometries using COMSOL to determine the Eigen frequencies or what is so-called the natural frequencies and the corresponding mode shapes for all the suggested geometries. The acoustic simulations took a couple of minutes to solve the Helmholtz equation. Once the acoustic simulations are done, the excitable modes and frequencies are checked. Then, the ultrasonic probe is introduced to work at the same frequency to trigger a resonance condition. This resonance condition will enhance the sonochemical process and make it more efficient. Figure 4.31 presents the differences in the acoustic shapes and modes for sonoreactors with 3 sonotrodes at 20 kHz (left) and corresponding Eigen frequencies (right). As seen in the case of hexagonal sonoreactor with 3 sonotrodes, the magnitude of the negative pressure increased from -2.54×10^6 to -2.23×10^6 , thus increase the possibility of cavitation. The results revealed that, in some cases, when operating

the sonoreactor at the Eigen frequency, it will trigger resonance that affects the maximum magnitude of the negative pressure. The hexagonal sonoreactor is tested at the eigenfrequency of 19903 Hz; however, the results are not in favor with the safe operation of the sonoreactor and may lead to collapse. Therefore, a follow-up study is conducted using another eigenfrequency of 20206 Hz showing a reasonable average pressure distribution. For comparison, Figure 4.32 presents the differences in the acoustic shapes and modes for sonoreactors when the sonoreactors are featured with 5 probes at 20 kHz.

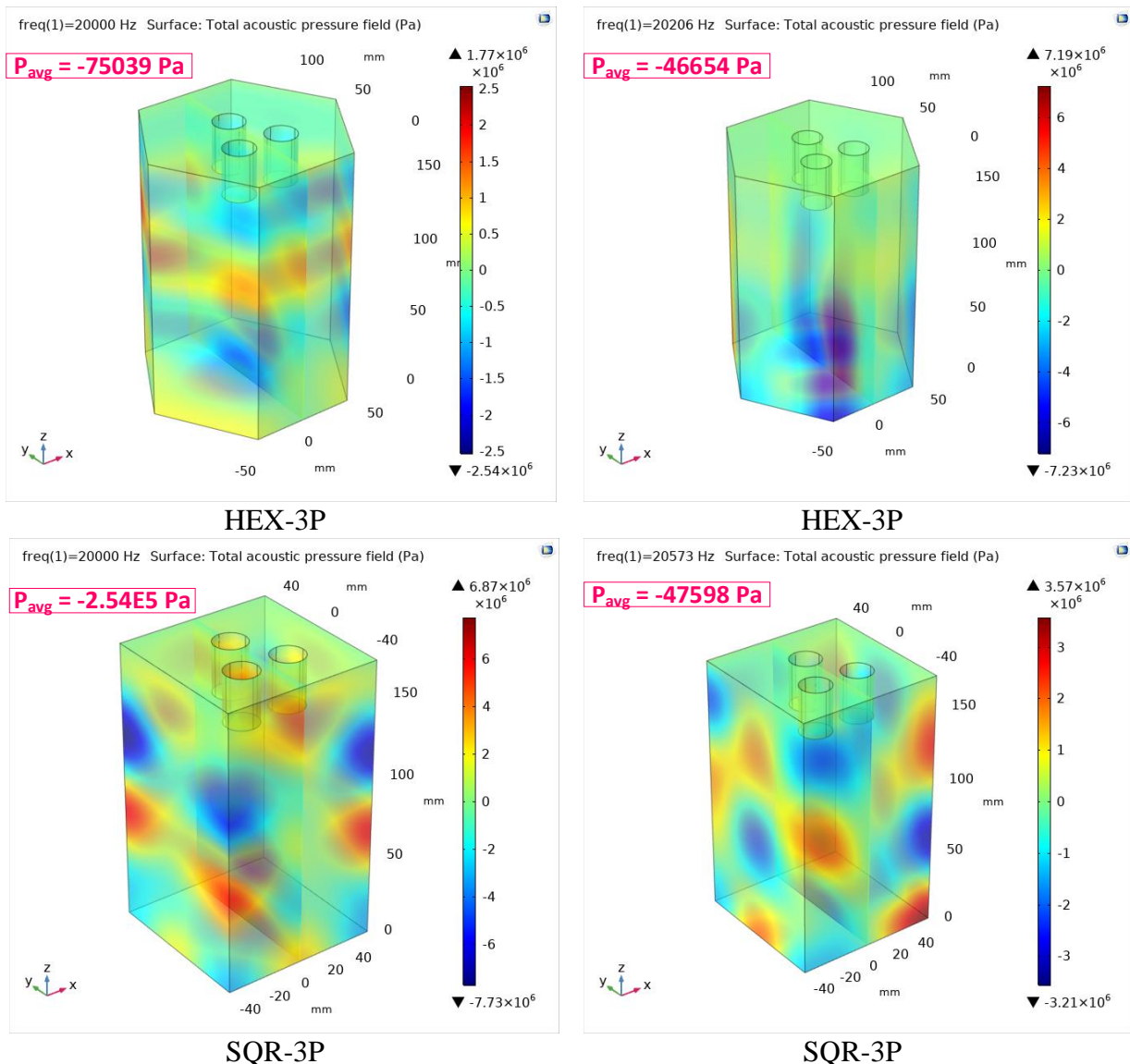


Figure 4.31: Acoustic shapes and modes for sonoreactors at 20 kHz (left) and corresponding Eigen frequencies (right) with different ultrasonic probes; the average pressure is taken over the volume from the COMSOL Acoustic Module Solution. Note that the vapor pressure for cavitation is 3171.47 Pa at 25.0 °C.

At the same time, the sonoreactors are tested while operating under the Eigen frequency conditions. The results are sorted, and it has been revealed that operating a Hexagonal sonoreactor at the following conditions: Eigen Frequency of 19331 Hz with 5 sonotrodes may adversely affect the sonoreactor body due to the build-up pressure that the sonoreactors with the following dimensions (HEX sonoreactor, 5 sonotrodes, 170 cm long, 50 cm diagonal length) cannot stand and it may collapse. Therefore, another Eigen frequency is chosen for the hexagonal and square sonoreactors and reported in Figure 4.32.

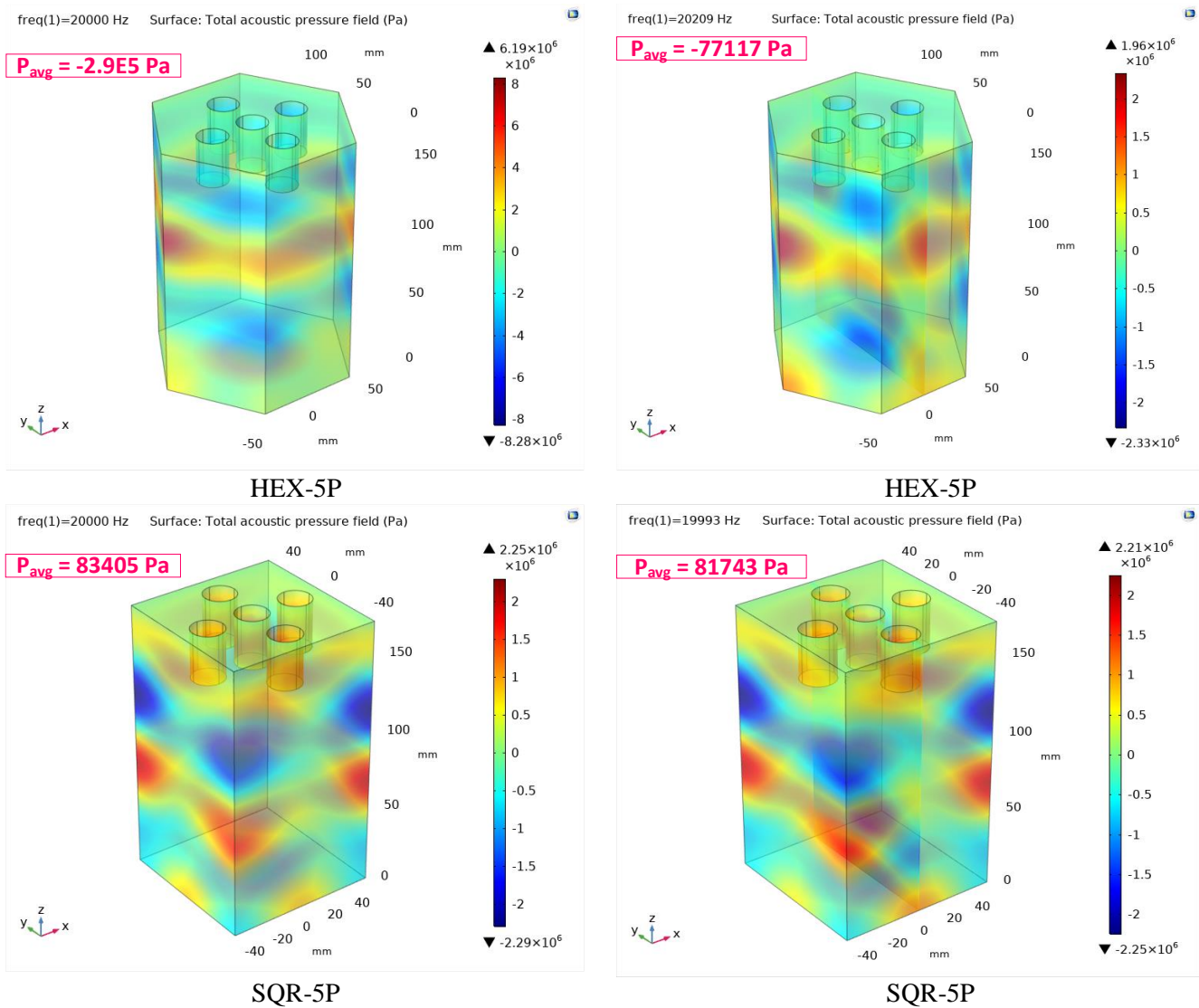


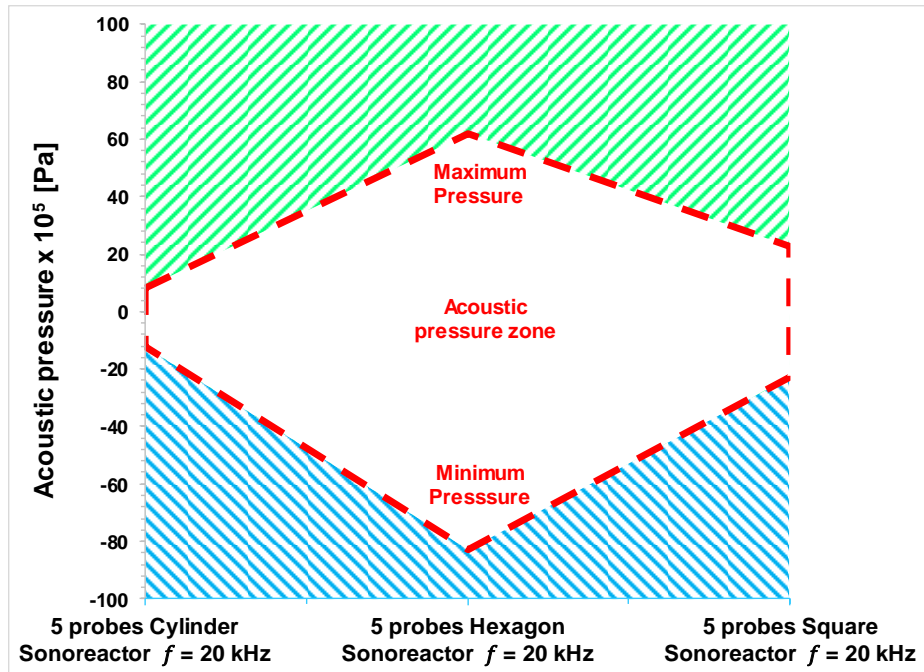
Figure 4.32: Acoustic shapes and modes for sonoreactors at 20 kHz (left) and corresponding eigenfrequency (right) with 5 transducers each; the average pressure is taken over the volume from the COMSOL Acoustic Module Solution. Note that the vapor pressure for cavitation is 3171.47 Pa at 25.0 °C.

The main observation from such analysis is that, in order to generate cavitation, the average pressure has to fall below the vapor pressure, which is 3171.47 Pa at 25.0 °C. The results showed that the square sonoreactor is considered not reasonable for generating acoustic cavitation bubbles as its average pressure is almost atmospheric. Figure 4.32 presents the differences in the acoustic shapes and modes for sonoreactors when the sonoreactors are featured with 5 probes at 20 kHz (left) and corresponding Eigen frequencies (right). The maximum and minimum pressure magnitudes are reported; after conducting the Eigen frequency test for all geometry in 3-D, which improved the maximum magnitude of the negative pressure and the cavitation energy and compared them with the typical ultrasonic frequency of 20 kHz. Figure 4.31 presents that the hexagon reactor at 20 kHz showed no significant difference with its Eigen frequency, while the square showed much better at its natural frequency. The differences in the magnitude of the negative pressure between all geometries are shown in Table 4.8 regarding optimization and comparing different geometries. A similar observation is found by Zhang et al. [144] in their study on the influence of sound directions on acoustic field characteristics within a rectangle-shaped sonoreactor.

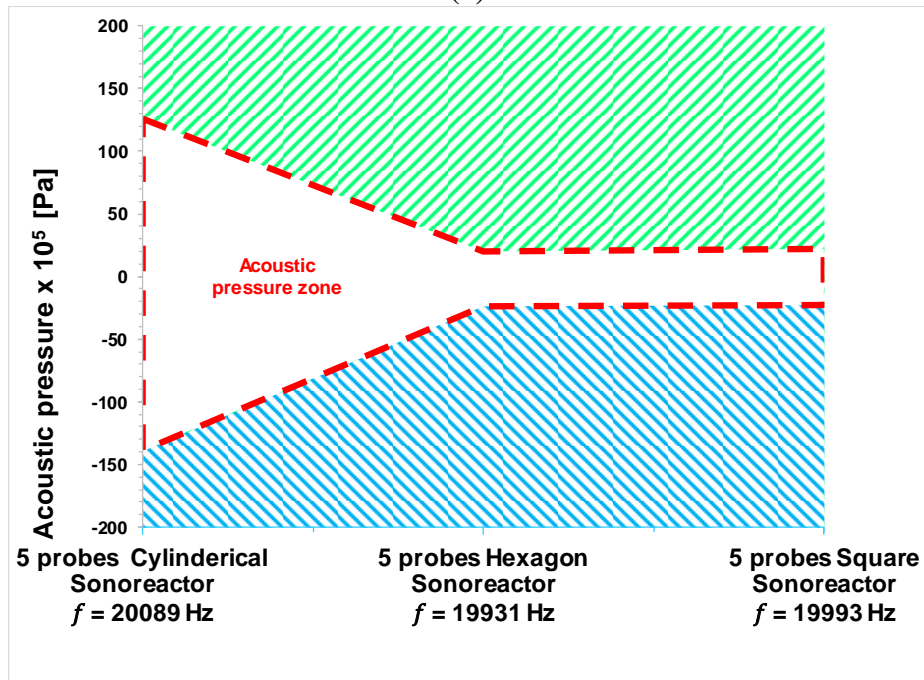
Table 4.8: Optimization and comparison on the effect of different geometries for the 5 sonotrodes analysis

Geometries	Cylinder	Hexagon	Square
Frequency [Hz]	$f=20000$		
Minimum pressure [Pa]	-1.22×10^6	-8.28×10^6	-2.29×10^6
Eigen Frequency [Hz]	20089	20209	19993
Minimum pressure [Pa]	-1.39×10^7	-2.33×10^6	-2.25×10^6

Further contrast is made to compare the geometries' performance with 3 sonotrodes and geometries with 5 sonotrodes on the maximum magnitude of the minimum pressure. At 20 kHz, there are no differences in the negative pressure in the cylindrical sonoreactor when 3 or 5 sonotrodes are applied. However, the hexagonal sonotrode with 5 probes showed a significant change. This can be attributed to the constructive interference of the sound waves when having 5 sonotrodes. Opposite observation is found when having the square sonoreactor. The constructive interference takes place when having 3 sonotrodes. It does not matter how many sonotrodes are introduced in the sonoreactor, but the most important thing is when constructive interference would occur.



(a)



(b)

Figure 4.33: Maximum and minimum acoustic pressure for all geometries at (a) 20kHz and (b) Eigen frequencies for geometries featured with 5 probes

In closing, this analysis is meant to investigate which sonoreactor has a higher possibility of generating acoustic cavitation by understanding the physics and the maximum magnitude of the negative pressure associated with each sonoreactor. However, the number of bubbles increases

significantly when the ultrasonic frequency increases. This observation is matching with some reports in the literature. It is not possible to make a clear comparison since most literature studies are performed experimentally at different conditions as compared to our study, including the ultrasonic frequency, acoustic intensity, and acoustic amplitude.

4.5.3 Characterization of the cavitation zone

The Blake Cavitation Threshold characterizes the cavitation zone. The actual limit separating linear and inertial cavitation is known as the Blake threshold. The black threshold P_{BL} is characterized by the Blake radius R_0 , static pressure P_∞ , and the water vapor pressure P_v as follows:

$$P_{BL} = P_0 - P_V + \frac{2}{3\sqrt{3}} \left(\frac{2\sigma}{R_0} \right)^{3/2} \left(P_0 - P_V + \frac{2\sigma}{R_0} \right)^{-1/2} \quad (4.1)$$

Where σ is the surface tension of water, the blake cavitation threshold is quantified according to equation 12 by Figure 4.34. It can be seen that the cavitation threshold decreases exponentially while the radius of nuclei increases within the assumed radius range between $0.1 \mu\text{m}$ to $10 \mu\text{m}$.

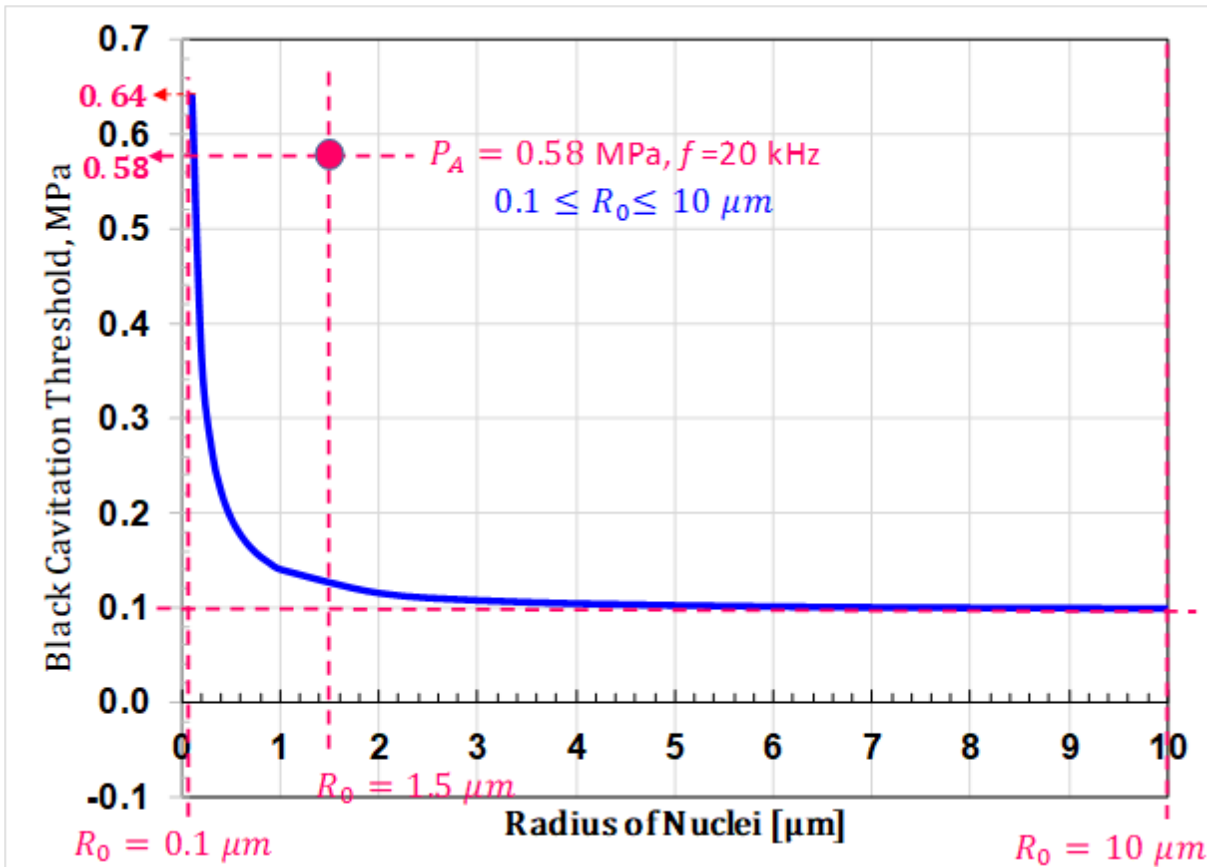


Figure 4.34: Blake Cavitation Threshold concerning the nuclei radius,

At the minimum radius of nuclei is $0.1 \mu\text{m}$ the cavitation threshold exceeds 0.64 MPa , regarded as the severe cavitation threshold. When the initial radius of the nuclei is higher than $10 \mu\text{m}$, this is corresponding to the minimum cavitation threshold. Thus, the predicted cavitation volume is quantified compared to the total volume of the sonoreactors with different configurations. Figure 4.35 presents a comparison between all sonoreactor in the present study. The figure presents the cavitation volume percentage, and the severe cavitation volume percentage as compared to the total volume of the sonoreactor corresponds to 100%. The rest of the volume is water with no predicted cavitation. The cavitation volume is identified using COMSOL Multiphysics by allocating the nodes whose pressure higher than the cavitation threshold. In contrast, the severe cavitation volume is quantified by allocating the number of nodes whose pressure higher at the pressure corresponds to $0.1 \mu\text{m}$.

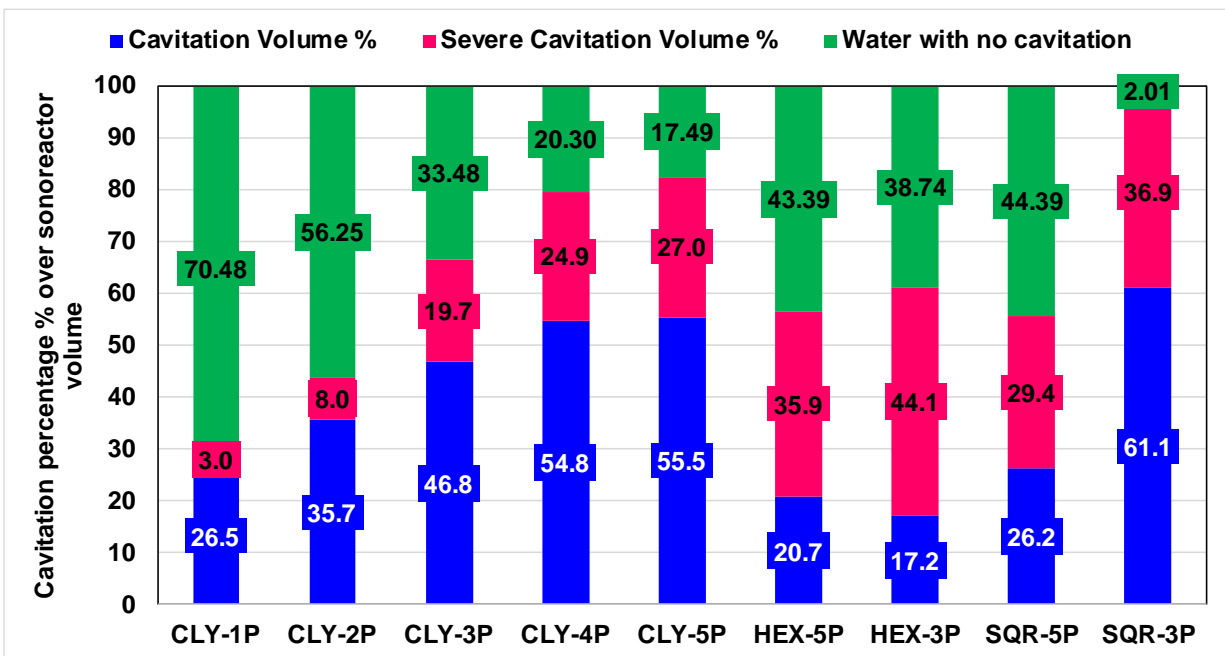


Figure 4.35: Cavitation percentage over the sonoreactor volume

It can be concluded that, under the cylindrical sonoreactor, the higher the number of probes, the higher the cavitation volume and the severe cavitation volume. As seen, the minimum cavitation percentage is recorded by CLY-1P because it has only 1 probe, which made the probability of generating cavitation is the lowest due to the high volume of the sonoreactor as compared to the probe volume. On the other hand, between the cylindrical sonoreactors, the maximum cavitation

volume can be generated by CLY-4P and CLY-5P, approximately 55%. However, the maximum cavitation recorded overall is recorded by the SQR-3P. Noting that, the case SQR-3P has its sonoreactor volume full by the cavitation volume 61.1% and severe cavitation volume of 36.9. In contrast, the maximum severe cavitation is recorded for HEX-3P with 44.1% of its volume covered with bubble radiuses lower than $0.1 \mu\text{m}$. This study is crucial as it gives an insight into the cavitation threshold and the predicted cavitation required for hydrogen production.

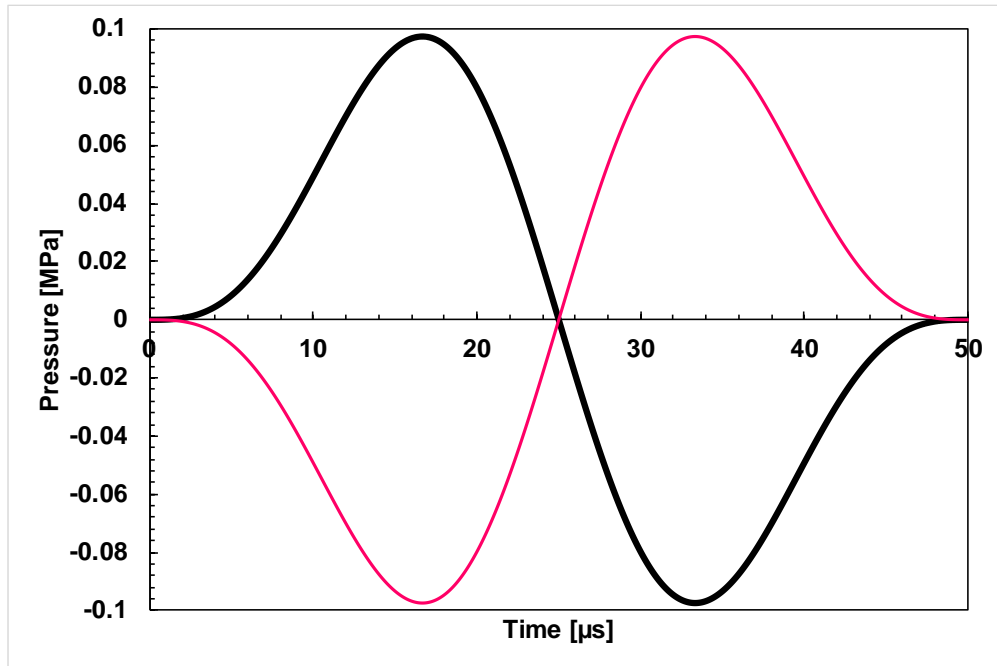
4.7 Chemical Kinetics Modeling Results

A comprehensive numerical study is performed to establish a link between the acoustic cavitation bubble activity's primary effect and the consequent effect of the chemical kinetics mechanism associated with the sonochemical process. We studied a possible reaction kinetics mechanism for the sonochemical hydrogen production in this work, which we called the sonohydrogen process. The reaction kinetics mechanism consists of 19 reversible reactions inside the acoustic cavitation micro-bubble at different conditions. The reaction kinetics simulation is validated and utilized to quantify the amount of hydrogen produced by a single bubble that is initially saturated with water vapor/oxygen. The results from the bubble dynamics model and the chemical kinetics model are compared with two different literature experiments.

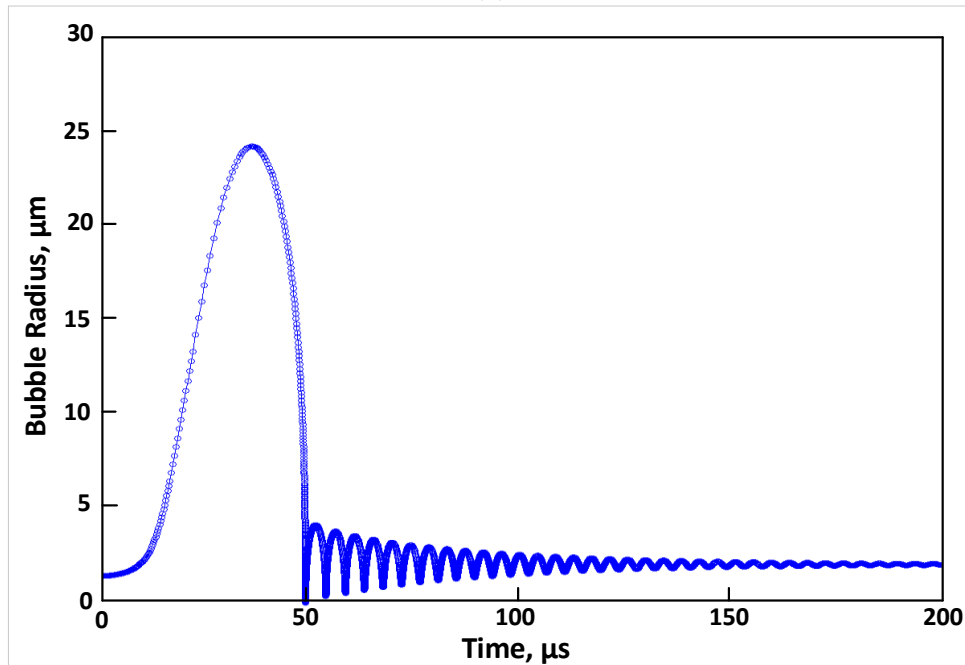
4.6.1 Bubble Dynamics Results

This section starts with the bubble dynamics results, followed by the chemical kinetics model validation and results—the range of ultrasound frequency changes with the sonoreactor configuration. The sonoreactor configuration alters based on the location where the ultrasound waves are introduced to the liquid medium. The most commonly used ultrasonic frequency in sonochemistry or the sono-hydrogen process is 20 kHz, and the corresponding initial bubble radius is known to be $2 \mu\text{m}$ [64,106]. Hence, at $f = 20 \text{ kHz}$ and an acoustic pressure amplitude of 0.1 MPa, the numerical results of the radial bubble dynamics presented in Figure 4.36, in terms of the pulse pressure and the bubble radius, all concerning the time. The pulse pressure is reported in Figure 4.36 and can be defined as the pressure emitted from the ultrasonic wave and exposed to the bubble. The pulse pressure applied by the transducer probe drawn for one acoustic cycle ($50 \mu\text{s}$ at 20 kHz). Also, the bubble radius presented as a function of time. The bubble radius is initially at $1.5 \mu\text{m}$. The bubble radius behavior matches the radius behavior reported by Kim et al. [78] and

shows an expansion within the first period of the cycle and has gone to collapse after two consecutive cycles at 100 μs .



(a)



(b)

Figure 4.36: The simulated bubble dynamics results at 20 kHz for a bubble radius of 1.5 μm and acoustic amplitude of 0.1 MPa (a) the pulse pressure introduced to the bubble, (b) bubble radius expansion at the aforementioned conditions

The bubble radius reaches a resonance size 25 μm at 20 kHz. After solving the Keller-Miksis equation considering the bubble-dynamics model, the results reported that the maximum radius is 25 μm . By knowing the maximum bubble radius and the initial bubble radius (minimum bubble radius) at the acoustic operating conditions (frequency 20 kHz and acoustic amplitude 0.1 MPa), will allow us to calculate the maximum bubble pressure ≈ 4000 atm by recalling equation (6), and the maximum bubble temperature $\approx 6000\text{K}$ from recalling equation (7). According to these results, these extreme conditions produced from a single bubble collapse will bring a unique chemical environment where high-energy chemical reactions occur. In the following section, we present the chemical kinetics model results, including the model validation and the effect of different bubble temperatures on the evolution of each species, primarily hydrogen and hydrogen radicals.

4.6.2 Chemical kinetics validation

The validation study for the chemical kinetics model is carried out to ascertain the proposed model's accuracy by using the “Chemical Species Transport” module in COMSOL. While the “Reaction Engineering” submodule is chosen to investigate a series of 19 reversible chemical reactions. The possible chemical kinetics mechanism consists of 19 possible chemical reactions from previous kinetic data for combustion [145–149] and sonochemical. The present model is compared to the work done by Merouani et al. [57] in 2014 about a theoretical estimation of the temperature and pressure within the collapsing acoustic bubble. The validation study is performed to assure the proposed kinetics model's accuracy for hydrogen production out of water molecules' dissociation due to the sonohydrogen process. The kinetic mechanism's evolution concerning the time at pressure and temperature conditions corresponds to the acoustic conditions.

Table 4.9: The initial concentration of the mixture species present study

Species	The initial condition set by Merouani et al. [57]
H_2	0
H	0
H_2O	0.39
H_2O_2	0
HO_2	0
O	0
O_2	0.61
OH	0

The analysis is estimated for a single bubble, which is initially composed of water vapor H_2O and O_2 . The initial concentration of the 9 species are given in Table 4.9. This series of chemical reaction simulation results at the same bubble conditions are presented in Figure 4.37. The analysis is performed for a single bubble that is initially saturated with a mixture of water vapor H_2O and oxygen O_2 . The water vapor and oxygen mole fractions' initial concentrations are 0.39 and 0.61 at the start of the dissociation reaction. As seen, H_2O and O_2 are consumed, and other species such as OH and H_2 are produced at a mole fraction of 0.18 and 0.01, respectively. Different species such as H_2O_2 , HO_2 , O , and H produced from such dissociation reactions are not included.

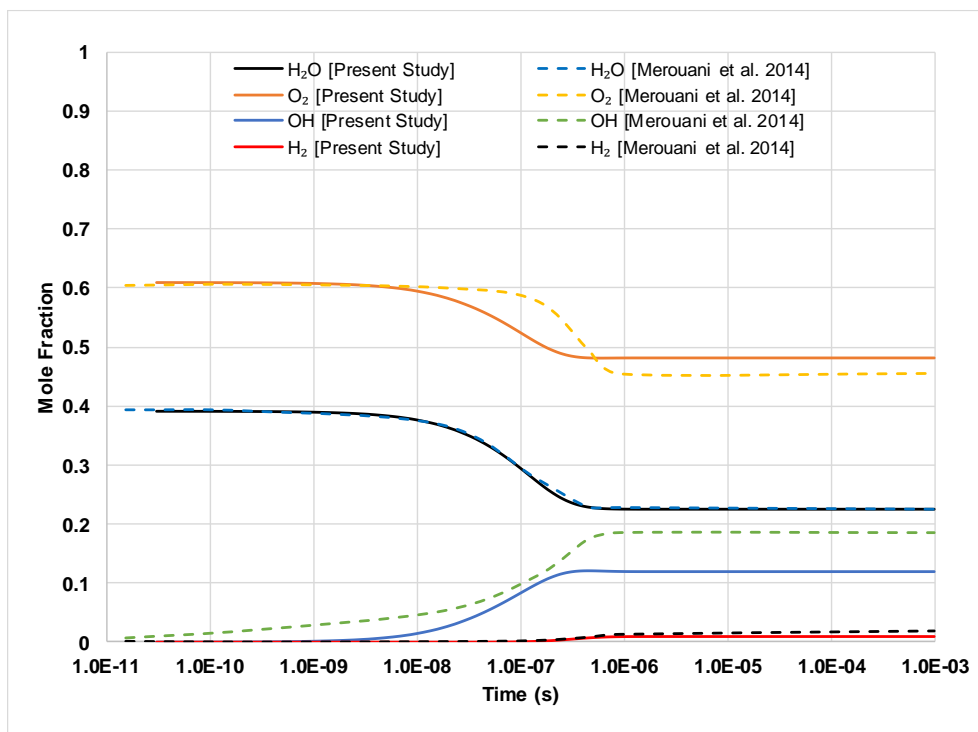


Figure 4.37: Validation of the chemical kinetics mechanism used in this study with the work done by Merouani et al. [57]

The comparison is drawn and reported in Figure 4.37. The solid lines denote the present study analysis and species concentrations, while the dashed lines indicate the previous data by Merouani et al. [57]. Generally, the present study's range of values is in good agreement with the values cited previously by Merouani et al. [57]. The reaction takes place at a time of micro-scale [μs], and the comparison results showed an excellent agreement regarding the values and profile. There is a slight difference in the OH concentration. This might be due to small differences in the experimental parameters such as Arrhenius values and the temperature exponent.

4.6.3 Effect of Bubble Temperature

It is well-known that the temperature inside the acoustic cavitation bubble has a significant impact on the dissociation reaction mechanism and the final concentration of hydrogen and other species. The effect of the bubble temperature is having a substantial effect on the H₂ production rate. The bubble temperature is one of the essential parameters that affect the mole fraction of the produced hydrogen from the sonochemical process. The study concluded that the OH radicals are the main product formed inside a bubble at the end of the bubble collapse. As per Momirlan and Boriaru [150], the influence of temperature on the hydrogen production process from water dissociation is recognized at a temperature higher than 2000 K. Another study by Xu et al. [151] stated that to attain a reasonable degree of water dissociation at the atmospheric pressure, and the temperature should be around 2500K. This is because the required temperature to dissociate a single molecule of water vapor entirely and produce hydrogen is 15000 K, as calculated earlier using thermodynamics analysis.

(a) H₂O/O₂ bubble case

In this sub-section, a parametric study on the effect of the temperature inside the bubble is performed and reported, which is initially saturated with water vapor and oxygen. The parametric study shows how the temperature variation is affecting the final products of the dissociation reactions. Hence, the text above explains why there is no reaction taking place at a bubble temperature of 2000 K. The species' concentration has not changed, which means the reaction did not even start at such a low temperature, as presented in Figure 4.38. At 4000 K, the reaction began to occur with a slight increase in the species' concentration. Water vapor and oxygen started to be consumed, and the highly reactive radicals are started to form. Heavy consumption of the water vapor/oxygen begins when the bubble temperature starts to exceed 5000 K. However, the hydrogen is not evolved until the bubble temperature becomes higher than 3000 K. This is due to the 15000 K temperature limit calculated earlier to dissociate water into hydrogen completely. The higher the bubble temperature, the higher the depletion of the water vapor/oxygen mole number to generate more reactive radicals for 8000 K. For the sake of clear presentation, Figure 4.39 and Figure 4.40 are considering the concentrations of both H₂ and H radical per unit volume of a single bubble. The higher the bubble temperature, the higher the generated mole fractions for both species. As mentioned, the bubble collapse will cause a tremendous amount of energy that goes

up to thousands in Kelvins. Hydrogen and hydrogen radicals are of importance because they are contributed to the final production rate of hydrogen. As per the numerical analysis and simulations presented in those figures accordingly, the trends showed continuous hydrogen production concerning time. However, these trends will change, and hydrogen production will not remain constant if the dissolved gas changed.

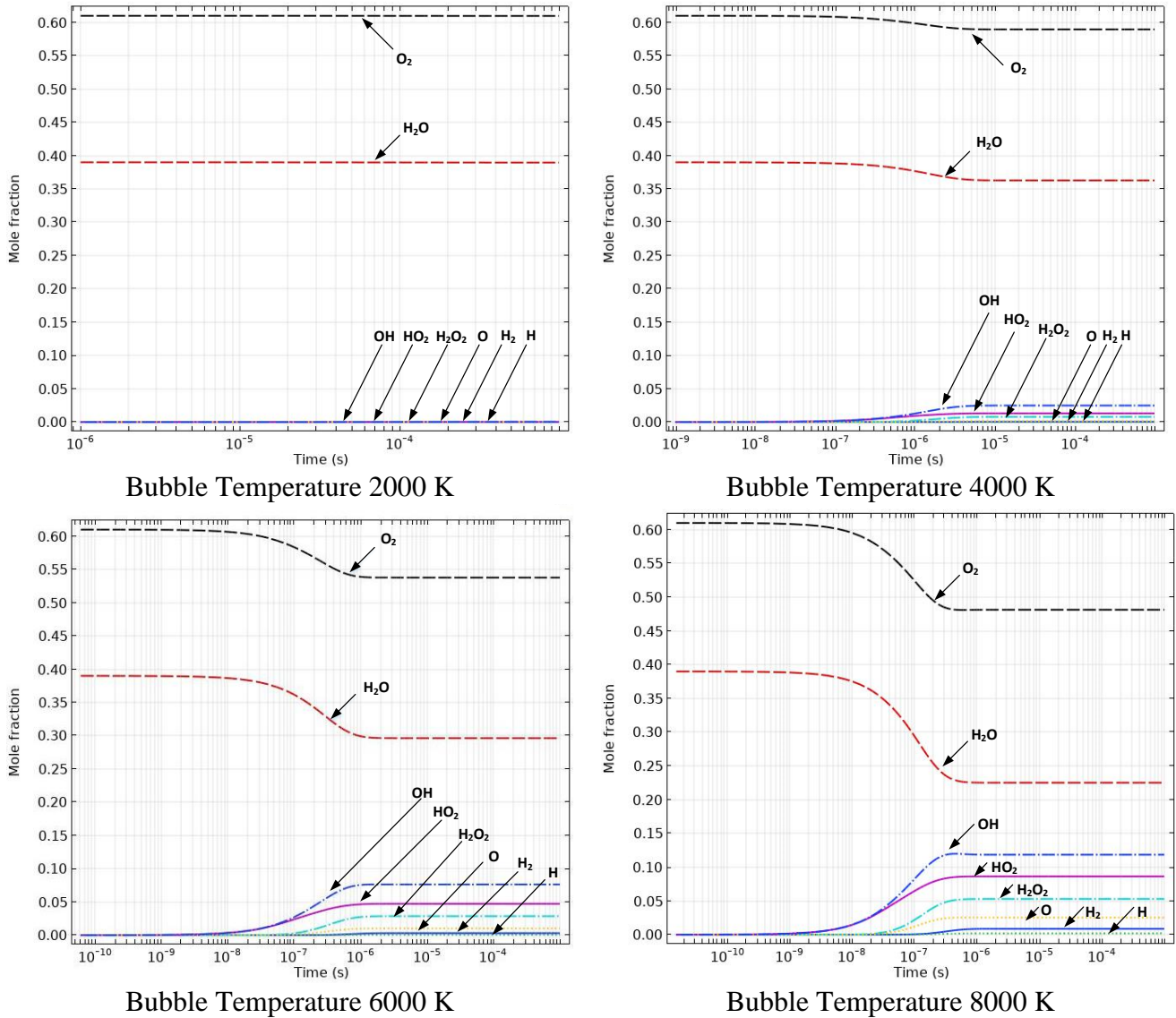


Figure 4.38: Evolution of the kinetic mechanism involving hydrogen with time at different bubble temperatures for a single bubble initially composed of H_2O/O_2

The hydrogen production rate is quantified in the next section by equation (4.6). Therefore, the production rate mainly depends on the mole number of radicals inside the bubble, which is

controlled by the bubble temperature. The concentrations are given in mole fraction per unit volume of the reactor. Knowing that as the reactor volume is the volume of a single bubble, then these values should be multiplied by the bubble volume calculated at the maximum radius R_{max} .

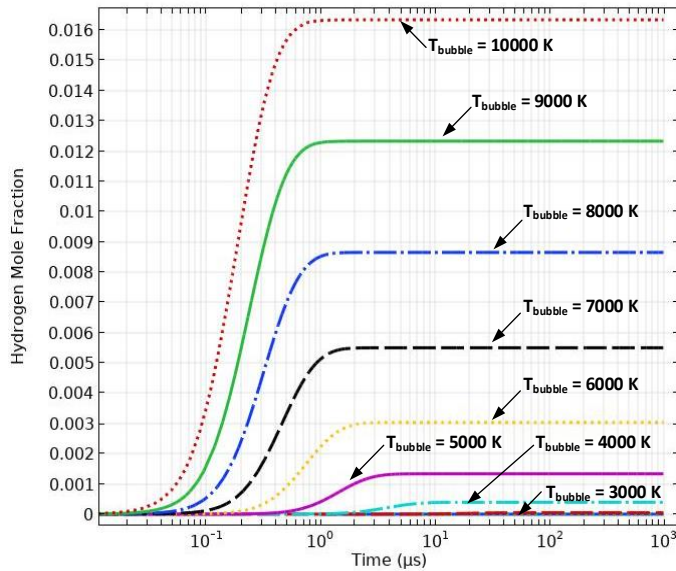


Figure 4.39: Evolution of the mole number of H_2 concerning the time at different bubble temperatures

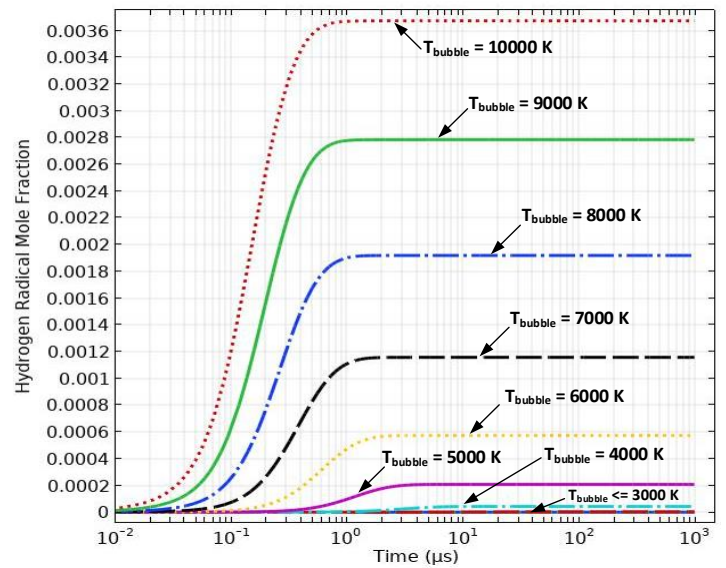


Figure 4.40: Evolution of the mole number of $*H$ concerning the time at different bubble temperatures

As seen in Figure 4.41, the hydrogen and hydrogen radicals almost have no production below a temperature of 3000 K. The mole number of both H_2 and H are presented in, which is given in mole per unit reactor volume. The reactor volume is the single bubble. Thus, the maximum radius's bubble volume should be multiplied by the mole number obtained from the figure. The correlation between the bubble temperature and the mole fraction of H_2 and H radical formed inside a single water vapor/oxygen bubble per collapse has a good agreement with the results reported by Merouani et al. [57]. The curves will be used later on for the hydrogen production quantification in the last section.

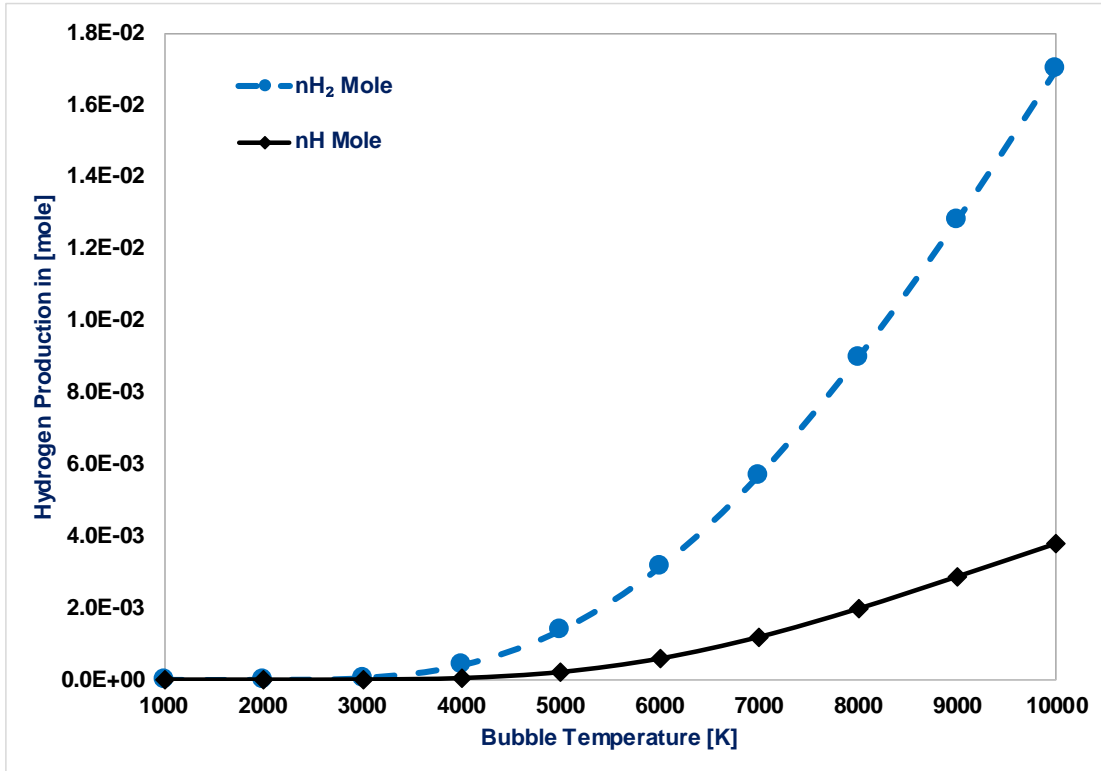


Figure 4.41: The hydrogen and hydrogen radical produced in moles

(b) H₂O/CO₂ bubble case

Another parametric study shows how the temperature variation affects the final products of the dissociation reactions but in the case of the H₂O/CO₂ bubble. It is well-known that the bubble temperature is having a significant impact on the dissociation reaction mechanism and the final concentration of hydrogen and other species. The effect of the bubble temperature has a substantial impact on the H₂ production rate, which is presented in Figure 4.42. The bubble temperature is one of the essential parameters that affect the mole fraction of the produced hydrogen from the sonochemical process. The study concluded that the OH radicals are the main product formed inside a bubble at the end of the bubble collapse. As per Momirlan and Boriaru [150], the influence of temperature on the hydrogen production process from water dissociation is recognized at a temperature higher than 2000 K. Another study by Xu et al. [151] stated that to attain a reasonable degree of water dissociation at the atmospheric pressure, and the temperature should be around 2500 K. Hence, this explains why there is no reaction taking place at a bubble temperature of 2000 K; the species' concentration is not changed, which means the reaction did not even start at such low temperature as presented in Figure 4.42. At 4000 K, the reaction began to take place with a

slight increase in the species' concentration. Water vapor and oxygen started to be consumed, and the highly reactive radicals are started to form. The water vapor consumption begins when the bubble temperature starts to exceed 5000 K. However; the hydrogen isn't evolved until the bubble temperature becomes higher than 3000 K. From the parametric study, the higher the bubble temperature, the higher the depletion of the water vapor/carbon dioxide mole number to generate more reactive radicals, as shown in Figure 4.42 for 8000 K. Therefore, the bubble is acting as a micro-combustion chamber or intense plasma where very high temperatures up to 20000 K are predicted and measured by Schanz et al. [77].

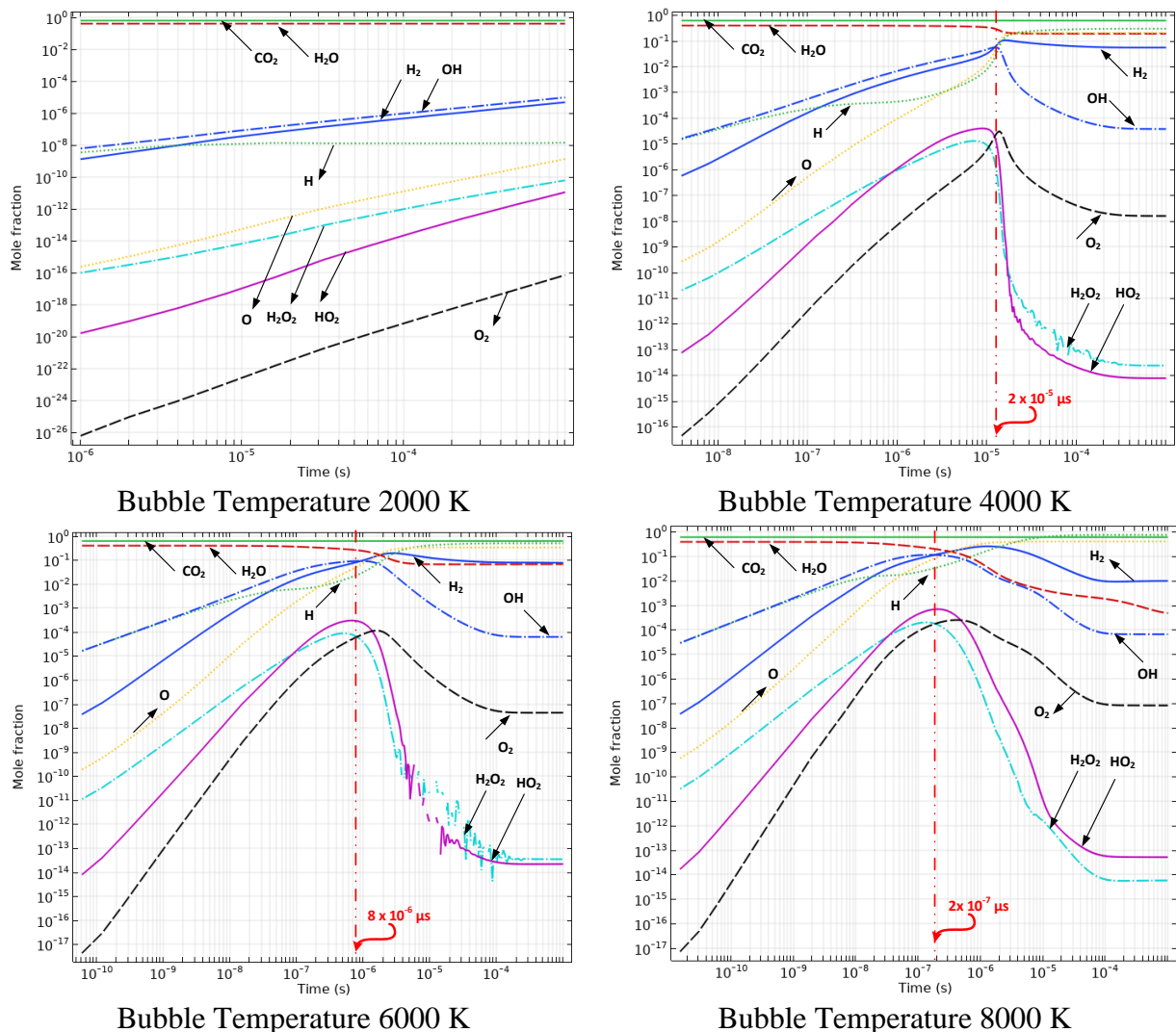


Figure 4.42: Predicted species production vs. time at different bubble temperatures for H_2O/CO_2

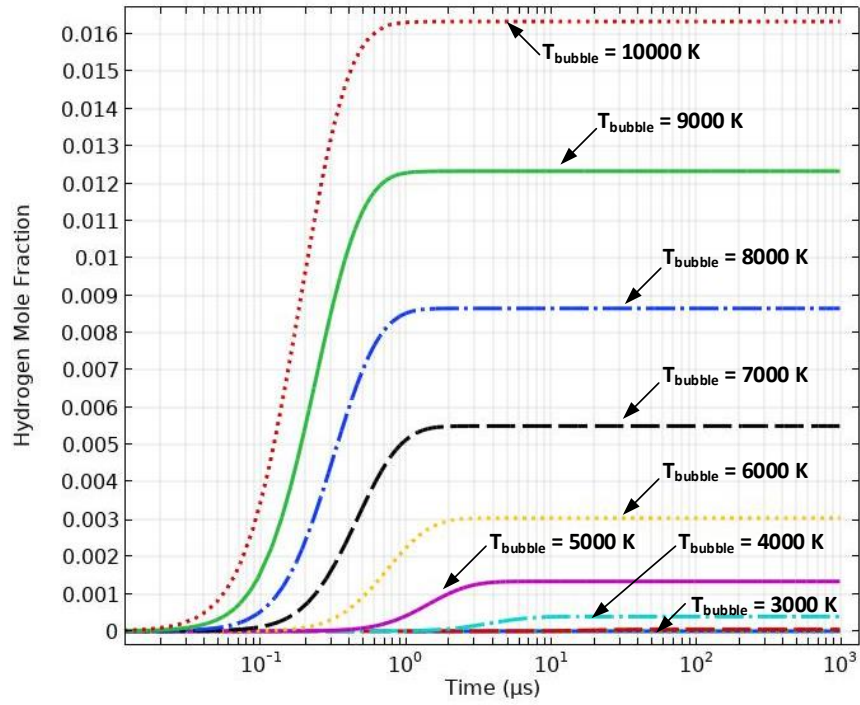


Figure 4.43: Predicted H_2 production vs. time of reaction at different temperatures for the $\text{H}_2\text{O}/\text{O}_2$ bubble

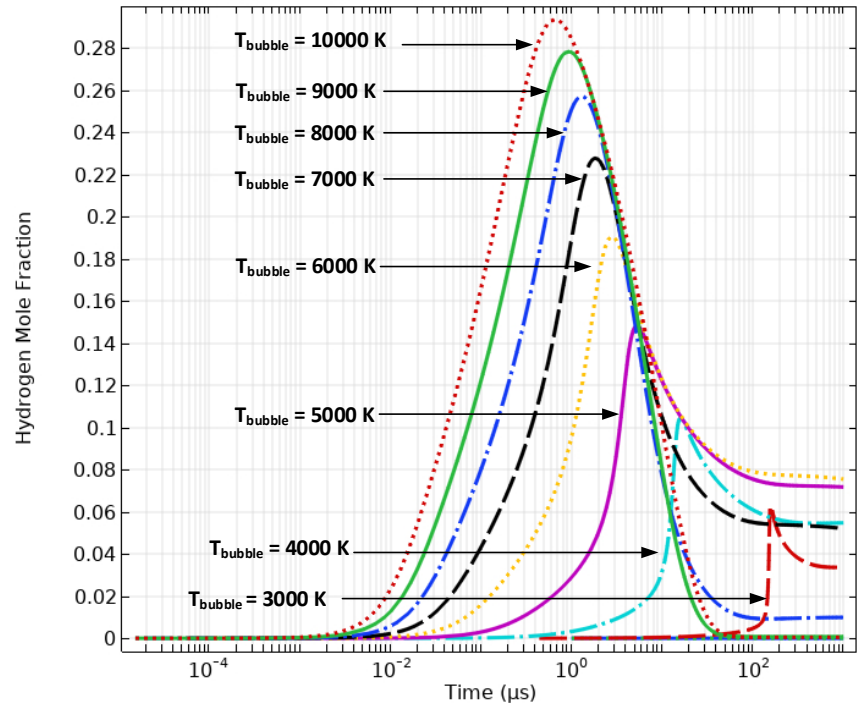


Figure 4.44: Predicted H_2 production vs. time of reaction at different temperatures for the $\text{H}_2\text{O}/\text{CO}_2$ bubble

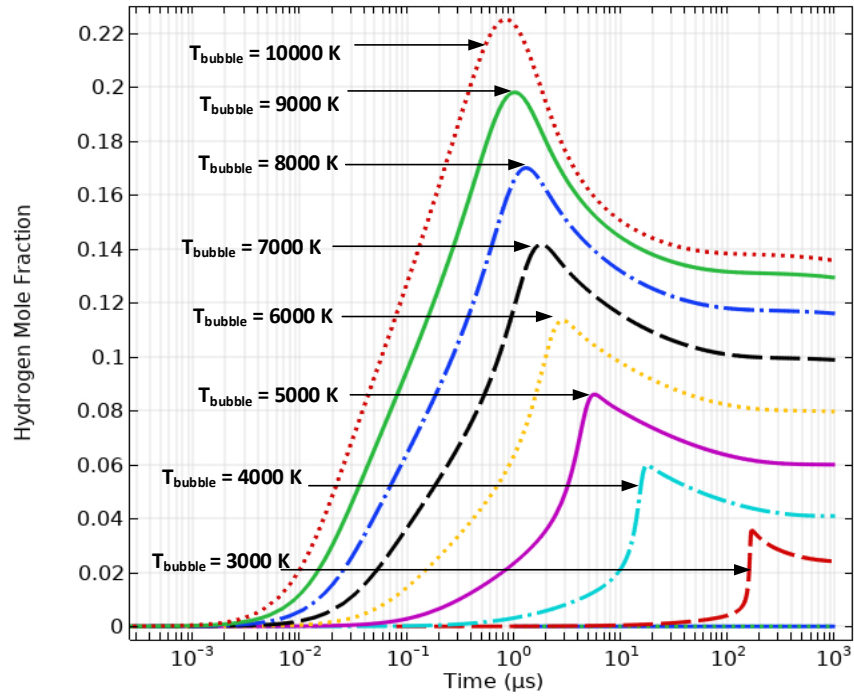


Figure 4.45: Predicted H₂ production vs. time of reaction at different temperatures for the H₂O/Ar bubble

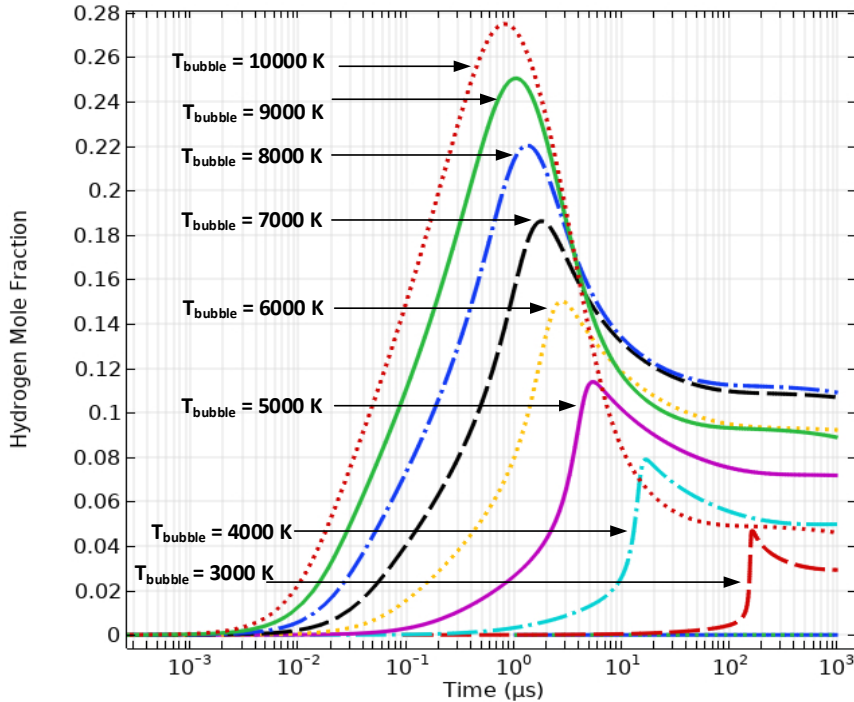


Figure 4.46: Predicted H₂ production vs. time at different bubble temperatures for the H₂O/Air bubble

Hydrogen and hydrogen radicals are of importance because they are contributed to the final production rate of hydrogen. As per the numerical analysis and simulations presented in those figures accordingly, the trends showed continuous hydrogen production. However, these trends change, and hydrogen production will not be constant if the dissolved gas changed. The hydrogen production rate is calculated later in the following section by equation (4.5).

Therefore, the production rate mainly depends on the number of radicals inside the bubble controlled by the bubble temperature. The concentrations are given in mole fraction per unit volume of the reactor. Knowing that as the reactor volume is the volume of a single bubble, and then the bubble volume calculated at the maximum radius should be multiplied by these values. As seen from the figures below, the hydrogen and hydrogen radicals almost have no production below a temperature of 2000-3000 K. based on the acoustical parameters. The higher the bubble temperature, the slower the reaction time. This is because of the high reaction rate. The figure indicates the reaction time while using CO₂ as a dissolved gas. The reaction time scale changes while changing the bubble temperature. For H₂O/O₂ bubble, the mole number of H₂ is presented in Figure 4.43 as predicted by the chemical kinetics model from the parametric study on the bubble temperature. Thus, the mole number obtained from the figure should multiply by the bubble volume at the maximum radius. The correlation between the bubble temperature and the mole fraction of H₂ and H radical formed inside a single water vapor/oxygen bubble per collapse is in good accordance with the results reported by Merouani et al. [57]. The curves will be used later on for the hydrogen production quantification in the last section of the results. For H₂O/CO₂ bubble, the mole number of H₂ is presented in Figure 4.44 in a mole per unit reactor volume, knowing that the reactor volume is the single bubble. The results considering the H₂O/Argon bubble are presented in Figure 4.42, given in moles extracted directly from the chemical kinetics model in COMSOL. The correlation between the bubble temperature and the mole fraction of H₂ and H radically produced in one water bubble should be employed to get the final output of hydrogen from the sonochemical process. H₂O/Argon chemical kinetics reaction results seemed to be consistent with the reaction time. No overlapping between the trends of hydrogen production concerning the differences in temperatures, which contradicts the trends found in the H₂O/Air bubble in Figure 4.46. In conclusion, when we compare the results of all dissolved gases, we will find that CO₂ has a significant contribution to enhancing the overall hydrogen production. This will be presented in the last subsection.

(c) H₂O/Ar bubble case

The previous sections, where the bubble temperature effects are presented for bubbles, contain H₂O/O₂ and H₂O/CO₂. In this section, the effect of varying the bubble temperature when simulating an H₂O/Argon bubble. In all sections, the water vapor fraction WVF is fixed to be 39%. Significant differences are seen when comparing all cases; this is due to the variation of the physical and chemical properties of all dissolved gases used. The effect of the bubble temperature has a substantial impact on the H₂ production rate, presented in Figure 4.47.

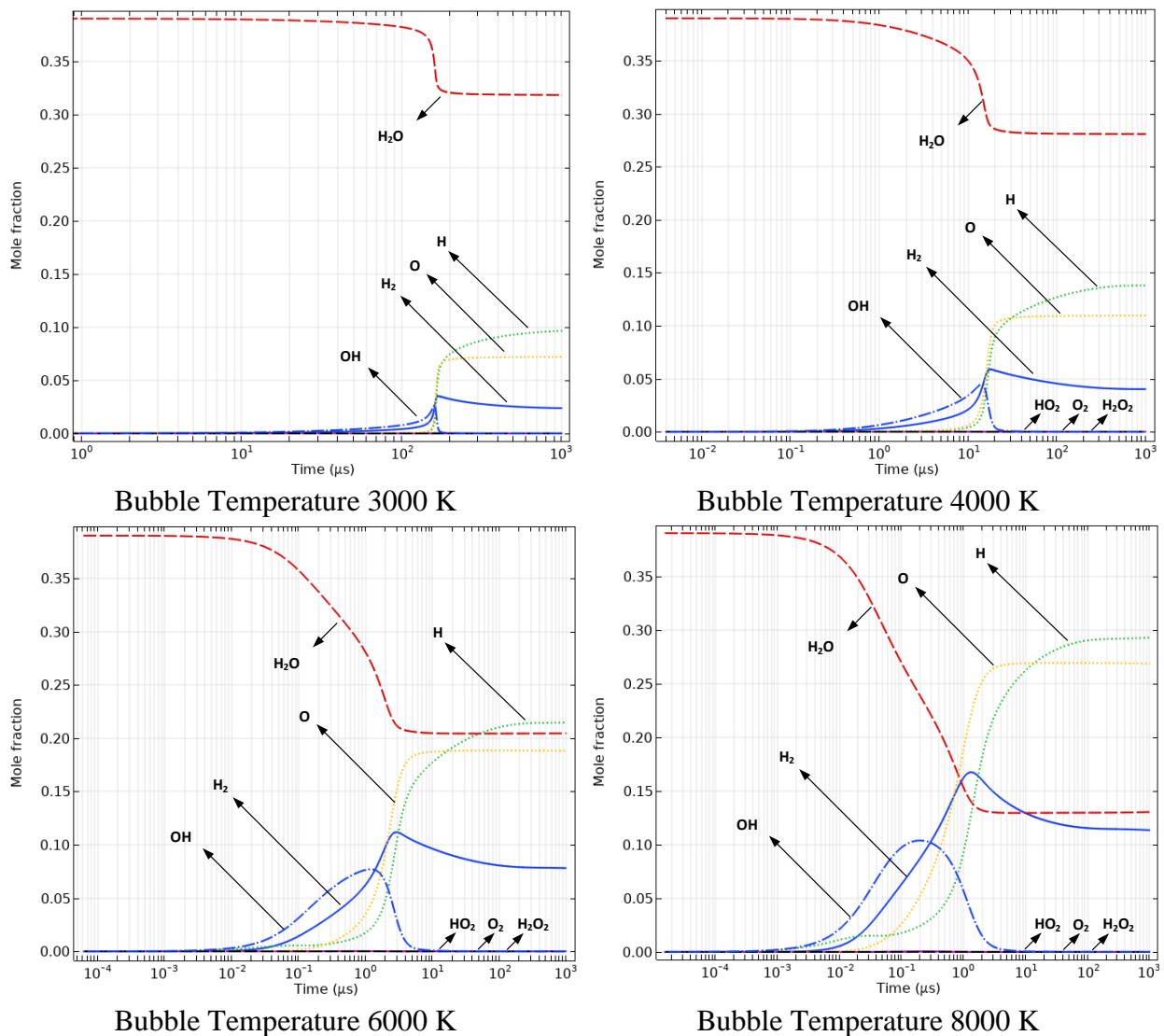


Figure 4.47: Predicted species production vs. time at different bubble temperatures for H₂O/Ar

The bubble temperature is one of the essential parameters that affect the mole fraction of the produced hydrogen from the sonochemical process. As seen from the figures below, the hydrogen and hydrogen radicals almost have no production below a temperature of 2000-3000 K. The higher the bubble temperature, the slower the reaction time. Hence, this explains why there is no reaction taking place at a bubble temperature before 3000 K; the species' concentration is not changed, which means the reaction did not start at such a low temperature. At 4000 K, the reaction began to occur with a slight increase in the species' concentration of around 0.04. Simultaneously, the hydrogen mole fraction recorded an increase to 0.075 and 0.125 when the bubble temperature increased to be 6000 K and 8000 K, respectively. Water vapor started to be consumed, and the highly reactive radicals are started to form, including H, O, OH, while other radicals are produced and consumed simultaneously, such as HO₂, O₂, and H₂O₂.

As per the numerical analysis and simulations presented in those figures accordingly, the trends showed continuous hydrogen production. However, these trends change, and hydrogen production will not be constant if the dissolved gas changed. The hydrogen production rate is calculated later in the following section by equation (4.5). The concentrations are given in mole fraction per unit volume of the reactor. Knowing that as the reactor volume is the volume of a single bubble, and then the bubble volume calculated at the maximum radius should be multiplied by these values.

(d) H₂O/Air bubble case

The previous sections, where the bubble temperature effects are presented for bubbles, contain H₂O/O₂, H₂O/CO₂, and H₂O/Ar. In this section, the effect of the bubble temperature when simulating an H₂O/Air bubble. In all sections, the water vapor fraction WVF is fixed to be 39%.

The effect of the bubble temperature has a substantial impact on the H₂ production rate, presented in Figure 4.48. As seen from the figures below, the hydrogen and hydrogen radicals almost have no production below a temperature of 2000-3000 K. The higher the bubble temperature used in the parametric study, the slower the reaction time. Hence, this explains why there is no reaction taking place at a bubble temperature before 3000 K; the species' concentration is not changed, which means the reaction did not start at such a low temperature. At 4000 K, the reaction began to occur with a slight increase in the species' concentration of around 0.05. Simultaneously, the hydrogen mole fraction recorded an increase to 0.09 and 0.11 when the bubble temperature increased to 6000 K, and 8000 K. Water vapor started to be consumed. The highly reactive radicals

are started to form, including H, O, OH, while other radicals are produced and consumed simultaneously, such as HO₂, O₂, and H₂O₂. As per the numerical analysis and simulations presented in those figures accordingly, the trends showed continuous hydrogen production. However, these trends change, and hydrogen production will not be constant if the dissolved gas changed. The hydrogen production rate is calculated later in the following section by equation (4.5). The concentrations are given in mole fraction per unit volume of the reactor. Knowing that as the reactor volume is the volume of a single bubble, and then the bubble volume calculated at the maximum radius should be multiplied by these values.

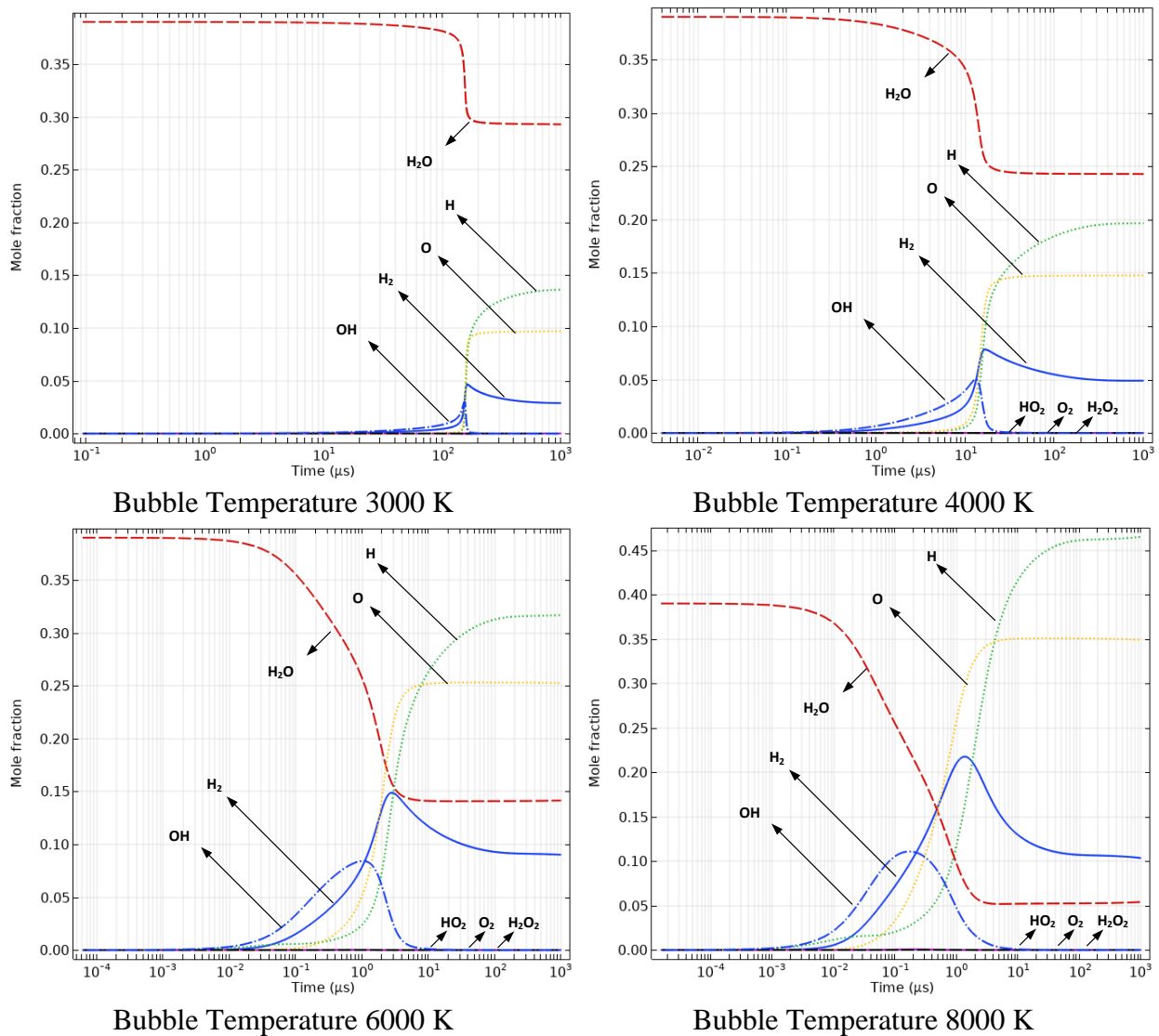


Figure 4.48: Predicted species production vs. time at different bubble temperatures for H₂O/Air

(e) Hydrogen production & quantification

In this section, the sonohydrogen process's hydrogen will be quantified from the chemical kinetics model. The analysis is calculated based on a single bubble initially saturated with (H₂O/O₂) with a mole fraction of water vapor of 0.39 and 0.61 inspired by previous data in the literature. The most commonly used ultrasonic frequency for the sonochemical process is 20 kHz. The chemical reaction mechanism occurs, and many produced radicals are released when the bubble reaches the collapse phase, at which the maximum bubble pressure and temperature are achieved. The previous study [4] found that the majority of hydrogen produced because of the recombination of the highly reactive radicals H^* and *OH after the collapse phase through the following reaction $H^* + ^*OH \rightleftharpoons H_2 + O$. The H_2 rate of reaction r_{H_2} can be given as follows [29]:

$$r_{H_2} = N \times n_{H_2} + k' [H^*]^2 \quad [mol/s] \quad (4.2)$$

where n_{H_2} is the radical hydrogen mole, N is the sum of bubbles that collapse in per unit volume per unit time ($L^{-1}s^{-1}$), and k' is the reactive fluid rate constant. The hydrogen production rate comes from two parts; the first part comes from the vapor phase of the hydrogen produced from this reaction $H^* + ^*OH \rightleftharpoons H_2 + O$, and the second part is associated with the radical development from the reaction $H^* + H^* \rightleftharpoons H_2$. The development of radical hydrogen can then be defined as follows:

$$r_{H^*} = N \times n_{H^*} - 2k' [H^*]^2 \quad [mol/s] \quad (4.3)$$

Here, n_{H^*} is the hydrogen radicals mole number. Noting that, under steady-state conditions, the radical hydrogen reaction rate is $r_{H^*} \sim 0$, this contributes to:

$$\frac{1}{2} \times N \times n_{H^*} = k' [H^*]^2 \quad [mol/s] \quad (4.4)$$

By substituting, we have achieved the overall production rate of H₂ that is written as follows:

$$r_{H_2} = N \times n_{H_2} + \frac{1}{2} \times N \times n_{H^*} \quad [mol/s] \quad (4.5)$$

Once the “mole number” for H and H₂ is obtained from Figure 4.41, it has to be multiplied by the number of bubbles produced. The acoustic field's complexity and the non-homogeneous conduct of the bubbles' density on the sonoreactor are very challenging and limited in the literature. The value of N is defined in some references and is presumed to be a constant number; for example, Louisnard's [152] work and Vanhille et al. [153]. In reality, during the process of sound hydrogen, millions of bubbles formed in the reactor. N bubbles depend heavily on acoustic parameters for

sonic operation, including the frequency of ultrasound and acoustic amplification[61]. Thus, a recent study by Merouani et al. [61] predicts the number of bubbles from the sonochemical process. The number of bubbles is recorded depends only on the ultrasonic frequency. They have reported that at 20 kHz, the possible number of generated bubbles can be in the range between 7.2705×10^3 and 1.1425×10^4 this per L per sec. For example, in a further study, Merouani et al. [29] related the number of bubbles to the applied ultrasonic frequency, stating that the number of bubbles at 20 kHz and 355 kHz respectively had been in the order of 10^4 and 10^8 . The value of N is defined as a constant number based on the ultrasound frequency in other references. For instance, Petrier and Francony [59] reported the number of bubbles $N = 26,173,800 L^{-1}.hr^{-1}$ and Jiang et al. [60], who used a bubble density is $N = 41,130,000 L^{-1} hr^{-1}$. Both experiments are conducted at an ultrasonic frequency of about 20 kHz and an acoustic pressure of 0.1 MPa. The effect of ultrasonic frequency ranged from 20-800 kHz is studied experimentally in both literature studies. The numbers of bubbles at different ultrasound frequencies have been recorded for these literature studies and has been used to calculate the hydrogen production of the sonohydrogen process.

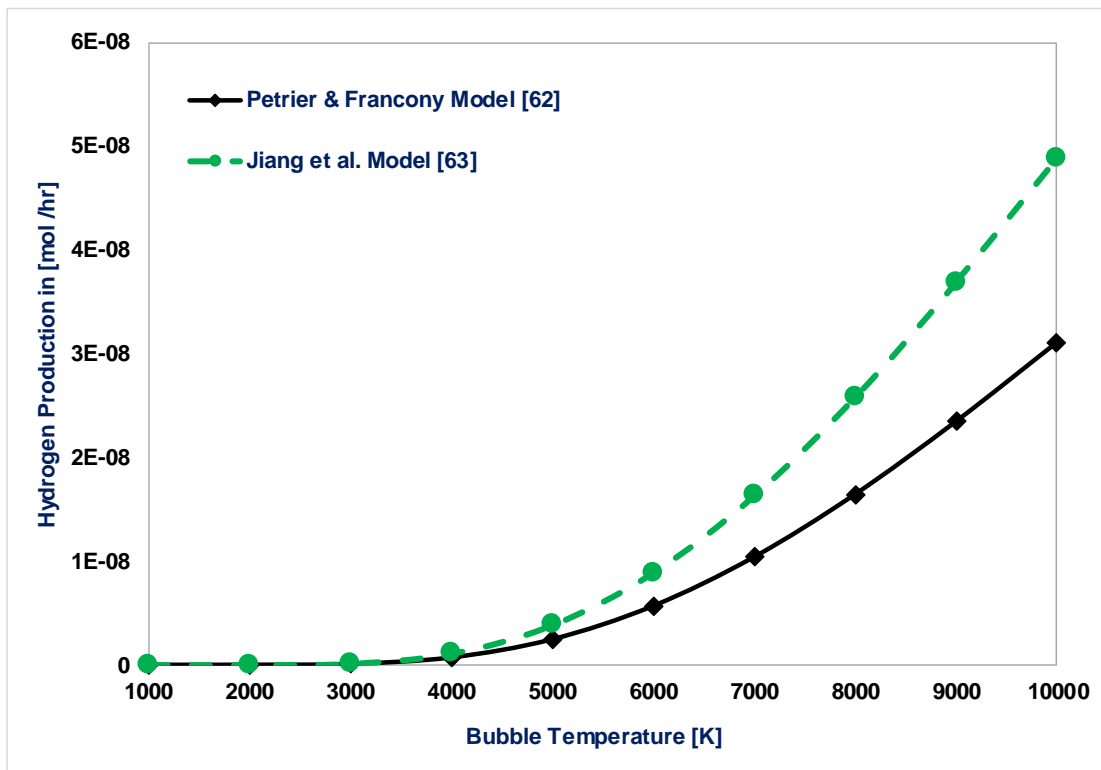


Figure 4.49: Predicted H₂ output rate in $\mu\text{mol/hr}$ at $f = 20 \text{ kHz}$ and 30 kW using different experimental models

These models are then used and compared to the quantity of hydrogen produced and shown in Figure 4.49. Furthermore, these experimental experiments are accurate as they are used by Merouani et al. [61], validating the numerical model. Therefore, those models are used to measure the hydrogen that all bubbles have the same size compared to that created. The chemical reaction mechanism implemented in this study should first be determined to determine the hydrogen production rate. Any bubble collapse shall produce the mole fraction of H₂ and *H that can be obtained from both Figure 4.39 and Figure 4.40. It is possible to quantify the production of the gas phase of the bubbles via the chemical reaction process, and the total hydrogen production rate (r_{H_2}) can be defined as:

$$r_{H_2} = \left[N \times n_{H_2} + \frac{1}{2} \times N \times n_{H^*} \right] [mol/m^3] \times \forall_{bubble} \left[\frac{m^3}{bubble} \right] \quad [\mu mol/hr] \quad (4.6)$$

$$\times N_{bubbles} [hr^{-1}] \times 10^6$$

where N is the bubble number ($L^{-1}s^{-1}$) collapsed per the volume a (liter) unit by the time unit (s), n_{H_2} is the mole number of H₂ output from a single bubble (mol/m^3) That is evaluated from the mechanism for the chemical reaction. In the bubble with H₂O/O₂, chemical reactions simulation begins on $R = R_{max}$ radius. The initial bubble radius is 2 μm , and, following the defined acoustical conditions, the maximum bubble radius (18) is obtained from the bubble-dynamic model. Therefore, the bubble dynamics simulation began earlier to achieve the optimum bubble radius for calculating the bubble's volume.

(f) Energy consumption

The energy consumption calculation for producing a μmol of H₂ by sonohydrogen is reported in Figure 4.50. Petrier & Francony [59] and Jian et al. [60] have studied the sonohydrogen process with the following conditions: 20 kHz, 30 W, and an acoustic pressure $P_A = 5$ bar. The ambient bubble radius is a function of frequency as well as the maximum bubble radius. The energy consumption is made to determine mico moles can be generated from two models because those models reported different number of bubbles in their studies. However, their reports of the number of bubbles has been taken as a reference in different research studies. This is due to the lack of scientific evidance of the relation between the number of bubbles and the acoustical paraemters.

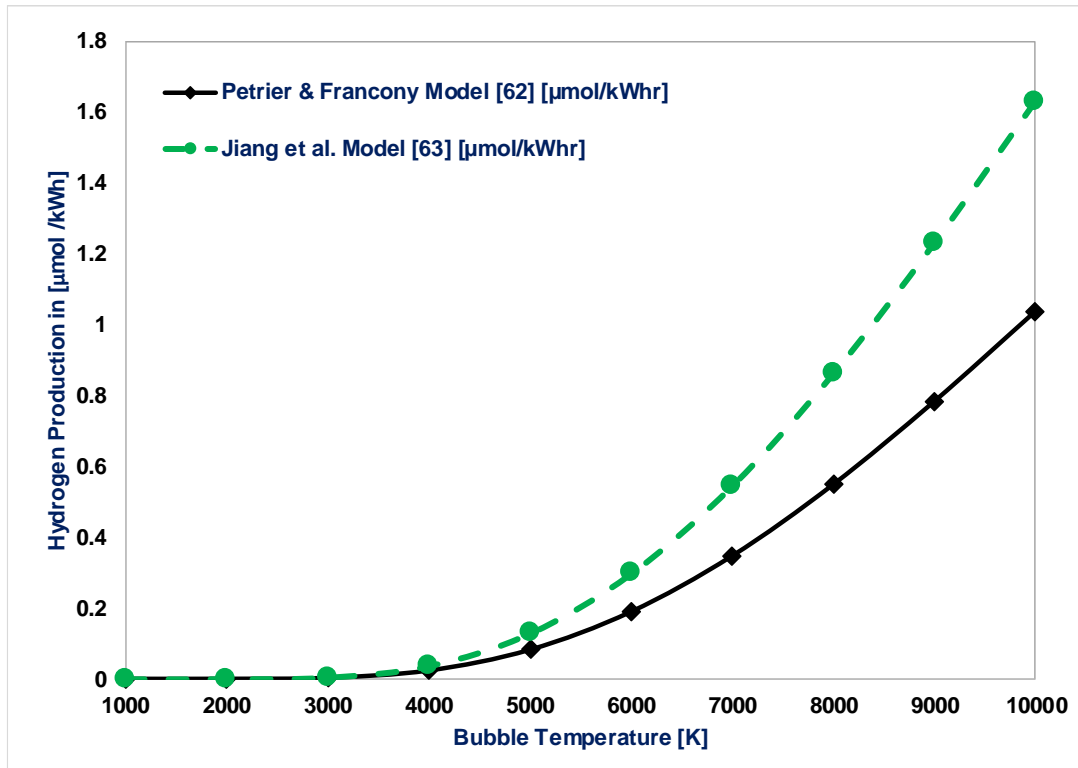


Figure 4.50: Predicted H_2 energy consumption in $\mu\text{mol/kWh}$ at $f = 20 \text{ kHz}$ and 30 kW using different experimental models

Many studies' standard radius has been $8 \mu\text{m}$, as defined by different reference numbers [130,131]. They suggested that an extensive range of acoustic power (20-320 W) has not altered the initial radius. The higher the temperature of the bubble, the higher the output of hydrogen. Also, the energy required to generate μmol of H_2 according to Petrier & Francony [59] is $0.15 \mu\text{mol/kWh}$, while the emitted hydrogen is approximately $0.07 \mu\text{mol/kWh}$ as per Jiang et al. [60]. The comparison is at different bubble temperatures; however, essentially, the number of bubbles created in each case is the main difference between the two. In closing, the steam gas reforming thermochemical method [24] has a big downside to producing a huge amount of carbon dioxide. Electrochemical electrolysis requires high electrical consumption. The photobiological approach has improved efficiency. Photo-electrochemical using water splitting have a variety of longevity problems. Sono-hydrogen technology drives the need to minimize carbon dioxide emissions and drive productivity and production ability. Table 4.6 provides a conceptual distinction between the five production forms of hydrogen, including production rates and costs.

Table 4.10: Energy consumption comparison between the most common H₂-production technologies

H₂ Production Technologies	H₂-Production rate and cost	Ref.
Thermochemical	50 kg/kWh	[24]
Electrochemical	53.4-70.1 kg/kWh	[25]
Photobiological	0.07-96 E-03 μmol L ⁻¹ h ⁻¹	[26]
Photoelectrochemical	39 kWh/ kg 17.3 \$/kg of H ₂	[27,28]
Sonochemical or sonohydrogen	5.46E-06 – 8.59E-06 μmol/h for H ₂ O/O ₂ bubble or 20-30 μmol/kWh for H ₂ O/Ar bubble	[108,109]

4.6.4 Effect of dissolved gases

There are several main parameters for developing hydrogen output: acoustic frequency, acoustic strength, dissolved gas, and bubble temperature. However, no attempt is made to research the effect on the sonication technique of dissolved gas. The effect of dissolved gas is between three important physical properties on hydrogen production efficiency; (1) specific heat capacity C_p [kJ/m³/K], (2) thermal conductivity k [W/m. K], and thermal diffusivity $\alpha = k/\rho \cdot C_p$ [m²/s]. The dissolved gas could accumulate at higher temperatures with higher heat capacity. On the other hand, Dissolved gases have low heat dissipation and are capable of pinning more temperatures in the bubble. Hence, the combination of both higher heat capacity and lower thermal conductivity results in lower thermal heat diffusiveness. As a result, the selection of dissolved gas with high thermal potential and low thermal conductivity achieves optimum selection to improve the process of water vapor dissociation, resulting in further hydrogen production in exchange. In Table 4.11, Air's substitution by Argon in the bubble mixture resulted in a higher mixture density of 28.28 percent, a lower thermal conductivity of 20.9 percent, which is favorable, and a lower heat capacity 16.49 percent, which is not favorable. However, when all properties are combined, this leads to a 5% low thermal diffusivity, which improves the hydrogen production rate and efficiency. Similarly, the transport properties of a bubble saturated with a 100% H₂O bubble often vary from those of the H₂O / CO₂ bubble and all other dissolved gases. This is due to major variations in the physical properties of CO₂ and H₂O [6–7]. Additionally, the evolution of the temperature during collapse is described by

recalling equation 3.27, $T = T_{\infty}(R_{max}/R)^{3(\gamma-1)}$. According to this equation, the temperature is governed by the polytropic index. The controlling parameter is then the polytropic index, which is the only parameter intervening in the equation and related to the dissolved gas's nature.

Table 4.11: Tabulated properties of H₂O/Air and H₂O/Ar mixture [154]. The negative sign refers to a decrease in the tabulated properties

	H₂O/Air mixture 39% WVF	H₂O/Ar mixture 39% WVF	% change H₂O/Air → H₂O/Ar 39% WVF
Density [kg/m³]	0.99	1.27	28.28%
Thermal Conductivity [W/m. K]	0.027393	0.021664	-20.9%
Vol. heat capacity [kJ/m³/K]	1.243	1.038	-16.49%
Thermal Diffusivity [m²/s]	2.20×10 ⁻⁰⁵	2.09×10 ⁻⁰⁵	-5%

(a) Quantification of hydrogen production

In this section, a series of numerical simulations of the bubble dynamics and reaction kinetics mechanism occurring in a single bubble are performed for 6 saturating gases (Ar, CO₂, N₂, CO, He, Air). The evolution of the reaction system is evaluated as a function of time around the end of the bubble collapse with an acoustic pressure amplitude of 0.1 MPa. Figure 4.51 represents a series of numerical investigations of chemical reactions taking place inside the acoustic cavitation bubble carried out for six saturating gases at the same bubble temperature, 8000 K, and an acoustic pressure amplitude of 0.1 MPa. To achieve a high temperature, it is recommended that the sonoreactor be operated at an ultrasonic frequency in the range between 20 – 40 kHz. The figure shows that the hydrogen production for CO₂ is a batch reaction that peaks at around 1μs and then diminishes with time. The hydrogen production peaks simultaneously as other dissolved gases; however, the production remains higher. The hypothesis behind this finding lies in lower thermal conductivity, higher thermal capacity, and lower thermal diffusivity. If all of these parameters are achieved, the optimal production of hydrogen is achieved.

In order to illustrate the significant variations in physical properties of CO₂, N₂, Ar, CO, H, O₂, in 298 K and 8000 K, Table 4.12 and Table 4.13 tabulate the characteristics of the various mixtures. As shown, the H₂O/CO₂ has reported the higher density of all mixtures, resulting in a more

remarkable heating ability than other mixtures, which increases the production rate of hydrogen directly. Additionally, CO₂ has recorded the lowest thermal conductivity, highest heat capacity, and most moderate thermal diffusivity, which, if all of these factors are combined, it achieves the optimum hydrogen production rate. The discussion of the influence of the nature of dissolved gas on the results of the simulations is strictly carried out based on the parameters used as inputs in the model. Thus, the influence of dissolved gases based on the model adopted by Rashwan et al. [108,109] and Merouani et al. [29,57], using as input physical parameter related to the nature of dissolved gas the polytropic index γ .

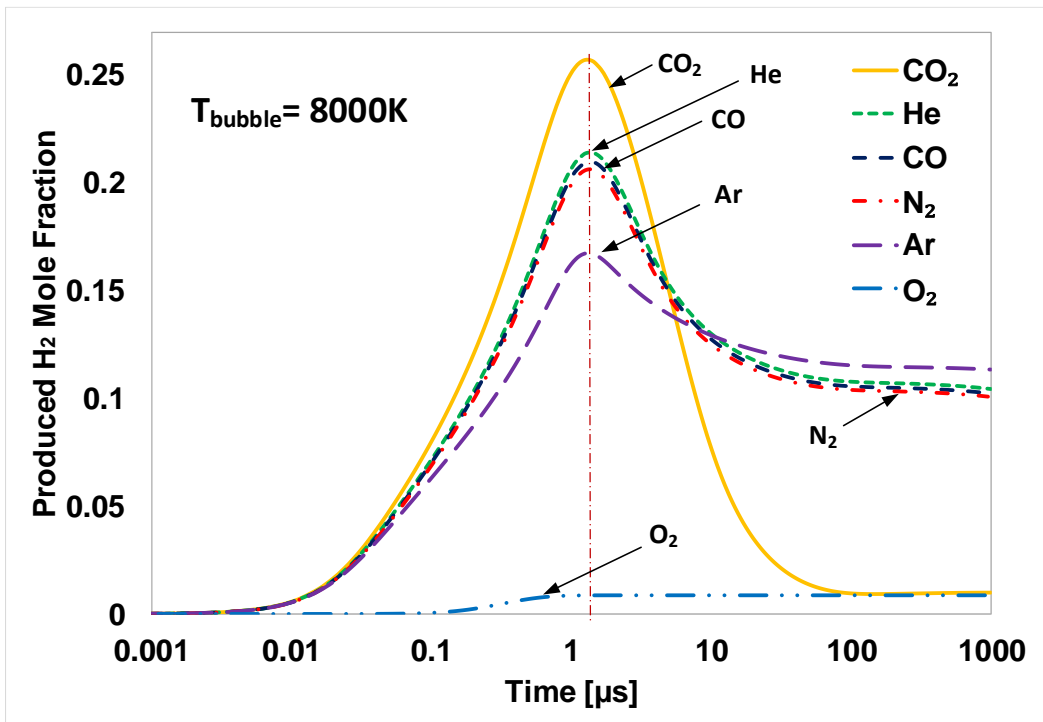


Figure 4.51: The predicted output of H₂ from a single bubble vs. the reaction time for various dissolved gases

For clarification purposes, a comparison is also made of the effect of adding CO₂ to the water vapor mixture with only H₂O and shown in respectively Table 4.14 and Table 4.15, at 298 K and 8000 K. A H₂O / CO₂ mixture achieved ideal density-related characteristics of +87.6%, decreased thermal conductivity -19.41%, increased the volumetric heat capacity by +22.2% and reduced heat diffusivity by -24.10%, leading to higher hydrogen output. The tables show that the decrease in thermal diffusiveness will definitely encourage the production rate of hydrogen. Their comparisons are presented. The dissolved gases type and bubble temperature can be maneuvered according to acoustically modified parameters.

Table 4.12: Tabulated properties of H₂O and different bubble mixtures at 298 K [154]. All at the same WVF of 0.39

	H ₂ O	H ₂ O/CO ₂	H ₂ O/N ₂	H ₂ O/Ar	H ₂ O/CO	H ₂ O/He	H ₂ O/O ₂
Density [kg/m ³]	0.73	1.37	0.97	1.27	0.97	0.38	1.07
Thermal Conductivity [W/m. K]	0.02587	0.020855	0.02740	0.02165	0.02692	0.08505	0.02733
Vol. heat capacity [kJ/m ³ /K]	1.18	1.442	1.242	1.038	1.242	1.038	1.248
Thermal Diffusivity [m ² /s]	1.92E-5	1.45E-5	2.21 E-5	2.09 E-5	2.17 E-5	8.19 E-5	2.19 E-5

Table 4.13: Tabulated properties of H₂O and different bubble mixtures at 8000 K [154]. All at the same WVF of 0.39

	H ₂ O	H ₂ O/CO ₂	H ₂ O/N ₂	H ₂ O/Ar	H ₂ O/CO	H ₂ O/He	H ₂ O/O ₂
Density [kg/m ³]	0.03	0.05	0.04	0.05	0.04	0.01	0.04
Thermal Conductivity [W/m. K]	0.7567	0.28143	0.3733	0.364190	0.405340	1.04080	0.48624
Vol. heat capacity [kJ/m ³ /K]	0.082	0.047	0.051	0.051	0.050	0.051	0.070
Thermal Diffusivity [m ² /s]	9.23E-3	5.99E-3	7.33E-3	7.14E-3	8.09E-3	2.04E-2	6.95E-3

Table 4.14: Tabulated properties of H₂O and H₂O/CO₂ mixture at 298 K [154]. The negative sign refers to a decrease in the tabulated properties

	H ₂ O	H ₂ O/CO ₂ mixture 39% WVF	% change H ₂ O → 39% H ₂ O/CO ₂
Density [kg/m ³]	0.73	1.37	+87.6
Thermal Conductivity [W/m. K]	0.025879	0.020855	-19.41
Vol. heat capacity [kJ/m ³ /K]	1.18	1.442	+22.20
Thermal Diffusivity [m ² /s]	1.92E-05	1.45E-05	-24.10

Table 4.15: Tabulated properties of H₂O and H₂O/CO₂ mixture at 8000 K [154]. The negative sign refers to a decrease in the tabulated properties

	H ₂ O	H ₂ O/CO ₂ mixture 39% WVF	% change H ₂ O → 39% H ₂ O/CO ₂
Density [kg/m ³]	0.03	0.05	+88.02
Thermal Conductivity [W/m. K]	0.756770	0.281430	-62.81
Vol. heat capacity [kJ/m ³ /K]	0.082	0.047	-42.72
Thermal Diffusivity [m ² /s]	9.23E-03	5.99E-03	-35.07

(b) Comparison between H₂O/CO₂ and H₂O/O₂ bubbles

The chemical kinetics mechanism and the predicted species production change while changing the dissolved gases and the initial bubble composition. The study is carried out on a single bubble initially filled with H₂O/O₂. The results of this sequence of simulations of chemical reactions under the same bubble conditions are described in Figure 4.52 and predicted species production of the O₂/H₂O bubble at a temperature of 8000 K. At the start of the dissociation reaction, the initial concentrations or mole component of the water and oxygen are 0.39 and 0.61. The intake of H₂O and O₂ and other species' development, including OH and H₂, is shown to be 0.18 and 0.01. Different radicals are produced, such as H₂O₂, HO₂, O, and H, produced from dissociation reactions and shown in the comparison figures below.

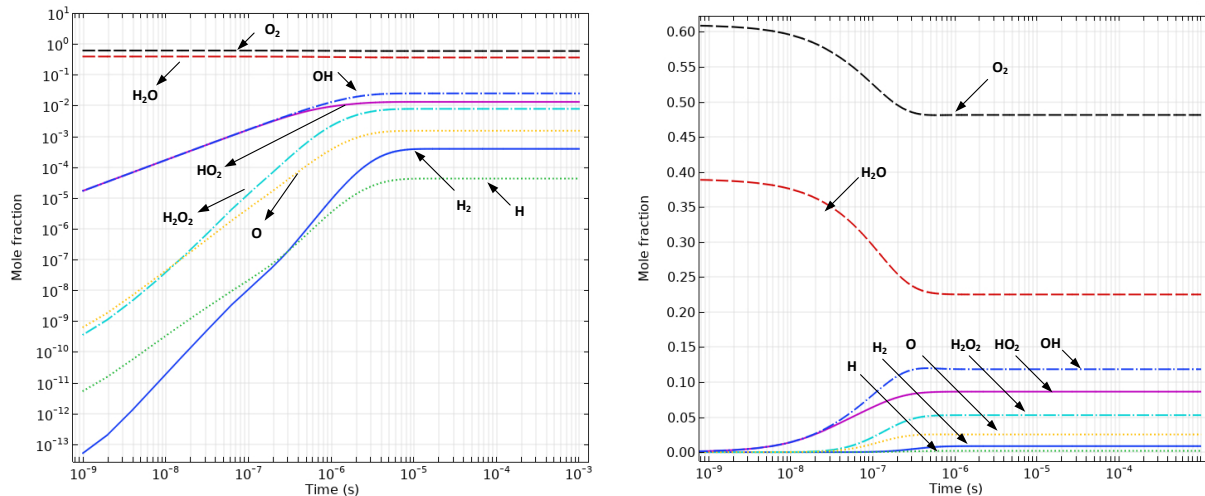


Figure 4.52: Predicted species production of the O₂/H₂O bubble concerning the time

In addition, a single bubble initially saturated with H₂O water vapor mixture and CO₂ carbon dioxide is analyzed. Figure 4.53 shows the effects of this sequence of simulation chemical reactions under the same bubble conditions. The figure presents the predicted species from the H₂O/CO₂ bubble at a temperature of 8000 K, 20 kHz at the end of the bubble collapse of 1.83 μs. At the beginning of the dissociation reaction, the same initial concentrations are applied. As seen, H₂O only is consumed, and H₂ is produced at a mole fraction of 0.06, while carbon dioxide is slightly consumed. It recorded a 50% increase in hydrogen production.

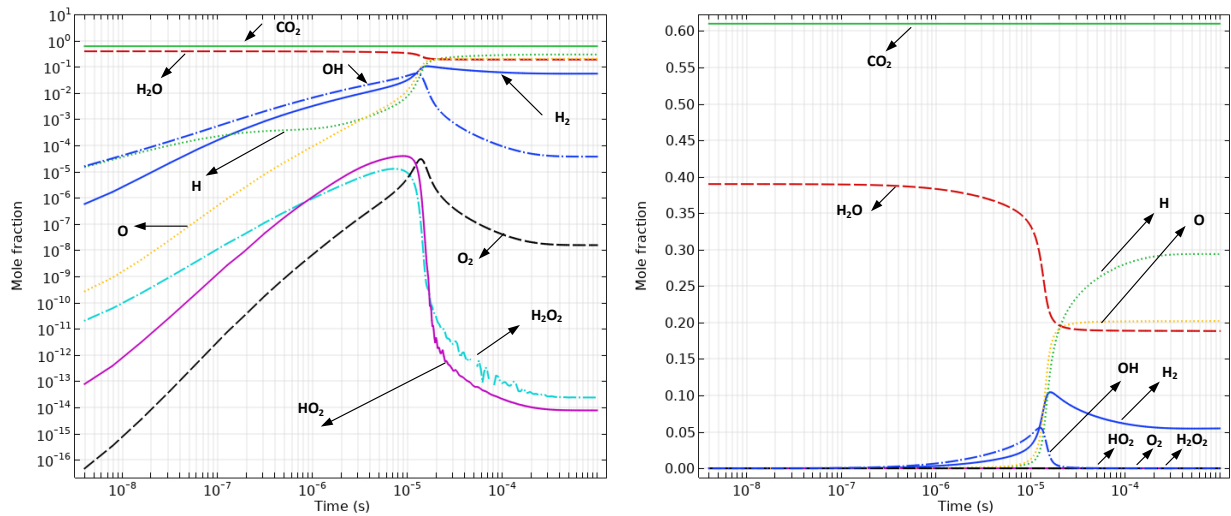


Figure 4.53: Predicted species production from the H₂O/CO₂ bubble concerning the time.

Table 4.16: Select properties of H₂O/O₂ and different H₂O/CO₂ mixtures at 298 K [154]. WVF is the water vapor fraction. The negative sign refers to a decrease in the tabulated properties.

	H ₂ O/O ₂ mixture 39% WVF	H ₂ O/CO ₂ mixture 39% WVF	% change H ₂ O → 39% H ₂ O/CO ₂
Density [kg/m ³]	1.07	1.37	27.61%
Thermal Conductivity [W/m. K]	0.027336	0.020855	-23.71%
Vol. heat capacity [kJ/m ³ /K]	1.248	1.442	15.55%

For clarification purposes, Table 4.16 showed the effect of diluting CO₂ to H₂O in a mixture and compared the results with a mixture of H₂O/O₂. A combination of H₂O/CO₂ achieved the ideal

density by an increase of +27.16%, the lower thermal conductivity of -23.71%, higher heat capacity +22.2%, and lower thermal diffusivity -24.10%, leading to a higher output rate of hydrogen. This study shows why more hydrogen can be expected when using CO₂ as a diluted gas. The next section presents the energy consumption needed for the sonohydrogen process, and a comparison is drawn between two different bubble compositions at various bubble temperatures.

(c) Energy consumption analysis

Once obtained, the "mole number" of $\cdot H$ and H_2 from Figure 4.54 at the required temperature of the bubble. The number of bubbles is used to determine the total hydrogen output from equation (45). A strong correlation is made with the results recorded by Merouani et al. [57] between the bubble temperature and the mole fraction of H radical and H_2 within a single bubble of H₂O/O₂. The estimate of 1 μ mol of sonohydrogen is then presented in the theoretical calculation of energy consumption. Petrier & Francony [59] and Jian et al. [60] conducted two experimental studies that tested the sonohydrogen procedure with 20 kHz, 30 W. Both the maximum and ambient bubble radii are a function of frequency, as well as the maximum bubble radius. The standard radius of 8 μ m, as defined by different references [130,131], has been reported in several studies. They indicated that the initial radius for a large acoustic power range had not been modified (20-320 W). A distinction between the two cases is provided in Figure 4.55 on energy consumption. The first case is when the bubble is CO₂-saturated, and the second one is O₂.

In addition to the energy consumption, the effect of the bubble temperature variation is also incorporated in the study—the greater the bubble temperature, the greater the hydrogen production as a major forecast performance findings. In addition, energy consumption is estimated to be up to 1.05 μ mol/kWh for generating hydrogen in the case of an O₂/H₂O bubble, as per Petrier & Francony [59]. While the hydrogen output using the Jiang et al. [60] model is 1.63 μ mol/kWh. The comparison is made at different bubble temperatures; however, the difference between both models is basically due to the number of bubbles produced in each case. However, in the case of the CO₂/H₂O bubble, the hydrogen produced showed an outstanding improvement as per Petrier & Francony [59]. The energy efficiency may go up to 22.26 μ mol/kWh, Whereas, Jiang et al. [60], the hydrogen produced is 34.98 μ mol/kWh.

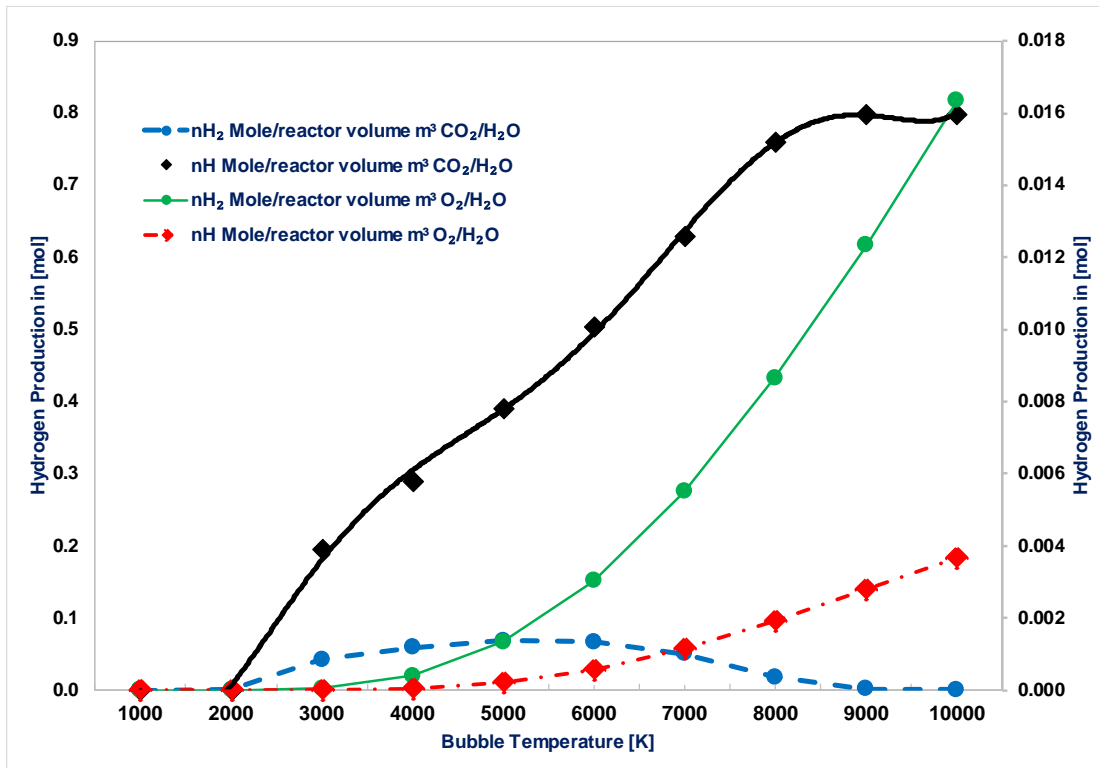


Figure 4.54: Predicted number of moles of H₂ and *H vs. at different bubble temperatures for CO₂/H₂O (left Y-axis) and O₂/H₂O (right Y-axis)

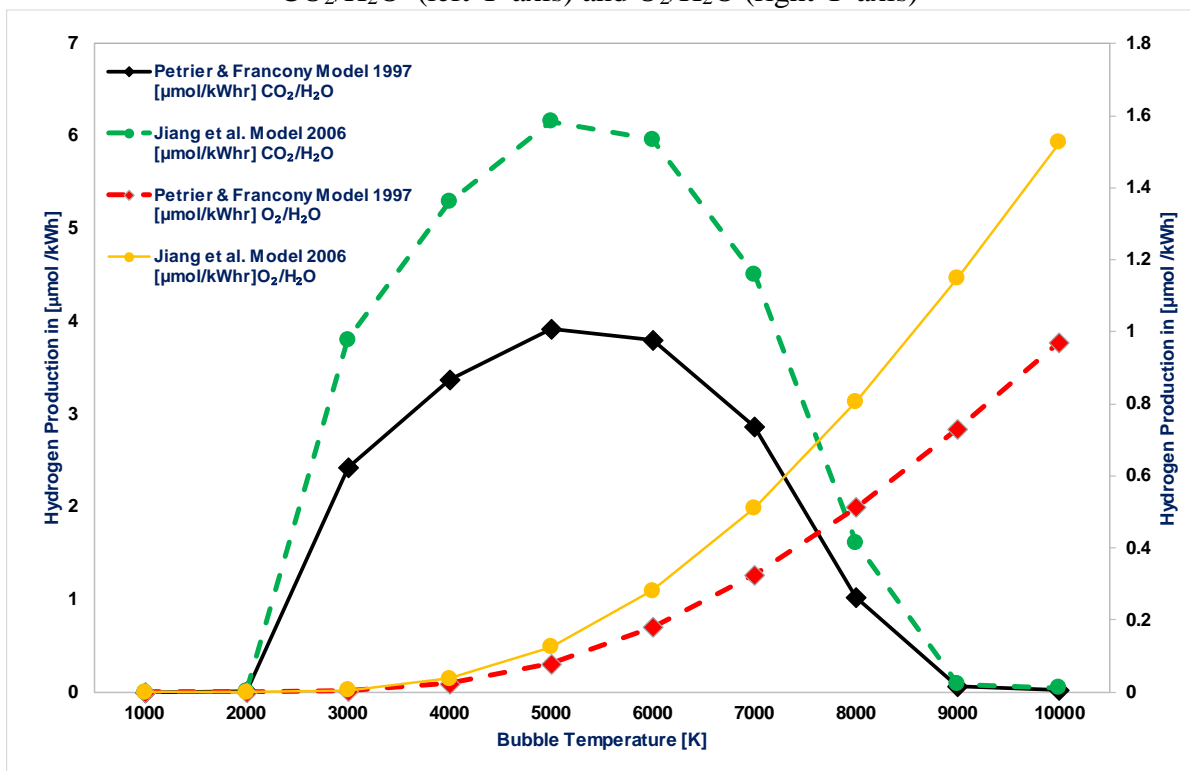


Figure 4.55: Predicted H₂ production in μmol/kWh for CO₂/H₂O (left y-axis) and O₂/H₂O (right y-axis)

Figure 4.56 predicted the number of moles of H₂ and H vs. at different bubble temperatures as extracted from the simulation results. The greater the bubble temperature, the greater the hydrogen production as a major forecast performance findings. The figure shows both hydrogen molecules and hydrogen radicals as both are involved in the calculation of the hydrogen production rate. In addition, energy consumption is estimated and presented in Figure 4.57. In both figures, the results are compared to the *primary reference case of H₂O/O₂ bubbles*. It is revealed that the energy consumption in the case of an O₂/H₂O bubble is in the range between 1.05-1.63 μmol/kWh for generating hydrogen in the case of Petrier & Francony [59] and Jiang et al. [60], respectively. The comparison is made at different bubble temperatures; however, the difference between both models is basically due to the number of bubbles produced in each case. However, in the case of the Air/H₂O bubble, the hydrogen produced showed an outstanding improvement, and the energy consumption is recorded to be in the range between 25-35 μmol/kWh. The results are repeated and compared in the case of the H₂O /Argon bubble.

Figure 4.58 predicted the number of moles of H₂ and H vs. at different bubble temperatures as extracted from the simulation results. The greater the bubble temperature, the greater the hydrogen production as a major forecast performance findings. The figure shows both hydrogen molecules and hydrogen radicals as both are involved in the calculation of the hydrogen production rate. In addition, energy consumption is estimated and presented in Figure 4.59. In both figures, the results are compared to the *primary reference case of H₂O/O₂ bubbles*. The comparison is made at different bubble temperatures; however, the difference between both models is basically due to the number of bubbles produced in each case. However, in the H₂O/Ar bubble, the hydrogen produced showed an outstanding improvement as per Petrier & Francony [59] and Jiang et al. [60] to be in the range between 20-30 μmol/kWh. The results are repeated and compared in the case of the H₂O/Ar bubble.

In conclusion, the best energy consumption is recorded when using carbon dioxide as a dissolved gas. Then the second-best energy consumption goes to air, then argon and oxygen come at the last place. This study recommends the dissolved gas that has to be selected in order to obtain the optimum hydrogen production. In the next section, the bubble composition effect is illustrated in-depth, and recommendations have been given accordingly.

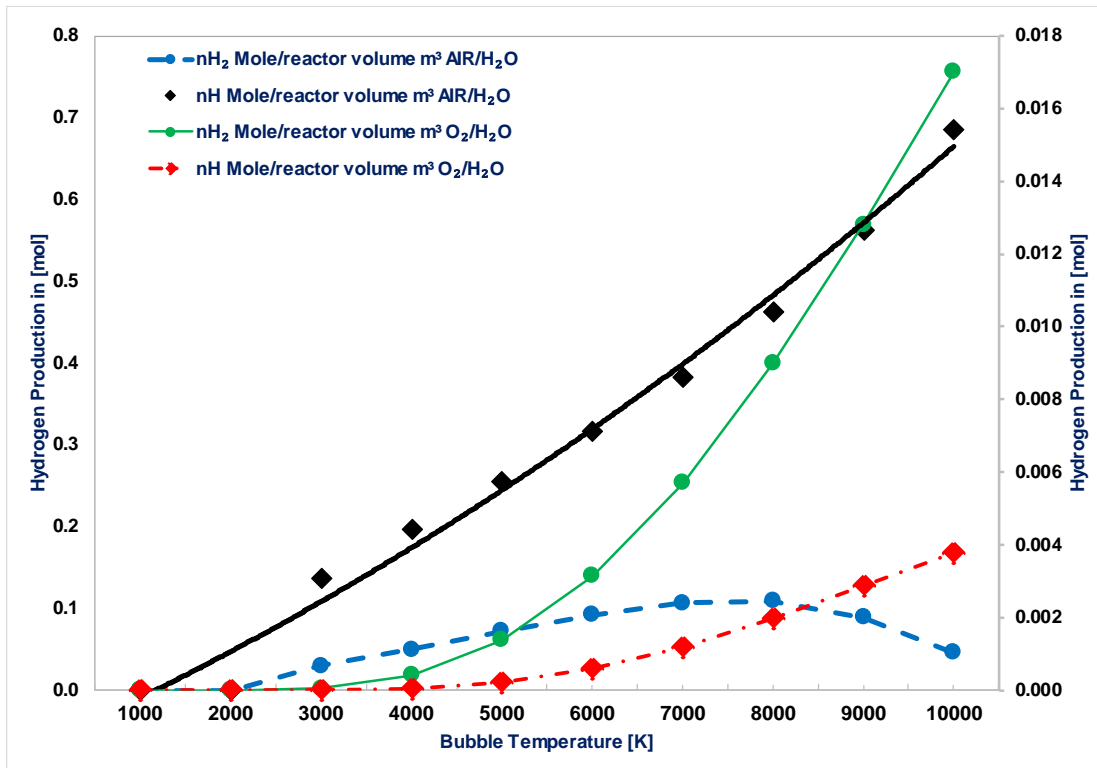


Figure 4.56: Predicted number of moles of H₂ and H vs. at different bubble temperatures for Air/H₂O (left Y-axis) and O₂/H₂O (right Y-axis)

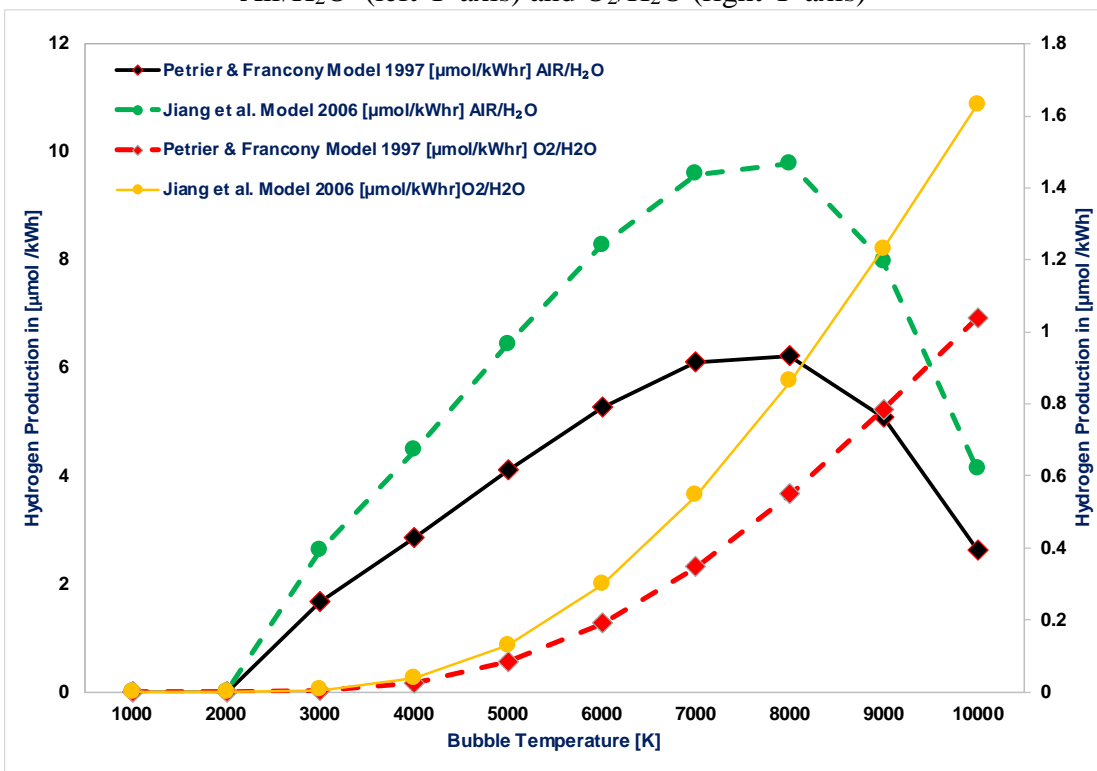


Figure 4.57: Predicted H₂ production in μmol/kWh for Air/H₂O (left y-axis) and O₂/H₂O (right y-axis)

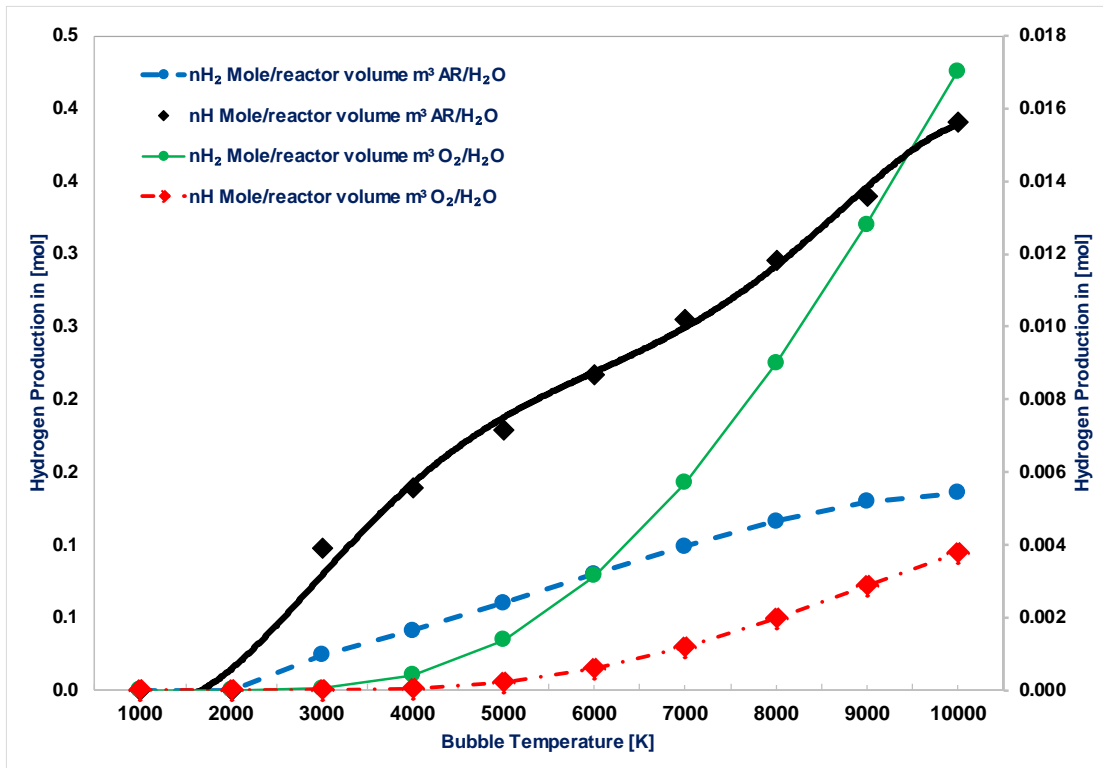


Figure 4.58: Predicted number of moles of H₂ and H vs. at different bubble temperatures for Ar/H₂O (left Y-axis) and O₂/H₂O (right Y-axis)

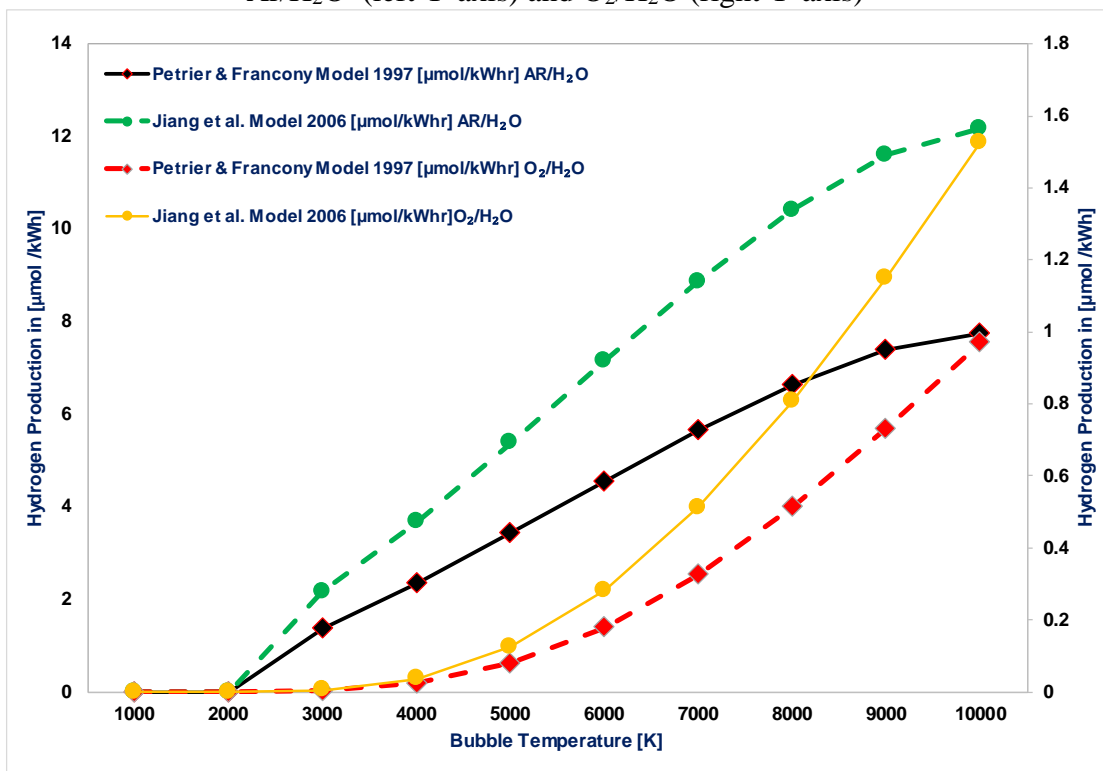


Figure 4.59: Predicted H₂ production in μmol/kWh for Ar/H₂O (left y-axis) and O₂/H₂O (right y-axis)

(d) Effect of bubble composition

This section presents the bubble composition effect because of its importance on the hydrogen production rate. This is considered a significant factor that is not explored yet. It has not been considered one of the factors affecting the sonochemical process as per the previous literature review. Therefore, a series of numerical simulations of the bubble dynamics and reaction kinetics mechanism occurring in a single bubble are performed for 4 selected saturating gases: Carbon Dioxide, Air, Argon (Ar) Oxygen. The hydrogen evolution from the chemical kinetics reaction system is evaluated as a function of time around the end of the bubble collapse with an acoustic pressure amplitude of 0.1 MPa. Figure 4.60 represents a series of numerical investigations of chemical reactions taking place inside the acoustic cavitation bubble carried out for six saturating gases at the same bubble temperature, 8000 K, at the same water volume fraction of 39%, and an acoustic pressure amplitude of 0.1 MPa. To achieve a high temperature, it is recommended that the sonoreactor be operated at an ultrasonic frequency in the range between 20 – 40 kHz. The figure shows that the hydrogen production for CO₂ is a batch reaction that peaks at around 1 μs and then diminishes with time to 0.02 and at the end of the chemical reaction. The hydrogen production peaks simultaneously as other dissolved gases; however, the production remains at a high mole fraction for air and argon at around 0.125. The hypothesis behind this finding lies in lower thermal conductivity, higher thermal capacity, and lower thermal diffusivity. If all of these parameters are achieved, the optimal production of hydrogen is achieved.

For comparison, another parametric study is conducted accordingly to investigate a higher water vapor fraction. Thus, the mole fraction of hydrogen is evaluated at a WVF of 50%, and the results are presented in Figure 4.61. As compared to the previous figure, more hydrogen could be produced while using carbon dioxide as a dissolved gas is when increasing the water vapor fraction. This is due to the reaction becomes continuous instead of a batch reaction. Another parametric study is conducted to show the effect of the bubble's initial concentration on hydrogen production. Such a study is reported in Figure 4.62 and Figure 4.63 for both hydrogen and hydrogen peroxide. The results showed a consistent trend when the mole fraction of CO₂ in CO₂/H₂O bubbles is up to 0.5. A concentration of a CO₂ higher than 0.5 showed a negative impact on the hydrogen produced as the reaction kinetics stops. From these studies, it is concluded that the water vapor fraction WVF has to be at least 50% or more in order to have a reasonable amount of hydrogen mole fraction.

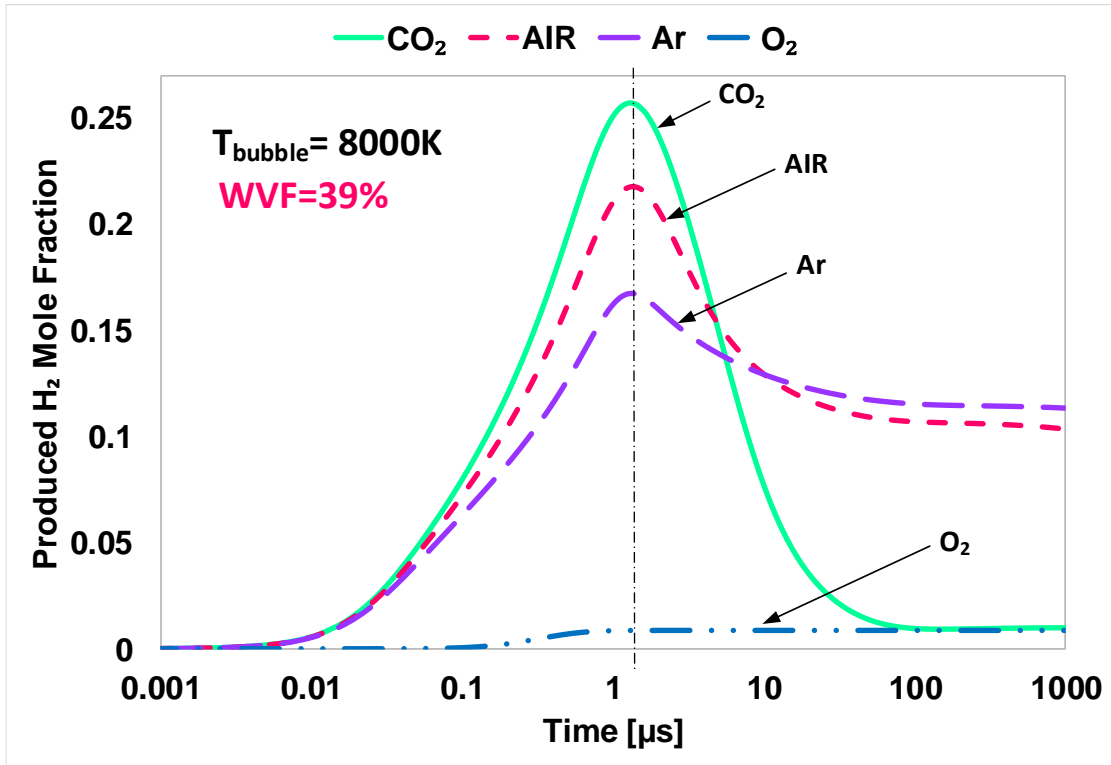


Figure 4.60: The predicted output of H₂ from a single bubble vs. the reaction time for various dissolved gases at a water volume fraction WVF = 39%

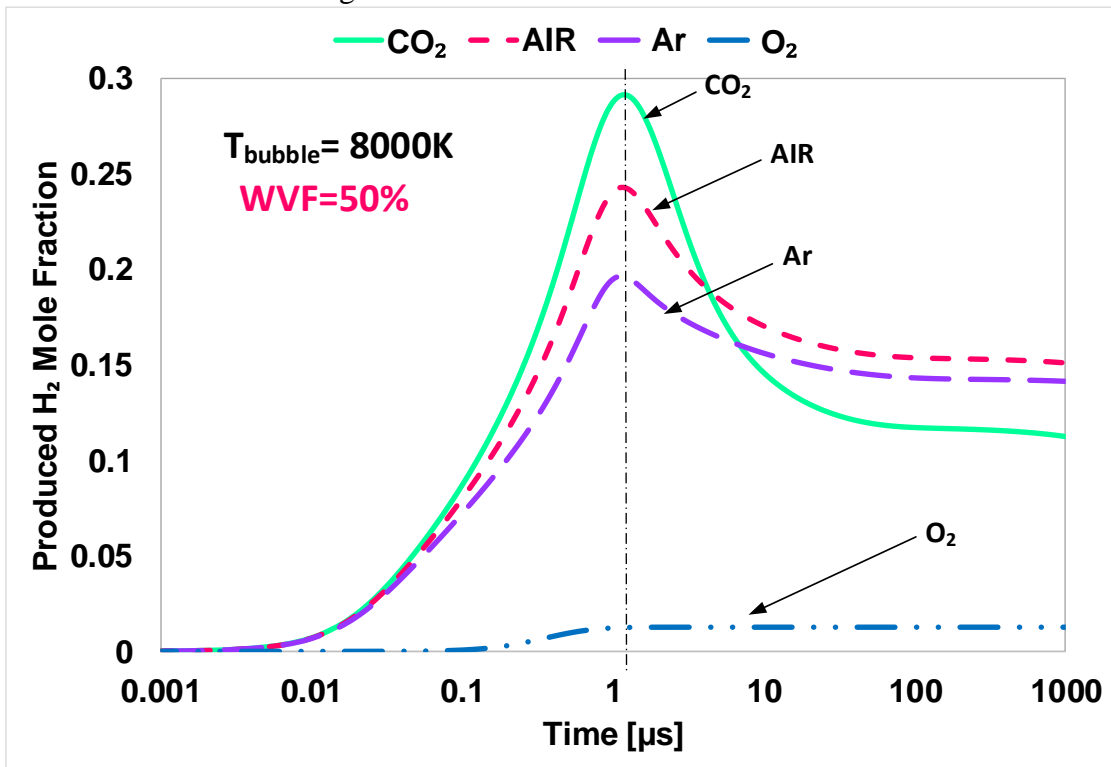


Figure 4.61: The predicted output of H₂ from a single bubble vs. the reaction time for various dissolved gases at a water volume fraction WVF = 50%

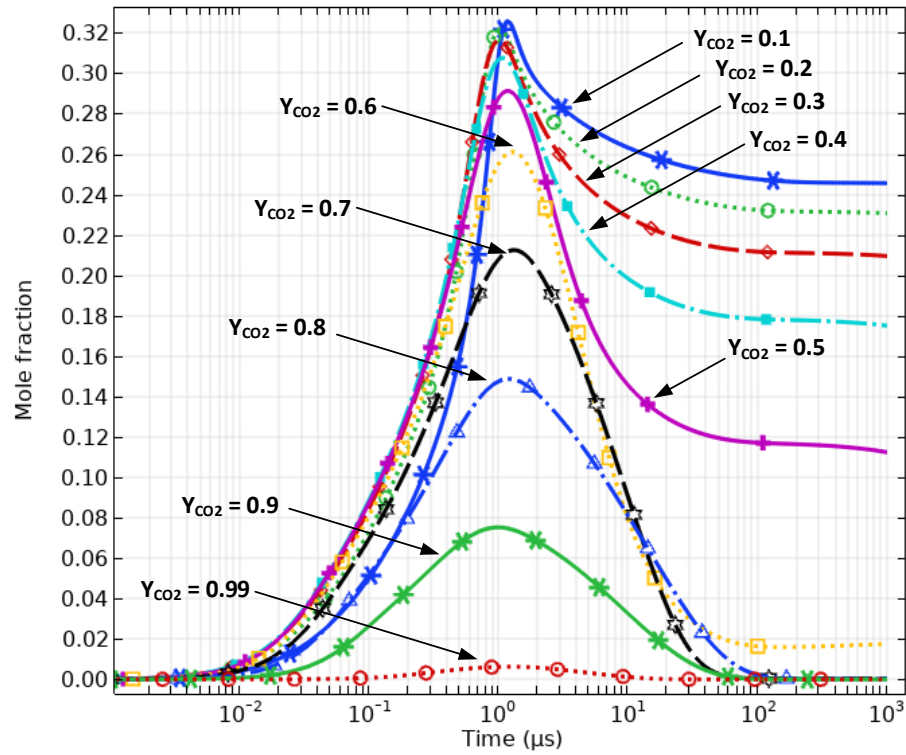


Figure 4.62: The effect of the initial bubble concentration on H_2 production of an H_2O/CO_2 bubbles

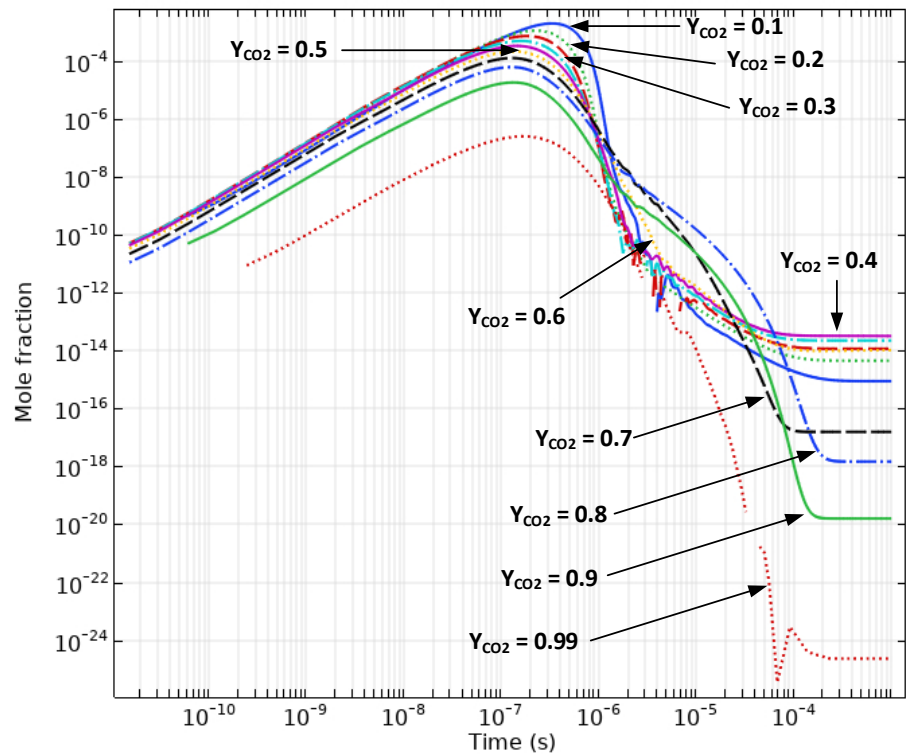


Figure 4.63: The effect of the initial bubble concentration on H_2O_2 production of an H_2O/CO_2 bubbles

The hydrogen produced stops and becomes non-continuous. Hydrogen peroxide is also of importance. It is found in many households at low concentrations of 3-9% for medicinal applications and as clothes and hair bleach. In industry, hydrogen peroxide at higher concentrations is used as a bleach for textiles and paper, as a component of rocket fuels, and for producing foam rubber and organic chemicals. Meanwhile, H_2O_2 can be toxic if ingested, inhaled, or by contact with the skin or eyes. The production of hydrogen peroxide from the sonochemical process is displayed in Figure 4.63. As seen, the mole fraction is very low due to a batch chemical reaction that does not harm the surroundings. The trends of different bubble concentrations do not show consistent results. All trends peak at almost the same reaction time, then they fall significantly, causing a drop in hydrogen peroxide production.

(e) Energy Performance Analysis

In this chapter, the hydrogen yield and energy efficiency performances of the sonochemical process are identified, and they will be presented in detail. The hydrogen yield is extracted from the chemical kinetics module's model solution at the end of the chemical reaction time.

4.7.1 Hydrogen yield

A study on the hydrogen yield from the sonochemical process is performed concerning different acoustic bubble temperatures. The bubble temperature affects the hydrogen yield because it depends on the acoustical parameters such as ultrasonic and acoustic pressure amplitude. The bubble temperature varies based on the acoustical parameters referring to the following equation considering the maximum bubble temperature $T = T_\infty (R_{max}/R)^{3(\nu-1)}$. The maximum bubble temperature is a function of the maximum bubble radius that is correlated to the ultrasonic frequency and the acoustic pressure amplitude by the following equation as: $R_{max} = (3 \times 10^3/f)(P_A - 1)(P_A)^{-1/2}[1 + 2(P_A - 1)/3]^{1/3}$. Back to the hydrogen yield from our process, the chemical reaction mechanism takes place at the maximum bubble temperature, and the water vapor is consumed, and many radicals are produced, such as O, OH, H, H_2O_2 , HO_2 as well as hydrogen H_2 molecule. The consumption of the water vapor X_{H_2O} trapped inside the acoustic bubble can be calculated from the following equation:

$$X_{H_2O} = \frac{n_{H_2O}(t = 0) - n_{H_2O}(t)}{n_{H_2O}(t = 0)} \quad (4.7)$$

where $n_{H_2O}(t = 0)$ is the number of moles of H₂O before the reaction, and $n_{H_2O}(t)$ is the mole fraction of water after the dissociation reaction or at any time t. While the hydrogen yield Y_{H_2} can be given as follows:

$$Y_{H_2} = \frac{n_{H_2}(t) - n_{H_2}(t = 0)}{n_{H_2O}(t = 0) - \int_0^t \dot{n}_{H_2O}(t)dt} \quad (4.8)$$

4.7.2 Sonohydrogen energy efficiency

To the best of the author's knowledge, no studies have reported the overall energy efficiency of the sonohydrogen process. Thus, this work is considered the first to report the energy efficiency of such an approach. The energy efficiency is defined as the total output divided by the summation of the total input, including the energy required for the dissociation of water H₂O into the radicals OH and H following this reaction: $H_2O \rightarrow OH + H$. It is worth mentioning that the amount of energy required for such dissociation is 493.4 kJ/mol. Which is considered half of the amount of energy needed for the separation of water into hydrogen and oxygen molecules based on this reaction equation: $H_2O \rightarrow H_2 + O$ that is 920 kJ/mol. Additionally, as carbon dioxide is contributed to the chemical reaction as a diluent, then its effect has to be neglected in the input energy. The ultrasonic power has to be added to the energy input, and it should be multiplied by the irradiation time. The general energy efficiency of the sonohydrogen process in the case of H₂O/CO₂ bubbles dissociation can be expressed as follows:

$$\eta_{sonoxygen} = \frac{n_{H_2}(t) * \overline{HV}_{H_2}}{P_{US} \cdot \Delta t_{US}} \Big]_{H_2O/dissolved\ gas} \quad (4.9)$$

Where $n_{H_2}(t)$ is the produced hydrogen number of moles, \overline{HV}_{H_2} the heating value of hydrogen 242 kJ/mol. Knowing that the energy required to dissociate the water molecule into OH and H, the electrical energy input accounts for it, can be obtained from any thermodynamics book [155]. $(P_{US} \cdot \Delta t_{US})$ is the ultrasonic power multiplied by the ultrasonic irradiation time to obtain the power in k joules. The hydrogen yield and the overall efficiency of the sonohydrogen process are extracted and calculated when the reaction time ends and not at the corresponding peak time. Therefore, Figure 4.64 displays the hydrogen yield and the process's overall energy efficiency for a bubble that is initially contained 39% H₂O/CO₂. The optimum hydrogen production can be

achieved at a temperature of 5400 K. The maximum H₂ yield achieved is 18%, meaning that only 18% has been transformed from 39% H₂O/CO₂. The maximum overall efficiency is around 8% within the limited time of the ultrasonic irradiation, which is considered the time at which the chemical reaction stops. Surprisingly, the increase in bubble temperature decreases the hydrogen production because of the presence of a dissolved gas like CO₂, which has a higher specific heat at constant pressure, which would absorb the excessive heat from the dissociation reaction. Hence, any additional heat added to the dissociation reaction would not benefit the process, but also it will deteriorate it. As mentioned earlier, the reaction did not start, or hydrogen won't be produced unless the minimum temperature of 2000 K is achieved through the acoustic conditions. Moreover, the general energy efficiency of the sonohydrogen process in the case of H₂O/O₂ bubbles dissociation is going to be the same. The only difference is the number of moles generated while using different dissolved gases. The hydrogen yield and the overall efficiency of the sonohydrogen process are extracted and calculated when the reaction time ends and not at the corresponding peak time. Therefore, Figure 4.65 displays the hydrogen yield and the process's overall energy efficiency for a bubble that is initially contained 39% H₂O/O₂. The optimum hydrogen production can be achieved at a temperature of 10000 K. The maximum H₂ yield obtained is less than 4%, meaning that only 3.8% has been transformed from 39% H₂O/O₂. The maximum overall efficiency is around 2% within the ultrasonic irradiation's limited time, which is considered when the chemical reaction stops. Surprisingly, the increase in bubble temperature did not affect the hydrogen production significantly because of the presence of a dissolved gas like O₂, which has a high thermal diffusivity, which would have less efficiency to contaminate the heat and it would result in releasing excessive heat from the bubble, which will decrease the hydrogen production. Hence, any additional heat added to the dissociation reaction would not benefit the process significantly, as a considerable part of it will be diffused. The critical observation for the dissociation of H₂O/O₂ bubbles is that the reaction did not start, or hydrogen will not be produced unless the minimum temperature of 4000 K is achieved through the acoustic conditions. On the other hand, the minimum temperature is 2000 K in the case of an H₂O/CO₂ bubble. In the case of the H₂O/Air bubble, the hydrogen yield and the overall efficiency of the sonohydrogen process are extracted and calculated when the reaction time ends and not at the corresponding peak time. Therefore, Figure 4.66 displays the hydrogen yield and the process's overall energy efficiency initially containing 39% H₂O/Air bubble. The optimum hydrogen production can be achieved at a

temperature of 7900 K. The maximum H₂ yield achieved is 28%, meaning that only 28% has been transformed from 39% H₂O/Air.

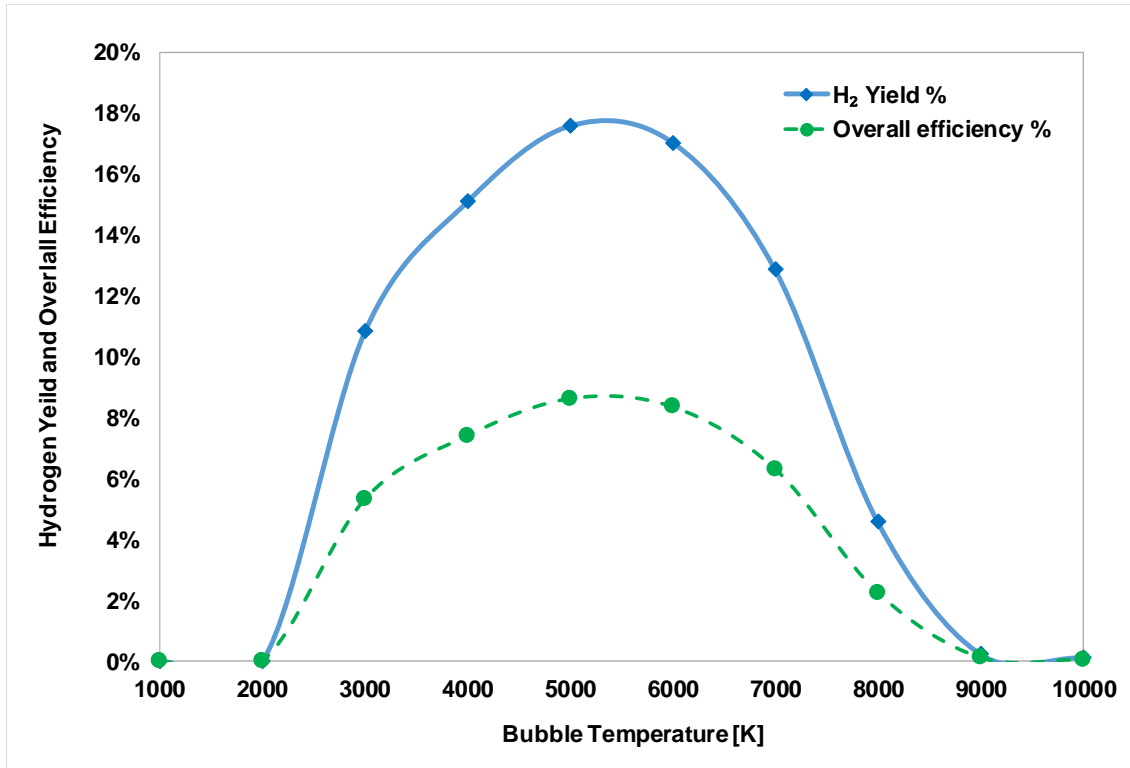


Figure 4.64: Hydrogen yield and energy efficiency vs. acoustic bubble temperature of H₂O/CO₂ bubble

The maximum overall efficiency is around 14% within the limited time of the ultrasonic irradiation, which is considered the time at which the chemical reaction stops. Surprisingly, the increase in bubble temperature decreases hydrogen production. Hence, any further heat added to the dissociation reaction would not benefit the process, but also it will deteriorate it. As mentioned earlier, the reaction did not start or hydrogen will not be produced unless the minimum temperature of 2000 K is achieved through the acoustic conditions. The hydrogen yield and the overall efficiency of the sonochemical process are extracted and calculated when the chemical reaction time ends and not at the corresponding peak time.

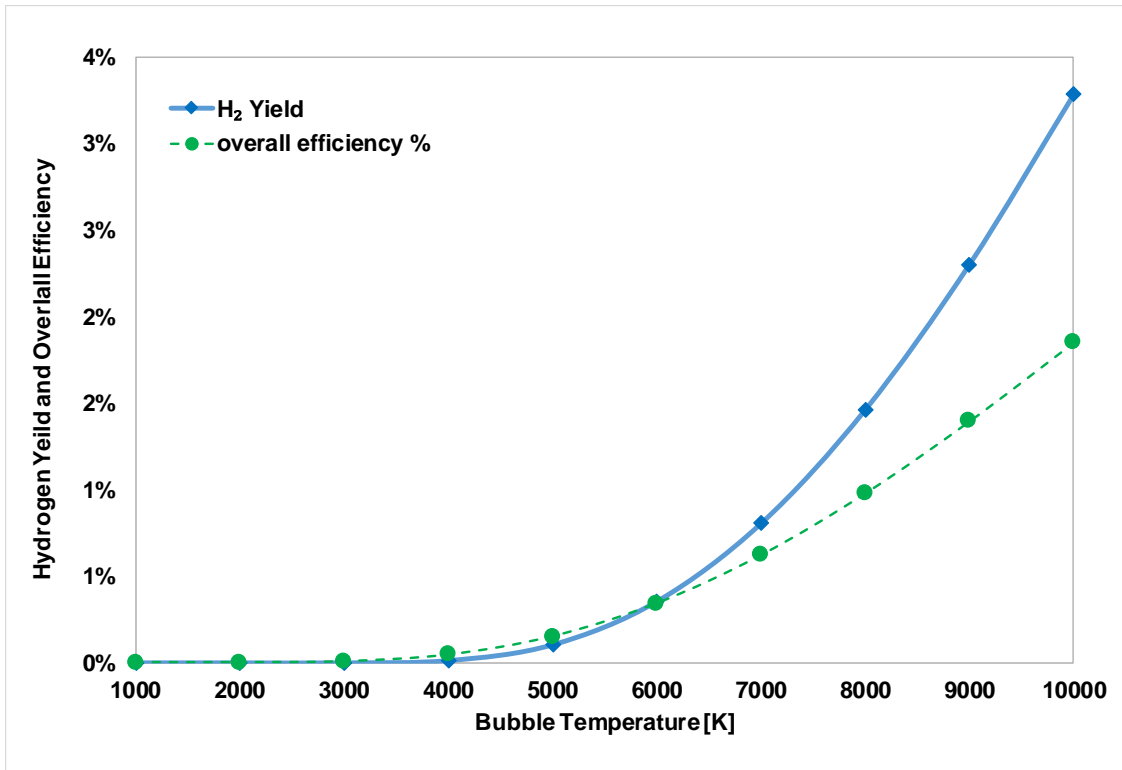


Figure 4.65: Hydrogen yield and energy efficiency vs. acoustic bubble temperature of H₂O/O₂ bubble

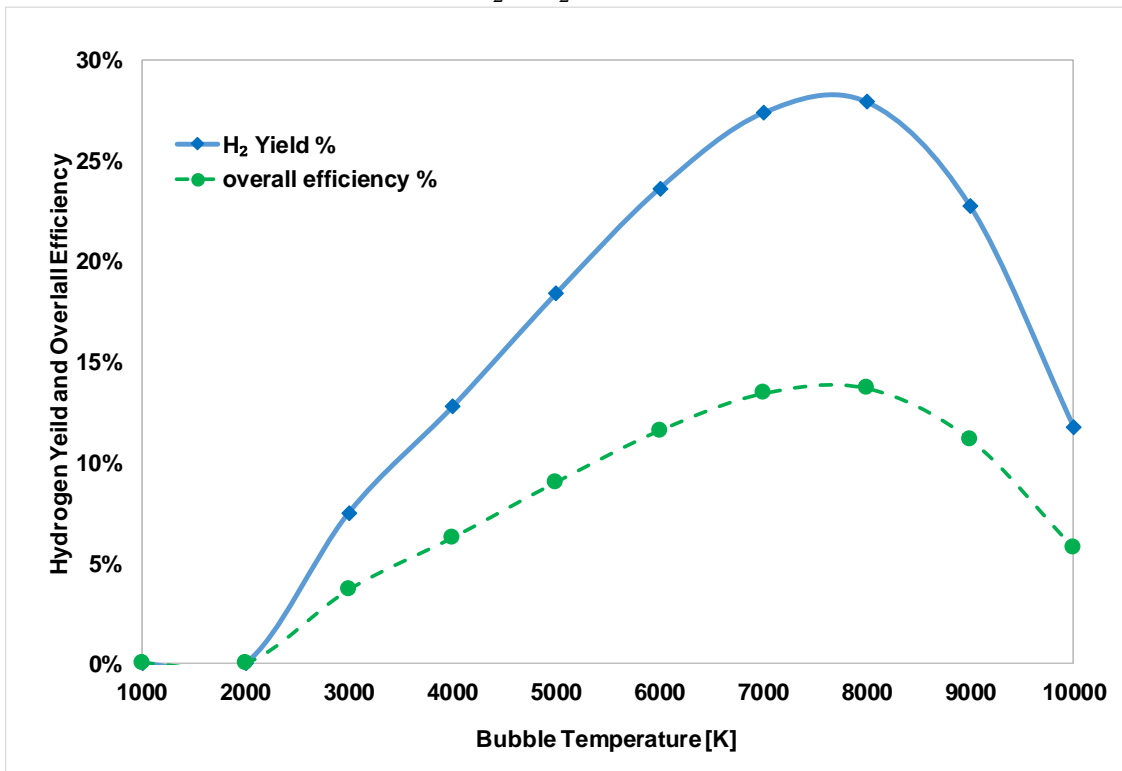


Figure 4.66: Hydrogen yield and energy efficiency vs. acoustic bubble temperature of H₂O/Air bubble

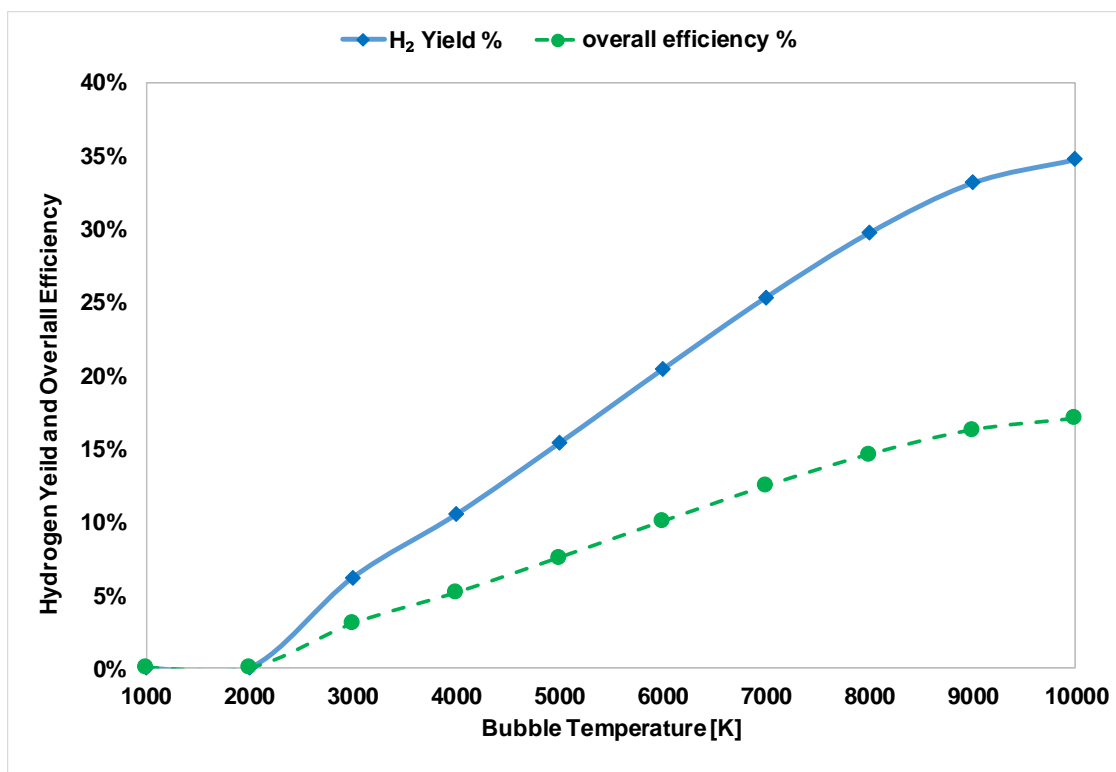


Figure 4.67: Hydrogen yield and energy efficiency vs. acoustic bubble temperature of H₂O/Ar bubble, argon bubble

Therefore, Figure 4.67 displays the hydrogen yield and the process's overall energy efficiency for a bubble that is initially contained 39% H₂O/Ar. The optimum hydrogen production can be achieved at a temperature of 10000 K. The maximum H₂ yield obtained is 35%, meaning that only 35% has been transformed from 39% H₂O/Ar. The maximum overall efficiency is around 16% within the ultrasonic irradiation's limited time, which is considered when the chemical reaction stops. Surprisingly, the argon recorded the best performance in comparison to all dissolved gases; from the trend, it seems that it almost reaches the optimum hydrogen yield and it is about to decrease, expecting that if the bubble temperature increased a couple of more thousands of kelvins, the yield would decrease and the overall efficiency.

4.7.3 Comparison of energy efficiency

At the end time of the chemical reaction mechanism, the yield of hydrogen and the corresponding sonochemical efficiency for different dissolved gases and different bubble temperatures are reported in Figure 4.68 and Figure 4.69, respectively. In Figure 4.68, the hydrogen yield is presented concerning the bubble temperature. Interestingly, the argon bubble showed the best

performance at the maximum bubble temperature. A turning point is also shown at the highest temperature used in the simulation. The oxygen bubble records the same trend. However, it has the lowest hydrogen yield performance. It would require a very high acoustic amplitude in order to improve the performance slightly. The air bubble achieved higher performance than the CO₂ bubble.

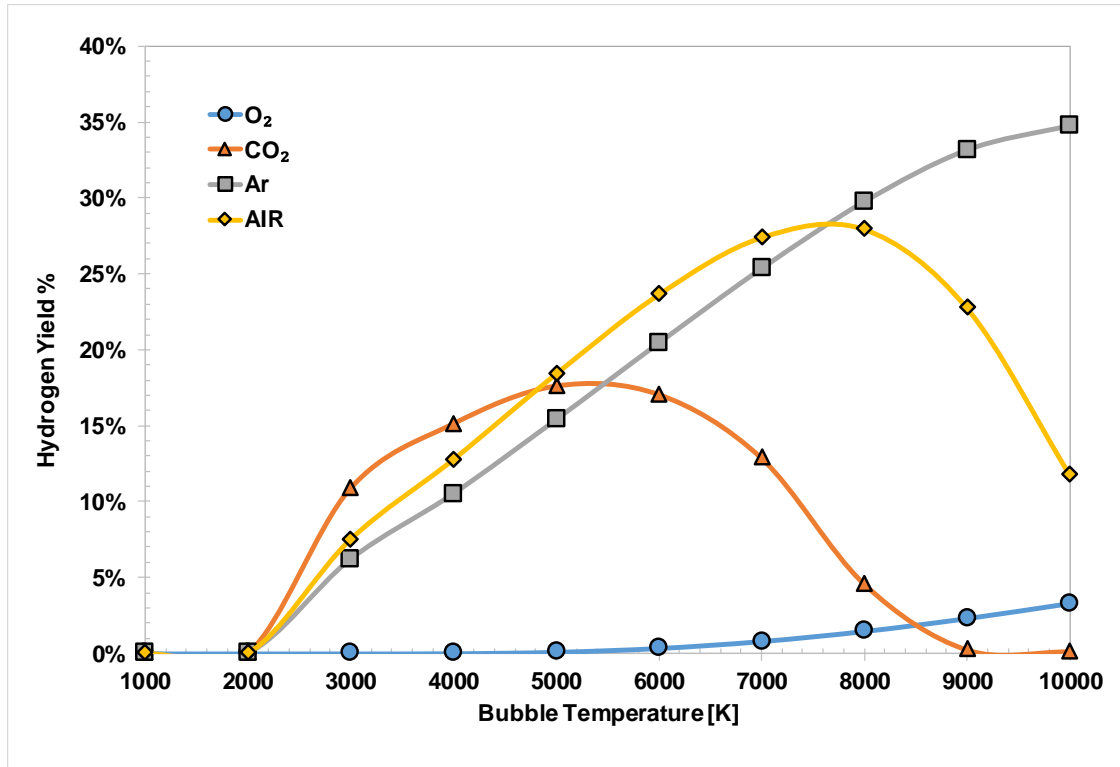


Figure 4.68: Hydrogen yield Comparison for different bubble temperatures and different dissolved gases

In Figure 4.69, the sonohydrogen efficiency is presented with respect to the bubble temperature. Interestingly, the argon bubble showed the best performance at the maximum bubble temperature; a turning point is also shown at the highest temperature used in the simulation. The oxygen bubble records the same trend; however, it has the lowest hydrogen yield performance. It would require a very high acoustic amplitude to improve the performance slightly. The air bubble achieved higher performance than the CO₂ bubble.

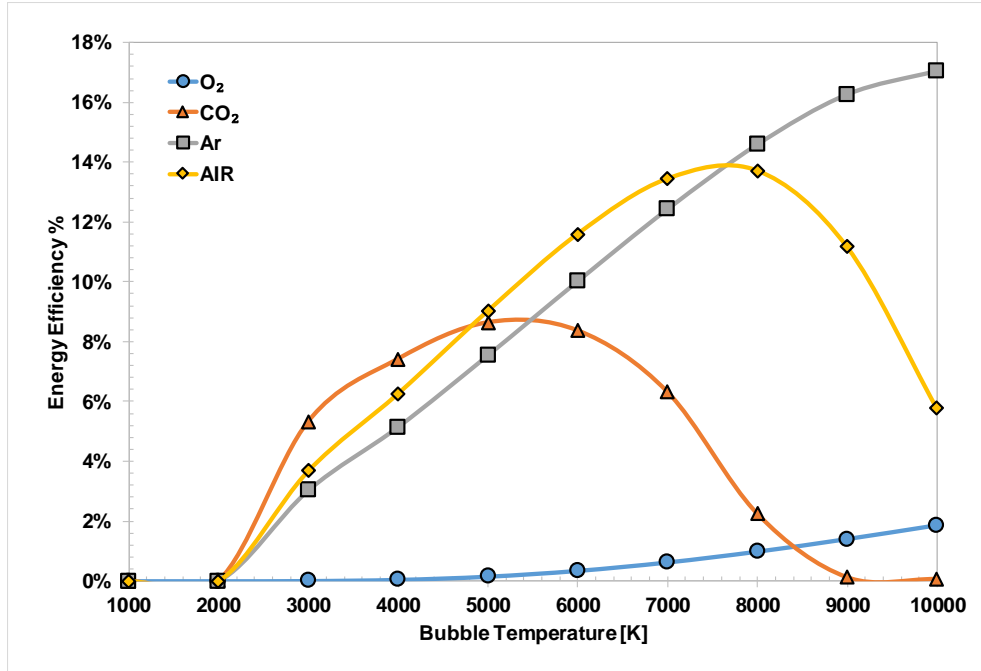


Figure 4.69: Energy Efficiency Comparison for different bubble temperatures and different dissolved gases

4.7.4 Cavitation and sonohydrogen efficiency

To scale-up the sonochemical reactors for industrial use, we have to investigate the efficiencies and the factor affecting the sonochemical process. The calorimetry method is not used here to calculate the input power because of the large heat dissipation due to the container's large surface area. Consequently, the input power has to be measured using a multi-meter. An ultrasonic cavitation meter is used for measuring the average cavitation energy in the sonoreactor. Unfortunately, the lack of experimental facilities made us assume and use the previous experimental works to assess the amount of cavitation energy and the corresponding sonohydrogen energy consumption. A standard method to calibrate the sonochemical efficiency of the sonoreactor is initially reported by Koda et al. [89]. They carried out the sonication experiment using distilled water at 25 °C. They performed a calibration analysis and concluded the ultrasonic power dissipation into a liquid can be calculated by the following equation:

$$P_{US} = M_{US} C_{pUS} \frac{\Delta T}{\Delta t} \quad (4.10)$$

Where (M_{US}) is the water mass [kg], (C_{pUS}) is the water's specific heat at a constant pressure of 4.19 kJ/kg-K, and ($\Delta T/\Delta t$) is the temperature change per unit irradiation time. The continuous ultrasonic irradiation into the liquid medium leads to a temperature rise of 5-10 K. The calorimetric

effect in this analysis is shown, and temperature simulations are conducted to see the effect of having an ultrasonic sonotrode emitting sound waves into a liquid medium on the temperature increase of the water as in Figure 4.70.

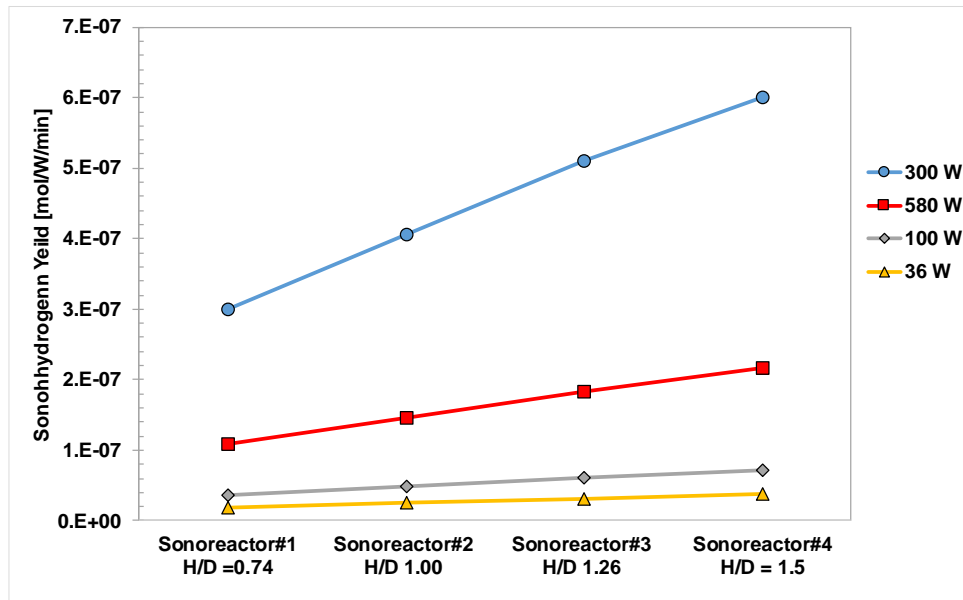


Figure 4.70: Average sonoreactor temperature with sonication time

The cavitation energy and cavitation yield are used to estimate the hydrogen quantity emitted by the sonohydrogen sonoreactor. The cavitation yield is defined as the number of reaction products per unit of irradiation time in seconds per unit of energy consumption in kWh. The cavitation energy gives an indication about the energy dissipated from the supplied input/electrical energy, and it can be described in terms of the input power as per equations (3.9) and (3.10). The acoustic cavitation has a threshold. The cavitation threshold can be defined as the power at which the cavitation bubble forms in a liquid at which the minimum power amplitude is required from a minimum cavitation density. Once the cavitation threshold is reached, low-density cavitation is presented in pressure antinodes. This cavitation is generally not uniform and generally not useful for any application, either sonohydrogen or ultrasonic cleaning. Above the cavitation threshold, cavitation density increases as power increased. Better cavitation bubble density is observed and may be seen with increased power within a certain range. The cavitation energy converted from the input power is displayed in Figure 4.71, along with the energy conversion efficiency. The conversion efficiency decreases while increasing the input power due to an increase in the surroundings' energy loss. The energy conversion can be identified as the ratio

between the cavitation energy output over the input power, measuring how much of the input energy is converted to the cavitation energy. This process's losses are due to the heat dissipated into the water inside the sonoreactor and losses of energy through the sonoreactor body.

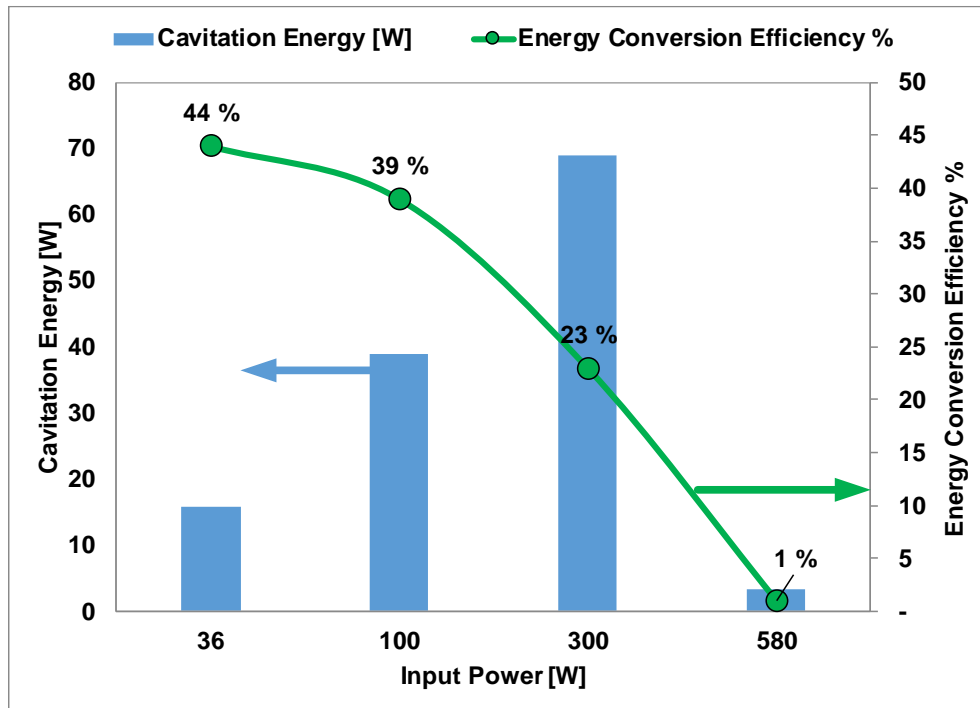


Figure 4.71: Input power vs. Cavitation Energy (y-axis-left) and Energy Conversion Efficiency (y-axis-right)

The onset of surface cavitation occurs when the acoustic cavitation bubbles starts to form on the surface of the ultrasonic transducer probe at a particular power amplitude rather than developing within the body of the liquid. In Figure 4.72, we present the input power vs. the cavitation energy. It shows how much input power is converted to cavitation energy. It also shows that after 300 W input power, the cavitation energy decreases because of the onset of surface cavitation is reached. Suppose the acoustic power amplitude exceeded the onset of surface cavitation. In that case, the forces required to couple vibrational energy to the liquid are exceeded, and additional power would not increase cavitation density. However, it would result in accelerating the transducer probe tip's erosion that may result in premature transducer failure.

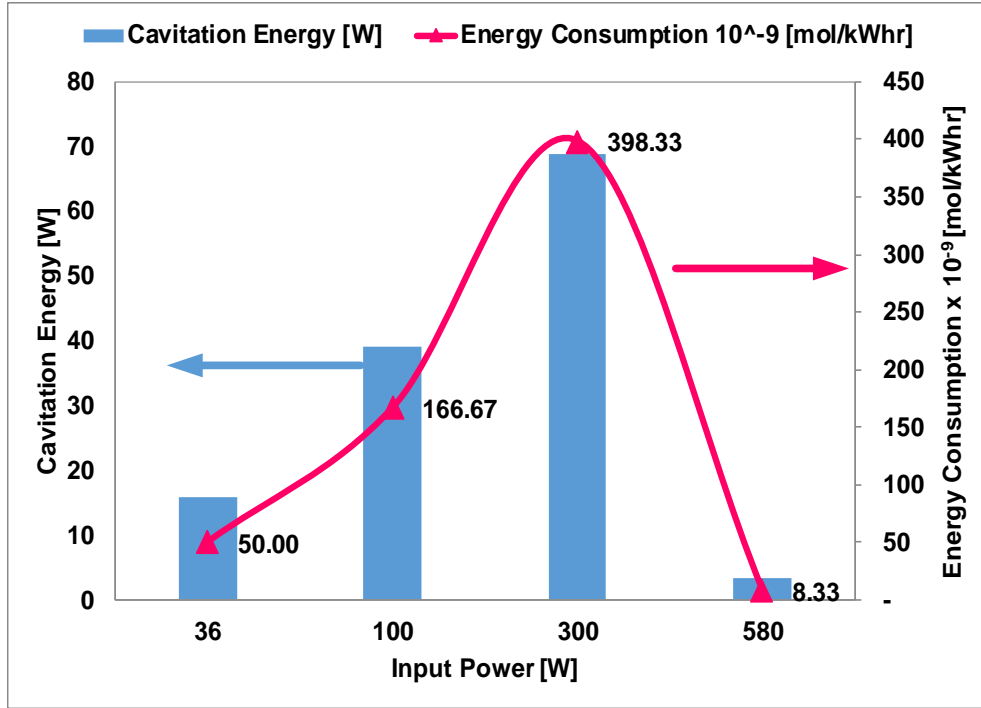


Figure 4.72: Input power vs. Cavitation Energy y-axis-left and Sonohydrogen Efficiency y-axis-right

In the case of multiple sonotrodes, the analysis is re-conducted using the same methodology to quantify the amount of hydrogen. The cavitation energy converted from the input power is displayed in Figure 4.73, along with the energy conversion efficiency. The conversion efficiency decreases while increasing the input power due to an increase in the surroundings' energy loss. As seen, the cavitation energy has a linear relation with the input energy with no drop in the conversion efficiency when using up to 5 sonotrodes with a capacity rate of 180 W or 36 W each. The trend for energy consumption is also increasing while increasing the number of sonotrodes and power, as seen in Figure 4.74.

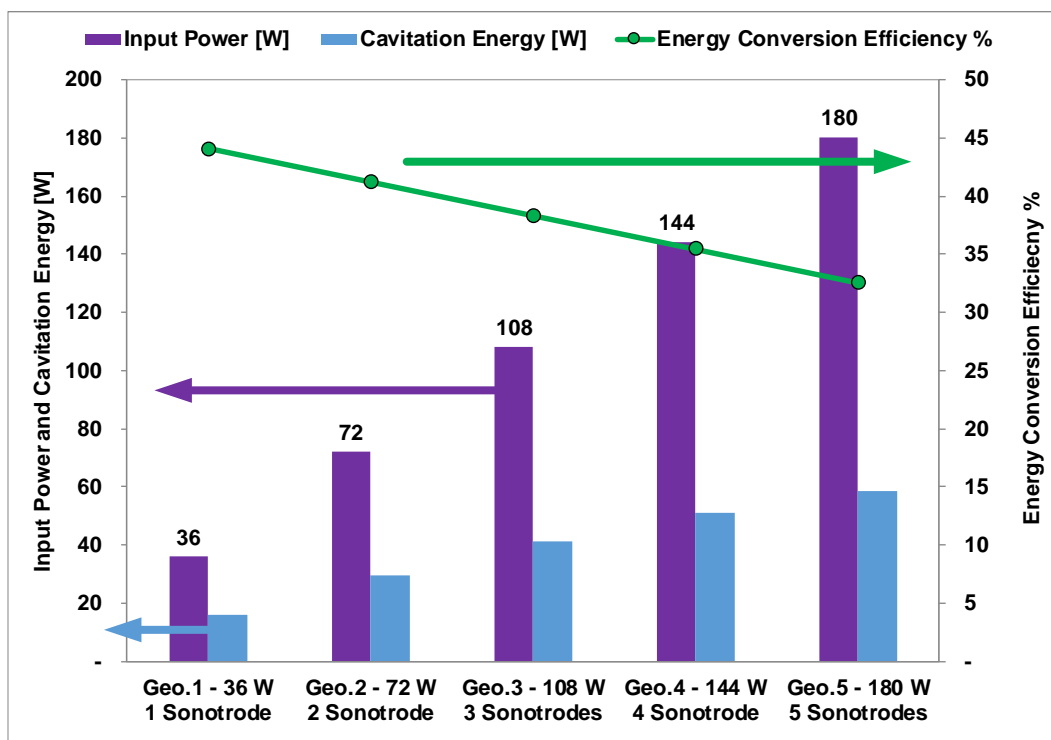


Figure 4.73: Input power vs. Cavitation Energy (y-axis-left) and Energy Conversion Efficiency (y-axis-right)

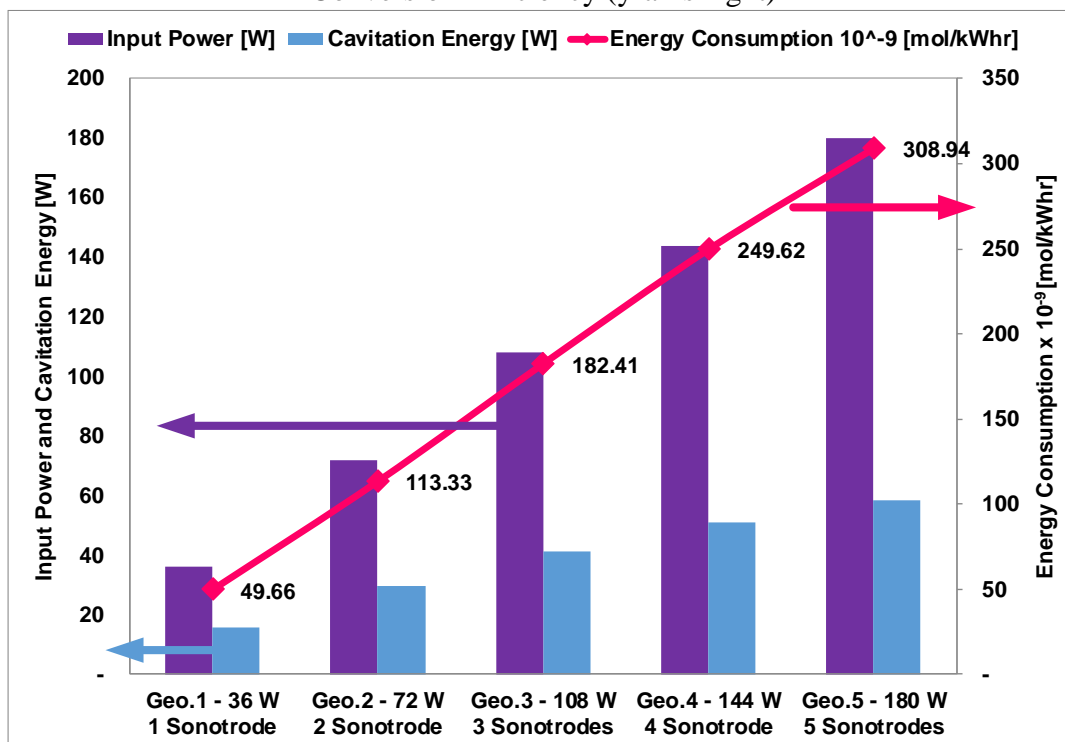


Figure 4.74: Input power vs. Cavitation Energy (y-axis) left and Sonohydrogen Efficiency (y-axis) right

Chapter 5. Conclusions and Recommendations

This chapter presents the conclusions of the work, research, and results in this Ph.D. Thesis. Then the chapter goes to the recommendation section, which provides recommendations that are inferred from the results of the thesis. Note that the recommendations also introduce ideas for studies that can be proposed and further analyze ideas that are out of this thesis's scope and objectives.

5.1 Conclusions

The main novelty that this Ph.D. thesis offers as the main contribution to the field is the established link between the ultrasonic sonication process and the chemical reactions associated with hydrogen production, which is identified and given the name the “sonohydrogen” process. The sonohydrogen process occurs in a sonoreactor type-A, where an ultrasonic transducer is immersed from the top side of the sonoreactor. The thesis aims to investigate and quantify the amount of hydrogen production out of the sonohydrogen process. The study provides characteristics of the acoustic field and flow field of the sonohydrogen process and quantifies hydrogen. Various numerical models and studies are established and simulated, including the acoustic pressure study, acoustic streaming study, bubble dynamics study, reaction kinetics study, and geometric optimization study. The acoustics model relates the acoustic parameters to the sonoreactor performance, such as frequency, acoustic power amplitude, and acoustic intensity. Simultaneously, the Keller-Miksis equation is solved to simulate the bubble dynamics study needed as input parameters to simulate the chemical engineering module.

The acoustic model focused on numerical simulations for characterizing the acoustic and flow field due to acoustic streaming within the sonoreactor and is successfully validated. A secondary study is performed to quantify the hydrogen production from the cavitation energy and determine the corresponding sonohydrogen efficiency. The main findings of the research, modeling, simulation, and analyses of this thesis are summarized as follows:

- The ultrasonic frequency can significantly alter the minimum pressure of the sonoreactor due to its direct impact on forming the acoustic cavitation bubbles. Changing the diameter will alter the length of the sound hard boundaries and will change the phase of the reflected waves.
- The minimum acoustic pressure did not alter significantly from 20 kHz to 50 kHz before the negative pressure's maximum amplitude takes place between 60 to 80 kHz. The negative

pressure amplitude starts to decrease when the frequency increased beyond the 80 kHz. Then any further increase will increase the negative pressure. These phenomena change the wave interactions and hence the acoustic pressure and the sound pressure levels.

- CLY-4P and CLY-5P generate the maximum cavitation volume of around 55%. The case of SQR-3P has its sonoreactor volume full by the cavitation volume 61.1% and severe cavitation volume of 36.9. The number of sonotrodes would promote hydrogen production efficiency to a certain limit. If this limit is exceeded, the forces required to couple vibrational energy to the liquid are exceeded, and additional power would not increase cavitation density.
- The minimum temperature limit of the H₂O/O₂ bubble required is 4000 K. This temperature limit changes when changing the dissolved gases. At a frequency of 20kHz, acoustic power of 30 W, and H₂O/O₂ bubble, the H₂ production rate produced ranged between 5.46×10^{-6} to 8.59×10^{-6} $\mu\text{mol/h}$. The energy consumption required to produce hydrogen is 2.22×10^{-2} $\mu\text{mol/kWh}$.
- For the sake of contrast, a brief comparison is drawn between two dissolved gases, H₂O/CO₂ and H₂O/O₂, and we predicted and compared the energy consumption might vary between 1.05-1.63 $\mu\text{mol/kWh}$. Conversely, in the CO₂/H₂O bubble, the hydrogen rate significantly improved to range from 22.26 to 34.98 $\mu\text{mol/kWh}$. The dissolved gases are considered one of the most critical parameters affecting the hydrogen production rate. It is attributed that the mixture of H₂O/CO₂ has higher heat capacity, lower thermal conductivity, and, consequently, lower thermal diffusivity, which achieves the optimum atmosphere that benefits hydrogen production.
- The maximum hydrogen production is recorded at 300 W for 2.5×10^{-9} mol/J when increasing the input power to one sonotrode mounted in a typical sonoreactor cylindrical shape at an energy conversion efficiency of 23%. For the study on the multiple sonoreactor, the amount of hydrogen produced is 308×10^{-9} mol/kWh at 180 W with an energy conversion efficiency of 33%.

5.2 Recommendations

In this section, a set of recommendations are provided to further study considerations that can be built upon the work and results presented in this thesis. The work in this thesis investigates the unexplored field of using ultrasonic waves in the hydrogen production process. It also investigates the integration between acoustics and the hydrogen production field. This Ph.D. thesis is based on

numerical modeling and simulation analyses. The COMSOL Multiphysics solver is used throughout the whole study. However, there are still many opportunities to be probed and discovered. In order to further investigate the proposed systems and expand on the introduced field of sonochemical systems and the recommendations and some proposed experimental work is summarized as follows:

- Expanding the developed work of the sonohydrogen to be integrated with an electrolyzer system to promote the hydrogen production rate. The integrated system is novel with limited contribution in the literature. The integrated system is called Ultrasonic-Aided Electrolyzer System for hydrogen production
- Expanding the developed model of the sonohydrogen process to simulate complex-geometries to enhance the pressure distribution and promote the acoustic streaming effects inside the sonohydrogen reactor. Expand the acoustic-geometric parametric study by applying multiple probes with different arrays inside various sonoreactor geometries
- Investigating the distribution of the generated acoustic cavitation bubbles inside different and complex-sonoreactor geometries taking into consideration non-linear effects of the bubble dynamics model
- Investigating the potential efficiency improvement by using catalysts or nanoparticles to enhance the heat transfer characteristics and improve the hydrogen production rate
- The developed one-dimensional chemical kinetics mechanism can be extended to two dimensional or three dimensional within a single and multiple bubbles
- Performing cost and exergy-economic cost analysis on the proposed systems, including the savings due to the sonohydrogen process
- An experimental study of the sonohydrogen process is highly recommended to investigate the performance of the proposed system
- Experimental investigation of the sonohydrogen process while using different liquids such as water-methanol blends and other different wastewater compositions
- Experimental investigation of the ultrasonic effects on the disintegration of the sewage sludge wastewater is recommended as well as an experimental investigation of the ultrasonic-aided coagulation and flocculation process for wastewater treatment and possible hydrogen production using ultrasound

The main opportunity that should be discovered is to perform an experimental investigation. The main points are illustrated in detail in order to investigate the sonohydrogen process experimentally. This would benefit the readers and incoming grad students to do tests and examinations and come out with a novel contribution to the sonohydrogen field. Ultrasound-induced cavitation bubbles can be a source of energy due to bubble oscillation. The production of these sound pressure waves can be attributed to two reasons; the first reason is that these pressure waves is a result of the bubbles collapse, whereas the second reason is that these pressure waves are produced from the interaction between the bubbles, the wall and the reflected ultrasound waves from the walls. It is not yet clear that the production of these sound pressure waves is due to which of these reasons. Therefore, further experimental investigations should be carried out. An overview of different experimental configurations and recent experimental work procedure and their significance in understanding the *Sonohydrogen* production approach is presented. The author recommends using one of the three main configurations of sonoreactors, as mentioned earlier in Figure 2.2, section 2.2.4. The ultrasonic transducer probe (Type-A), the ultrasonic transducer bath (Type-B), and an indirect irradiation bath (Type-C). Differences between each type are mentioned earlier in section 2.2.4. However, researchers in the field of Ultrasonic Sonochemistry recommended performing experimental work on Type-A in order to strengthen the quality of the work. In conclusion, greater concentrated energy will be available in type-A (immersed ultrasonic probe reactor), and almost 15% lower power dissipation is found in the case of type-B (ultrasonic bath reactor) [49]. Therefore, type-A is recommended to continue the study in the future. The experiment is a typical immersed type sonoreactor system, Type-A. The ultrasonic transducer probe (Vibra-cell VCX-750, frequency 20 kHz, net power output 750 W, 2 cm diameter). The transducer tip is immersed 2 cm under the liquid water surface and mounted by a vertical movable mechanism in order to vary the immersed depth of the ultrasonic probe inside the sonoreactor model. The sonoreactor consists of cylindrical acrylic glass with a diameter of 13.5 cm and a length of 17 cm. The acrylic glass container is going to be filled with distilled water at 25°C. The water temperature will be monitored through a thermocouple immersed and located halfway of the liquid volume. Furthermore, the temperature will be maintained by means of circulating cooling water through the water jacket surrounded the sonoreactor. A hydrophone will be used to track and monitor the acoustic pressure fluctuation using the FFT spectrum analyzer. The amount of hydrogen produced will be measured using gas chromatography (CP-4900, Varian) equipped with

a molecular sieve column, which enables hydrogen, oxygen, and nitrogen separation. The chromatography will also be attached with a thermal conductivity detector, which allows gas identification. The gas sampling is going to be made by a gastight syringe. The sampling pipe will be inserted at the top of the sonoreactor through a duct with a porous septum in rubber and Teflon. The sample will be taken and injected into the gas chromatography to analyze and identify the gas composition.

REFERENCES

- [1] Industrial Energy Demand by Fuel, Reference Case n.d. <https://www.cerrec.gc.ca/en/data-analysis/canada-energy-future/2018/chapter-3-reference-high-low-price-case-results.html>.
- [2] Arafa N, Mohany A. Developments and Recent Patents on Thermoacoustic Devices. *Recent Patents Mech Eng* 2012;5:79–88. doi:10.2174/1874477X11205020079.
- [3] Rashwan SS, Dincer I, Mohany A. Sonication to hydrogenization: Sono-hydro-gen. *Int J Energy Res* 2019;43:1045–8. doi:10.1002/er.4339.
- [4] Rashwan SS, Dincer I, Mohany A, Pollet BG. The Sono-Hydro-Gen process (Ultrasound induced hydrogen production): Challenges and opportunities. *Int J Hydrogen Energy* 2019;44:14500–26. doi:10.1016/j.ijhydene.2019.04.115.
- [5] Malerød-Fjeld H, Clark D, Yuste-Tirados I, Zanón R, Catalán-Martinez D, Beeaff D, et al. Thermo-electrochemical production of compressed hydrogen from methane with near-zero energy loss. *Nat Energy* 2017;2:923–31. doi:10.1038/s41560-017-0029-4.
- [6] Sherbo RS, Delima RS, Chiykowski VA, MacLeod BP, Berlinguette CP. Complete electron economy by pairing electrolysis with hydrogenation. *Nat Catal* 2018;1:501–7. doi:10.1038/s41929-018-0083-8.
- [7] Xie G-J, Liu B-F, Wang R-Q, Ding J, Ren H-Y, Zhou X, et al. Bioaggregate of photo-fermentative bacteria for enhancing continuous hydrogen production in a sequencing batch photobioreactor. *Sci Rep* 2015;5:16174. doi:10.1038/srep16174.
- [8] Brinkert K, Richter MH, Akay Ö, Liedtke J, Giersig M, Fountaine KT, et al. Efficient solar hydrogen generation in microgravity environment. *Nat Commun* 2018;9:2527. doi:10.1038/s41467-018-04844-y.
- [9] Zhang Y, Xu P, Liang S, Liu B, Shuai Y, Li B. Exergy analysis of hydrogen production

- from steam gasification of biomass: A review. *Int J Hydrogen Energy* 2019;44:14290–302. doi:10.1016/j.ijhydene.2019.02.064.
- [10] Guo Y, Wang SZ, Xu DH, Gong YM, Ma HH, Tang XY. Review of catalytic supercritical water gasification for hydrogen production from biomass. *Renew Sustain Energy Rev* 2010;14:334–43. doi:10.1016/j.rser.2009.08.012.
- [11] Chang ACC, Chang H-F, Lin F-J, Lin K-H, Chen C-H. Biomass gasification for hydrogen production. *Int J Hydrogen Energy* 2011;36:14252–60. doi:10.1016/j.ijhydene.2011.05.105.
- [12] Safari F, Dincer I. Development and analysis of a novel biomass-based integrated system for multigeneration with hydrogen production. *Int J Hydrogen Energy* 2019;44:3511–26. doi:10.1016/j.ijhydene.2018.12.101.
- [13] Dincer I, Acar C. Review and evaluation of hydrogen production methods for better sustainability. *Int J Hydrogen Energy* 2014;40:11094–111.
- [14] Raptis D, Seferlis AK, Mylona V, Politis C, Lianos P. Electrochemical hydrogen and electricity production by using anodes made of commercial aluminum. *Int J Hydrogen Energy* 2019;44:1359–65. doi:10.1016/j.ijhydene.2018.11.202.
- [15] Zhang JY, Qi H, He ZZ, Yu XY, Ruan LM. Investigation of light transfer procedure and photobiological hydrogen production of microalgae in photobioreactors at different locations of China. *Int J Hydrogen Energy* 2017. doi:10.1016/j.ijhydene.2017.06.079.
- [16] Eroglu E, Melis A. Photobiological hydrogen production: Recent advances and state of the art. *Bioresour Technol* 2011;102:8403–13. doi:10.1016/j.biortech.2011.03.026.
- [17] Photobiological Hydrogen Production – Prospects and Challenges. *Microbe* 2009. doi:10.1016/j.tibtech.2010.01.007.
- [18] Ahmed M, Dincer I. A review on photoelectrochemical hydrogen production systems: Challenges and future directions. *Int J Hydrogen Energy* 2019;44:2474–507. doi:10.1016/j.ijhydene.2018.12.037.
- [19] Yu S-C, Huang C-W, Liao C-H, Wu JCS, Chang S-T, Chen K-H. A novel membrane reactor for separating hydrogen and oxygen in photocatalytic water splitting. *J Memb Sci* 2011;382:291–9. doi:10.1016/j.memsci.2011.08.022.
- [20] Hisatomi T, Kubota J, Domen K. Recent advances in semiconductors for photocatalytic and photoelectrochemical water splitting. *Chem Soc Rev* 2014;43:7520–35.

doi:10.1039/C3CS60378D.

- [21] Maeda K. Photocatalytic water splitting using semiconductor particles: History and recent developments. *J Photochem Photobiol C Photochem Rev* 2011;12:237–68.
doi:10.1016/j.jphotochemrev.2011.07.001.
- [22] Kato H, Kudo A. Photocatalytic water splitting into H₂ and O₂ over various tantalate photocatalysts. *Catal. Today*, vol. 78, 2003, p. 561–9. doi:10.1016/S0920-5861(02)00355-3.
- [23] Haryanto A, Fernando S, Murali N, Adhikari S. Current Status of Hydrogen Production Techniques by Steam Reforming of Ethanol: A Review. *Energy & Fuels* 2005;19:2098–106. doi:10.1021/ef0500538.
- [24] Collodi G, Wheeler F. Hydrogen Production via Steam Reforming with CO₂ Capture. *Chem Eng Trans* 2010. doi:10.3303/CET1019007.
- [25] Ivy J. Summary of Electrolytic Hydrogen Production - Milestone Completion Report. 2004. doi:10.1126/science.1066771.
- [26] Bandyopadhyay A, Stöckel J, Min H, Sherman LA, Pakrasi HB. High rates of photobiological H₂ production by a cyanobacterium under aerobic conditions. *Nat Commun* 2010. doi:10.1038/ncomms1139.
- [27] Šingliar M. SOLAR ENERGY USING FOR HYDROGEN PRODUCTION. *Pet Coal* 2007;49:40–7.
- [28] Landman A, Dotan H, Shter GE, Wullenkord M, Houaijia A, Maljusch A, et al. Photoelectrochemical water splitting in separate oxygen and hydrogen cells. *Nat Mater* 2017;16:646–51. doi:10.1038/nmat4876.
- [29] Merouani S, Hamdaoui O, Rezgui Y, Guemini M. Mechanism of the sonochemical production of hydrogen. *Int J Hydrogen Energy* 2015;40:4056–64.
doi:10.1016/j.ijhydene.2015.01.150.
- [30] Venault L. De l'influence des ultrasons sur la réactivité de l'uranium (U (IV)/U (VI)) et du plutonium (PU (III)/PU (IV)) en solution aqueuse nitrique. 1997.
- [31] Penconi M, Rossi F, Ortica F, Elisei F, Gentili PL. Hydrogen production from water by photolysis, sonolysis and sonophotolysis with solid solutions of rare earth, gallium and indium oxides as heterogeneous catalysts. *Sustain* 2015;7:9310–25.
- [32] Moriguchi N. The Influence of Supersonic Waves on Chemical Phenomena. III. *Nippon*

- KAGAKU KAISHI 1934. doi:10.1246/nikkashi1921.55.8_749.
- [33] Li S-D, Wang C-C, Chen C-Y. Water electrolysis in the presence of an ultrasonic field. *Electrochim Acta* 2009. doi:10.1016/j.electacta.2009.01.087.
- [34] Compton RG, Eklund JC, Marken F. *Sonoelectrochemical Processes: A Review*. *Electroanalysis* 1997. doi:10.1002/elan.1140090702.
- [35] Crum LA, Fowlkes JB. Acoustic cavitation generated by microsecond pulses of ultrasound. *Nature* 1986. doi:10.1038/319052a0.
- [36] WALKER R, WALKER CT. Hardening of immersed metals by ultrasound. *Nature* 1974;250:410–1. doi:10.1038/250410a0.
- [37] Mitragotri S. Healing sound: the use of ultrasound in drug delivery and other therapeutic applications. *Nat Rev Drug Discov* 2005;4:255–60. doi:10.1038/nrd1662.
- [38] Nieminen HJ, Laidmäe I, Salmi A, Rauhala T, Paulin T, Heinämäki J, et al. Ultrasound-enhanced electrospinning. *Sci Rep* 2018. doi:10.1038/s41598-018-22124-z.
- [39] Bhandari P, Novikova G, Goergen CJ, Irudayaraj J. Ultrasound beam steering of oxygen nanobubbles for enhanced bladder cancer therapy. *Sci Rep* 2018. doi:10.1038/s41598-018-20363-8.
- [40] Mason TJ. Ultrasound in synthetic organic chemistry. *Chem Soc Rev* 1997. doi:10.1039/cs9972600443.
- [41] Cravotto G, Cintas P. Power ultrasound in organic synthesis: moving cavitation chemistry from academia to innovative and large-scale applications. *Chem Soc Rev* 2006;35:180–96. doi:10.1039/B503848K.
- [42] Bang JH, Suslick KS. Applications of ultrasound to the synthesis of nanostructured materials. *Adv Mater* 2010. doi:10.1002/adma.200904093.
- [43] Chen D. Ultrasound in Synthetic Applications and Organic Chemistry. *Handb. Appl. Ultrasound*, CRC Press; 2011, p. 235–84. doi:10.1201/b11012-16.
- [44] Tao Y, Sun DW. Enhancement of Food Processes by Ultrasound: A Review. *Crit Rev Food Sci Nutr* 2015. doi:10.1080/10408398.2012.667849.
- [45] Chandrapala J, Oliver C, Kentish S, Ashokkumar M. Ultrasonics in food processing. *Ultrason Sonochem* 2012. doi:10.1016/j.ultsonch.2012.01.010.
- [46] Ashokkumar M. The characterization of acoustic cavitation bubbles - An overview. *Ultrason. Sonochem.*, vol. 18, 2011, p. 864–72. doi:10.1016/j.ultsonch.2010.11.016.

- [47] Klíma J, Frias-Ferrer A, González-García J, Ludvík J, Sáez V, Iniesta J. Optimisation of 20 kHz sonoreactor geometry on the basis of numerical simulation of local ultrasonic intensity and qualitative comparison with experimental results. *Ultrason Sonochem* 2007;14:19–28. doi:10.1016/j.ultsonch.2006.01.001.
- [48] Tuziuti T, Yasui K, Sivakumar M, Iida Y, Miyoshi N. Correlation between Acoustic Cavitation Noise and Yield Enhancement of Sonochemical Reaction by Particle Addition. *J Phys Chem A* 2005;109:4869–72. doi:10.1021/jp0503516.
- [49] Gogate PR, Tatake PA, Kanthale PM, Pandit AB. Mapping of sonochemical reactors: Review, analysis, and experimental verification. *AIChE J* 2002;48:1542–60.
- [50] Yasui K. *Acoustic Cavitation and Bubble Dynamics*. Nagoya: Springer Briefs in Molecular Science; 2017.
- [51] Leighton TG, Apfel RE. The Acoustic Bubble. *J Acoust Soc Am* 1994;96:2616–2616. doi:10.1121/1.410082.
- [52] Lee J, Kentish SE, Ashokkumar M. The effect of surface-active solutes on bubble coalescence in the presence of ultrasound. *J Phys Chem B* 2005. doi:10.1021/jp0476444.
- [53] Lee J, Tuziuti T, Yasui K, Kentish S, Grieser F, Ashokkumar M, et al. Influence of Surface-Active Solute on the Coalescence, Clustering, and Fragmentation of Acoustic Bubbles Confined in a Microspace. *J Phys Chem C* 2007;111:19015–23. doi:10.1021/jp075431j.
- [54] S. Rashwan S, Dincer I, Mohany A. Sonication to Hydrogenization: Sono-hydro-gen. *Int J Energy Res* 2018:1–4. doi:10.1002/er.4339.
- [55] Merouani S, Hamdaoui O, Rezgui Y, Guemini M. Computational engineering study of hydrogen production via ultrasonic cavitation in water. *Int J Hydrogen Energy* 2016;41:832–44. doi:10.1016/j.ijhydene.2015.11.058.
- [56] Merouani S, Hamdaoui O, Rezgui Y, Guemini M. Sensitivity of free radicals production in acoustically driven bubble to the ultrasonic frequency and nature of dissolved gases. *Ultrason Sonochem* 2015. doi:10.1016/j.ultsonch.2014.07.011.
- [57] Merouani S, Hamdaoui O, Rezgui Y, Guemini M. Theoretical estimation of the temperature and pressure within collapsing acoustical bubbles. *Ultrason Sonochem* 2014;21:53–9. doi:10.1016/j.ultsonch.2013.05.008.
- [58] Brotchie A, Grieser F, Ashokkumar M. Effect of Power and Frequency on Bubble-Size

- Distributions in Acoustic Cavitation. *Phys Rev Lett* 2009;102:084302.
doi:10.1103/PhysRevLett.102.084302.
- [59] Pétrier C, Francony A. Ultrasonic waste-water treatment: Incidence of ultrasonic frequency on the rate of phenol and carbon tetrachloride degradation. *Ultrason Sonochem* 1997. doi:10.1016/S1350-4177(97)00036-9.
- [60] Jiang Y, Petrier C, Waite TD. Sonolysis of 4-chlorophenol in aqueous solution: Effects of substrate concentration, aqueous temperature and ultrasonic frequency. *Ultrason Sonochem* 2006. doi:10.1016/j.ultsonch.2005.07.003.
- [61] Merouani S, Ferkous H, Hamdaoui O, Rezgui Y, Guemini M. A method for predicting the number of active bubbles in sonochemical reactors. *Ultrason Sonochem* 2015;22:51–8. doi:10.1016/j.ultsonch.2014.07.015.
- [62] MA Margulis YD. Energetics and mechanism of acoustochemical reactions. Yields of hydrogen and hydrogen peroxide in different aqueous systems. *Russ J Phys Chem* 1984.
- [63] Kerboua K, Hamdaoui O. Numerical estimation of ultrasonic production of hydrogen: Effect of ideal and real gas based models. *Ultrason Sonochem* 2018;40:194–200. doi:10.1016/j.ultsonch.2017.07.005.
- [64] Sutkar VS, Gogate PR. Design aspects of sonochemical reactors: Techniques for understanding cavitation activity distribution and effect of operating parameters. *Chem Eng J* 2009. doi:10.1016/j.cej.2009.07.021.
- [65] Krefting D, Mettin R, Lauterborn W. High-speed observation of acoustic cavitation erosion in multibubble systems. *Ultrason. Sonochem.*, 2004. doi:10.1016/j.ultsonch.2004.01.006.
- [66] Marangopoulos IP, Martin CJ, Hutchison JMS. Measurement of field distributions in ultrasonic cleaning baths: Implications for cleaning efficiency. *Phys Med Biol* 1995. doi:10.1088/0031-9155/40/11/009.
- [67] Zeqiri B, Gélat PN, Hodnett M, Lee ND. A novel sensor for monitoring acoustic cavitation. Part I: Concept, theory, and prototype development. *IEEE Trans Ultrason Ferroelectr Freq Control* 2003. doi:10.1109/TUFFC.2003.1244751.
- [68] Zeqiri B, Lee ND, Hodnett M, Gélat PN. A novel sensor for monitoring acoustic cavitation. Part II: Prototype performance evaluation. *IEEE Trans Ultrason Ferroelectr Freq Control* 2003. doi:10.1109/TUFFC.2003.1244752.

- [69] Kim HJ, Chi MH, Hong IK. Effect of ultrasound irradiation on solvent extraction process. *J Ind Eng Chem* 2009;15:919–28. doi:10.1016/j.jiec.2009.09.025.
- [70] Gallego-Juárez JA, Graff KF. *Power Ultrasonics: Applications of High-Intensity Ultrasound*. 2014. doi:10.1016/C2013-0-16435-5.
- [71] elipe Gaitan D, Crum LA, Church CC, Roy RA. Sonoluminescence and bubble dynamics for a single, stable, cavitation bubble. *J Acoust Soc Am* 1992. doi:10.1121/1.402855.
- [72] Flannigan DJ, Suslick KS. Inertially confined plasma in an imploding bubble. *Nat Phys* 2010. doi:10.1038/nphys1701.
- [73] Kappus B, Khalid S, Chakravarty A, Putterman S. Phase transition to an opaque plasma in a sonoluminescing bubble. *Phys Rev Lett* 2011. doi:10.1103/PhysRevLett.106.234302.
- [74] Khalid S, Kappus B, Weninger K, Putterman S. Opacity and transport measurements reveal that dilute plasma models of sonoluminescence are not valid. *Phys Rev Lett* 2012. doi:10.1103/PhysRevLett.108.104302.
- [75] Toegel R, Gompf B, Pecha R, Lohse D. Does water vapor prevent upscaling sonoluminescence? *Phys Rev Lett* 2000. doi:10.1103/PhysRevLett.85.3165.
- [76] Rosselló JM, Dellavale D, Bonetto FJ. Energy concentration and positional stability of sonoluminescent bubbles in sulfuric acid for different static pressures. *Phys Rev E - Stat Nonlinear, Soft Matter Phys* 2013. doi:10.1103/PhysRevE.88.033026.
- [77] Schanz D, Metten B, Kurz T, Lauterborn W. Molecular dynamics simulations of cavitation bubble collapse and sonoluminescence. *New J Phys* 2012. doi:10.1088/1367-2630/14/11/113019.
- [78] Kim KY, Byun KT, Kwak HY. Temperature and pressure fields due to collapsing bubble under ultrasound. *Chem Eng J* 2007;132:125–35. doi:10.1016/j.cej.2007.01.037.
- [79] Colussi AJ, Weavers LK, Hoffmann MR. Chemical Bubble Dynamics and Quantitative Sonochemistry. *J Phys Chem A* 1998;102:6927–34. doi:10.1021/jp980930t.
- [80] OSTERMAN A, DULAR M, SIROK B. Numerical Simulation of a Near-Wall Bubble Collapse in an Ultrasonic Field. *J Fluid Sci Technol* 2009;4:210–21. doi:10.1299/jfst.4.210.
- [81] Philipp A, Lauterborn W. Cavitation erosion by single laser-produced bubbles. *J Fluid Mech* 1998. doi:10.1017/S0022112098008738.
- [82] Rooze J, Rebrov E V., Schouten JC, Keurentjes JTF. Dissolved gas and ultrasonic

- cavitation - A review. *Ultrason Sonochem* 2013;20:1–11.
doi:10.1016/j.ultsonch.2012.04.013.
- [83] Niazi S, Hashemabadi SH, Razi MM. CFD simulation of acoustic cavitation in a crude oil upgrading sonoreactor and prediction of collapse temperature and pressure of a cavitation bubble. *Chem Eng Res Des* 2014.
- [84] Sutkar VS, Gogate PR, Csoka L. Theoretical prediction of cavitation activity distribution in sonochemical reactors. *Chem Eng J* 2010;158:290–5. doi:10.1016/j.cej.2010.01.049.
- [85] Wei Z. Scale-up Design of Ultrasound Horn for Advanced Oxidation Process Using COMSOL Simulation 2013:1–6.
- [86] Wang L, Memoli G, Butterworth I, Hodnett M, Zeqiri B. Characterisation of a multi-frequency cavitation vessel. *IOP Conf. Ser. Mater. Sci. Eng.*, 2012. doi:10.1088/1757-899X/42/1/012013.
- [87] Memoli G, Gélat PN, Hodnett M, Zeqiri B. Characterisation and improvement of a reference cylindrical sonoreactor. *Ultrason Sonochem* 2012;19:939–52.
doi:10.1016/j.ultsonch.2011.12.010.
- [88] Kinsler L, Frey A, Coppens A, Sanders J. *Fundamentals of Acoustics*. 3rd ed. New York: 1982.
- [89] Koda S, Kimura T, Kondo T, Mitome H. A standard method to calibrate sonochemical efficiency of an individual reaction system. *Ultrason Sonochem* 2003. doi:10.1016/S1350-4177(03)00084-1.
- [90] Yasui K, Iida Y, Tuziuti T, Kozuka T, Towata A. Strongly interacting bubbles under an ultrasonic horn. *Phys Rev E* 2008;77:016609. doi:10.1103/PhysRevE.77.016609.
- [91] Son Y, Lim M, Khim J, Ashokkumar M. Acoustic emission spectra and sonochemical activity in a 36 kHz sonoreactor. *Ultrason Sonochem* 2012;19:16–21.
doi:10.1016/j.ultsonch.2011.06.001.
- [92] Cotana F, Rossi F. Study of Water Photosonolysis for Hydrogen Production. 3rd Int. green energy Conf., 2007, p. 3–8.
- [93] Capelo-Martínez JL. *Ultrasound in Chemistry: Analytical Applications*. 2009.
doi:10.1002/9783527623501.
- [94] Rubinetti D, Weiss DA, Wahlen A, Müller J. Numerical Modeling and Validation Concept for Acoustic Streaming Induced by Ultrasonic Treatment. 2016 COMSOL Conf

- Munich 2016:12–4.
- [95] Son Y, Lim M, Ashokkumar M, Khim J. Geometric Optimization of Sonoreactors for the Enhancement of Sonochemical Activity. *J Phys Chem C* 2011;115:4096–103. doi:10.1021/jp110319y.
- [96] Trujillo FJ, Knoerzer K. A computational modeling approach of the jet-like acoustic streaming and heat generation induced by low frequency high power ultrasonic horn reactors. *Ultrason Sonochem* 2011;18:1263–73. doi:10.1016/j.ultronch.2011.04.004.
- [97] Moudjed B, Botton V, Henry D, Millet S, Garandet JP, Ben Hadid H. Near-field acoustic streaming jet. *Phys Rev E* 2015;91:033011. doi:10.1103/PhysRevE.91.033011.
- [98] Comsol Multiphysics Software. Ultrasonic Flow Meter with Piezoelectric Transducers : Coupling between FEM and DG n.d.
- [99] Niazi S, Hashemabadi SH, Noroozi S. Numerical simulation of operational parameters and sonoreactor configurations for the highest possibility of acoustic cavitation in crude oil. *Chem Eng Commun* 2014;201:1340–59.
- [100] Abdelmwigoud M, Shaaban M, Mohany A. Flow dynamics and azimuthal behavior of the self-excited acoustic modes in axisymmetric shallow cavities. *Phys Fluids* 2020;32. doi:10.1063/5.0026552.
- [101] Ramírez-Del-Solar M, de la Rosa-Fox N, Esquivias L, Zarzycki J. Kinetic study of gelation of solventless alkoxide-water mixtures. *J Non Cryst Solids* 1990. doi:10.1016/0022-3093(90)90101-Q.
- [102] Asakura Y, Yasuda K, Kato D, Kojima Y, Koda S. Development of a large sonochemical reactor at a high frequency. *Chem Eng J* 2008. doi:10.1016/j.cej.2007.08.007.
- [103] Mhetre AS, Gogate PR. New design and mapping of sonochemical reactor operating at capacity of 72L. *Chem Eng J* 2014. doi:10.1016/j.cej.2014.07.075.
- [104] Valitov G, Jamshidi R, Rossi D, Gavriilidis A, Mazzei L. Effect of acoustic streaming on continuous flow sonocrystallization in millifluidic channels. *Chem Eng J* 2020. doi:10.1016/j.cej.2019.122221.
- [105] Yasui K, Tuziuti T, Iida Y. Optimum bubble temperature for the sonochemical production of oxidants. *Ultrasonics* 2004;42:579–84. doi:10.1016/j.ultras.2003.12.005.
- [106] Jamshidi R, Pohl B, Peuker UA, Brenner G. Numerical investigation of sonochemical reactors considering the effect of inhomogeneous bubble clouds on ultrasonic wave

- propagation. Chem Eng J 2012. doi:10.1016/j.cej.2012.02.029.
- [107] Keller JB, Miksis M. Bubble oscillations of large amplitude. J Acoust Soc Am 1980. doi:10.1121/1.384720.
- [108] Rashwan SS, Dincer I, Mohany A. A unique study on the effect of dissolved gases and bubble temperatures on the ultrasonic hydrogen (sonohydrogen) production. Int J Hydrogen Energy 2020;45:20808–19. doi:10.1016/j.ijhydene.2020.05.022.
- [109] Rashwan SS, Dincer I, Mohany A. An investigation of ultrasonic based hydrogen production. Energy 2020;205:118006. doi:10.1016/j.energy.2020.118006.
- [110] Mason TJ, Lorimer JP. Applied sonochemistry. The uses of power ultrasound in chemistry and processing. 2002. doi:10.1002/352760054X.
- [111] NIST Chemical Kinetics Database, <<http://kinetics.nist.gov/index.php>> (date last viewed 27/9/2012). n.d.
- [112] http://combustion.berkeley.edu/gri-mech/data/nasa_plnm.html n.d.
- [113] Hart EJ, Henglein A. Sonochemistry of aqueous solutions: H₂-O₂ combustion in cavitation bubbles. J Phys Chem 1987. doi:10.1021/j100297a038.
- [114] Mišík V, Riesz P. EPR study of free radicals induced by ultrasound in organic liquids II. Probing the temperatures of cavitation regions. Ultrason Sonochem 1996. doi:10.1016/1350-4177(95)00036-4.
- [115] Fischer CH, Hart EJ, Henglein A. Hydrogen/deuterium isotope exchange in the molecular deuterium-water system under the influence of ultrasound. J Phys Chem 1986;90:222–4. doi:10.1021/j100274a003.
- [116] Kamath V, Oğuz HN, Prosperetti A. Bubble oscillations in the nearly adiabatic limit. J Acoust Soc Am 1992. doi:10.1121/1.405253.
- [117] Didenko YT, Pugach SP. Spectra of water sonoluminescence. J Phys Chem 1994. doi:10.1021/j100090a006.
- [118] Ashokkumar M, Hall R, Mulvaney P, Grieser F. Sonoluminescence from aqueous alcohol and surfactant solutions. J Phys Chem B 1997. doi:10.1021/jp972477b.
- [119] Löfstedt R, Weninger K, Putterman S, Barber BP. Sonoluminescing bubbles and mass diffusion. Phys Rev E 1995. doi:10.1103/PhysRevE.51.4400.
- [120] Wu CC, Roberts PH. Shock-wave propagation in a sonoluminescing gas bubble. Phys Rev Lett 1993. doi:10.1103/PhysRevLett.70.3424.

- [121] Hua I, Hoffmann MR. Kinetics and mechanism of the sonolytic degradation of CCL4: Intermediates and byproducts. *Environ Sci Technol* 1996. doi:10.1021/es9502942.
- [122] Baulch DL, Pilling MJ, Cobos CJ, Cox RA, Frank P, Hayman G, et al. Evaluated Kinetic Data for Combustion Modeling. Supplement I. *J Phys Chem Ref Data* 1994. doi:10.1063/1.555953.
- [123] Hart EJ, Henglein A. Free radical and free atom reactions in the sonolysis of aqueous iodide and formate solutions. *J Phys Chem* 1985. doi:10.1021/j100266a038.
- [124] Lohse D, Hilgenfeldt S. Inert gas accumulation in sonoluminescing bubbles. *J Chem Phys* 1997. doi:10.1063/1.474939.
- [125] Flynn HG. Cavitation dynamics. II. Free pulsations and models for cavitation bubbles. *J Acoust Soc Am* 1975. doi:10.1121/1.380799.
- [126] Rayleigh, Lord. VIII. On the pressure developed in a liquid during the collapse of a spherical cavity. London, Edinburgh, Dublin *Philos Mag J Sci* 1917. doi:10.1080/14786440808635681.
- [127] Naidu DVP, Rajan R, Kumar R, Gandhi KS, Arakeri VH, Chandrasekaran S. Modelling of a batch sonochemical reactor. *Chem Eng Sci* 1994. doi:10.1016/0009-2509(94)80024-3.
- [128] Tsang W, Hampson RF. Chemical Kinetic Data Base for Combustion Chemistry. Part I. Methane and Related Compounds. *J Phys Chem Ref Data* 1986. doi:10.1063/1.555759.
- [129] Sochard S, Wilhelm AM, Delmas H. Modelling of free radicals production in a collapsing gas-vapour bubble. *Ultrason Sonochem* 1997. doi:10.1016/S1350-4177(97)00021-7.
- [130] Burdin F, Tsochatzidis NA, Guiraud P, Wilhelm AM, Delmas H. Characterisation of the acoustic cavitation cloud by two laser techniques. *Ultrason. Sonochem.*, 1999. doi:10.1016/S1350-4177(98)00035-2.
- [131] Tsochatzidis NA, Guiraud P, Wilhelm AM, Delmas H. Determination of velocity, size and concentration of ultrasonic cavitation bubbles by the phase-Doppler technique. *Chem Eng Sci* 2001. doi:10.1016/S0009-2509(00)00460-7.
- [132] Mohany A, Ziada S. Numerical Simulation of the Flow-Sound Interaction Mechanisms of a Single and Two-Tandem Cylinders in Cross-Flow. *J Press Vessel Technol* 2009. doi:10.1115/1.3110029.
- [133] Mohany A, Arthurs D, Bolduc M, Hassan M, Ziada S. Numerical and experimental

- investigation of flow-acoustic resonance of side-by-side cylinders in a duct. *J Fluids Struct* 2014. doi:10.1016/j.jfluidstructs.2014.03.015.
- [134] Arafa N, Mohany A. Flow-Excited Acoustic Resonance of Isolated Cylinders in Cross-Flow. *J Press Vessel Technol Trans ASME* 2016. doi:10.1115/1.4030270.
- [135] Capelo-Martínez JL. *Ultrasound in Chemistry: Analytical Applications*. 2009. doi:10.1002/9783527623501.
- [136] Suslick KS, Didenko Y, Fang MM, Hyeon T, Kolbeck KJ, McNamara WB, et al. Acoustic cavitation and its chemical consequences. *Philos Trans R Soc A Math Phys Eng Sci* 1999. doi:10.1098/rsta.1999.0330.
- [137] Memoli G, Gélat P, Hodnett M, Zeqiri B. The importance of temperature control in the operation of high power ultrasound reactors. *Proc. 38th Annu. Symp. Ultrason. Ind. Assoc. UIA* 2009, 2009. doi:10.1109/UIA.2009.5404027.
- [138] Berliner S, Cove G. *ULTRASONICFLUD PROCESSING SYSTEM*, 1991.
- [139] Dahlem O, Reisse J, Halloin V. The radially vibrating horn: A scaling-up possibility for sonochemical reactions. *Chem Eng Sci* 1999;54:2829–38. doi:10.1016/S0009-2509(98)00356-X.
- [140] Rashwan SS, Dincer I, Mohany A. Investigation of acoustic and geometric effects on the sonoreactor performance. *Ultrason Sonochem* 2020;68:105174. doi:10.1016/j.ultsonch.2020.105174.
- [141] Schenker MC, Pourquié MJB, Eskin DG, Boersma BJ. PIV quantification of the flow induced by an ultrasonic horn and numerical modeling of the flow and related processing times. *Ultrason Sonochem* 2013;20:502–9. doi:10.1016/j.ultsonch.2012.04.014.
- [142] Slama RBH, Gilles B, Chiekh M Ben, Bera JC. Characterization of focused-ultrasound-induced acoustic streaming. *Exp Therm Fluid Sci* 2019;101:37–47. doi:10.1016/j.expthermflusci.2018.10.001.
- [143] Son Y. Simple design strategy for bath-type high-frequency sonoreactors. *Chem Eng J* 2017;328:654–64. doi:10.1016/j.cej.2017.07.012.
- [144] Zhang Z, Gao T, Liu X, Li D, Zhao J, Lei Y, et al. Influence of sound directions on acoustic field characteristics within a rectangle-shaped sonoreactor: Numerical simulation and experimental study. *Ultrason Sonochem* 2018;42:787–94. doi:10.1016/j.ultsonch.2017.12.024.

- [145] Rashwan SS, Ibrahim AH, Abou-Arab TW, Nemitallah MA, Habib MA. Experimental investigation of partially premixed methane-air and methane-oxygen flames stabilized over a perforated-plate burner. *Appl Energy* 2016. doi:10.1016/j.apenergy.2016.02.047.
- [146] Rashwan SS, Ibrahim AH, Abou-Arab TW, Nemitallah MA, Habib MA. Experimental study of atmospheric partially premixed oxy-combustion flames anchored over a perforated plate burner. *Energy* 2017;122:159–67.
- [147] Rashwan SS, Nemitallah MA, Habib MA. Review on Premixed Combustion Technology: Stability, Emission Control, Applications, and Numerical Case Study. *Energy and Fuels* 2016. doi:10.1021/acs.energyfuels.6b02386.
- [148] Rashwan SS. The Effect of Swirl Number and Oxidizer Composition on Combustion Characteristics of Non-Premixed Methane Flames. *Energy & Fuels* 2018;32:2517–26.
- [149] Ramadan IA, Ibrahim AH, Abou-Arab TW, Rashwan SS, Nemitallah MA, Habib MA. Effects of oxidizer flexibility and bluff-body blockage ratio on flammability limits of diffusion flames. *Appl Energy* 2016;178:19–28. doi:10.1016/j.apenergy.2016.06.009.
- [150] Momirlan M, Boriaru N. Pressure and temperature effects on water dissociation reaction for hydrogen production over zeolites. *Renew Energy* 2000;19:243–8. doi:10.1016/S0960-1481(99)00038-5.
- [151] Xu D, Dong L, Ren J. Introduction of Hydrogen Routines. *Hydrog. Econ., Elsevier*; 2017, p. 35–54. doi:10.1016/B978-0-12-811132-1.00002-X.
- [152] Louisnard O. A simple model of ultrasound propagation in a cavitating liquid. Part I: Theory, nonlinear attenuation and traveling wave generation. *Ultrason Sonochem* 2012;19:56–65. doi:10.1016/j.ultsonch.2011.06.007.
- [153] Vanhille C, Campos-Pozuelo C. Nonlinear ultrasonic standing waves: Two-dimensional simulations in bubbly liquids. *Ultrason Sonochem* 2011;18:679–82. doi:10.1016/j.ultsonch.2010.09.002.
- [154] Colorado State University n.d. <http://navier.engr.colostate.edu/code/code-2/index.html>.
- [155] Cengel YA, Boles MA. *Thermodynamics: an Engineering Approach* 8th Edition. 2015. doi:10.1017/CBO9781107415324.004.

APPENDICES

Copyright permissions

This thesis's high similarity is exclusively due to the candidate's six published journal papers, which are based on this thesis. As a result, some critical information, equations, and illustrations, which cannot be revised without losing the work's fundamental essence, are maintained. The similarity of the thesis and each of those papers is listed below. For this reason, permissions are duly obtained from the publishers to include this information in the thesis.

The following are the publishers' obtained permissions for the reuse of the published work based on this Ph.D. thesis.

a. Wiley: (International Journal of Energy Research)

Article C, in the Copyright transfer agreement:

“3. Final Published Version. The Owner hereby licenses back to the Contributor the following rights with respect to the final published version of the Contribution (the "Final Published Version"):”

“b. Re-use in other publications. The right to re-use the Final Published Version or parts thereof for any publication authored or edited by the Contributor (excluding journal articles) where such re-used material constitutes less than half of the total material in such publication. In such a case, any modifications must be accurately noted.”

b. Elsevier:

Article: Submission declaration and verification in the Guide for authors:

“Submission of an article implies that the work described has not been published previously (except in the form of an abstract, a published lecture or academic thesis, see 'Multiple, redundant or concurrent publication' for more information), that it is not under consideration for publication elsewhere, that its publication is approved by all authors and tacitly or explicitly by the responsible authorities where the work is carried out, and that, if accepted, it will not be published elsewhere in the same form, in English or in any other language, including electronically without the written consent of the copyright holder. To verify originality, your article may be checked by the originality detection service Crossref Similarity Check.”

The similarity of the thesis with each of the published work that is based on the Thesis:

Paper1: Rashwan SS, Dincer I, Mohany A, Pollet BG. The Sonohydrogen process (Ultrasound induced hydrogen production): Challenges and opportunities. International Journal of Hydrogen Energy. 2019, 7;44, (29):14500-26. doi.org/10.1016/j.ijhydene.2020.05.022

Similarity: 14%

Paper2: Rashwan SS, Dincer I, Mohany A. An investigation of ultrasonic based hydrogen production. Energy. 2020 Jun 10:118006. doi.org/10.1016/j.energy.2020.118006

Similarity: 9%

Paper3: Rashwan SS, Dincer I, Mohany A. Investigation of acoustic and geometric effects on the sonoreactor performance. Ultrasonics Sonochemistry. 2020 May 16:105174. doi.org/10.1016/j.ultsonch.2020.105174

Similarity: 9%

Paper4: Rashwan SS, Dincer I, Mohany A. A unique study on the effect of dissolved gases and bubble temperatures on the ultrasonic hydrogen (sono-hydrogen) production. doi.org/10.1016/j.ijhydene.2020.05.022

Similarity: 6%

Appendix A. Copy righted articles

A1. Copy rights permission by ELSEVIER of published articles

“Rashwan SS, Dincer I, Mohany A. An investigation of ultrasonic based hydrogen production”

Sherif Seif Eldin

From: Rights and Permissions (ELS) <Permissions@elsevier.com>
Sent: Monday, September 28, 2020 2:53 AM
To: Sherif Seif Eldin
Subject: Re: Obtain permission request - Journal (1060965) [200927-004137]

[EXTERNAL EMAIL]



Dear Dr. Sherif Seifeldin

We hereby grant you permission to reprint the material below at no charge **in your thesis** subject to the following conditions:

1. If any part of the material to be used (for example, figures) has appeared in our publication with credit or acknowledgement to another source, permission must also be sought from that source. If such permission is not obtained then that material may not be included in your publication/copies.
2. Suitable acknowledgment to the source must be made, either as a footnote or in a reference list at the end of your publication, as follows:
“This article was published in Publication title, Vol number, Author(s), Title of article, Page Nos, Copyright Elsevier (or appropriate Society name) (Year).”
3. Your thesis may be submitted to your institution in either print or electronic form.
4. Reproduction of this material is confined to the purpose for which permission is hereby given
5. This permission is granted for non-exclusive world **English** rights only. For other languages please reapply separately for each one required. Permission excludes use in an electronic form other than submission. Should you have a specific electronic project in mind please reapply for permission.
6. As long as the article is embedded in your thesis, you can post/ share your thesis in the University repository
7. Should your thesis be published commercially, please reapply for permission.
8. Posting of the full article/ chapter online is not permitted. You may post an abstract with a link to the Elsevier website www.elsevier.com, or to the article on ScienceDirect if it is available on that platform.

Thanks & Regards,
Roopa Lingayath
Sr Copyrights Coordinator - Copyrights Team
ELSEVIER | Health Content Operations
E-mail: r.lingayath@elsevier.com | url: www.elsevier.com

From: Administrator
Date: Sunday, September 27, 2020 04:15 PM GMT

Dear Sherif Rashwan,

Thank you for contacting the Permissions Granting Team.

We acknowledge the receipt of your request and we aim to respond within seven business days. Your unique reference number is 200927-004137.

Please avoid changing the subject line of this email when replying to avoid delay with your query.

Regards,
Permission Granting Team

From: Sherif Rashwan
Date: Sunday, September 27, 2020 04:15 PM GMT

Submission ID: 1060965
Date: 27 Sep 2020 5:15pm

Name: Dr. Sherif Seifeldin
Institute/company: UOIT
Address: 2238 Minsky PL
Post/Zip Code: L1L 1C4
City: Oshawa
State/Territory: Ontario
Country: Canada
Telephone: 2899434127
Email: sherif.seifeldin@uoit.ca

Type of Publication: Journal

Title: Energy
Auhtors: Sherif S. Rashwan, Ibrahim Dincer, Atef Mohany
Year: 2020
From page: 118006
To page: 118006
ISSN: 0360-5442
Volume: 205
Article title: An investigation of ultrasonic based hydrogen production

I would like to use: Figure(s)

Quantity of material: 15
I am the author of the Elsevier material: Yes
Involvement: First and Corresponding Author

In what format will you use the material: Print and Electronic
Translation: No

Proposed use: Reuse in a thesis/dissertation

“Rashwan SS, Dincer I, Mohany A. A unique study on the effect of dissolved gases and bubble temperatures on the ultrasonic hydrogen (sonohydrogen) production”

Sherif Seif Eldin

From: Rights and Permissions (ELS) <Permissions@elsevier.com>
Sent: Monday, September 28, 2020 2:50 AM
To: Sherif Seif Eldin
Subject: Re: Obtain permission request - Journal (1060964) [200927-004087]

[EXTERNAL EMAIL]



ELSEVIER

Dear Dr. Sherif Seifeldin

We hereby grant you permission to reprint the material below at no charge **in your thesis** subject to the following conditions:

1. If any part of the material to be used (for example, figures) has appeared in our publication with credit or acknowledgement to another source, permission must also be sought from that source. If such permission is not obtained then that material may not be included in your publication/copies.
2. Suitable acknowledgment to the source must be made, either as a footnote or in a reference list at the end of your publication, as follows:
“This article was published in Publication title, Vol number, Author(s), Title of article, Page Nos, Copyright Elsevier (or appropriate Society name) (Year).”
3. Your thesis may be submitted to your institution in either print or electronic form.
4. Reproduction of this material is confined to the purpose for which permission is hereby given
5. This permission is granted for non-exclusive world **English** rights only. For other languages please reapply separately for each one required. Permission excludes use in an electronic form other than submission. Should you have a specific electronic project in mind please reapply for permission.
6. As long as the article is embedded in your thesis, you can post/ share your thesis in the University repository
7. Should your thesis be published commercially, please reapply for permission.
8. Posting of the full article/ chapter online is not permitted. You may post an abstract with a link to the Elsevier website www.elsevier.com, or to the article on ScienceDirect if it is available on that platform.

Thanks & Regards,
Roopa Lingayath
Sr Copyrights Coordinator – Copyrights Team
ELSEVIER | Health Content Operations
E-mail: r.lingayath@elsevier.com | url: www.elsevier.com

1

From: Administrator
Date: Sunday, September 27, 2020 04:03 PM GMT

Dear Sherif Rashwan,

Thank you for contacting the Permissions Granting Team.

We acknowledge the receipt of your request and we aim to respond within seven business days. Your unique reference number is 200927-004087.

Please avoid changing the subject line of this email when replying to avoid delay with your query.

Regards,
Permission Granting Team

From: Sherif Rashwan
Date: Sunday, September 27, 2020 04:03 PM GMT

Submission ID: 1060964
Date: 27 Sep 2020 5:02pm

Name: Dr. Sherif Seifeldin
Institute/company: University of Ontario Institute of Technology
Address: 2000 Simcoe St N, Oshawa, , PO 5069
Post/Zip Code: L1H 7K4
City: Oshawa
State/Territory: Ontario
Country: Canada
Telephone: 2899434127
Email: sherif.seifeldin@uoit.ca

Type of Publication: Journal

Title: International Journal of Hydrogen Energy
Auhtors: Sherif S. Rashwan, Ibrahim Dincer, Atef Mohany
Year: 2020
From page: 20808
To page: 20819
ISSN: 0360-3199
Volume: 45
Issue: 41
Article title: A unique study on the effect of dissolved gases and bubble temperatures on the ultrasonic hydrogen (sonohydrogen) production

I would like to use: Figure(s)

Quantity of material: 16
I am the author of the Elsevier material: Yes
Involvement: First and Corresponding Author

In what format will you use the material: Print and Electronic
Translation: No

“Rashwan SS, Dincer I, Mohany A, Pollet BG. The Sono-hydrogen process (Ultrasound induced hydrogen production): Challenges and Opportunities. International Journal of Hydrogen Energy”

Sherif Seif Eldin

From: Rights and Permissions (ELS) <Permissions@elsevier.com>
Sent: Monday, October 12, 2020 7:40 PM
To: Sherif Seif Eldin
Subject: Re: Obtain permission request - Journal (1066931) [201009-018284]

[EXTERNAL EMAIL]



Dear Sherief

Thank you for your email.

Please note that, as one of the Authors of this article, you retain the right to reuse it in your thesis/dissertation. You do not require formal permission to do so.

You are permitted to post this Elsevier article online if it is embedded within your thesis. Suitable acknowledgement to the source must be made, either as a footnote or in a reference list at the end of your publication.

You are also permitted to post your Author Accepted Manuscript online. However posting of the final published article is prohibited.

*“As per our [Sharing Policy](#), authors are permitted to post the Accepted version of their article on their institutional repository – as long as it is for **internal institutional use only**.*

It can only be shared publicly on that site once the journal-specific embargo period has lapsed. For a list of embargo periods please see: https://www.elsevier.com/data/assets/pdf_file/0005/78476/external-embargo-list.pdf

You are not permitted to post the Published Journal Article (PJA) on the repository.”

Please feel free to contact me if you have any queries.

Kind regards

Anita

Anita Mercy

Senior Copyrights Coordinator – Copyrights Team

Elsevier | Health Content Operations

(A division of Reed Elsevier India Pvt. Ltd.)

Ascendas International Tech Park, Crest – 12th Floor|Taramani, Chennai 600113 · India|

Tel: +91 4442994696

a.vethakkan@elsevier.com

Permissions Helpdesk please visit - [Permissions Helpdesk Support Center](#)

Join the Elsevier Connect Community
www.elsevier.com
[Twitter](#) | [Facebook](#) | [LinkedIn](#) | [Google+](#)

From: Administrator
Date: Friday, October 09, 2020 03:55 PM GMT

Dear Sherif Rashwan,

Thank you for contacting the Permissions Granting Team.

We acknowledge the receipt of your request and we aim to respond within seven business days. Your unique reference number is 201009-018284.

Please avoid changing the subject line of this email when replying to avoid delay with your query.

Regards,
Permission Granting Team

From: Sherif Rashwan
Date: Friday, October 09, 2020 03:55 PM GMT

Submission ID: 1066931
Date: 09 Oct 2020 4:54pm

Name: Dr. Sherif Seifeldin
Institute/company: University of Ontario Institute of Technology
Address: 2238 Minsky PL
Post/Zip Code: L1L 1C4
City: Oshawa
State/Territory: Ontario
Country: Canada
Telephone: 2899434127
Email: sherif.seifeldin@uoit.ca

Type of Publication: Journal

Title: International Journal of Hydrogen Energy
Auhtors: Sherif S. Rashwan, Ibrahim Dincer, Atef Mohany, Bruno G.Pollet
Year: 2019
From page: 14500
To page: 14526
ISSN: 0360-3199
Volume: 44
Issue: 29
Article title: The Sono-Hydro-Gen process (Ultrasound induced hydrogen production): Challenges and opportunities

I would like to use: Full article / chapter

2

“Rashwan SS, Dincer I, Mohany A. Investigation of acoustic and geometric effects on the sonoreactor performance. *Ultrasonics Sonochemistry*. 2020 May 16:105174.”

Sherif Seif Eldin

From: Rights and Permissions (ELS) <Permissions@elsevier.com>
Sent: Monday, October 12, 2020 7:37 PM
To: Sherif Seif Eldin
Subject: Re: Obtain permission request - Journal (1066930) [201009-018230]

[EXTERNAL EMAIL]



ELSEVIER

Dear Sherif

Thank you for your email.

Please note that, as one of the Authors of this article, you retain the right to reuse it in your thesis/dissertation. You do not require formal permission to do so.

You are permitted to post this Elsevier article online if it is embedded within your thesis. Suitable acknowledgement to the source must be made, either as a footnote or in a reference list at the end of your publication.

You are also permitted to post your Author Accepted Manuscript online.
However posting of the final published article is prohibited.

*“As per our [Sharing Policy](#), authors are permitted to post the Accepted version of their article on their institutional repository – as long as it is for **internal institutional use only**.*

It can only be shared publicly on that site once the journal-specific embargo period has lapsed. For a list of embargo periods please see: https://www.elsevier.com/data/assets/pdf_file/0005/78476/external-embargo-list.pdf

You are not permitted to post the Published Journal Article (PJA) on the repository.”

Please feel free to contact me if you have any queries.

Kind regards

Anita

Anita Mercy

Senior Copyrights Coordinator – Copyrights Team

Elsevier | Health Content Operations

(A division of Reed Elsevier India Pvt. Ltd.)

Ascendas International Tech Park, Crest – 12th Floor|Taramani, Chennai 600113 · India|

Tel: +91 4442994696

a.vethakkan@elsevier.com

1

Permissions Helpdesk please visit - [Permissions Helpdesk Support Center](#)

Join the Elsevier Connect Community
www.elsevier.com
[Twitter](#) | [Facebook](#) | [LinkedIn](#) | [Google+](#)

From: Administrator
Date: Friday, October 09, 2020 03:51 PM GMT

Dear Sherif Rashwan,

Thank you for contacting the Permissions Granting Team.

We acknowledge the receipt of your request and we aim to respond within seven business days. Your unique reference number is 201009-018230.

Please avoid changing the subject line of this email when replying to avoid delay with your query.

Regards,
Permission Granting Team

From: Sherif Rashwan
Date: Friday, October 09, 2020 03:51 PM GMT

Submission ID: 1066930
Date: 09 Oct 2020 4:51pm

Name: Dr. Sherif Seifeldin
Institute/company: University of Ontario Institute of Technology
Address: 2238 Minsky PL
Post/Zip Code: L1L 1C4
City: Oshawa
State/Territory: Ontario
Country: Canada
Telephone: 2899434127
Email: sherif.seifeldin@uoit.ca

Type of Publication: Journal

Title: Ultrasonics Sonochemistry
Auhtors: Sherif S. Rashwan, Ibrahim Dincer, Atef Mohany
Year: 2020
From page: 105174
To page: 105174
ISSN: 1350-4177
Volume: 68
Article title: Investigation of acoustic and geometric effects on the sonoreactor performance

I would like to use: Full article / chapter